U. S. ARMY
TRANSPORTATION RESEARCH COMMAND
FORT EUSTIS, VIRGINIA

TRECOM TECHNICAL REPORT 63-1

GETOL RESEARCH PROGRAM

FINAL REPORT

Task 1D121401A14701
(Formerly Task 9R38-11-011-01)
Contract DA 44-177-TC-722

August 1963

prepared by:

GENERAL DYNAMICS/CONVAIR
San Diego, California

4396-63

DISCLAIMER NOTICE

When Government drawings, specifications, or other data are used for any purpose other than in connection with a definitely related Government procurement operation, the United States Government thereby incurs no responsibility nor any obligation whatsoever; and the fact that the Government may have formulated, furnished, or in any way supplied the said drawings, specifications, or other data is not to be regarded by implication or otherwise as in any manner licensing the holder or any other person or corporation, or conveying any rights or permission, to manufacture, use, or sell any patented invention that may in any way be related thereto.

* * *

DDC AVAILABILITY NOTICE

Qualified requesters may obtain copies of this report from

Defense Documentation Center
Arlington Hall Station
Arlington 12, Virginia

* * *

This report has been released to the Office of Technical Services, U. S. Department of Commerce, Washington 25, D. C., for sale to the general public.

* * *

The findings and recommendations contained in this report are those of the contractor and do not necessarily reflect the views of the U. S. Army Mobility Command, the U. S. Army Materiel Command, or the Department of the Army.

HEADQUARTERS
U S ARMY TRANSPORTATION RESEARCH COMMAND
FORT EUSTIS, VIRGINIA

Under Contract DA 44-177-TC-722 with the U. S. Army Transportation Research Command, a research program was conducted by the Convair Division of General Dynamics Corporation for the Army and Navy to determine feasibility of and to develop design information on an aircraft concept utilizing the peripheral jet principle as a landing gear system (GETOL) enabling aircraft take-off and landing over relatively unprepared terrain. This program was conducted in three phases: model study and fabrication, model testing and data analysis, and GETOL aircraft design study.

The most significant aspect of this study is the advancement in the state of the art resulting from the extensive wind-tunnel testing and data compilation on the relatively new GETOL concept. This command agrees that a GETOL aircraft could be built and flown. However, at present, the significant advantage of this type of aircraft over existing and proposed Army VTOL systems remains somewhat in doubt. The aircraft design presented in this report does not appear to be physically compatible with the restricting application of Army air vehicles.

GARY N. SMITH
Project Engineer

PAUL J. CARPENTER
Group Leader
Applied Aeronautical Engineering Group

APPROVED.

FOR THE COMMANDER:

LARRY M. HEWIN
Technical Director

Task 1D121401A14701
(Formerly Task 9R38-11-011-01)
Contract DA 44-177-TC-722
TRECOM Technical Report 63-1
August 1963

GETOL RESEARCH PROGRAM

FINAL REPORT

GDC-62-370

Prepared by

General Dynamics/Convair
San Diego, California

for

U. S. ARMY TRANSPORTATION RESEARCH COMMAND
FORT EUSTIS, VIRGINIA

CONTENTS

ILLUSTRATIONS

SYMBOLS

A	duct nozzle exit area (sq. ft.)
AR	aspect ratio
b	wing span exclusive of tips (ft.)
B. L.	buttock line
c	wing chord (ft.)
$\bar{c}$	mean aerodynamic chord (ft.)
$c_{1/2}$	cycles to half amplitude
c_2	cycles to double amplitude
CG	center of gravity
$\mathbb{C}_L$	center line
C. P.	center of pressure
D	drag (lb.)
D/L	longitudinal acceleration
d_e	equivalent base diameter
g	acceleration of gravity (fps^2)
h	height above the ground plane
$\mathbb{H}_L$	hinge line
I_{xx}	moment of inertia about the principal roll axis, (slug-ft.^{2})
I_{yy}	moment of inertia about the principal pitch axis, (slug-ft.^{2})
I_{zz}	moment of inertia about the principal yaw axis, (slug-ft.^{2})
L	lift (1b.)
M	pitching moment about 35% chord
M/L$\bar{c}$	center of pressure change from 0.35$\bar{c}$
m	mass flow (slugs/sec.)

N	yawing moment
n	load factor
p_e	average static pressure at nozzle exit (psf)
p_o	ambient pressure (psf)
psi	pounds per square inch
p_{t_1}	total pressure upstream (psf)
p_{t_e}	total pressure at exit (psf)
q_o	free stream dynamic pressure (psf)
q_j	jet efflux dynamic pressure (psf)
q_T	wind tunnel dynamic pressure (psf)
q"	nozzle dynamic pressure (q" - q_o + T/A) — psf
R	rolling moment
rpm	revolutions per minute
S	wing area, (sq. ft.)
SHP	shaft horsepower
T	Thrust (lb.)
T_o	static free air thrust (lb.)
T_c"	thrust coefficient (T_c" - T/q" S)
V_o	free stream velocity
$\frac{V_o}{\sqrt{\frac{0.7\ nW}{\rho\ S}}}$	nondimensional speed parameter
V_j	jet efflux velocity
V_s	stall velocity

W	gross weight (lb.)
w_a	weight flow (lb./sec.)
W. L.	water line
W_{ST}	structural weight (lb.)
Y	side force (lb.)
C_D	drag coefficient
C_L	lift coefficient
C_L''	slipstream lift coefficient
C_{L_α}	lift coefficient per unit angle of attack
$C_{L_{\dot{\alpha}}}$	lift coefficient per unit angle of attack rate in nondimensional time
$C_{L_{\dot{\theta}}}$	lift coefficient per unit pitch rate in nondimensional time
C_{ℓ_β}	rolling moment coefficient per unit sideslip angle
C_{ℓ_p}	rolling moment coefficient per unit roll rate
C_{ℓ_r}	rolling moment coefficient per unit yaw rate
C_m	pitching moment coefficient
C_{m_α}	pitching moment coefficient per unit angle of attack
$C_{m_{\dot{\alpha}}}$	pitching moment coefficient per unit angle of attack rate in nondimensional time
$C_{m_{\dot{\theta}}}$	pitching moment coefficient per unit pitch rate in nondimensional time
C_{n_β}	yawing moment coefficient per unit sildeslip angle
C_{n_p}	yawing moment coefficient per unit roll rate
C_{n_r}	yawing moment coefficient per unit yaw rate

C_{y_β}	side force coefficient per unit sideslip angle
C_{y_p}	side force coefficient per unit roll rate
C_{y_r}	side force coefficient per unit yaw rate
α	wing angle of attack referenced to wing chord plane, positive nose up
δ_F	flap deflection (deg.)
δ_i	tip deflection, positive when tip leading edge up (deg.)
$\delta_{\text{INLET STATOR}}$	inlet stator deflection (deg.)
δ_S	horizontal stabilizer deflection, positive when leading edge up (deg.)
δ_V	thrust deflection vane deflection, positive when thrust deflected to rear
ρ	air density, slugs/cu. ft.
ϕ	roll angle, positive right wing down (deg.)
Ψ	yaw angle, positive nose right (deg.)
$\left\lvert \frac{\phi}{v_e} \right\rvert$	rolling parameter (deg./fps)

SUMMARY

This report presents the results of an experimental research program to determine the aerodynamic characteristics of a ground-effect take-off and landing (GETOL) airplane. The work was conducted under Contract DA 44-177-TC-722 for the U. S. Army Transportation Research Command, Fort Eustis, Virginia. With the Bureau of Naval Weapons as cosponsers, the scope of Contract DA 44-177-TC-722 included consideration of Navy requirements in its study and analysis of GETOL aircraft.

The GETOL concept promises the extension of airplane utility by using a ground-effect cushion for take-off and landing, thereby obviating the need for a prepared runway. This concept has been under study at General Dynamics/Convair for several years. The idea of replacing conventional landing gear with a high-pressure "bubble" of air evolved from studies in the ground-effect machine (GEM) regime and from investigations into the compatibility of low aspect-ratio wings with such machines. The GETOL vehicle can provide the most desirable feature of VTOL craft — no necessity for a prepared runway — and still maintain a significantly larger portion of conventional aircraft payload than a VTOL vehicle.

The Convair studies progressed to this experimental research program which has provided substantial data toward making the GETOL concept a reality.

CONCLUSIONS

Results of the experimental program show that that the external aerodynamic characteristics of the GETOL concept are amenable to the development of an all-surface aircraft with STOL performance. Figure 1 shows typical take-off characteristics for a GETOL transport-type aircraft.

Lift-to-static thrust ratios adequate to provide satisfactory ground clearance were achieved. This lift-to-thrust ratio is equal to or greater than the hovering value at all forward speeds, and increases rapidly when sufficient speed is attained to attach the external flow to the upper wing surface. Gains in lift-to-thrust ratio can be attained if the peripheral slot is extended across the fuselage. Also, evidence was obtained to show that peripheral nozzle development potential exists which will give still further improvement in this ratio.

As expected, forward movement of the center of pressure with increasing forward velocity was experienced. This trim change can be controlled by manipulation of the exit nozzle geometry without resort to additional thrust producing devices.

With the plain, peripheral-type slots tested, rearward deflection of the thrust for forward acceleration causes a drop in base pressures which is reflected by a loss in lift-to-thrust ratio. Therefore, when considering a configuration of this type, thrust for forward acceleration should be obtained from the cruise engines and/or other schemes, if possible.

Pressure and force data confirm the existence of three characteristic flow patterns — subcritical, transitional, and supercritical — in which the external flow is unattached to the leading edge, attached to the leading edge, and both attached to the leading edge and flowing over and under the vehicle, respectively. These flow patterns have a strong effect on the trim change with forward velocity and on ram drag which was less than theoretically expected in ground effect.

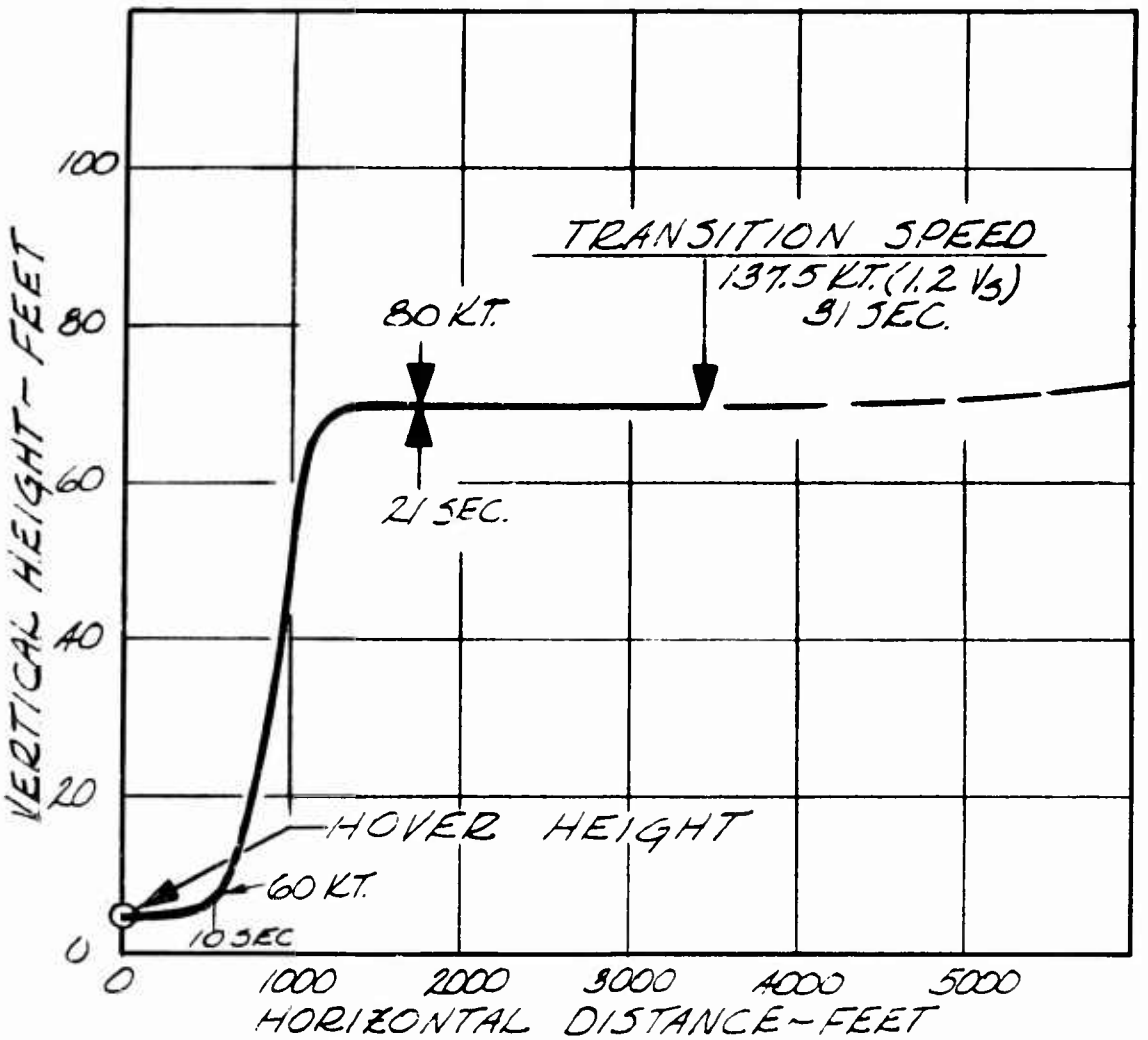

Figure 1. Typical GETOL Take-Off Using Experimental Data Gross Weight = 82,500 Pounds

RECOMMENDATIONS

This program has produced wind tunnel model test results which confirm the technical practicability of the GETOL aircraft concept. The work also has highlighted areas needing further aerodynamic research. The ability of the GETOL craft to obtain terrain freedom at an installed thrust level less than the vehicle gross weight is sufficient reason to pursue its development. Therefore, it is recommended that a program be initiated which will culminate in the flight test of a GETOL research vehicle. The following experimental programs are specifically recommended to support this work before further powered model testing:

1. A static program to develop: (a) a nozzle geometry which will provide inherent attitude stability in the height regime which is reasonable for normal GETOL operations, and (b) an effective and near-linear reaction control system compatible with the above nozzle geometry.

2. A semispan model wind tunnel test program to determine the effects of: (a) chordwise location of the fan inlet on pitching moment, and (b) relative chordwise location of propeller plane and fan inlets on longitudinal thrust and pitching moment.

3. A wind tunnel test program to develop a cruise configuration with satisfactory performance and flight handling characteristics.

INTRODUCTION

The GETOL experimental research program had two major objectives:

1. To furnish design information for a fan exit nozzle and a control system geometry arrangement to provide a vehicle with GETOL capability.

2. To use this design information to obtain a representative GETOL aircraft configuration.

The program was divided into three phases which had the following objectives:

Phase I — Design a powered wind tunnel model of a GETOL aircraft with sufficient power, control simulation, and pressure instrumentation to meet Phase II objectives.

Phase II — By using results of the powered wind tunnel model investigation, determine the contribution of the individual forces to the total lift and pitching moment and the variation of these forces with height above ground, airplane velocity and attitude, thrust, and thrust deflection.

Phase III — Use the information gained from Phase II to obtain a representative GETOL aircraft configuration.

Two other programs were conducted separately by Convair to support these objectives. One was a bench test program to obtain a proper nozzle geometry for the powered model. The other was a modification of the Convair Low-Speed Wind Tunnel to provide a large test section for powered model use. This large section was required to eliminate large tunnel wall effects on powered model data.

Phase II is represented by a sampling of data obtained from the heavily instrumented, three-dimensional model and shows the effects of various geometric and flight parameters on airplane forces and moments. The data then was used to conduct an airplane predesign study to substantiate concept capability and to fulfill the Phase III objective.

Calculations based on test results show that a GETOL transport system is capable of attaining take-off and landing distances over a 50-foot obstacle which are comparable with that of STOL aircraft while maintaining the terrain clearance advantage of VTOL aircraft. Also, it is significant that such performance is attainable with lift equal to 77% of the gross weight and with clearance heights of at least 5 feet.

PHASE I — CONTRACTUAL EFFORT

As previously indicated, the design and fabrication of the powered wind tunnel model were the objectives of the Phase I task. Basically, this work was separated into three areas. The first was the definition of the configuration to be simulated by the powered model. The second portion involved the actual model design, and the last consisted of model construction.

CONFIGURATION SELECTION

Selecting the configuration to be simulated largely meant using the experience gained from previous extensive Convair configuration studies. Synthesis studies were conducted on a short-range transport configuration with a payload capacity of approximately 8 tons. The resulting geometry from these studies generally established the model configuration, using a 0.08 scale factor. Further studies were conducted to provide the model with a configuration that could reflect maximum GETOL performance.

The wing planform was selected from previous studies. The low aspect-ratio configuration provided significant structural weight advantages as is indicated in Figure 2 and Reference 1. However, the simple, low aspect-ratio wing suffers prohibitively from performance deterioration at cruise. Therefore, Convair has completed various studies to rectify this problem which have indicated that proper wing tip design with addition of the horizontal tail outboard of the wing tips could provide low aspect-ratio wing performance essentially competitive with higher aspect-ratio designs (Figure 3). These studies then provided the basis for selection of the aspect ratio of one for the basic wing planform used on the model. The wing tip design was selected as the optimum from a series of wing tips tested with an aspect-ratio one wing (Reference 2).

Coupled with wing planform selection was the determination of the proper horizontal tail to be selected. Proper sizing was required to assure that the aerodynamic neutral point in cruise flight would be aft of the 35% chord point selected from ground-effect considerations to be discussed later. Earlier studies in the wing tunnel for various tail sizes tested on an aspect-ratio one wing indicated that a tail-area-to-wing-area ratio of 0.23 would satisfy the cruise flight requirements for a center of gravity at the 35% chord. The planform was selected with due consideration of the upwash patterns in cruise flight and the prospects of excessive dihedral effects from the canted wing tips near the stall speed.

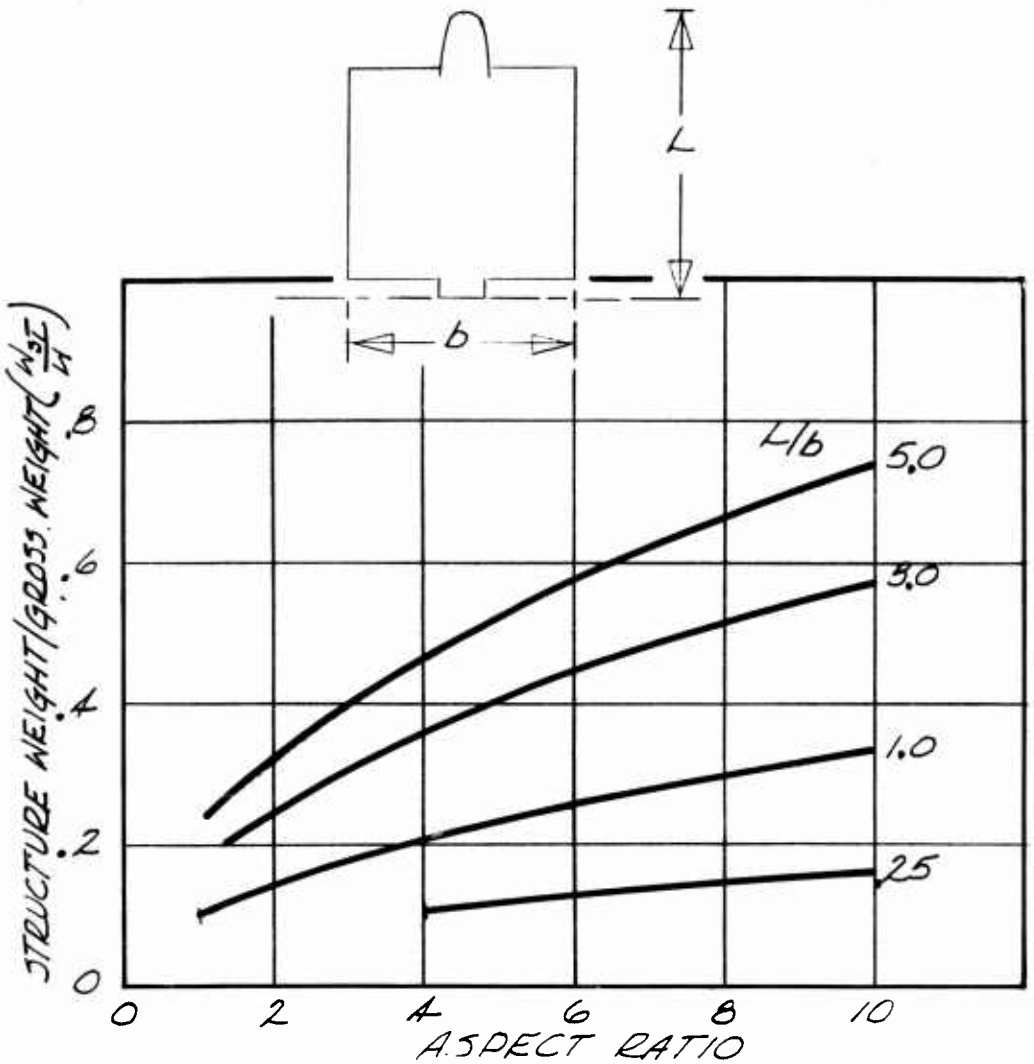

Figure 2. Structural Advantages of Low AR Wings

The base planform was selected to provide as large an area as possible within the periphery of the jets while still maintaining its center of pressure at the center of gravity. The size of the base then is dependent on the cg location. Therefore, the cg of the model was placed at the 35% chord point which was believed to be the most reasonable compromise between improved GETOL performance and excessive tail size.

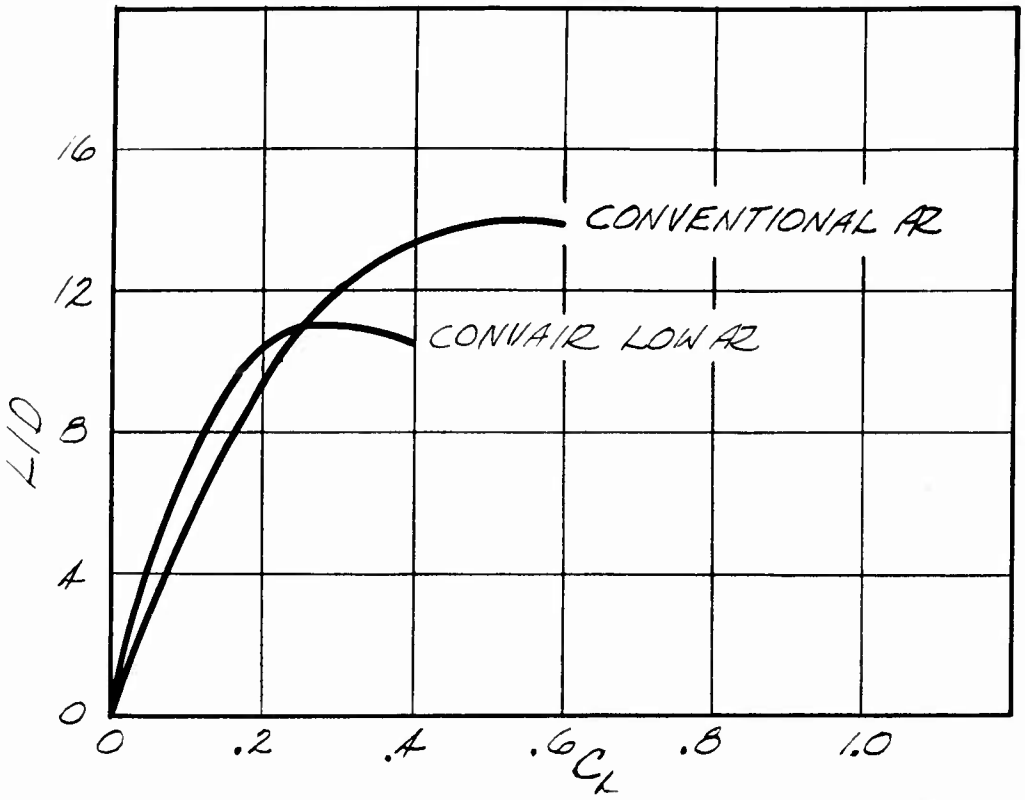

Figure 3. Performance Comparison of GETOL Research Low AR Configuration with Conventional Wing Configuration

The nozzle geometry for the model was selected primarily from the results of the hovering tests conducted concurrently with this program by Convair and discussed at length later in this report. However, consideration of the expected performance with forward speed was a factor prior to the final selection of the nozzles which were tested on the powered model.

Fan-area-to-wing-area ratio was selected as the result of earlier Convair-sponsored synthesis studies on a GETOL transport configuration. The location of the fan was selected so that the fan centerline was on the 35% chord point. The model wing span was limited so that model geometry located the lateral location of the fan. The fan itself was designated to be a model of the General Electric X353 system fan.

The cruise propulsion system was neglected on the powered model. It was decided at the start of the program that this system would be a separate

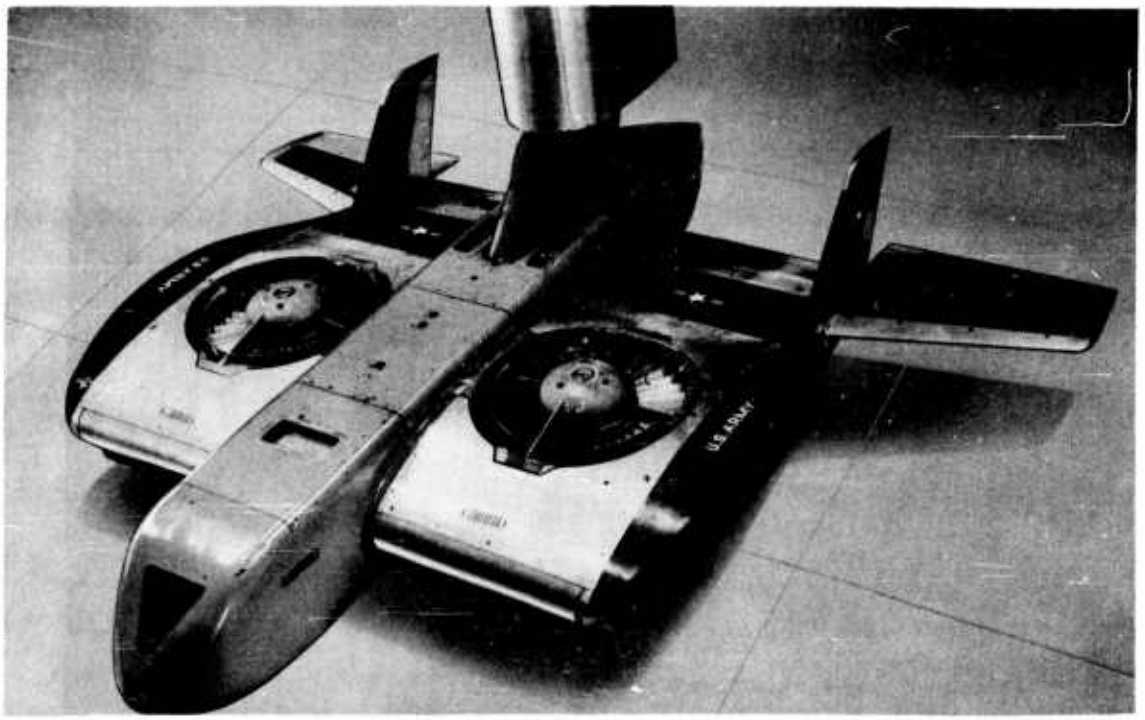

Figure 4a. GETOL Powered Model

consideration since its incorporation in the model would provide complications not commensurate with the results expected from this type of model.

MODEL DESIGN

Design Philosophy

A rather complex model was required to satisfy program objectives. Adequate separation of model forces and moments from fan forces and moments required that two balances be built into the model as well as pressure instrumentation. This philosophy of force and moment component determination prevailed throughout the design of the model. Total model forces and moments would not be enough to allow adequate understanding of the phenomena which were occuring over the model.

These systems were built into the model that was defined through the various configuration studies described earlier. A picture of the completed model is shown in Figures 4a and 4b; Figure 5 is a three-view drawing.

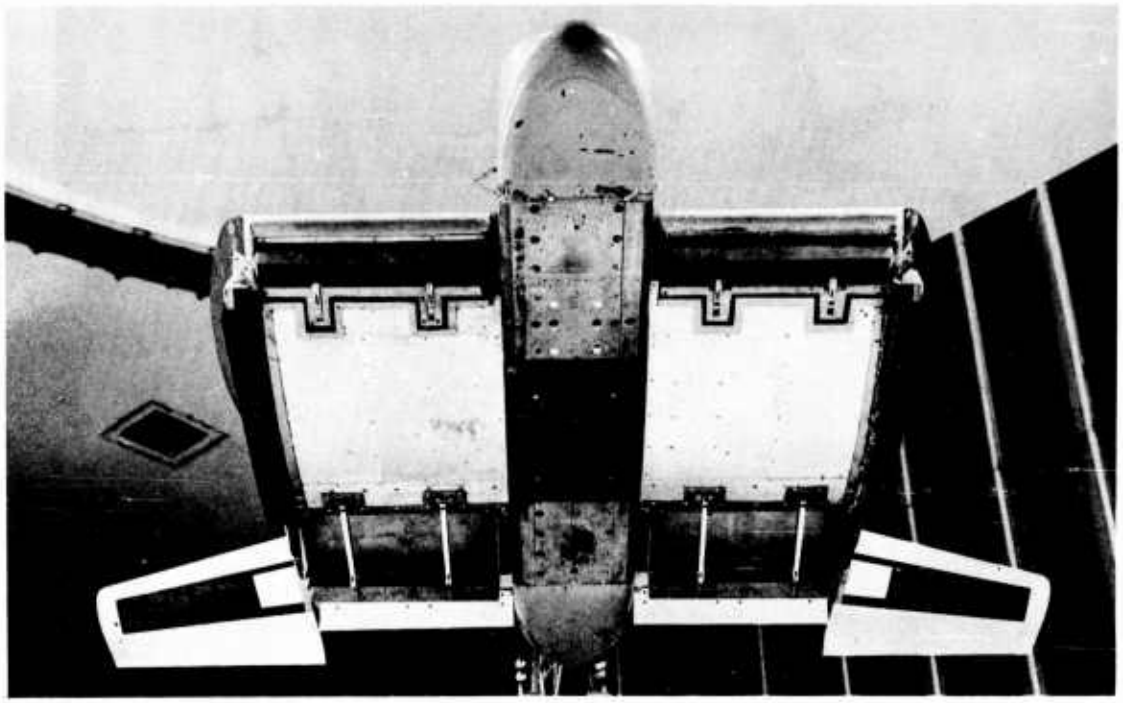

Figure 4b. GETOL Powered Model With Reaction Trimmer in Aft Position

Fans and Motors

Two Convair-owned, 32-hp, variable-frequency electric motors were selected to power the model. The motors were mounted in the model fuselage and drove the fans through two gear boxes. Since the motors were water-cooled, water lines were required to be brought into the model through the sting.

The fans selected were models of the General Electric X353 lift fans. The diameter of 10.4 inches was chosen so that the fans would be compatible with the motors. The hub-to-tip ratio on the fan was altered to 0.50 from the full-scale value of 0.40 due to hub gear box requirements. The gear boxes reduced the motor rpm by a factor of 0.685 into the fan. Gear-box oil lines were brought into the model through the sting.

Force Balances

The model was supplied with two 6-component balances, a fan balance, and a main balance. The fan balance measured forces on the thrusting system which included the fans, duct structure, fan motors, and gear boxes. The main balance

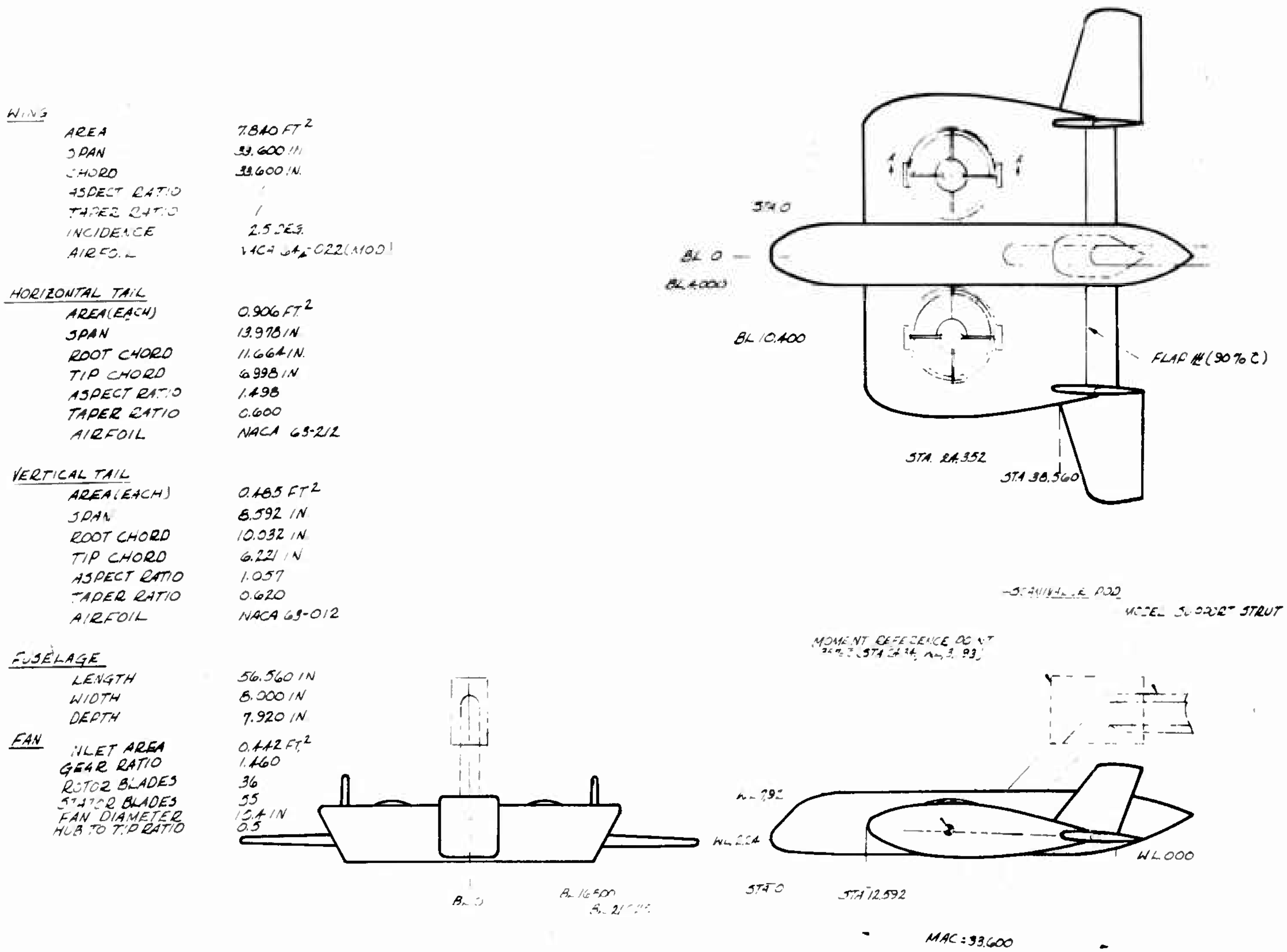

Figure 5. GETOL 0.080 Scale Model

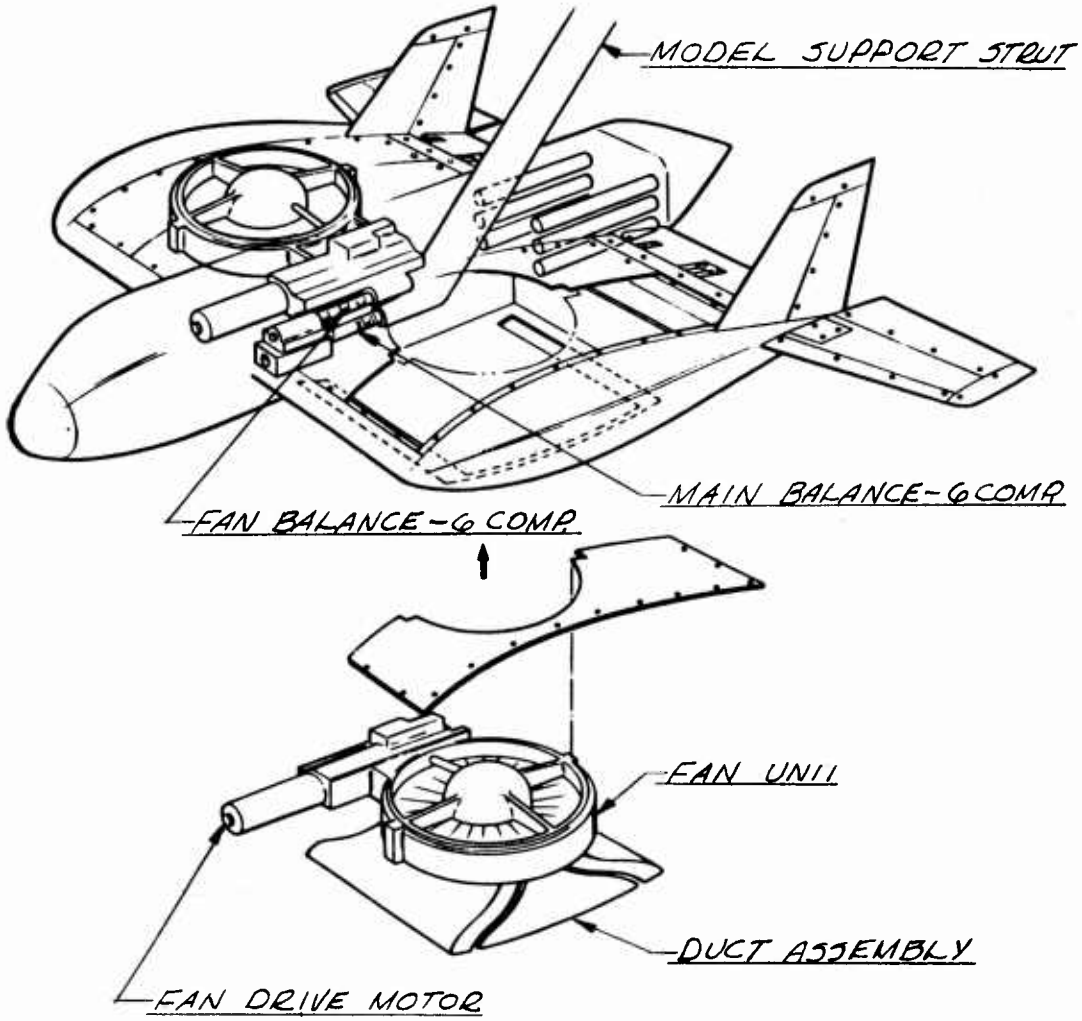

Figure 6. GETOL Model Cutaway

measured the total forces and moments on the model. A view of the system is shown in the cutaway drawing in Figure 6. Difficulties were encountered in the design because of the anticipated errors in the fan balance readings due to external pressures leaking in under the ducts and the interference effects between the model and the thrusting system caused by the motor power and water lines and the fan oil lines. Rubber seals were used to limit the leakage problem to acceptable tolerances; careful design and adequate model assembly time were combined to satisfactorily resolve the second difficulty.

Pressure Instrumentation

Pressure instrumentation was incorporated into the left half of the model. This included approximately 180 orifices located on the upper and lower surfaces of the wing and fuselage. Six pressure rakes also were added for the last two tests (CVAL 333A and 333B). These pressure rakes were located radially in a plane parallel to and under the left fan. Each rake consisted of four total and two static ports. They were intended to determine the flow distribution across the face of the fan and the weight flow through the fan. The pressures from the rakes and surface ports were read out through six scanivalves, located in the aft fuselage cone during test CVAL 333. This proved to be an inconvenient location because access for repair and maintenance required extensive dismantling of the model. Therefore, the scanivalves were moved to a streamlined pod on the model support sting after CVAL 333.

Nozzle Planforms

Based on results of the hovering tests (to be discussed later) and on anticipated performance with forward speed, two nozzle planforms were selected for testing in the wind tunnel. The first planform had 90% of the total area in the tip slot with the remaining 10% evenly distributed between the front and rear slots. This duct planform is referred to as the "A" duct configuration and was tested during CVAL 333. The second planform has 37.6% of the nozzle area in the tip slot and the remaining 62.4% evenly distributed between the forward and aft slot and is referred to as the "B" duct configuration. This duct configuration was tested during CVAL 333A and CVAL 333B. The "A" ducts were selected because of expected advantages with forward speed, while the "B" ducts were selected because of their high performance characteristics demonstrated statically.

Thrust Deflection Schemes

The model with the "B" duct configuration installed was provided with movable nozzle ends on the forward and aft slots (called eyelids) and deflector vanes for the tip slot. With the "A" duct configuration, only the tip vanes were used. These devices are shown in Figure 7. This permitted many different thrust deflection angle combinations to be tested. This was desirable in determining the maximum amount of acceleration or deceleration that could be derived from vectoring the thrust, while still maintaining an acceptable value for augmentation ratio. Also, it was useful to determine whether an improvement in augmentation ratio could be made by directing the flow under the wing; i.e., the forward eyelid facing aft and aft eyelid facing forward.

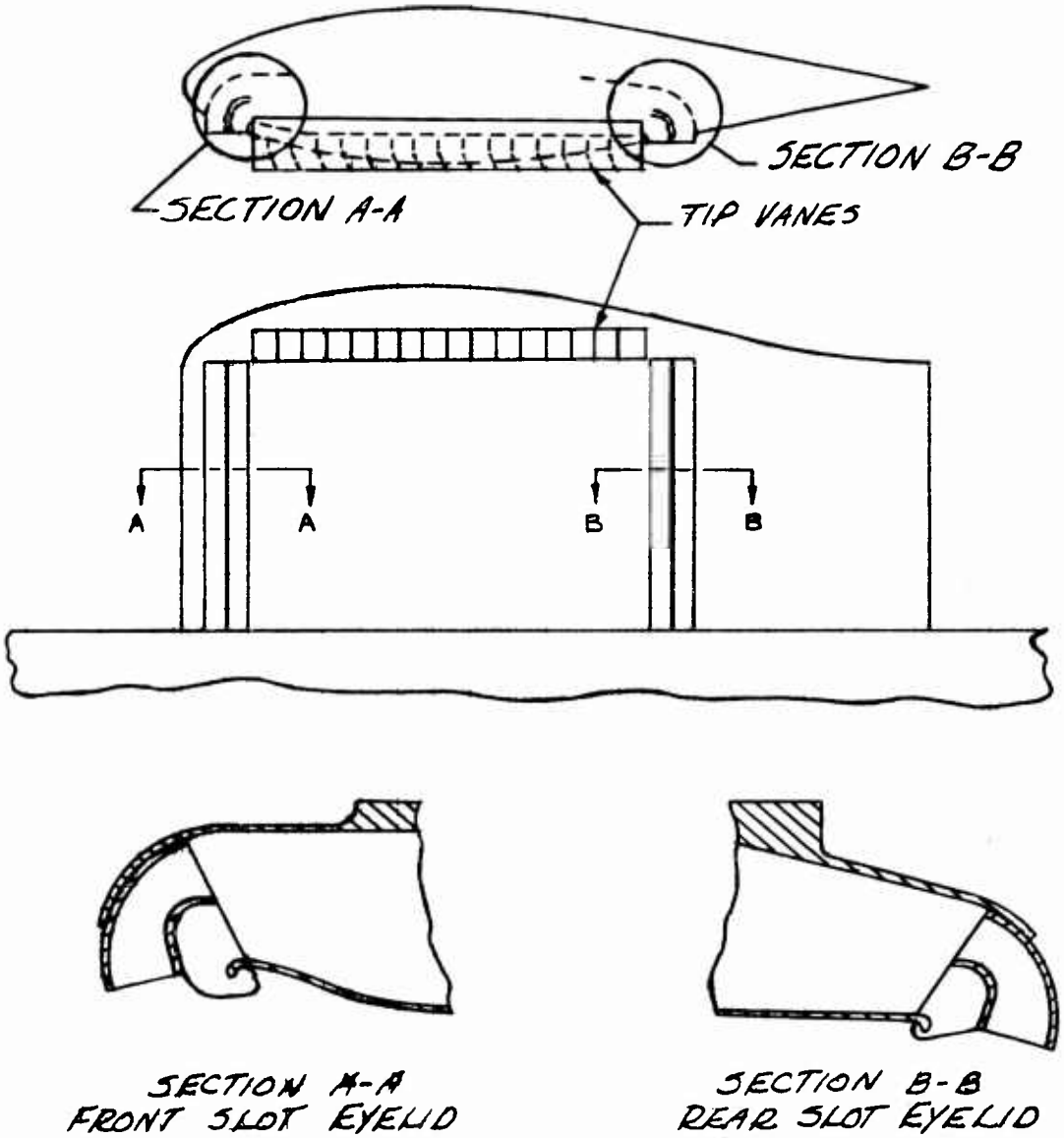

Figure 7. Thrust Deflection Schemes

Reaction Trimmer and Controls

During hover and during transition to cruise, this kind of airplane will operate at speeds too low for conventional aerodynamic controls to be effective. Therefore, the model was provided with various reaction-trimming and control devices

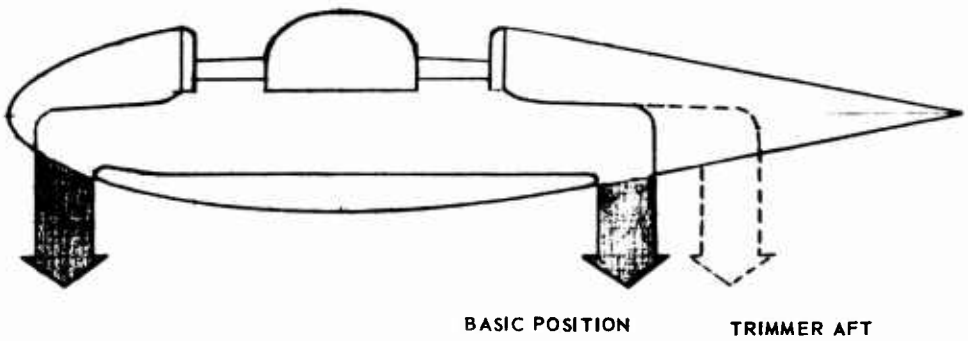

Figure 8. Reaction Trimmer — Schematic

to determine their effectiveness for trim and control in the hover and GETOL mode. One such device, called a reaction trimmer, is shown in Figure 8.

To accomplish trim of the nose-up pitching moments expected during transition flight, the eyelid of the aft duct was moved farther aft. The flow remained attached to the upper wall exiting at a point considerably aft of the basic position. This produced a nose-down pitching moment due to (1) the increased moment arm of the aft slot thrust, and (2) the increased base area aft of the cg position, thus moving the base center of pressure aft. Two different positions of the aft duct eyelid were tested in addition to the basic aft slot position. These positions were with the aft eyelid moved back 2.65 and 5.3 inches.

Reaction controls for pitch are shown in Figures 9 and 10. Figure 9 shows inlet guide stators, consisting of 28 radially mounted vanes located above the fan. The vanes covering the front half of the fan were deflected differentially from the vanes over the rear half of the fan. This directed the air into the fan blades at a different angle at the front half than at the rear half of the fan. This causes a differential mass flow between the front and rear slots, resulting in a pitching moment.

Figure 10 shows how wooden strips were used to partially plug either the front or rear slot. This was expected to cause a pitching moment by reducing the mass flow from the plugged slot. The aft slot plug was tested with the slot in both its basic and most aft positions.

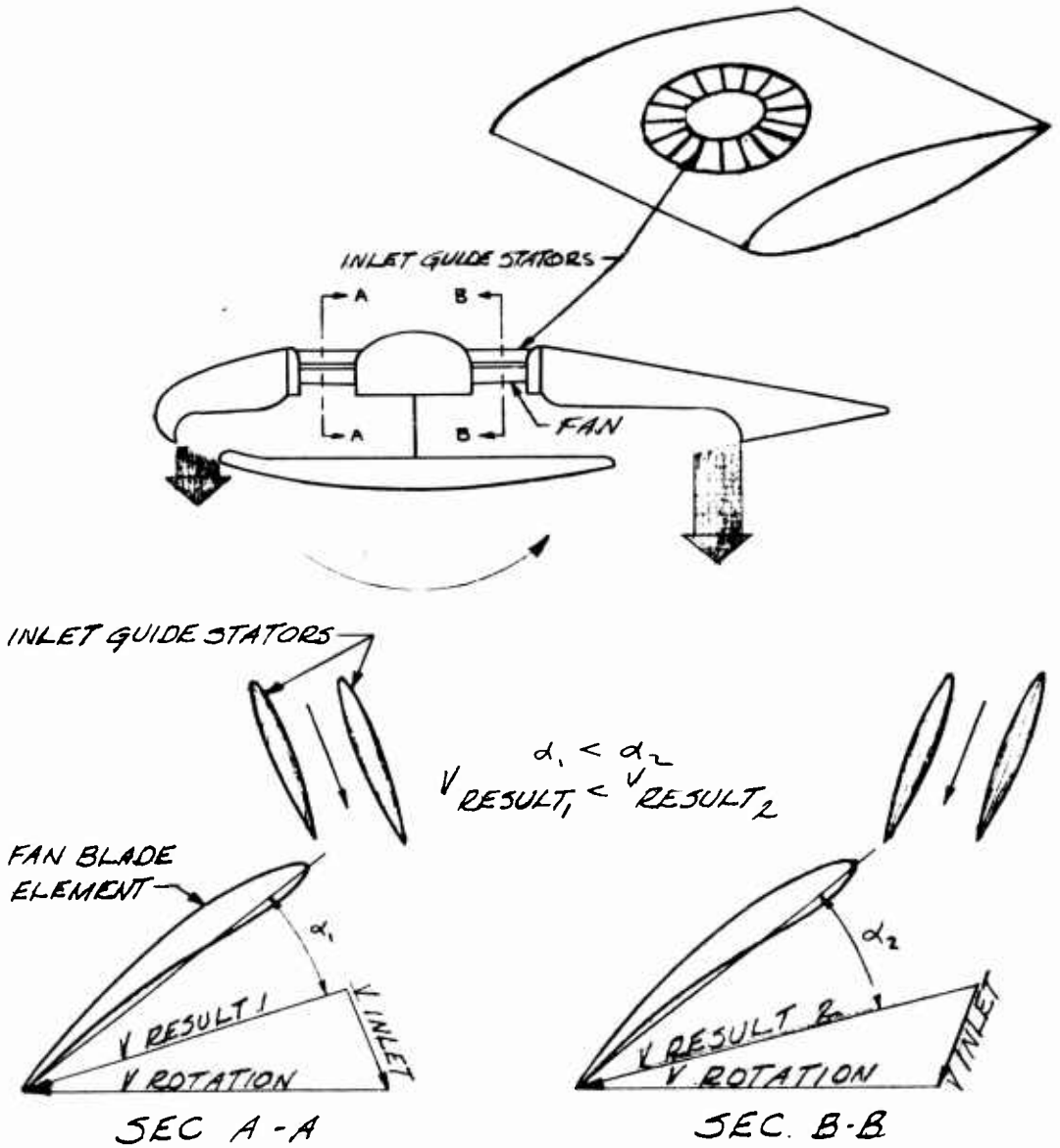

Figure 9. Pitch Control With Inlet Guide Stators

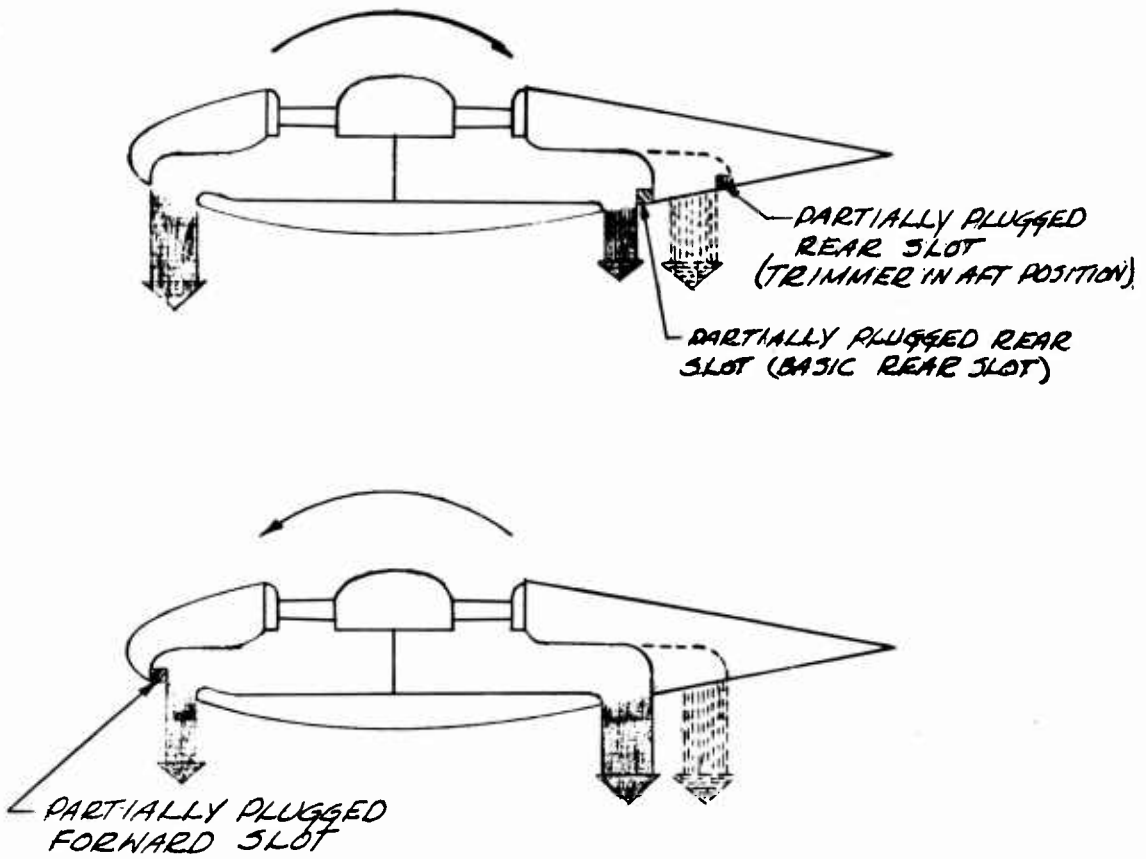

Figure 10. Pitch Control With Duct Plugs

Aerodynamic Controls

The only movable aerodynamic control surfaces on the model were the horizontal tails. These were infinitely adjustable between approximately +20° to -30° and were set by using a protractor. The horizontal surfaces were mounted so that they pivoted about 25% of their mean aerodynamic chord which was located at 90% of the wing chord.

A simple 10% $\bar{c}$ flap was included on the basic wing trailing edge; flap settings of 0°, 30° 45° and 60° were available.

PHASE I — NONCONTRACTUAL SUPPORT

It was recognized before starting the program that two supporting programs should be accomplished so that (1) wind tunnel testing could be focused on nozzle configurations that had been proven effective statically, and (2) the wind tunnel results could be as free of tunnel wall and boundary layer effects as possible. Two Convair-sponsored programs were conducted to achieve these objectives. The first was a hovering test program conducted over a period of approximately four months on a specially constructed static test facility. The second was a program to modify the existing Convair Low-Speed Wind Tunnel to provide a 16 by 20-foot test section complete with a special ground board equipped for boundary layer removal.

HOVERING TESTS

The primary objectives of the hovering tests were to determine a nozzle geometry that provided the most promise of satisfactory results for the powered model. In accomplishing this objective, the effects on augmentation and center of pressure of various model geometries were determined for the static case with respect to the following parameters:

1. Height above the ground.
2. Angle of attack.
3. Angle of roll.
4. Thrust deflection angle.

Facility

The testing was conducted at the facility shown in Figures 11a and 11b. As indicated in the drawing, air enters the facility through an air seal in the balance plane and is expanded through the diffuser until it reaches essentially plenum chamber conditions just before being exhausted through the model nozzle. The model is attached to the diffuser that is mounted on the balance. This balance is a 3-component strain-gage type, measuring forces in two directions and one moment. The forces and the moment measured are dependent on model orientation; however, during testing, the model was generally aligned so that normal force, drag, and pitching moment data could be recorded from the balance. The ground board is designed to permit rapid adjustment of ground height and angle

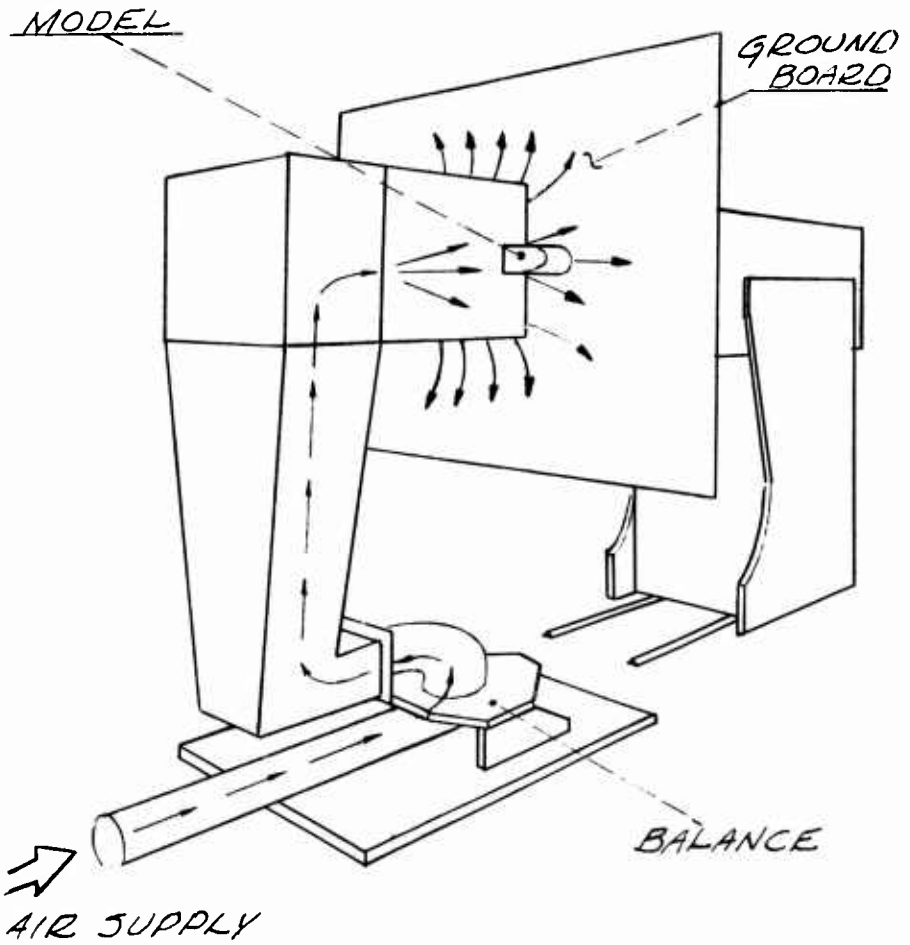

Figure 11a. Static Facility

relative to the model and is equipped with a Plexiglas center to facilitate flow visualization.

Model

The models consisted of square mahogany and aluminum blocks mounted in one end of the diffuser with the lower surface facing the ground board. The models contained various rectangular exit configurations differing only in slot width. Both flat and curved lower surfaces were tested.

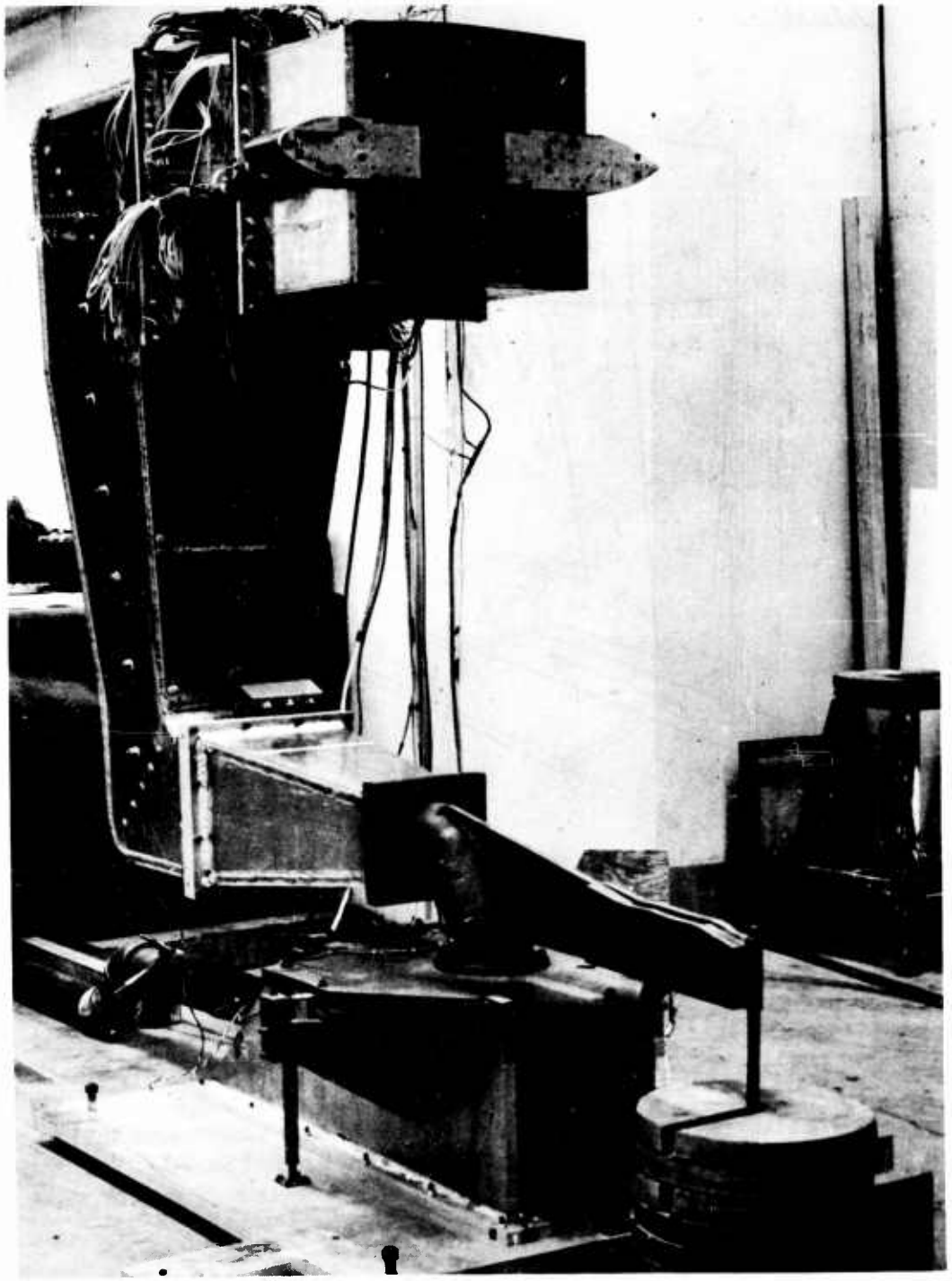

Figure 11b. Photograph of Static Test Facility With Model Installed

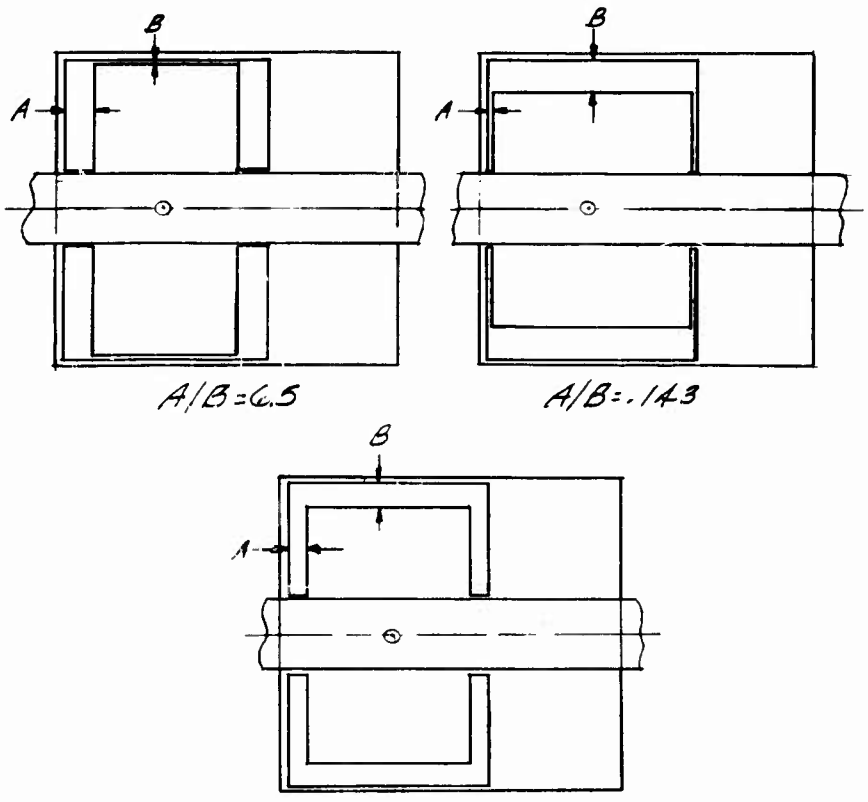

Figure 12. Model Nozzle Geometry

Each model simulated an aspect-ratio one wing with a fuselage extending from the leading and trailing edges. The model chord and span were both equal to 13.75 inches. The planform area of the peripheral nozzle was 27.5 square inches, and the enclosed base area was approximately 89 square inches for all model configurations. Three of the basic nozzle configurations are shown in Figure 12.

Various external components were tested with most exit configurations including several fuselage depths, flaps, and turning vanes. Different kinds of flaps were mounted on the wing lower surface (generally on the base) which included straight flaps extending downward at an angle of 90% to the lower surface, curved flaps, cusped flaps, and a screen flap. Fuselage depth was varied by the addition of blocks to the basic configuration. Turning vanes were mounted in the exit slots of several configurations.

All model blocks contained pressure orifices on the lower surface of the wing and fuselage. Approximately 120 orifices were located over one-half the model. The pressures were recorded through use of three scanivalves mounted on the diffuser.

Test Conditions

Testing was conducted generally at a weight flow (w_a) of 2.1 pounds per second. The air was supplied from the Convair air supply and was metered by a 3-inch orifice in a 4-inch supply line. It was controlled at the Convair Low-Speed Wind Tunnel air supply system control panel. This system provided weight flow accuracy of ±0.02 pound per second.

Total and static pressure probes were included in the diffuser immediately ahead of the model to provide a method of checking the weight flow as well as supplying total pressure data which would allow calculation of thrust at the nozzle. Flow uniformity in the diffuser was also evaluated by use of these pressure probes. Velocity distribution across the nozzles was uniform within ±5% around the nozzle periphery, as evaluated by a pressure survey.

Data Reduction

The force data from the hovering tests was analyzed and reduced to values of augmentation and center of pressure. The augmentation ratio was computed as follows:

$$\text{Augmentation ratio} = \frac{L}{T} = \frac{L}{\frac{w_a}{g} V_j + A (p_e - p_o)}$$

where

L = lift force measured by the balance (pounds)

T = nozzle thrust (pounds)

V_j = jet velocity at the nozzle exit (fps)

A = nozzle area (square feet)

p_e = average static pressure at nozzle exit (psf)

p_o = ambient pressure (psf)

The average static pressure at the exit (p_e) is determined from the upstream total pressure (p_{t_1}) and the weight flow, assuming a negligible total pressure loss from the diffuser total pressure probes to the nozzle exits.

$$p_{t_1} = p_{t_e} = \frac{1}{2} \rho V_j^2 + p_e$$

but

$$V_j = \frac{w_a}{\rho g A}$$

$$p_e = p_{t_1} - \frac{1}{2\rho} \left(\frac{w_a}{gA} \right)^2$$

where

$g = 32.2 \text{ fps}^2$

ρ = density (slug-cubic foot)

The center of pressure location was computed by:

$$\triangle CP \text{ (\%chord)} = \frac{\text{pitching moment (100)}}{\text{lift (chord length)}}$$

Results

The most significant results from the testing are presented in this report. Force results will be analyzed as much as possible with respect to the pressure data taken concurrently with the forces.

The behavior of augmentation with variation in height is indicated in Figure 13 for each of three slot width configurations. Of particular interest in this illustration is the augmentation deterioration in the presence of the ground when the tip slots are allowed to vary in width from the front and rear slots while maintaining a constant nozzle area. An examination of the pressure distributions in Figures 14 and 15 provide a clearer understanding of the phenomena occurring on the base when these nozzle width relationships are varied. For the constant

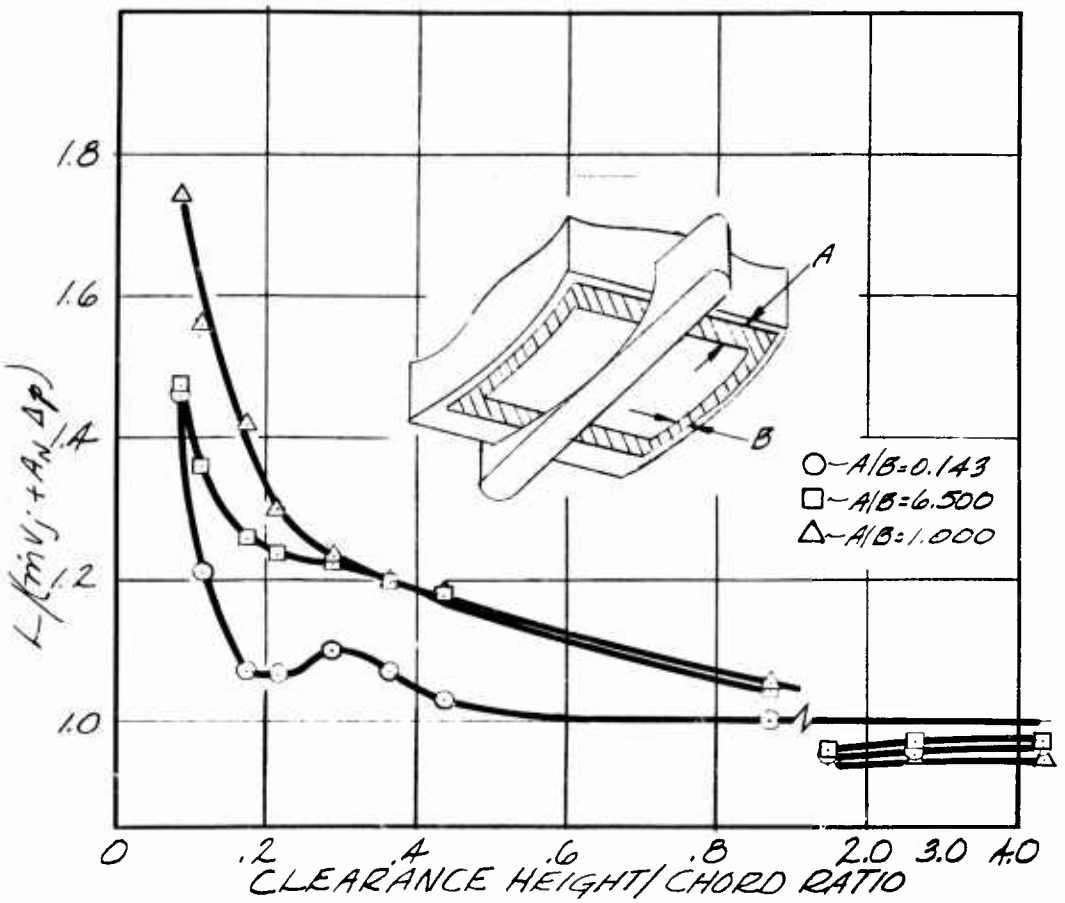

Figure 13. Hovering Test — Thrust Augmentation With Various Nozzle Width Ratios (α = 0)

slot width configuration (A/B = 1.0), the pressures on the base appear relatively even. However, large areas of negative pressure exist in the area of the oversized slot for the other two slot configurations. These pressures indicate that vortices are standing inboard and parallel to the oversized slot.

Various attempts were made either to reduce the effects of these vortices or to eliminate them completely. Among the devices tested were spoilers, inboard flaps to reduce the jet mixing length, and devices to pump a portion of the jet into the base opposing the rotation of the vortex. Although some of these methods were partially successful, at no time did the improvement in base pressure offset the physical decrease in clearance height caused by the attachment of the corrective

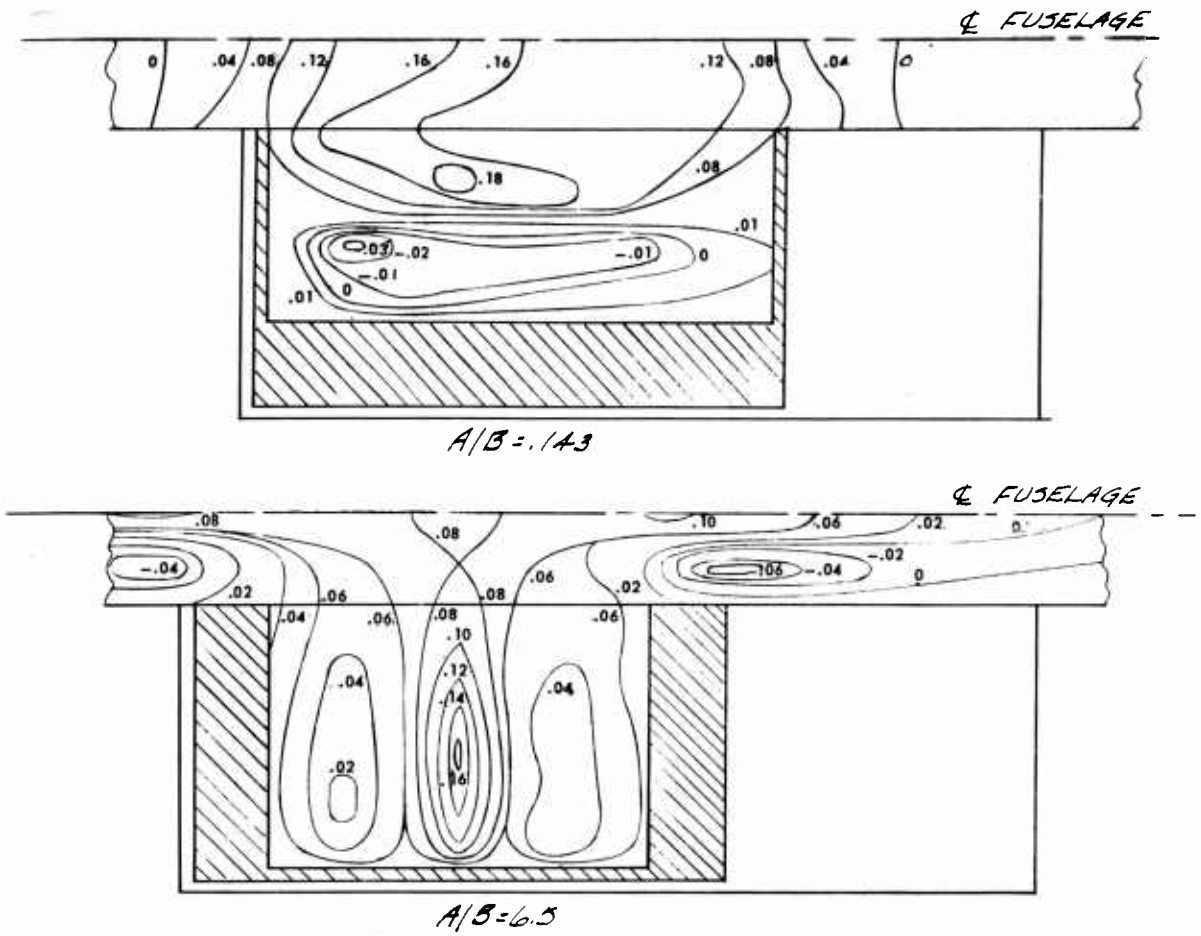

Figure 14. Hovering Test — Effect of Nozzle Width on Lower Surface Pressure Distribution (α = 0°, h/c = 0.087, $q_{jet} \cong$ 23.3 PSF, Isobars ~ PSI)

device to the lower surfaces for nozzle geometries with tip slot widths unequal to front and rear slot widths.

Other items of interest in Figure 13 are the height instability apparent at low heights for the wide tip slot configuration and the lack of "tulip" effect out of the influence of the ground. The height instability appears to be caused by the nature of the vortex development with increases in height. The vortex sits inboard of the wide tip slot and grows in size as the model leaves the vicinity of the ground. However, this growth is restricted due to the confines of the base and, as the growth is restricted, the vortex is forced away from the surface. This results

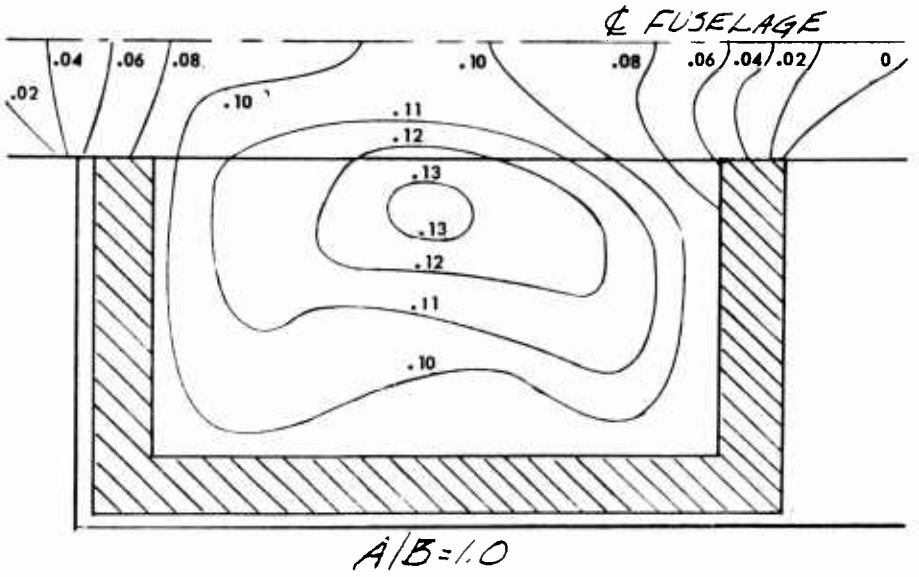

Figure 15. Hovering Test — Effect of Nozzle Width on Lower Surface Pressure Distribution (α = 0°, h/c = 0.087, $q_{jet} \cong$ 23.3 PSF, Isobars ~ PSI)

in increased pressure over the area of the base where the vortex previously was acting. Such action is reflected in the augmentation curve as a height instability. The same phenomenon apparently occurs on the wide front and rear slot configuration, but the vortex growth is curtailed closer to the ground due to the smaller chordwise dimension of the base. Therefore, the resulting forces are not reflected so severely in the augmentation curve of this configuration.

The lack of large negative pressures on the base out of ground effect ("tulip") cannot be explained completely. It is reasoned that the square corners on the base planform prevented the individual jets from coalescing adequately out of ground effect to produce the extreme negative pressures generally associated with the "tulip" effect.

The effect of angle of attack on augmentation is shown in Figure 16. For each of the height-to-chord ratios shown, the augmentation deteriorates with increasing positive angle of attack; as the model is rotated to negative angles of attack, the augmentation first improves and then deteriorates at about the same rate as at positive angles of attack. The pressure distributions in Figure 17 offer an explanation. At 10° angle of attack, a large negative pressure area is evident on

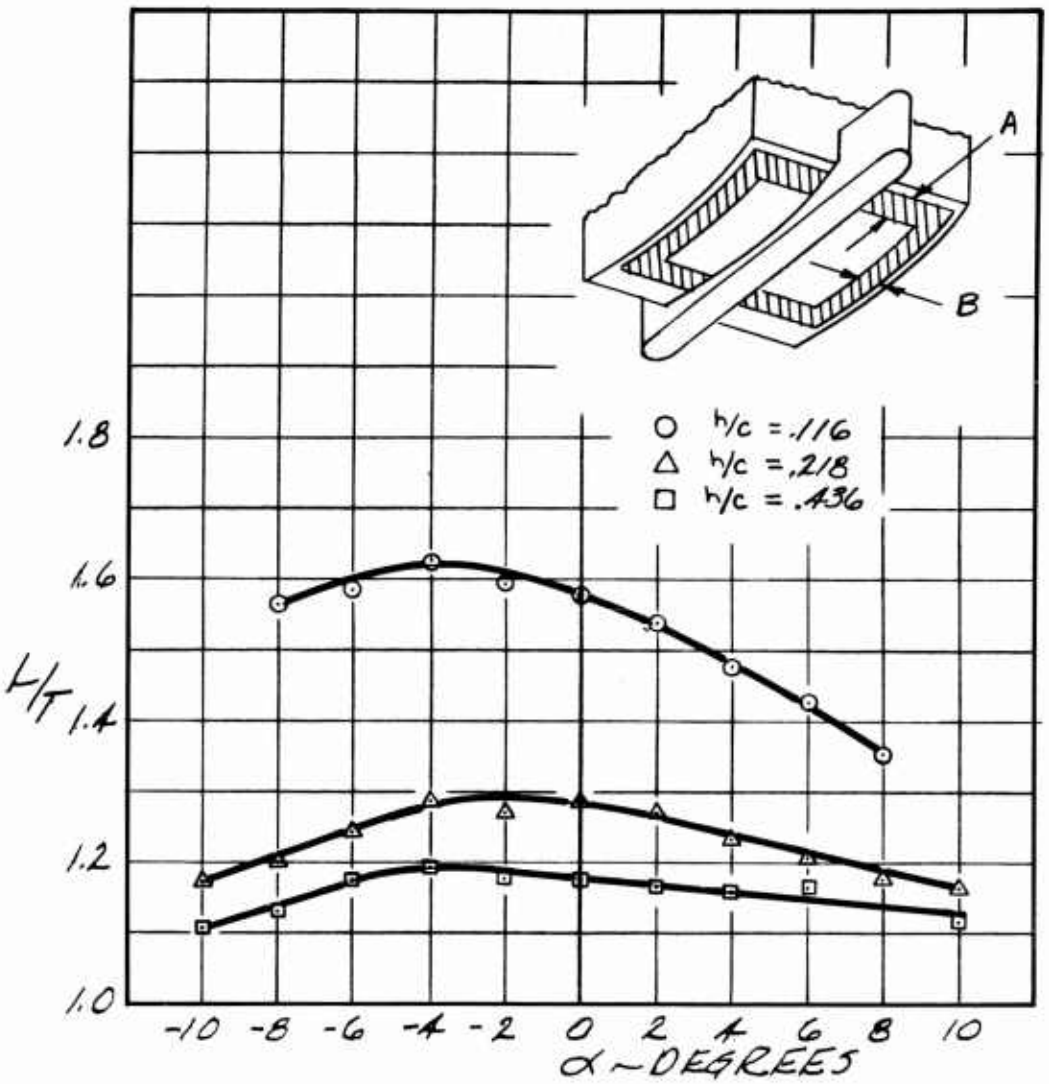

Figure 16. Hovering Test — Augmentation Ratio Variation With Angle of Attack (A/B = 1.0)

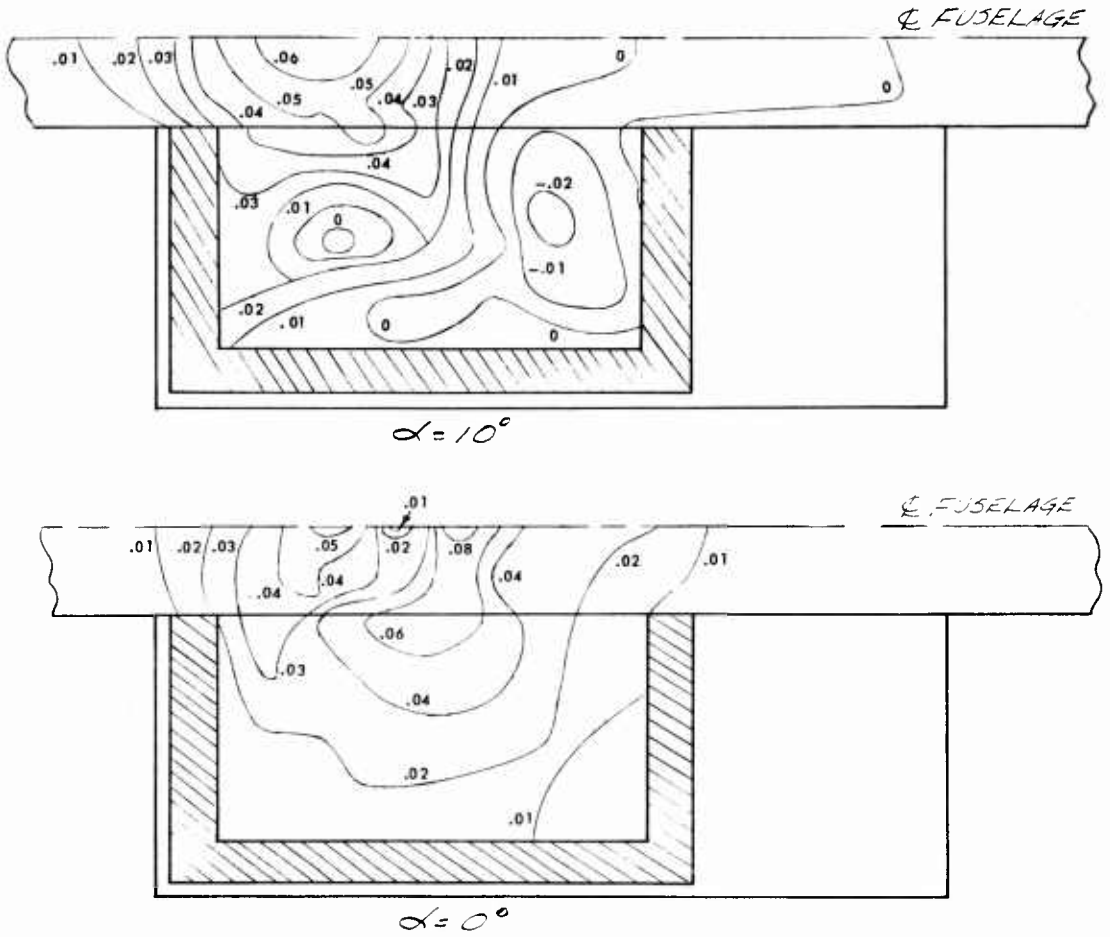

Figure 17. Hovering Test — Effect of Angle of Attack on Lower Surface Pressure Distribution (h/c = 0.219, q_{jet} = 23.3 PSF, Isobars ~ PSI, A/B = 1.0)

the trailing edge of the base where the pressure was slightly positive at zero angle of attack. The positive base pressures appear to shift forward, acting on a lesser area than at zero augmentation. Further, the negative pressures on the trailing edge aft of the rear nozzle increase negatively as the trailing edge gets closer to the ground with positive angle of attack. This results in a lift decrement for positive angles of attack and, since the negative pressures are reduced with negative angle of attack, a lift increment at negative angles of attack. This is the reason for the augmentation peak at a negative angle of attack.

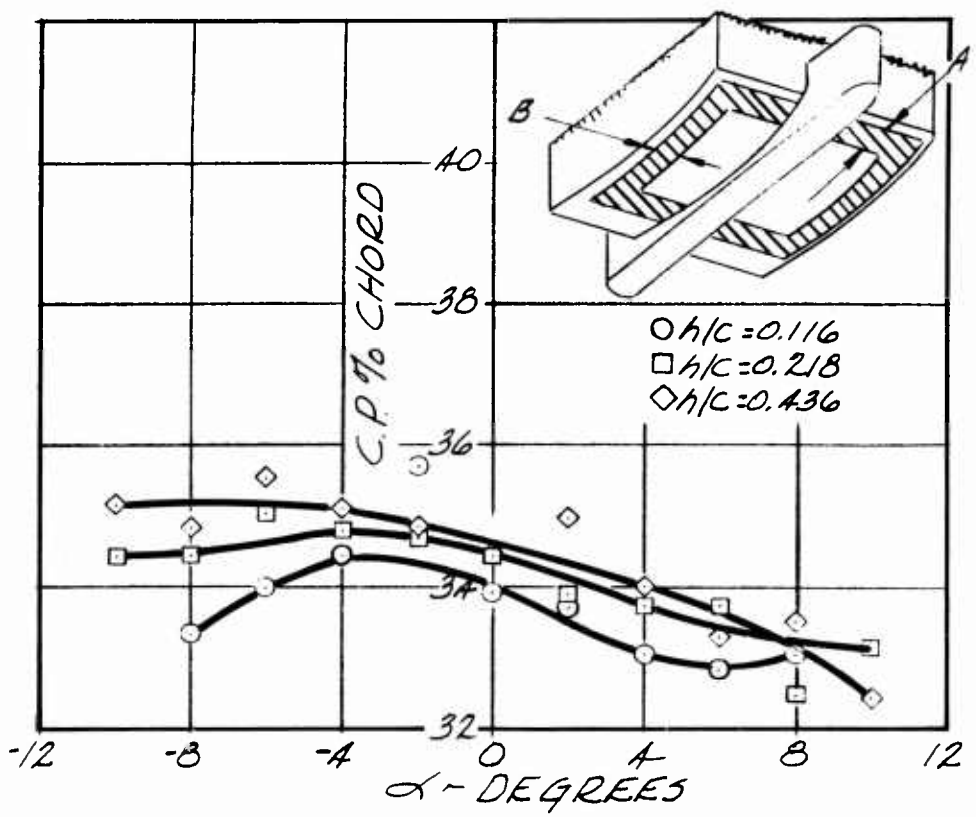

Figure 18. Hovering Test — Longitudinal Attitude Stability (A/B = 1.0)

Results of the longitudinal attitude stability investigation are shown in Figure 18. At all positive angles of attack and negative angles of attack from zero to -4°, the configuration appears to be slightly unstable. At angles of -4 to -10°, the configuration varies from being stable at the low height to neutrally stable at the highest ground height. In addition, the negative pressures on the wing trailing edge contribute to the unstable condition since they become more negative as the trailing edge gets closer to the ground.

The effects of thrust deflection vanes are shown in Figures 19 and 20. Severe lift losses are encountered when the flow is deflected aft for acceleration thrust. These losses are particularly severe considering that the effective deflection angle is approximately one-half the design deflection angle out of ground effect, and only one-quarter the design deflection angle at low heights in ground effect. For the configuration shown in the illustrations, deflection causes the pressures

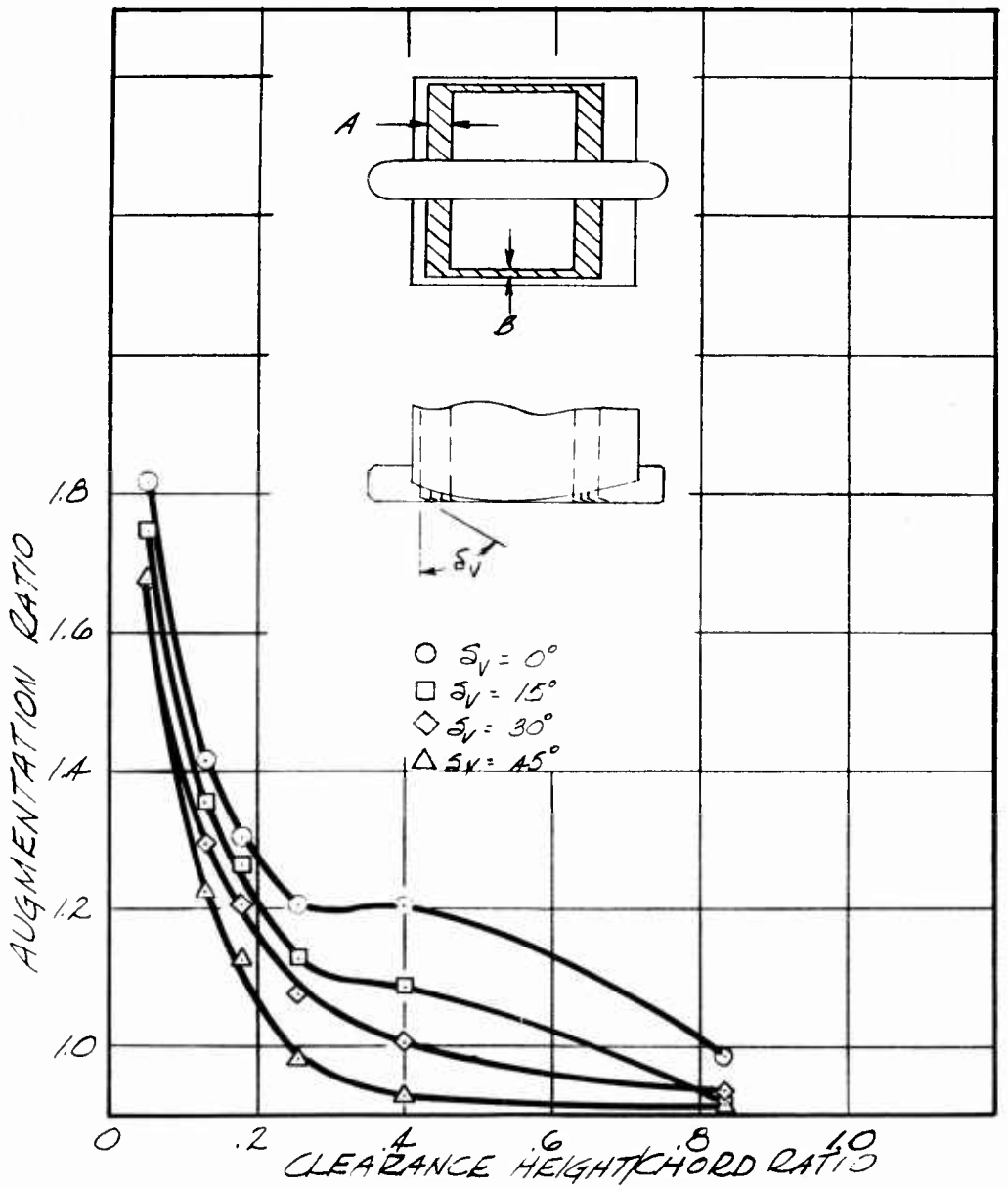

Figure 19. Hovering Test — Augmentation Versus Height/Chord Ratio for Various Values of Thrust Deflection Vane Angle δ_V ($\alpha = 0°$, $A/B = 2.65$)

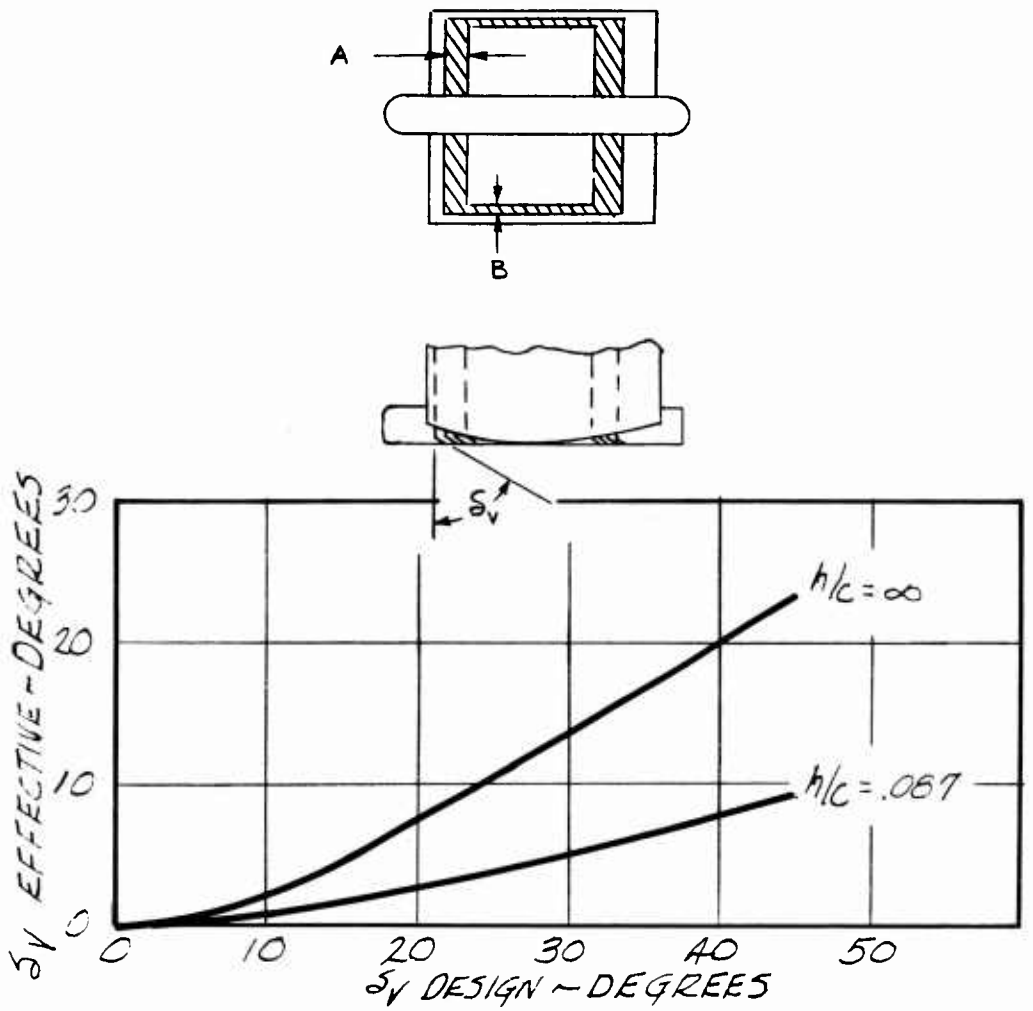

Figure 20. Hovering Test — Thrust Deflection Vane Effectiveness (α = 0°, A/B = 2.65)

to be reduced significantly on the base immediately aft of the front slot, depending on the deflection angle. Thus, the lift reduces more than would be expected by using the cosine of the thrust deflection angle.

Center-of-pressure travel with height is illustrated in Figure 21. The center of pressure tends to remain at the center of the base except at very low heights, when it moves forward about 2%. This movement is caused by negative pressures induced on the planform trailing edge when in ground effect.

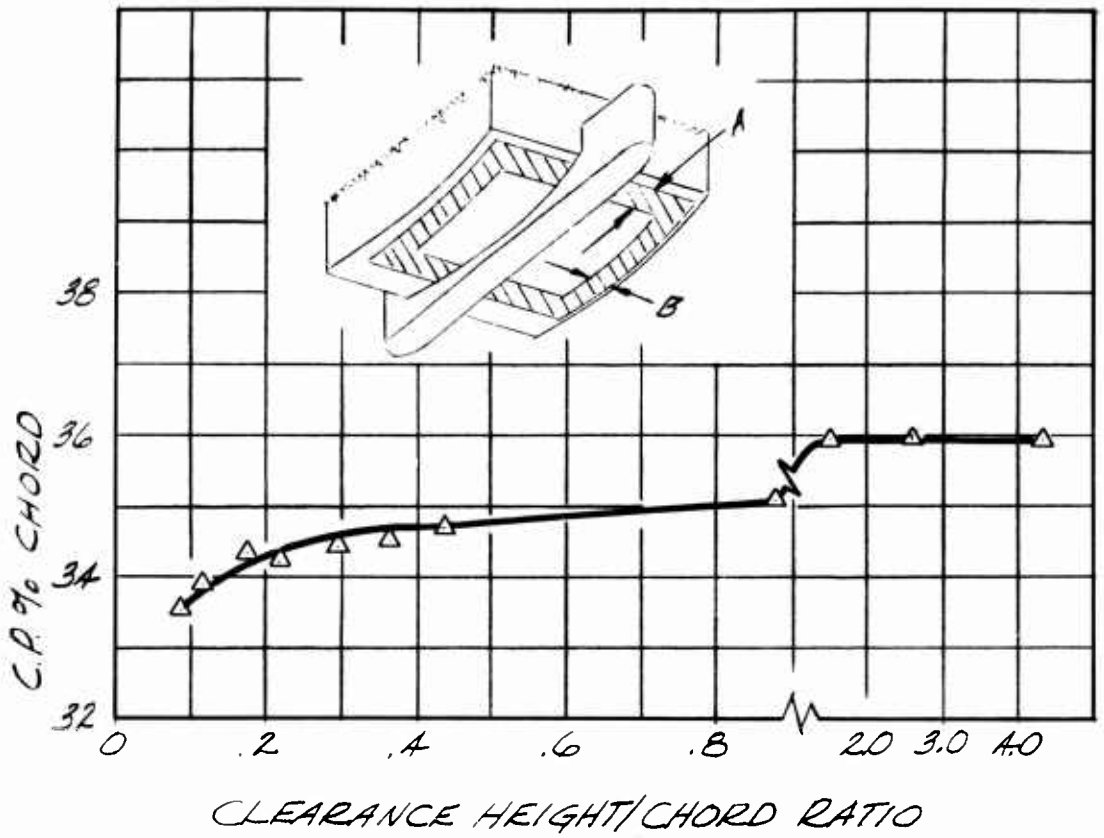

Figure 21. Hovering Test — Center of Pressure Variation With Height (α = 0°, A/B = 1.0)

The configuration appears to be from neutrally stable to slightly unstable in roll, depending on the height (see Figure 22). The low height tends to be close to neutrally stable. The intermediate height is unstable at both high positive and negative roll angles, becoming unstable at the angles near zero. An indication of the pressure distribution with roll angle is shown in Figure 23.

Two different longitudinal control schemes were investigated during the hovering tests. One provided for plugs of various widths to be put into either the front or the rear nozzle, restricting its flow, and thus providing a pitching moment in the desired direction. Figure 24 shows that this scheme worked with some success both in and out of ground effect. However, augmentation was affected adversely as expected.

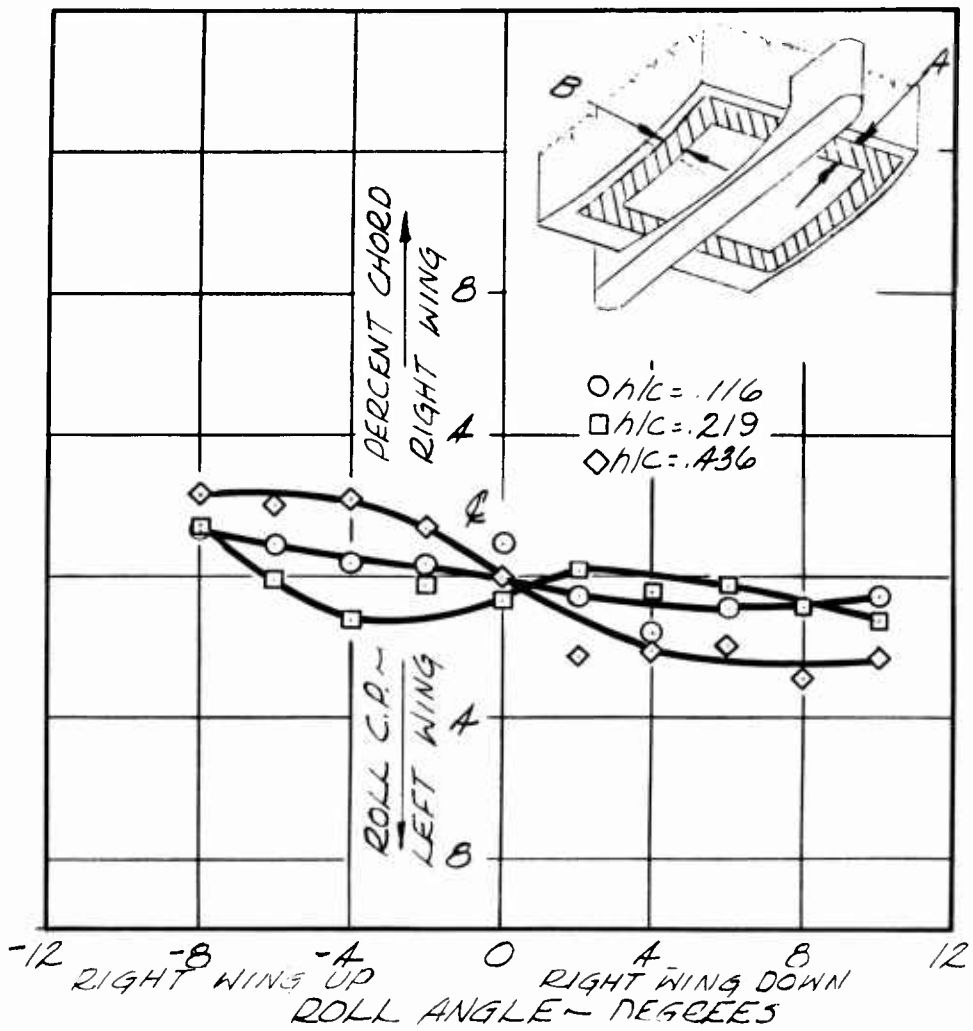

Figure 22. Hovering Test — Lateral Center of Pressure Versus Roll Angle (α = 0°, A/B = 1.0)

The other scheme involved moving the base itself. A constant nozzle area was maintained and, while either the front or the rear slot width was enlarged, the opposing slot width was reduced, thus producing a pitching moment. The results in Figure 25 indicate that this scheme is fairly satisfactory for out of ground effect operation, but the performance in ground effect is not satisfactory. An examination of the pressure distributions in ground effect (Figure 26) indicates the reason for this discrepancy. Apparently, when the one slot width enlarges

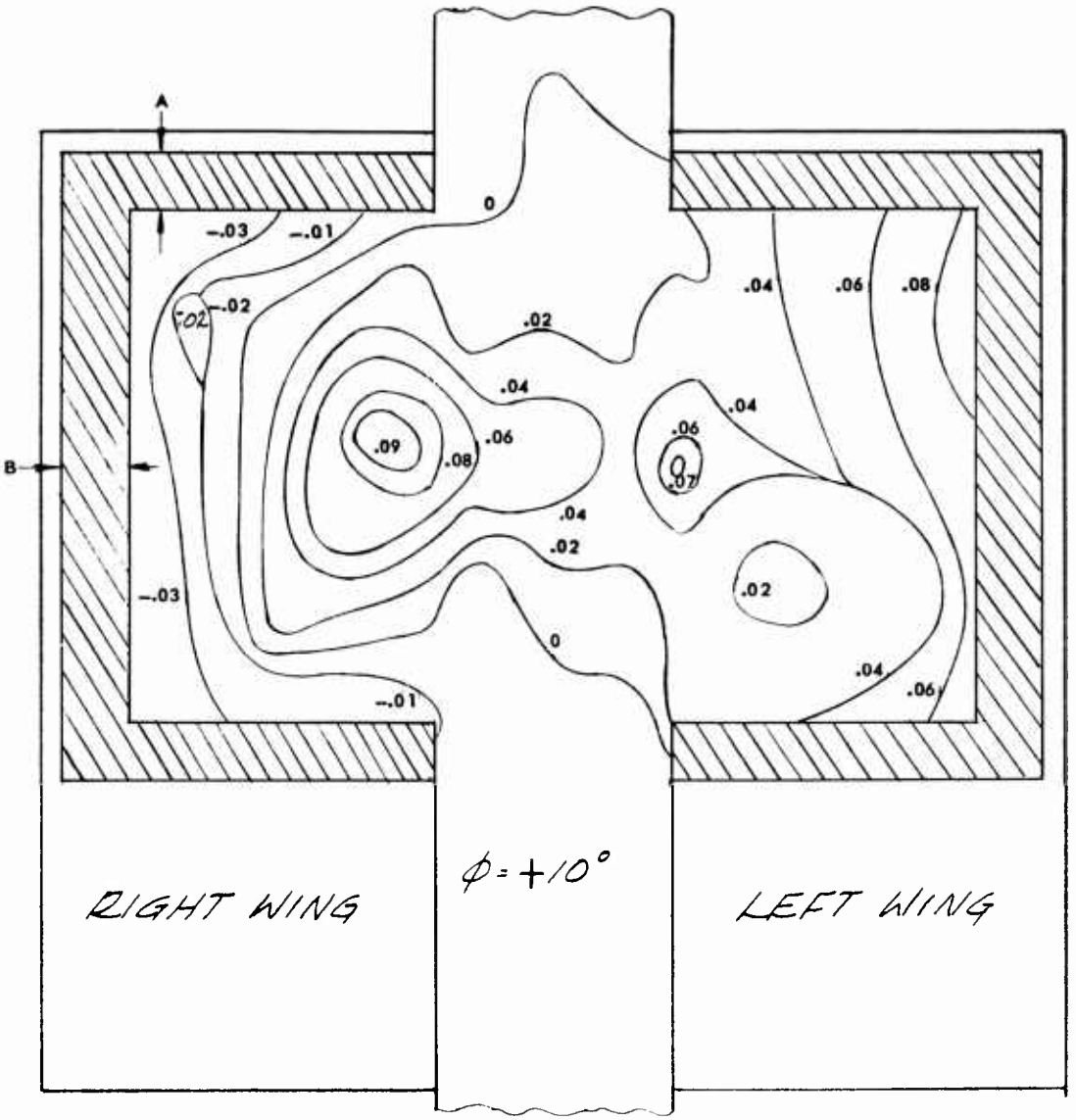

Figure 23. Hovering Test — Effect of Angle of Roll on Lower Surface Pressure Distribution ($\alpha = 0°$, $h/c = 0.116$, $q_{jet} \cong 23.3$ PSF, $A/B = 1.0$, Isobars ~ PSI, Right Wing Down)

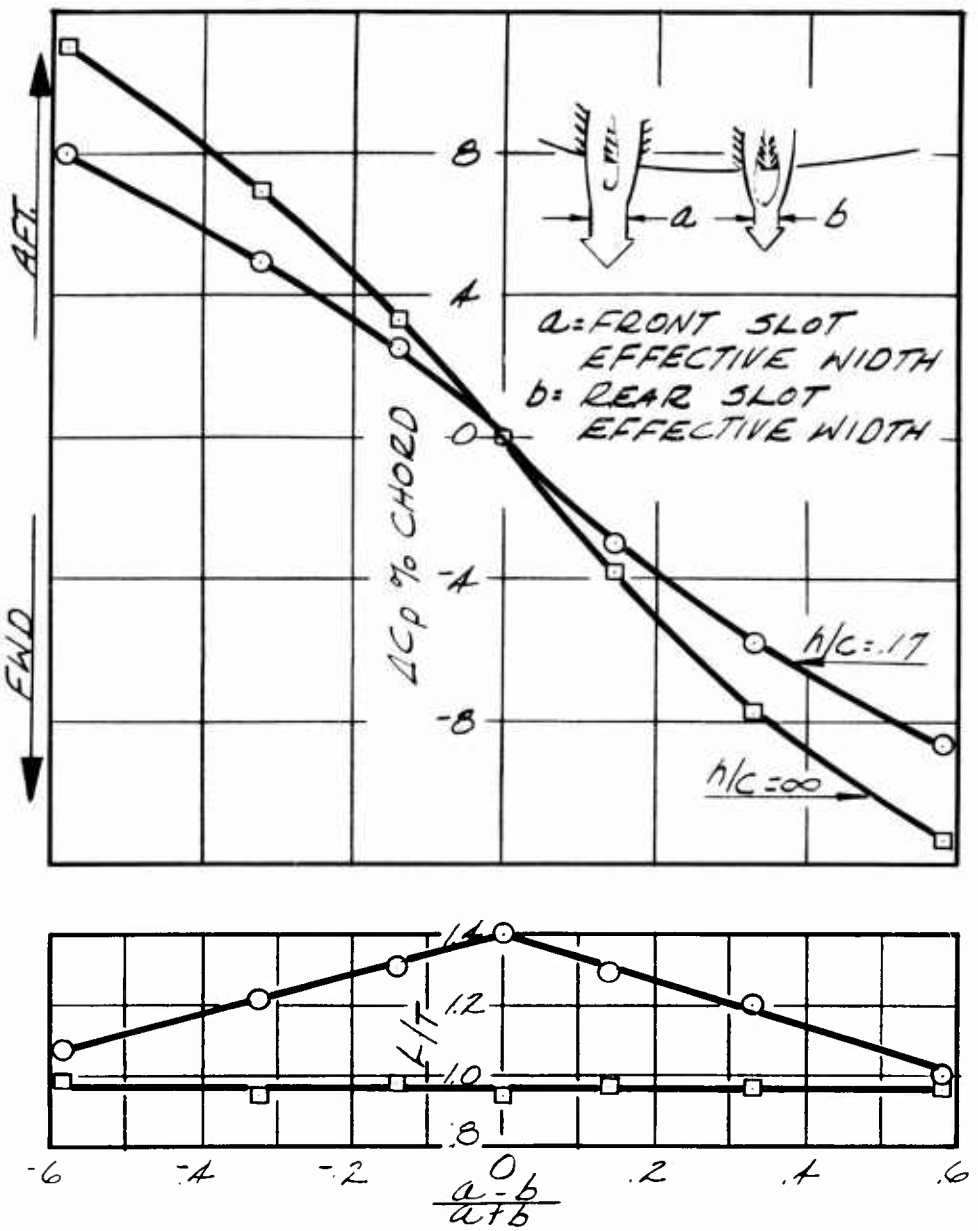

Figure 24. Hovering Test — Control Effectiveness of Control Plug Configuration (α = 0°, A/B = 1.0)

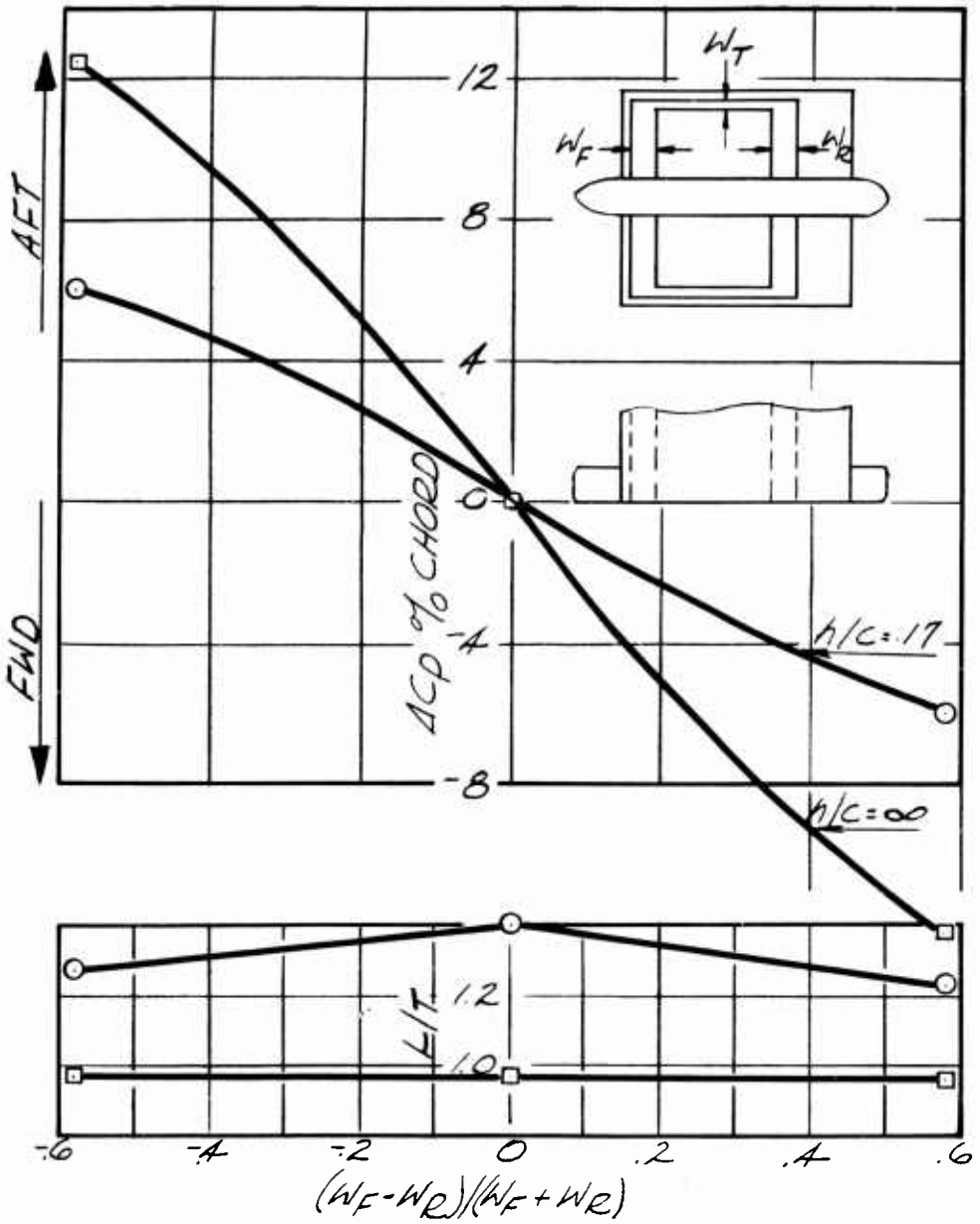

Figure 25. Hovering Test — Control Effectiveness of Base Translation Configuration ($\alpha = 0°$, $W_T/(W_F + W_R) = 0.19$)

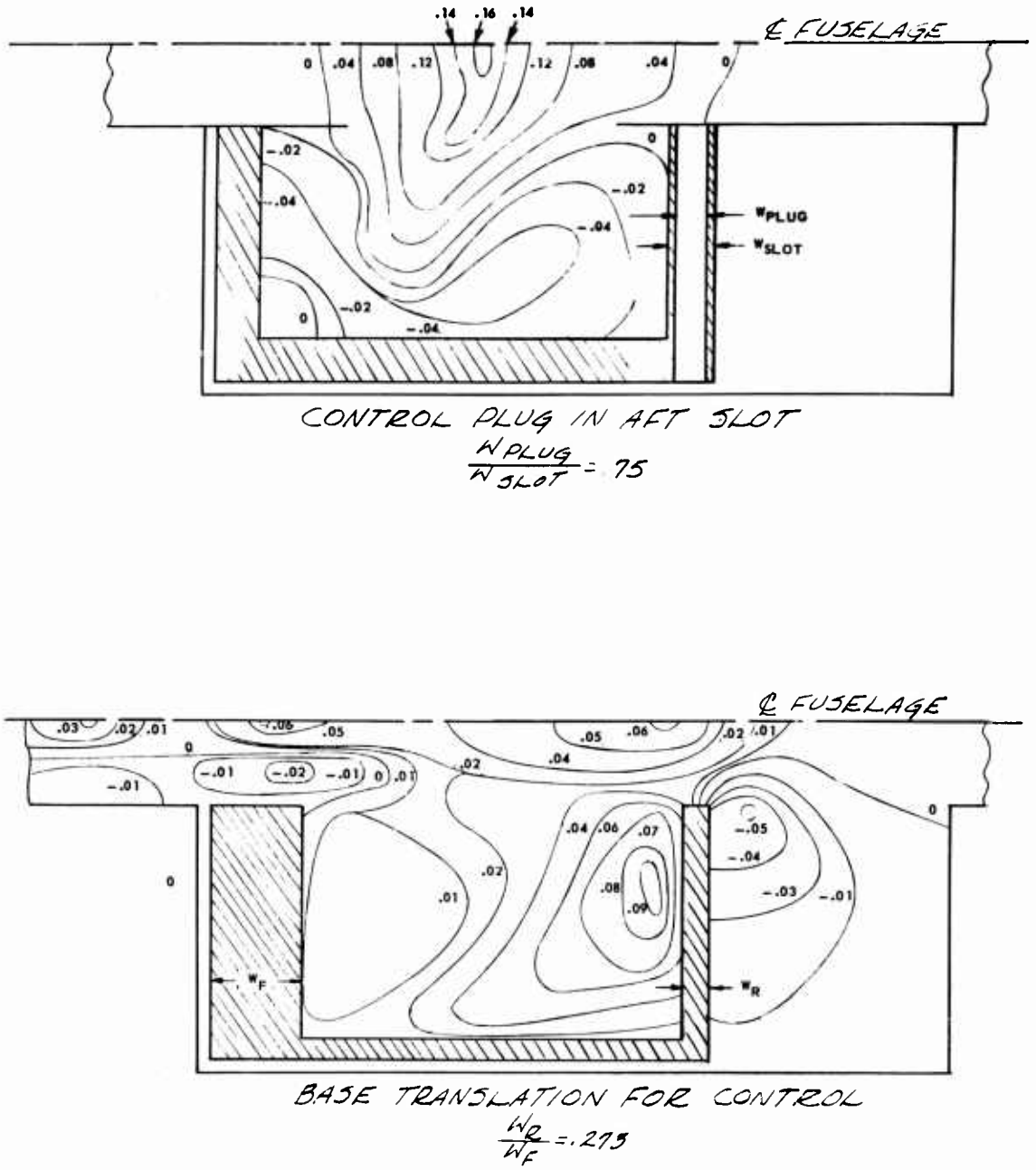

Figure 26. Hovering Test — Control Effects on Lower Surface Pressure Distribution (α = 0°, h/c = 0.172, $q_{jet} \cong$ 23.3 PSF, Isobars ~ PSI)

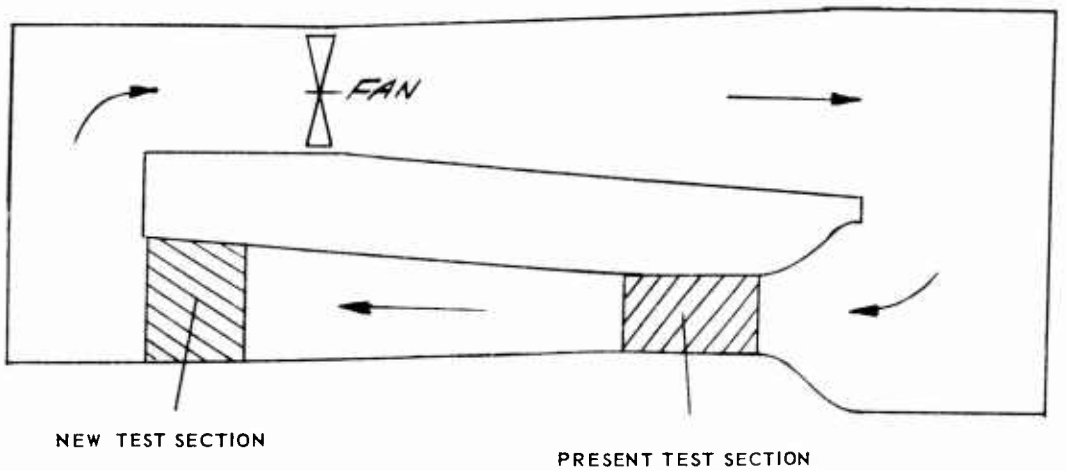

Figure 27. Convair Low-Speed Wind Tunnel

with respect to the base chord and the other slot, a large vortex is formed inboard of the large slot causing negative pressures which oppose the direction of the desired pitching moment. In the plug scheme, this effect also is present, but the negative pressure area does not cover such a large area of the base.

In general, the results of the hovering tests are considered encouraging. The augmentation ratios are in line with what was expected even though a discontinuity in the slot existed across the fuselage. It is expected that a significant improvement in augmentation ratio is available if this gap is closed. Further gains in augmentation ratio can be expected from later studies if the model geometry is not limited so strictly. The results provided a positive input into the powered model program. The even slot width configuration on which the majority of the wind tunnel testing was done was a direct outgrowth of these static tests.

WIND TUNNEL TEST FACILITY

Accurate wind tunnel simulation of the operating conditions of a GETOL configuration requires that tunnel walls be adequately separated from the model to prevent excessive wall effects and that the ground board be equipped so that no ground board boundary layer is present in the vicinity of the model. Early in the program, Convair initiated a modification to its Low-Speed Wind Tunnel to achieve the objectives stated above. A section of the tunnel was selected in the diffuser downstream of the normal 8 by 12-foot test section, as shown in Figure 27.

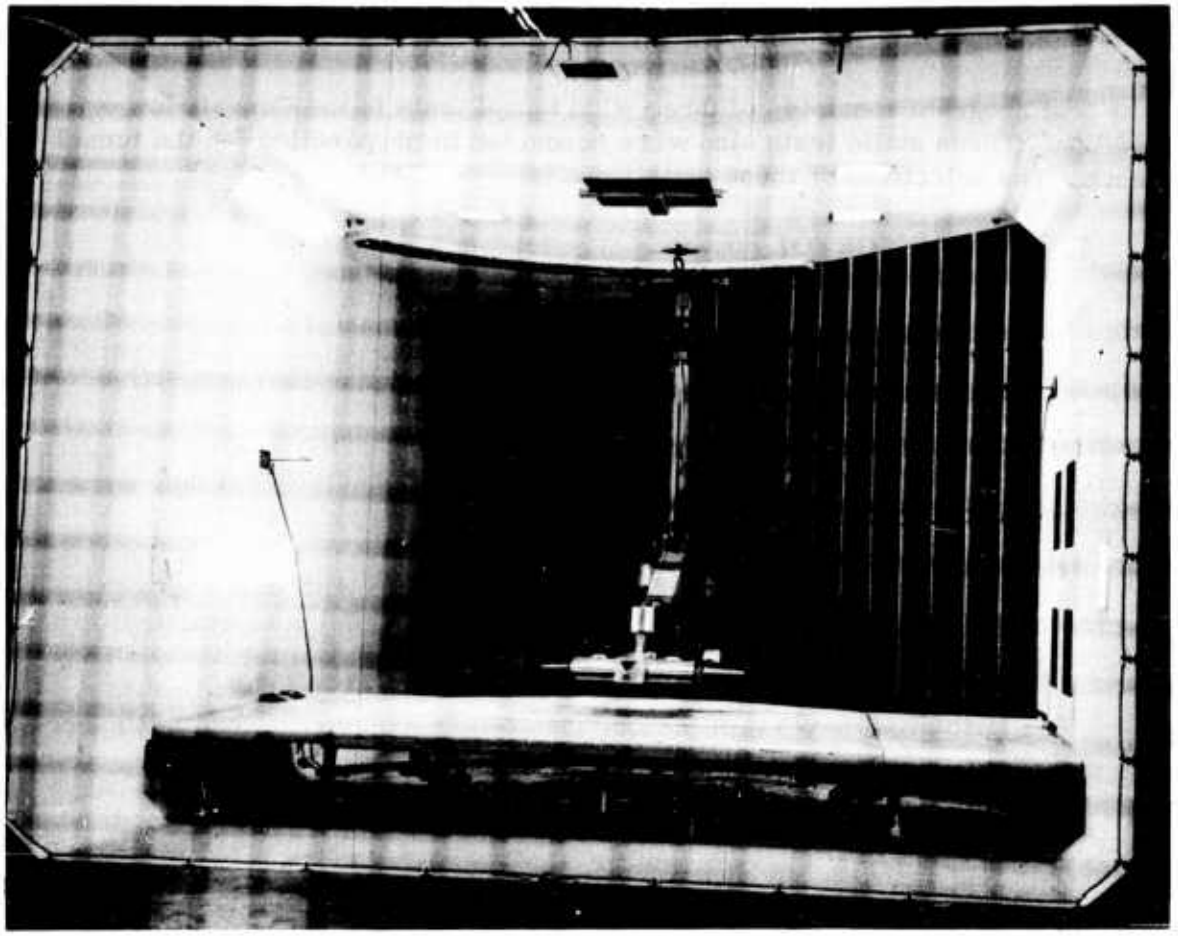

Figure 28. Large Test Section in Convair Low-Speed Wind Tunnel

This section is nominally a 16 by 20-foot section. A model support system was designed and constructed which is capable of remote control in heave and pitch. Further, yaw and roll can be achieved manually.

The special ground board is fitted in the section to extend completely across it. A suction slot is installed approximately one chord length ahead of the model to remove the ground board boundary layer.

Three screens of varying density, placed at appropriate stations upstream of the test section, were required to provide satisfactory flow distribution at two tunnel dynamics pressures (q_T). These two were q_T = 1.5 psf and q_T = 9.3 psf, both of which were used during the testing. The test section with its various components is shown in Figure 28.

PHASE II — MODEL TESTING AND DATA ANALYSIS

The test program consisted of three wind tunnel tests in the Convair low-speed facility. Three static tests also were conducted in preparation for the tunnel tests. The objectives of these tests were to:

1. Verify the GETOL concept.

2. Select efficient nozzle configuration.

3. Obtain data from which performance and handling characteristics could be calculated.

Following is a short description of each test in the order in which they were conducted:

1. Static test of the bare fans and also of the fans with duct configurations "A" and "B" attached. The fan and duct assembly was mounted on a three-component balance with pressure rakes aft of the fan and nozzle exits. Normal force, pitching moment, rolling moment, and total and static pressures aft of the fan and at the nozzle exits were measured during this test.

2. Initial tunnel test run with duct configuration "A" installed in the model. Tunnel speed, fan rpm, model height above the ground plane, angle of attack, and thrust vectoring were varied during the test.

3. Static test involving modification of the original concept of the "B" duct. Pressure data were taken both aft of the fan and at the nozzle exits to determine a configuration with better peripheral flow distribution than the original "B" duct.

4. Second tunnel test with the modified "B" duct installed in the model. Variables were the same as in the initial test.

5. Static test to determine effectiveness of seals between main and fan balances prior to entering tunnel for final test.

6. Final tunnel test involving further study of same configuration as tested in second test. A limited amount of roll and yaw data was obtained in this test in addition to the variables previously mentioned. Various control devices also were tested during this final test.

EVALUATION

Revision to Full-Scale Velocities

The wind tunnel data, reduced to coefficients, was not considered to be in the form most amenable to full-scale aircraft performance predictions. Therefore, the following method was derived for revision of the data to a more usable form:

Model theory states that for one system to represent another accurately, the model system must be dynamically, as well as geometrically, similar to the full-scale product. By the use of Bernoulli's equation and the continuity equation, it can be shown (Reference 3) that when dealing with propeller or rotor aircraft, the ratio $\frac{T}{A q_0}$ must be identical for the two systems for dynamic similarity to exist. Dimensional analysis has indicated that the methods employed for propeller testing are adequate for the scaling of lift fan model test data (Reference 4). Therefore, if the value of this ratio could be determined from wind tunnel data and applied to full-scale calculations, a method could be determined for converting the tunnel data to usable full-scale values.

The wind tunnel data has been nondimensionalized in the form of slip-stream coefficients. By proper manipulation of the thrust coefficient (T_c''), it can be determined that

$$\frac{T}{A q_0} = \frac{T_c''}{\frac{A}{S} - T_c''} \tag{1}$$

Now, looking at a full-scale airplane with a given wing loading $(\frac{W}{S})$

$$C_L'' = \frac{nW}{q'' S} \tag{2}$$

$$q'' = \frac{nW}{C_L'' S} \tag{3}$$

Since, by definition,

$$q'' = q_0 + \frac{T}{A} = q_0 \left(1 + \frac{T}{A q_0}\right) \tag{4}$$

$$\frac{nW}{C_L'' S} = q_o \left(1 + \frac{T}{A_{q_0}} \right) \tag{5}$$

Equation 5 as derived, applies to a full-scale airplane. However, since,

$$\left(\frac{T}{A_{q_0}} \right)_{\text{model}} = \left(\frac{T}{A_{q_0}} \right)_{\text{full scale}} , \tag{6}$$

Equation 5 may be revised to give

$$(q_0)_{\text{full scale}} = \frac{nW}{C_L'' S} \left[\frac{1}{1 + \frac{T}{A_{q_0}}_{\text{wind tunnel}}} \right] \tag{7}$$

Using Equation 1, full-scale, free-stream velocity in knots is

$$(V_0)_{\text{full scale}} = \sqrt{\frac{0.7\ nW}{\rho C_L'' S} \left[1 - \left(\frac{T_c''}{\frac{A}{S}} \right) \right]} \tag{8}$$

Equation 8 can be nondimensionalized to produce the following parameter:

$$\frac{(V_0)_{\text{full scale}}}{\sqrt{\frac{0.7}{\rho} \frac{nW}{S}}} = \sqrt{\frac{1}{C_L''} \left(1 - \frac{T_c''}{\frac{A}{S}} \right)} . \tag{9}$$

The date presented and analyzed in this section of the report is plotted against this parameter for maximum flexibility in usage. An example of how velocity is obtained from this parameter is given below:

Suppose

$$\frac{V_0}{\sqrt{\frac{0.7}{\rho} \frac{nW}{S}}} = 0.8 .$$

Now, if the aircraft with which we are working has a wing loading of 40 psf and is flying at a load factor of 1.0,

$$V_0 = 0.8\sqrt{\frac{0.7}{\rho}\frac{nW}{S}}$$

$$= 0.8\sqrt{\frac{(0.7)\ (1.0)\ (40)}{(0.002378)}}$$

$$= 86.8 \text{ knots.}$$

ANALYSIS

Static Tests

Static tests were conducted outside the wind tunnel to determine satisfactory operation and performance of the fans and ducts before entering the tunnel for the formal tests. The objectives of these tests were to check out the mechanical operation and evaluate the nozzle exit velocity distribution.

The initial static test of the bare fans with no ducts attached was considered an acceptance test of the fans to determine their conformance to specifications. The fans were mounted on a three-component balance measuring normal force, pitching moment, and rolling moment. Six radial pressure rakes at 60° increments around the fan were mounted 0.5 inch below the fan exit stators. The pressures thus measured were used to calculate weight flow through the fan. Power required to drive the model motors also was measured. The results, as shown in Figure 29, were excellent. The power required to drive the fans was slightly higher than predicted, but overall, the fans met predictions very well. Figure 30 shows the variation of thrust, weight flow, and power required with height above the ground plane. At a height-to-diameter ratio of approximately 1.25, the weight flow and power required began to fall off. This can be attributed to the onset of fan stall due to back pressure from the presence of the ground. It would be expected that thrust also would fall off corresonding to the falloff in weight flow. However, the thrust of the fan augmented by positive static pressures on the lower side of the fan hub and supporting frame to mask the expected decrease as seen by the balance.

The "A" ducts, "B" ducts, and modified "B" ducts also were tested statically before going into the wind tunnel. The fan and duct assembly was mounted on the three-component balance as described above, and pressure rakes were placed at

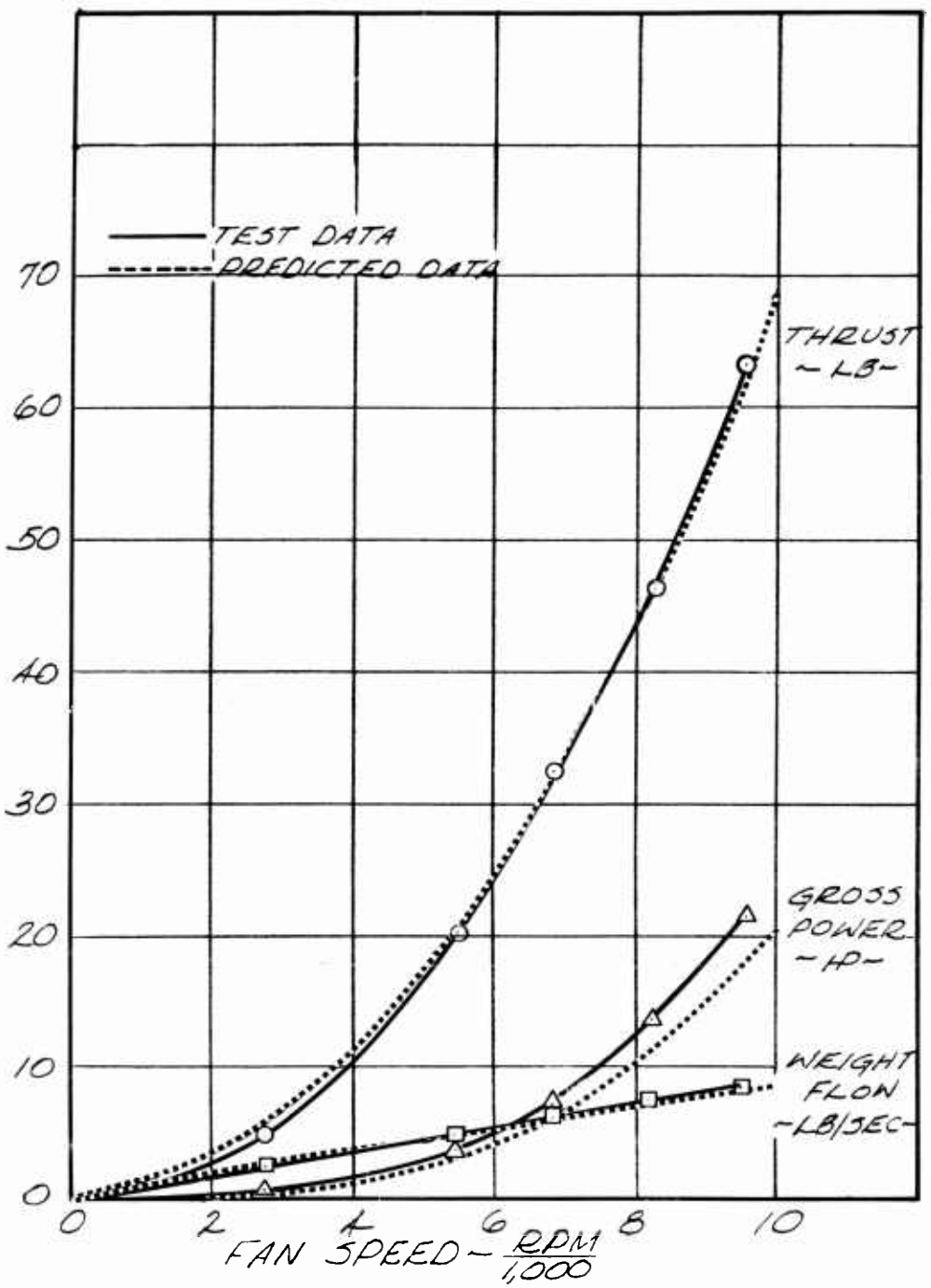

Figure 29. Model Fan Static Performance — No Ducts

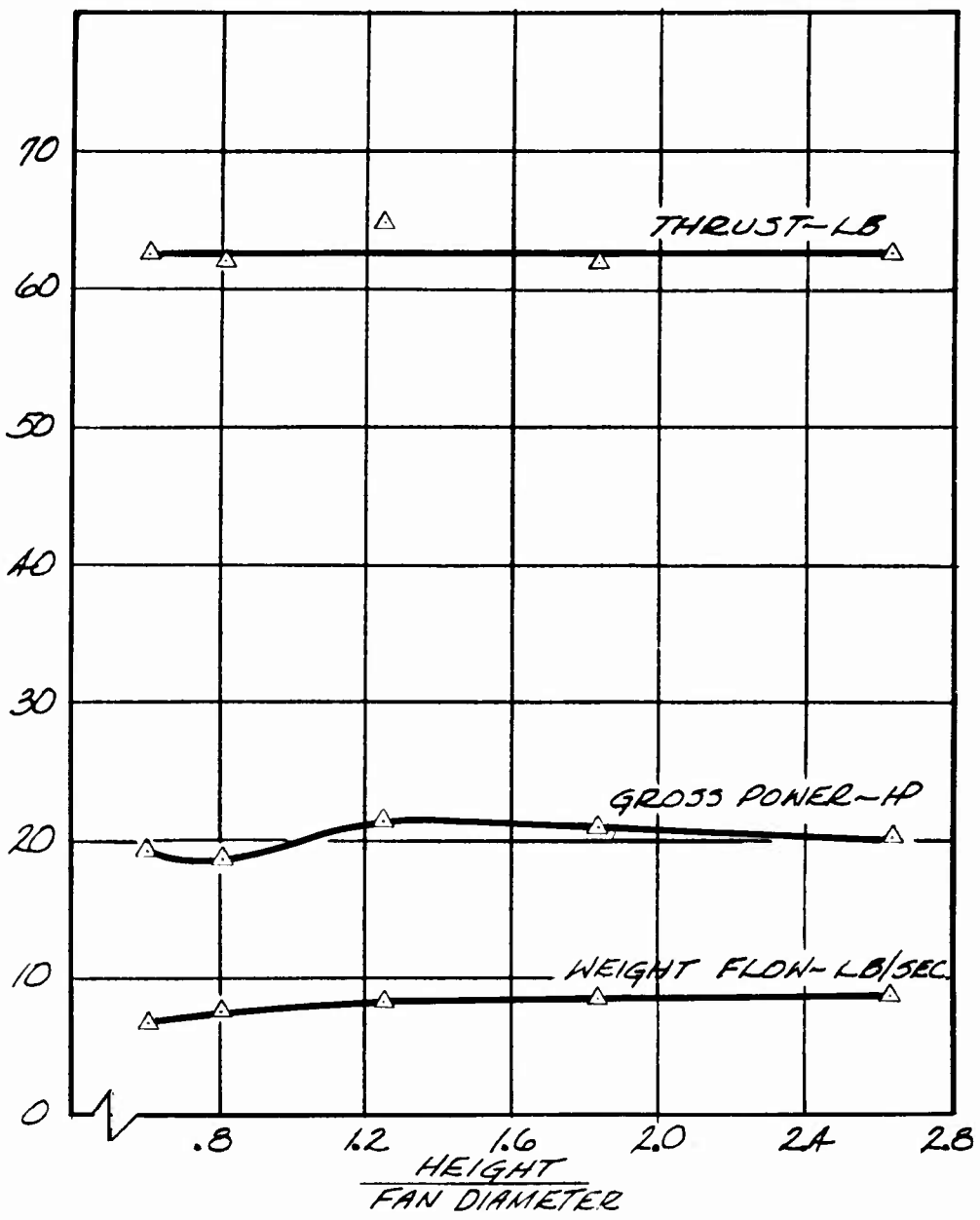

Figure 30. Effect of Height on Bare Fan Performance (Fan RPM = 9,590)

the duct exit nozzles to determine the velocity profile at the exits. Figure 31 shows the dynamic pressure distribution along each slot for the three-duct configurations. In general, it can be seen that the exit velocity distribution was smoother for the "A" ducts than for the "B" ducts. However, other considerations that are discussed later, rule out use of the "A" ducts, so an effort was made to improve the efficiency of the "B" duct. The result was the modified "B" duct shown in the figure. The velocity distribution, as well as the absolute value of velocity, was improved at all three slots over the original "B" configuration. This modified "B" duct was the duct configuration tested in the tunnel during the second and third tests.

A static test was conducted prior to the third wind tunnel test to check the effectiveness of the seals between the fan-duct assembly. Formal data was not recorded, but observations were made which indicated that the sealing methods used for the final test were reasonably effective; thus, the values of thrust read by the fan balance were usable.

WIND TUNNEL TESTS

Configuration "A" Ducts

The first wind tunnel test (CVAL 333) was run with the configuration "A" ducts installed in the model. Tunnel q, fan rpm, model height above the ground plane, model angle of attack, and thrust vectoring were variables in the test. Six-component force data was read from both the fan and main balances, and surface pressures were recorded.

As to the value of thrust used in the data reduction process, an attempt was made to measure the actual thrust output of the fan-duct assembly be isolated, or sealed off, from the surface pressures around the model. This was to be done by using a flexible rubber seal between the fan-duct assembly and the remainder of the model. However, oil leaking from the gear boxes resulted in rapid deterioration of the seals, and it was not until the third test that a reasonably effective and reliable seal was achieved. Therefore, all the data has been reduced using the static, out-of-ground value of thrust at any given rpm. By using this method, the assumption is made that the full-scale fan would act exactly as the model fan when in the presence of the ground and at forward speed. However, in either case there would be some differences between the model and a full-scale article when the fan is back-pressured by the presence of the ground plane because of the disparity in operating Reynolds' numbers. The assumption made above is normal wind tunnel testing procedure.

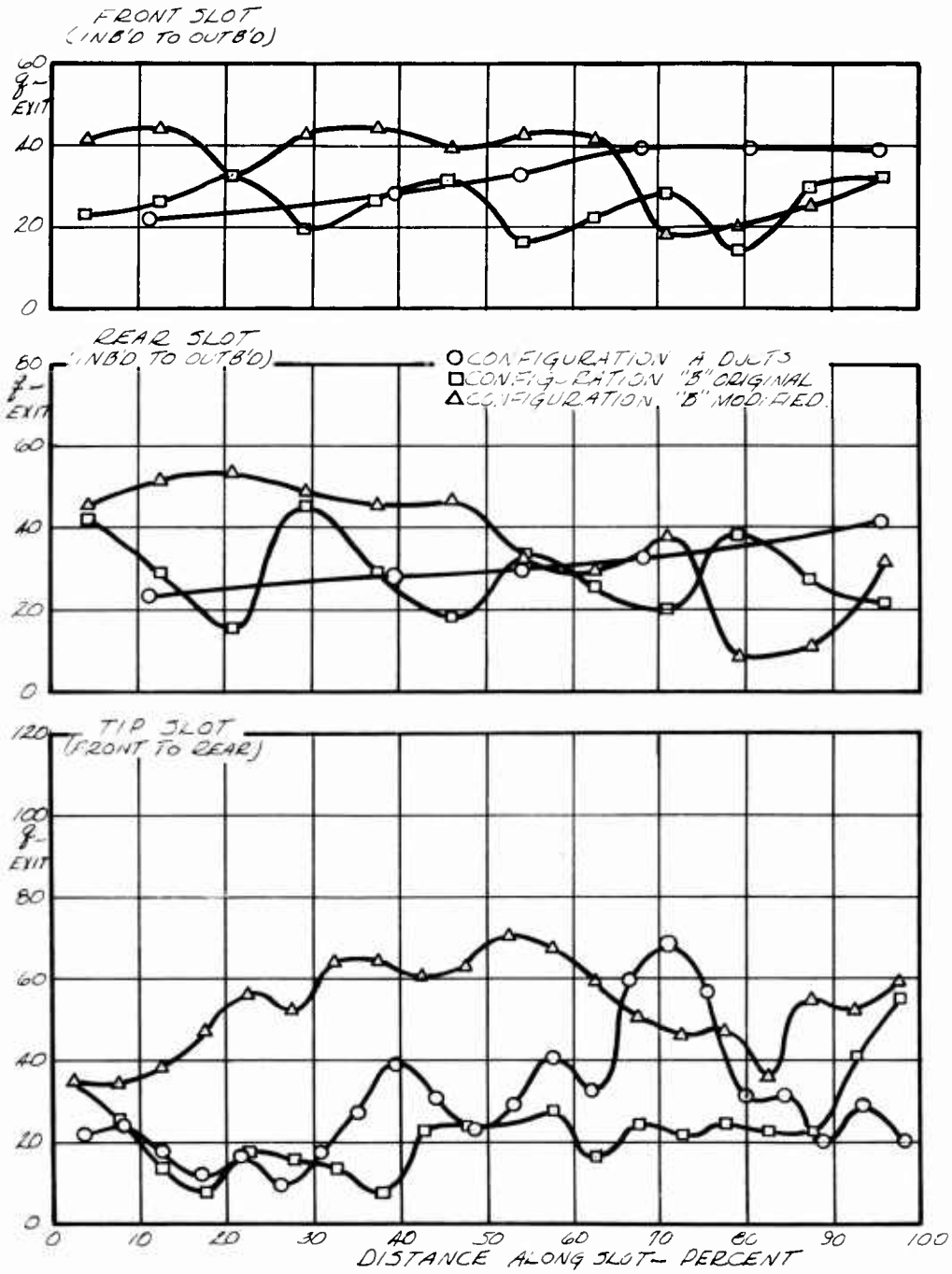

Figure 31. Exit Nozzle Dynamic Pressure Distribution in Free Air (Fan RPM = 10,275)

Effect of Thrust Deflection

Figure 32 shows the effect of rearward deflection of thrust with the "A" configuration ducts. The form in which the data is presented in this illustration will be the typical method of presentation in the report. The items presented are L/T_O - total lift to static, free air thrust; D/L - drag to lift ratio, which is a measure of the longitudinal acceleration; and M/L_C - center-of-pressure movement in per cent of chord from the 35% chord point, all as a function of the nondimensional velocity parameter discussed previously. The data as presented portrays a complete picture on one page of the longitudinal characteristics at any velocity.

Based on previous analytical work, a target value of the lift-to-static thrust ratio in ground effect for the GETOL research program was set at 1.40. Data is presented for 0°, 30° and 45° tip vane deflections at an angle cf attack of zero degrees and a height-to-chord ratio of 0.145, in ground effect. The lift-to-static thrust ratio decreases as the rearward vane deflection angle increases. This is expected, since the vertical component of thrust (and thus total lift) becomes less as the deflection angle increases. The curve representing the 30° deflection angle extends to higher velocities than the other two, and from it can be seen the characteristic shape of the lift-to-static thrust ratio curve in all configurations. The ratio remains relatively constant, or falls off slightly, until aerodynamic lift becomes effective; then the curve begins to break up, rather sharply in some instances. The static acceleration with the thrust deflected 45° is good (approximately 0.575g) but unusable as the lift-to-static thrust ratio at this point is less than 1.0. The rapid falloff of the lift-to-drag ratio is primarily due to the increase in ram drag as forward speed increases. Ram drag is discussed in detail in a later section of this chapter. The center of pressure moves forward quite rapidly with forward velocity in this configuration. With the thrust deflected 45°, it can be seen from the figure that the center of pressure would move forward approximately 35% at a velocity parameter value around 1.1. This would put the center of pressure at the leading edge of the wing. The subject of pitch-up with forward velocity also is covered more thoroughly in a later section of this chapter. Figure 33 shows the effect of tunnel q, which is analogous to forward speed, on the base pressures of the model in ground effect. The source of part of the increase in lift evidenced on the previous figure at the higher forward speed can be seen in the increased base pressures at the high tunnel q pressure profile as compared to the static case. Additional lift also is obtained at forward velocities due to the increased negative pressures on the wing upper surface.

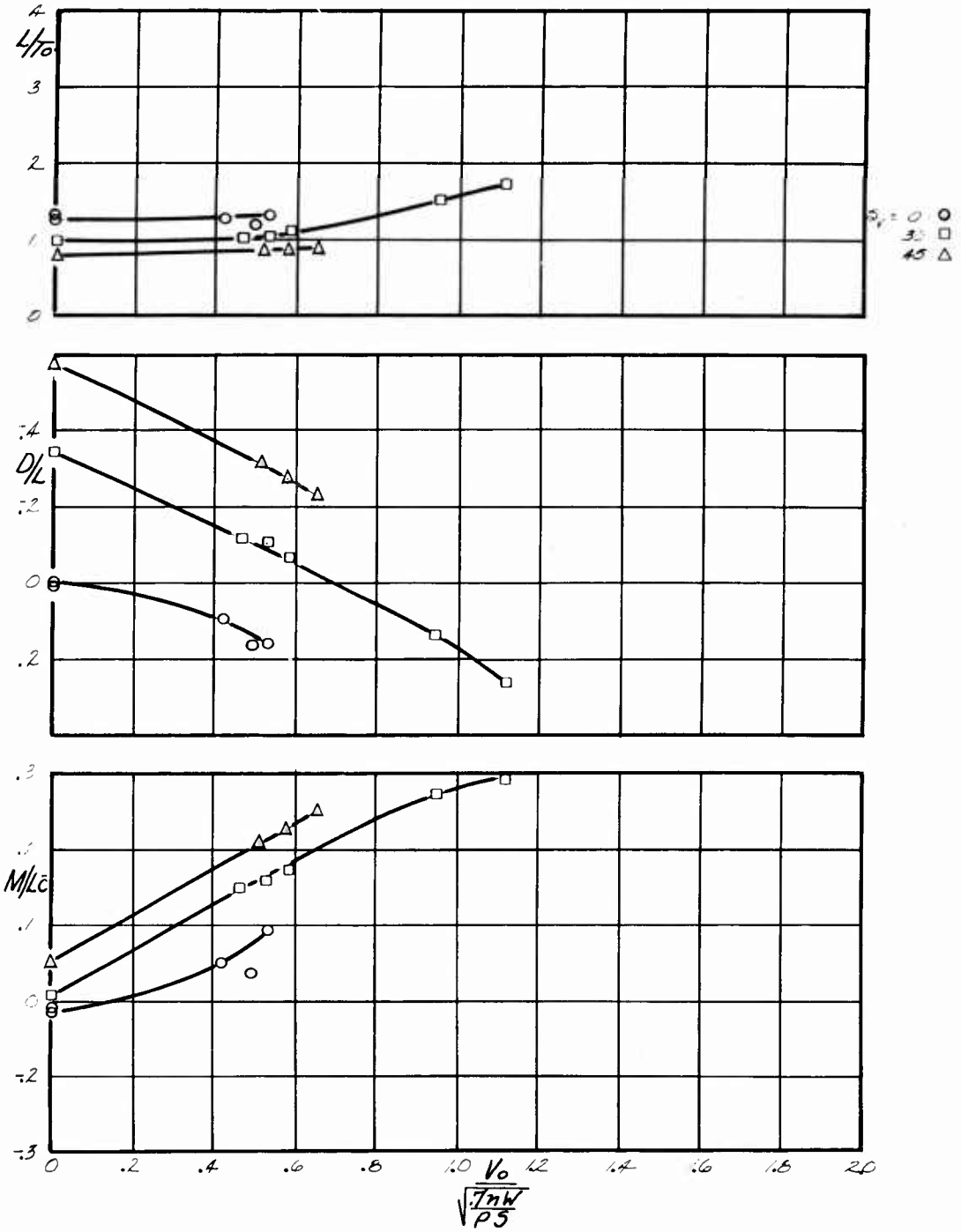

Figure 32. Effect of Tip Vane Deflection in Ground Effect — Configuration "A" Ducts (h/c = 0.145, α = 0°)

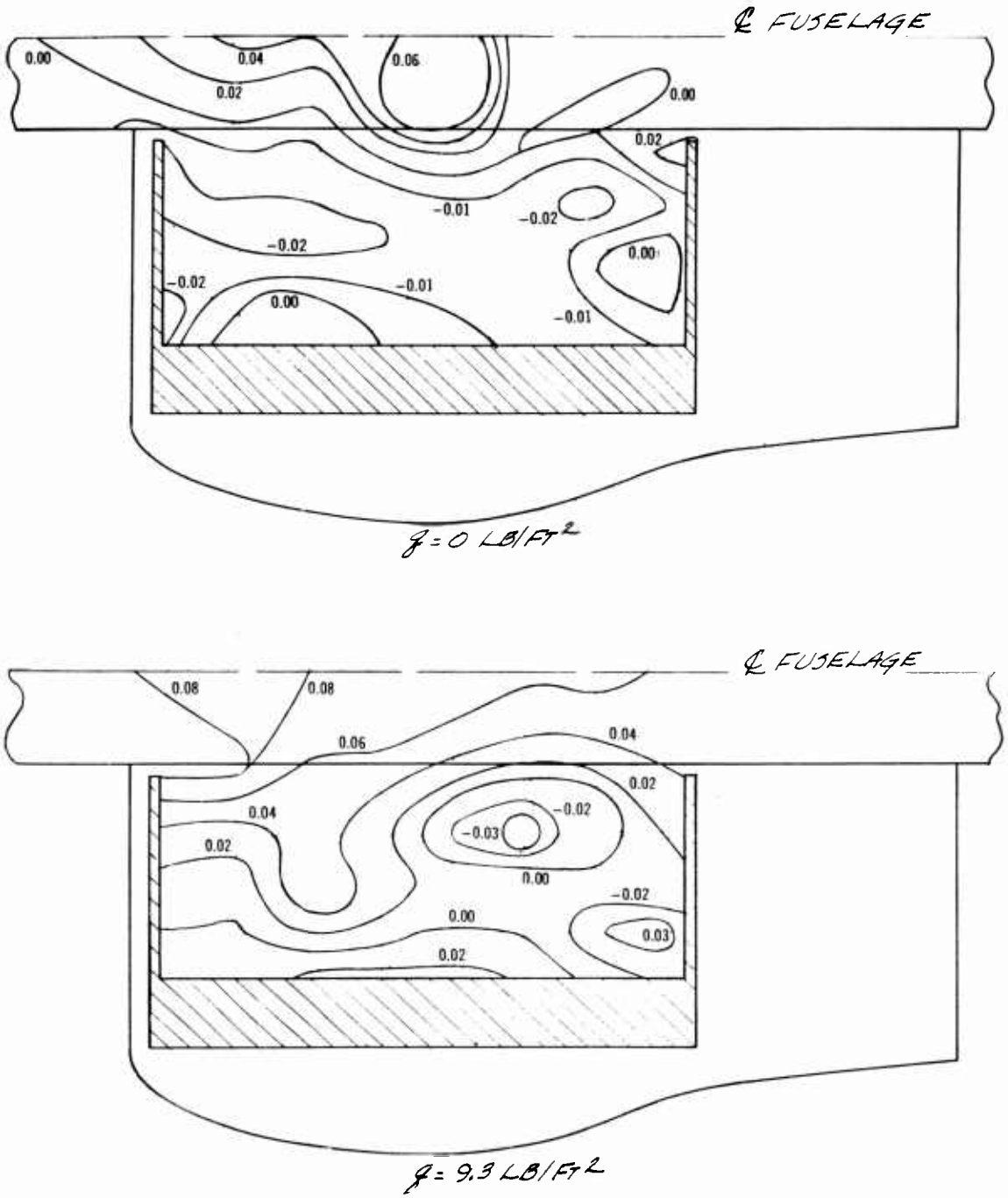

Figure 33. Effect of Free Stream Dynamic Pressure on Base Pressures — Configuration "A" Ducts ($\alpha = 0°$, $\delta_v = 0$, RPM = 12,500, $q_{jet} \cong 23$ PSF, $h/c = 0.146$, $\delta_i = 0°$, = Isobars ~ PSI

Effect of Angle of Attack

Figure 34 shows the effect of angle of attack on the parameters mentioned previously. In the range in which force data is available, angle of attack does not have an appreciable effect except on the drag-to-lift ratio. However, Figure 35 shows that in the higher speed range, an appreciable increase in lift can be expected at 10° angle of attack over that at zero degrees. At the higher angle of attack, isolated pressure peaks are eliminated and the overall pressure level is increased, thus producing increased lift. The increased drag at the higher angles of attack can be attributed to the fact that as the angle of attack is increased, with the thrust exiting normal to the wing chord plane, the component of thrust in the forward direction increases, thus causing a drag force on the model.

Effect of Height

The lift-to-static thrust ratio, drag-to-lift ratio, and center-of-pressure increment are shown in Figure 36 as a function of height-to-wing chord ratio. If it is desired to use height to equivalent base diameter ratio, the conversion can be made by use of Figure 37. It was shown in Figure 36 that the lift-to-thrust ratio has a dip at a height-to-chord ratio of approximately 0.175. This dip is believed caused by the lag between loss of effectiveness of the tip slots and the increasing effectiveness of the front and rear slots. Previous static tests on a configuration using only tip slots lead to this explanation. At height-to-chord ratios below 0.175, the lift-to-thrust ratio once again increases as height decreases. Figure 38 shows that the principal source of increased lift in ground effect is the base pressure on the lower surface of the fuselage. The pressures on the wing undersurface remain nearly the same in and out of ground effect. The low pressure on the undersurface of the wing is caused by the large tip slot overpowering the small front and rear slots and setting up a vortex which wipes out any pressure buildup on the wing. This detrimental effect is alleviated by going to approximately equal slots all around. The drag-to-lift ratio at $q_T = 0$ increases negatively as the height-to-chord ratio increases. This is apparently due to a change in the direction of the resultant thrust vector out of ground as compared to the low ground height. In the case of the $q_T = 1.5$ curve, ram drag overshadows this effect. In a later section it is shown that 100% of theoretical ram drag is experienced out of ground, while in ground effect the level is somewhat lower. Therefore, the slope of the drag curve for $q_T = 1.5$ is due to increasing ram drag as height above the ground plane is increased. In the static condition, the center of pressure moves forward approximately 8% as the model moves into ground effect. Previous static tests have shown this to be caused by negative pressure on the wing aft of the rear slot in ground effect. With a tunnel q of

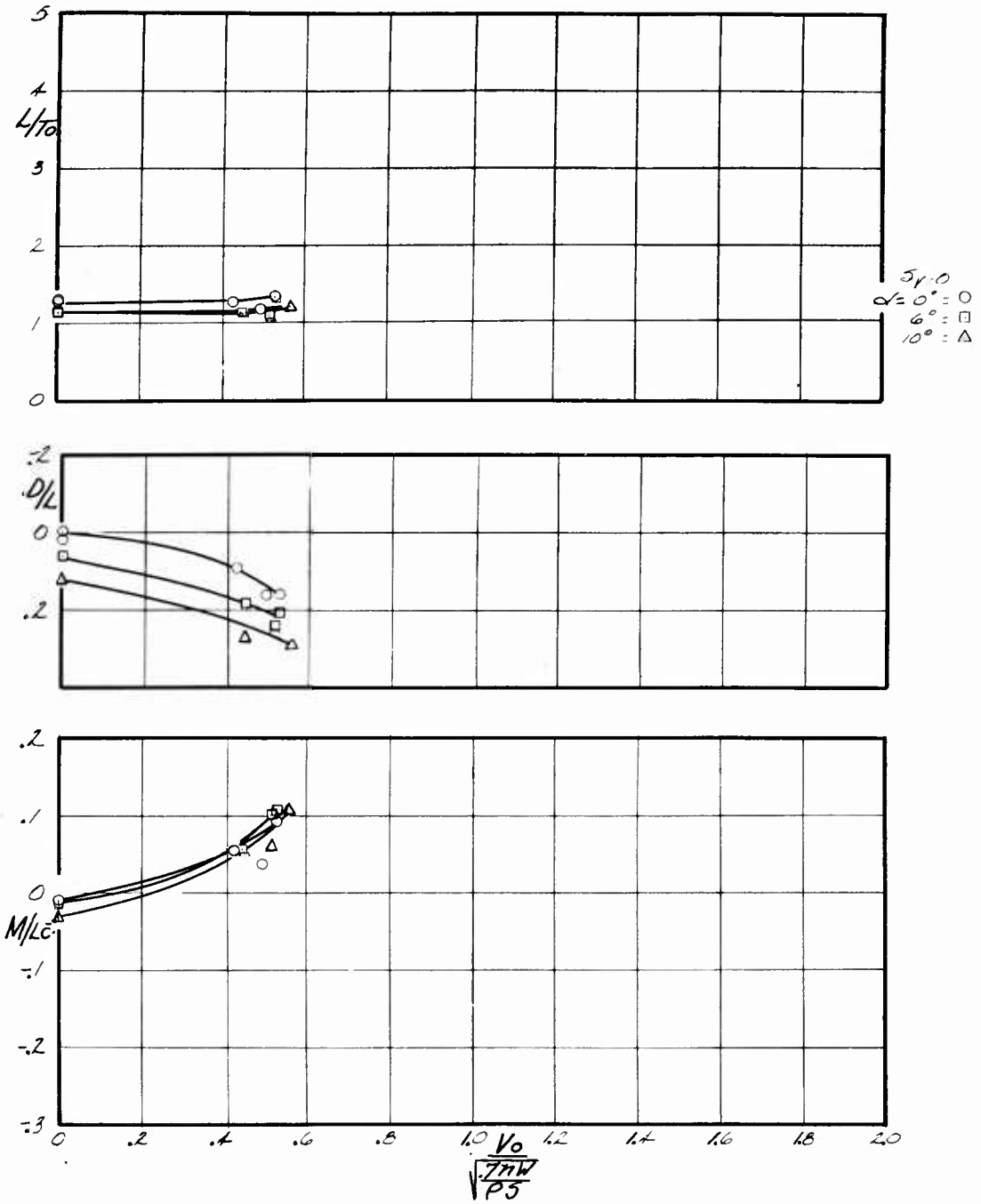

Figure 34. Effect of Angle of Attack in Ground Effect — Configuration "A" Ducts (h/c = 0.115, δ_V = 0°)

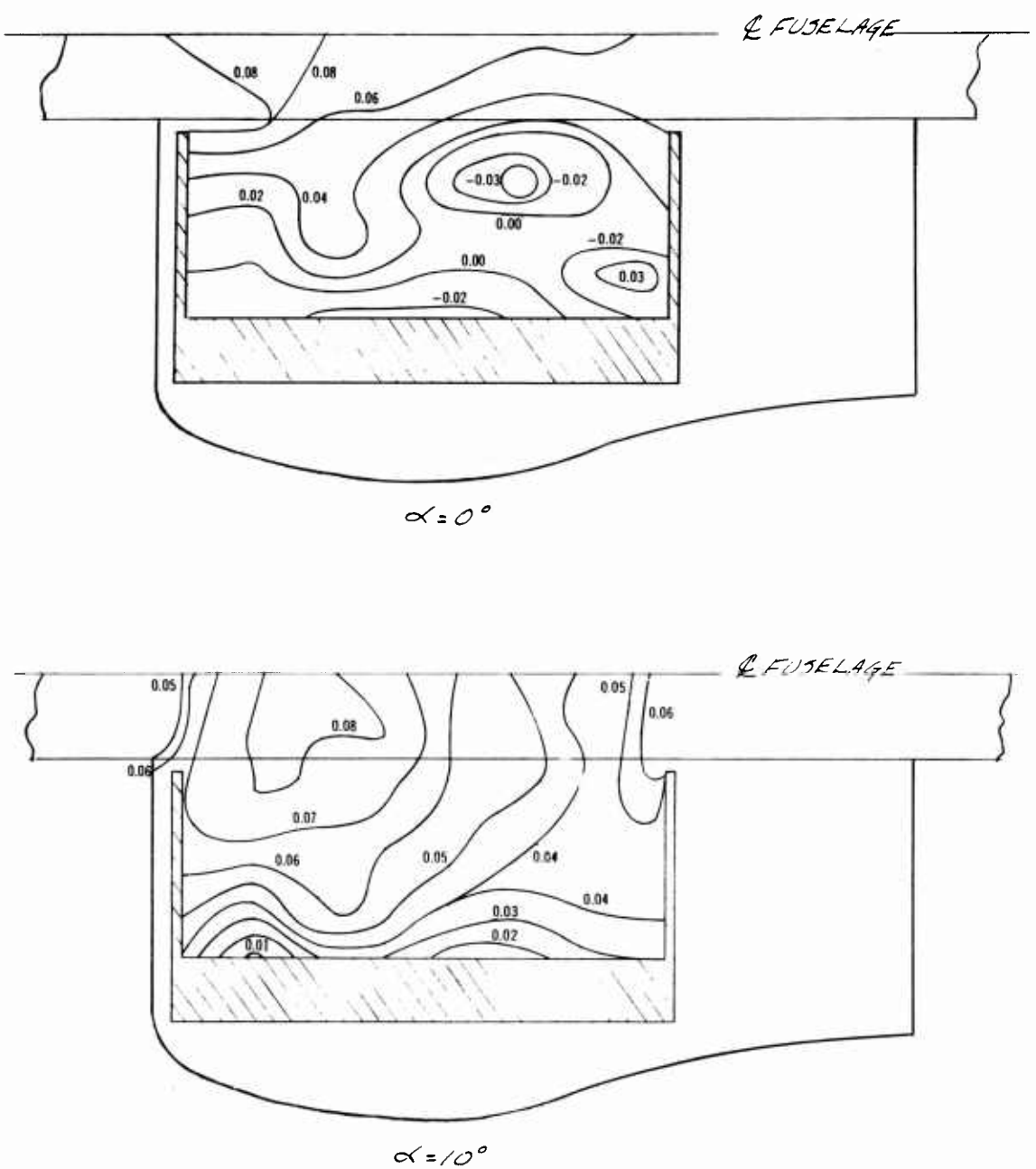

Figure 35. Effect of Angle of Attack on Base Pressures — Configuration "A" Ducts (q = 9.3 PSF, $\delta_V = 0°$, RPM = 12,500, $q_{jet} \cong 23$ PSF $\delta_i = 0°$, Isobars ~ PSI, h/c = 0.146)

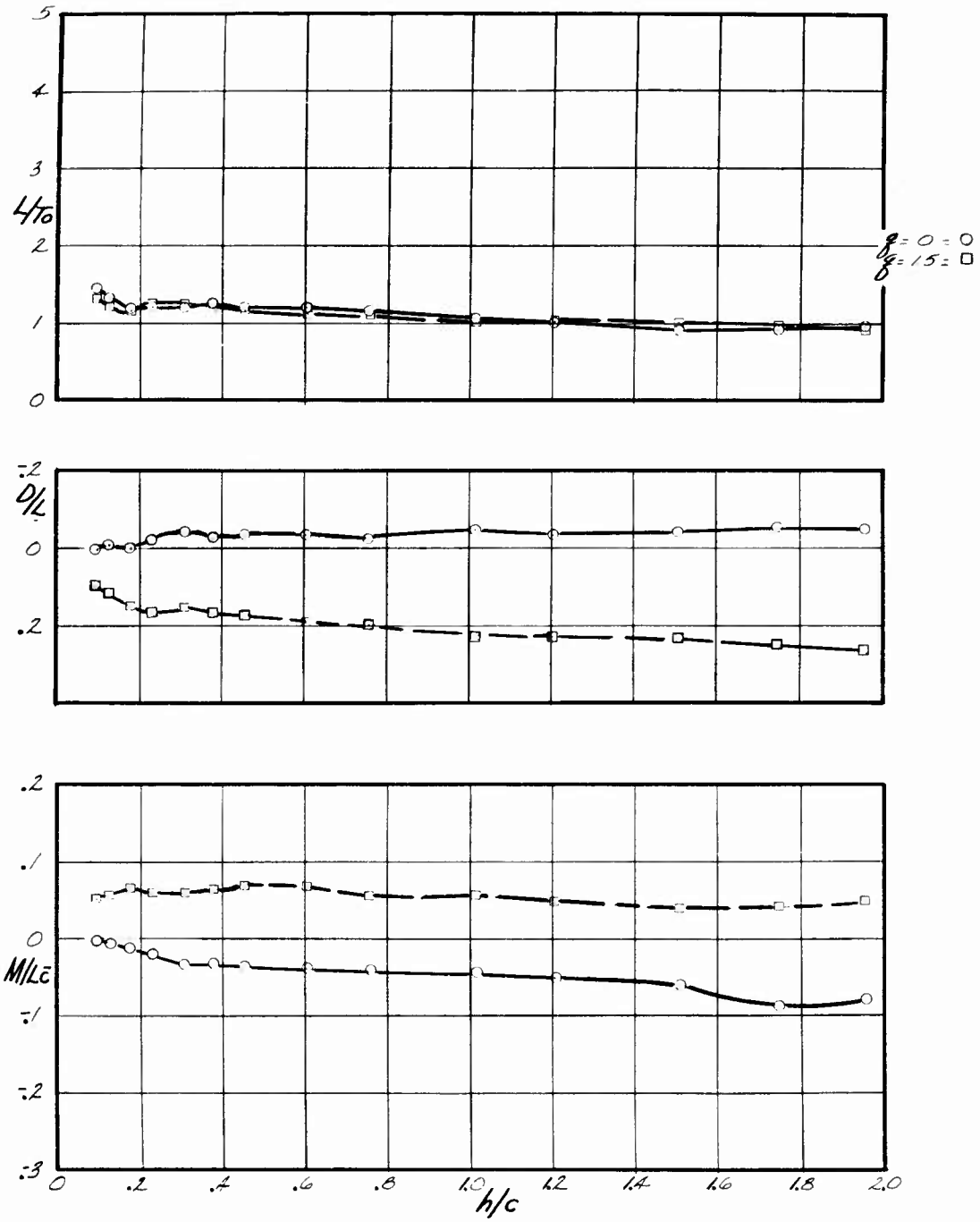

Figure 36. Effect of Height — Configuration "A" Ducts
(α = 0°, δ_V = 0°)

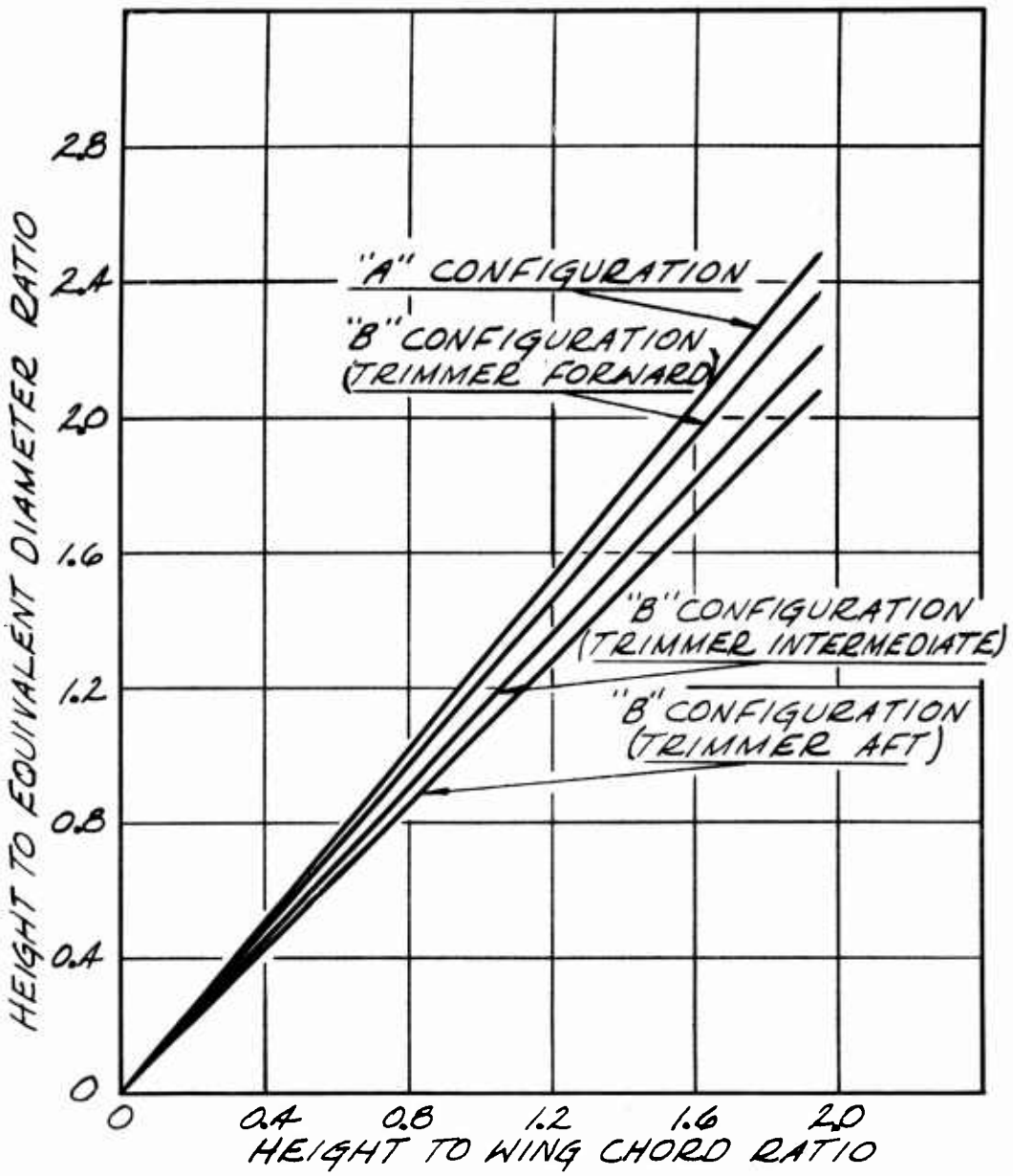

Figure 37. Height to Equivalent Base Diameter Ratio as a Function of Height to Wing Chord Ratio

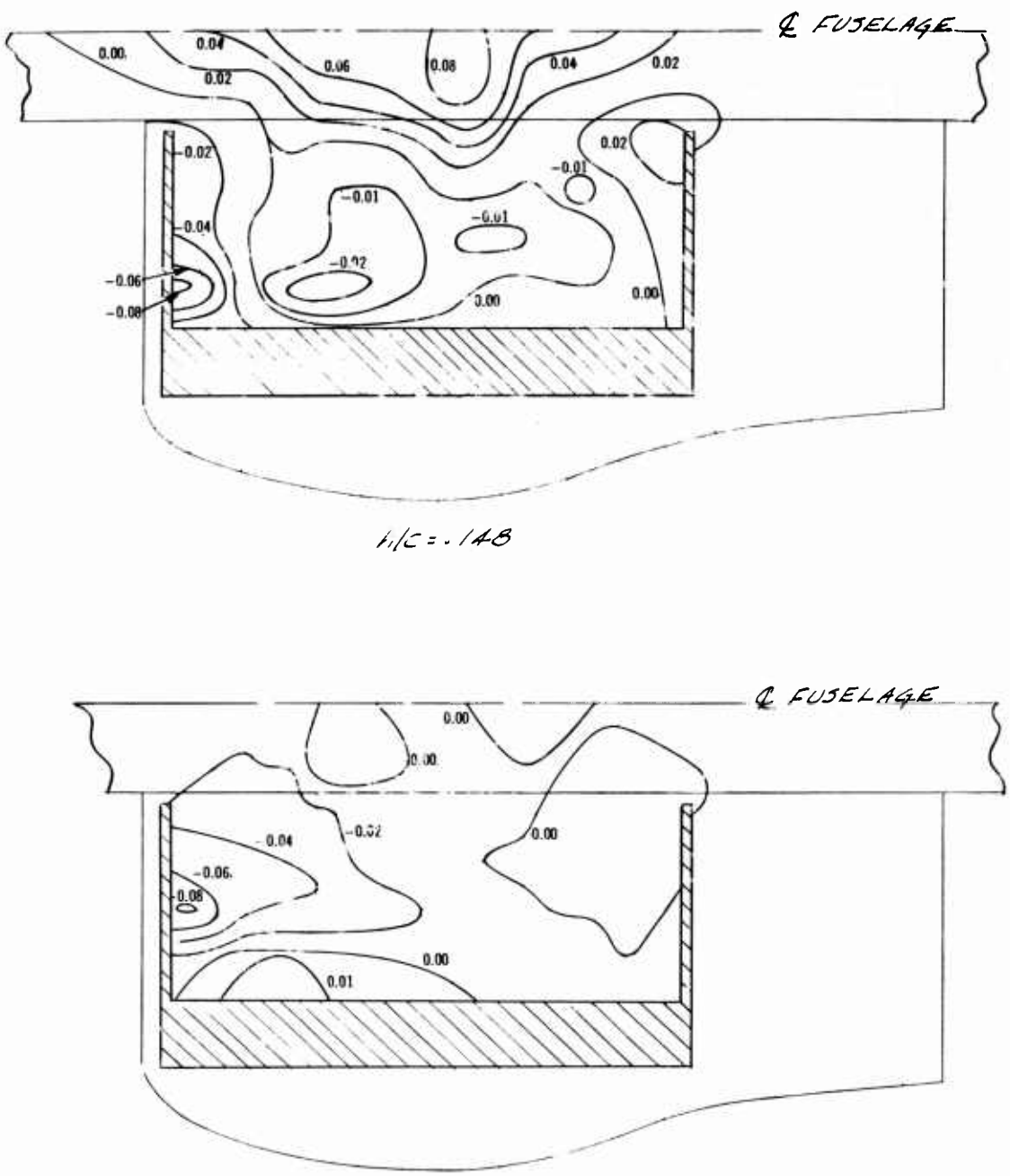

Figure 38. Effect of Height on Base Pressures — Configuration "A" Ducts (α = 0°, δ_V = 0°, RPM = 14,000, $q_{jet} \cong$ 29 PSF, q = 0 PSF, δ_i = 0°, Isobars ~ PSI)

1.5, the center-of-pressure movement is much less with height and at all heights is forward of its corresponding static position.

In summary, the "A" configuration ducts did not produce sufficient lift-to-thrust ratio and evidenced too much pitch-up with forward velocity to be practicable. Therefore, the "A" configuration was discarded in favor of the "B" ducts.

Configuration "B" Ducts

The second and third tests were run with the modified "B" ducts installed in the model. As explained previously, these ducts evolved from the original "B" ducts during static testing for improved peripheral velocity distribution. The modified "B" ducts hereafter are referred to as the "B" ducts for simplicity. Tunnel q, fan rpm, model height above the ground plane, model angle of attack, and thrust vectoring were variables in the test. Six-component force data was read from both the fan and main balances, and surface pressures were recorded. In addition, pressures were read from six radial rakes at 60° intervals around the fan mounted inside the left-hand duct, just below the fan exit stators, to estimate weight flow through the fan.

The problem associated with measuring the thrust of the fan-duct assembly was discussed in the previous section. However, in the final test, a seal configuration was achieved which allowed reasonably accurate measurements of thrust to be made. Figure 39 shows both the thrust used in the data-reduction procedure and the fan-balance thrust measured with the final seal configuration. The increase in indicated thrust from fan-balance readings at height/chord ratios below 0.3 is believed to result from base pressure loads on the seals, rather than an actual increase in thrust. This conclusion was reached after comparing the fan-balance data with bare fan data in the presence of the ground and with the difference between model balance readings and integrated external pressure force. Based on this data, it may be said that the lift-to-thrust ratios presented in this report are generally conservative for all values of height-to-chord ratio.

Nature and Effect of Flow Regimes

Before proceeding with the presentation and discussion of force and moment data for the model with the "B" ducts installed, some qualitative remarks on the nature of the flow field in the vicinity of the model are in order. Walker (Reference 5) defines three flow regimes through which a ground effect machine passes as forward speed increases.

1. Subcritical, in which the flow field is dominated by the jet efflux.

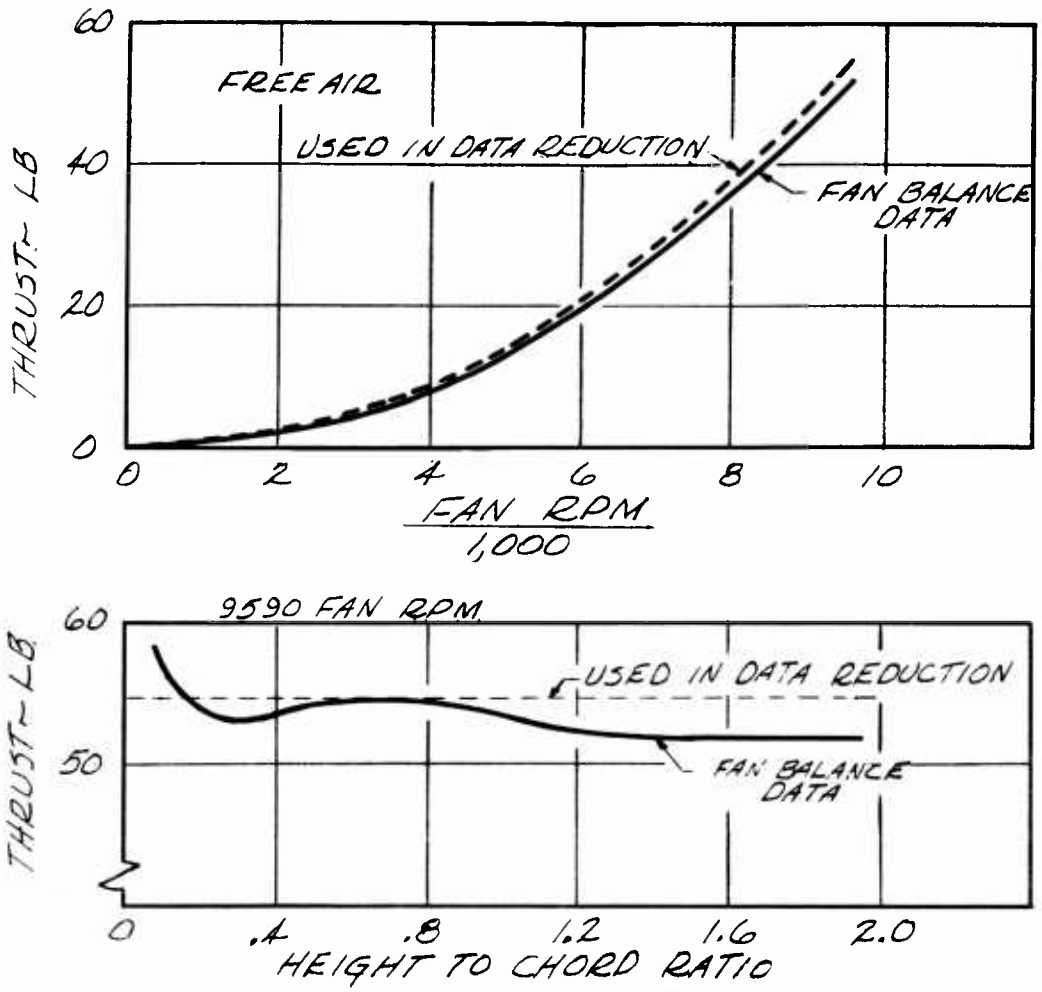

Figure 39. Thrust Available With Configuration "B" Ducts — Trimmer Forward ($q = 0$, $\alpha = 0°$, $\delta_V = 15°/-15°/0°$)

2. Transitional, in which the external flow attaches to the upper surface of the vehicle.

3. Supercritical, in which the external flow blows back the leading edge jet and passes underneath the vehicle.

Although no attempt has been made in this study to quantitatively determine the critical velocities defined by Walker, pressure and force data from the subject

test confirm the existence of these characteristic flow patterns. Figure 40 is a sketch of the subject GETOL model flow fields as envisioned at this time.

The subcritical, or low-speed regime, as stated above, is dominated by the jet efflux which flows forward, forms eddies, and flows back over the vehicle. For pipe-fed models in this flow regime, the external air does not touch the upper surface of the model. However, for the subject model, because of the fan, or sink, in the upper surface, the external flow does reattach to the upper surface, although not at the leading edge as shown in Figure 40, Detail (a). In this and the transition regimes, part of the air entering the fan is obtained from the free stream and part from the jet efflux which is engulfing the vehicle. As vehicle speed increases, the jet efflux burble is progressively forced closer to the ground and the vehicle leading edge until the external air conforms to the upper surface contour. This is shown in Figure 40, Detail (b). At this condition, the front jet is probably split with part of the flow being deflected aft and part forward. The high-speed regime, Figure 40, Detail (c), is dominated by the external flow which blows the jet efflux back under the base and allows the main stream to pass both under and over the vehicle. It appears that progressive deflection of the jet efflux aft, or increasing the clearance height of the vehicle, produces the same type of change in flow pattern as increasing speed. It appears also that increasing the angle of attack will decrease the speed at which the flow conforms to the upper surface.

The following observations are offered to provide a general understanding of the relationship of the above-defined flow regimes with the force data presented in subsequent sections of this report. At hovering, the pressure pattern on the wing upper surface through the fan centerline is as shown in Figure 41, Detail (a). As speed is increased, the point at which the free-stream flow conforms to the wing contour moved forward to the wing leading edge. The associated pressure patterns on the wing upper surface are as shown in Figure 41, Details (b) and (c). At the same time the pressure pattern on the wing lower surface through the fan centerline changes from the hovering condition, shown in Figure 42, Detail (a), to that shown in Figure 42, Detail (b).

In the following sections of this report it will be noted that, in ground effect operation without nozzle vane deflection, as speed is increased from zero, the lift-to-thrust ratio at first remains essentially constant at the hovering value. Then when the value of free-stream dynamic pressure is approximately two-tenths of the jet dynamic pressure the lift-to-thrust ratio increases rapidly with speed. Conformation of the free-stream flow to the wing contour from the wing leading edge to the fan inlet and the resulting pressure patterns shown in Figure 41, Detail (c) and Figure 42, Detail (b), appear to set the speed for increasing lift-thrust ratio. From Figures 43 and 44 it may be seen that the large

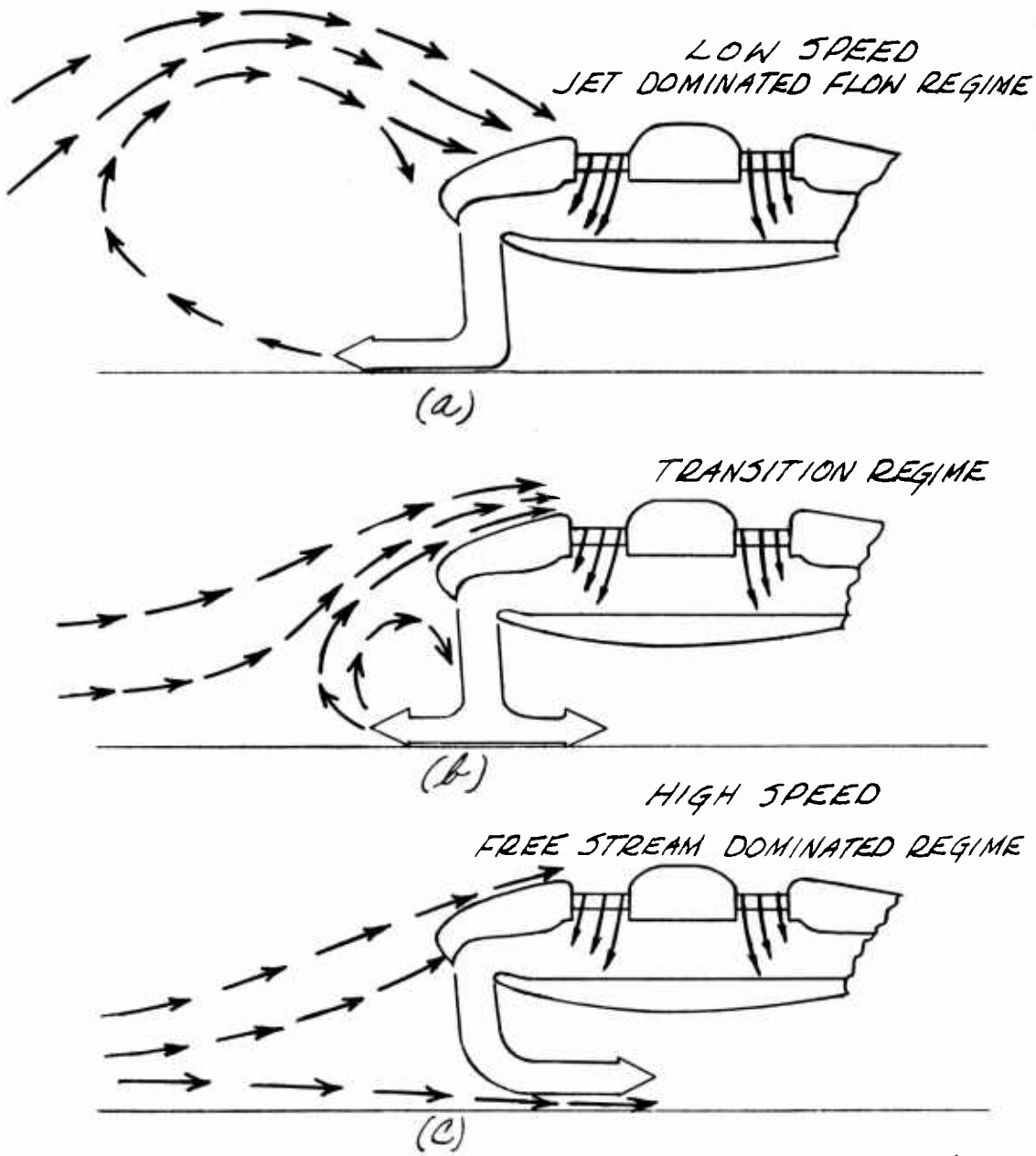

Figure 40. Characteristic Flow Patterns in Ground Effect

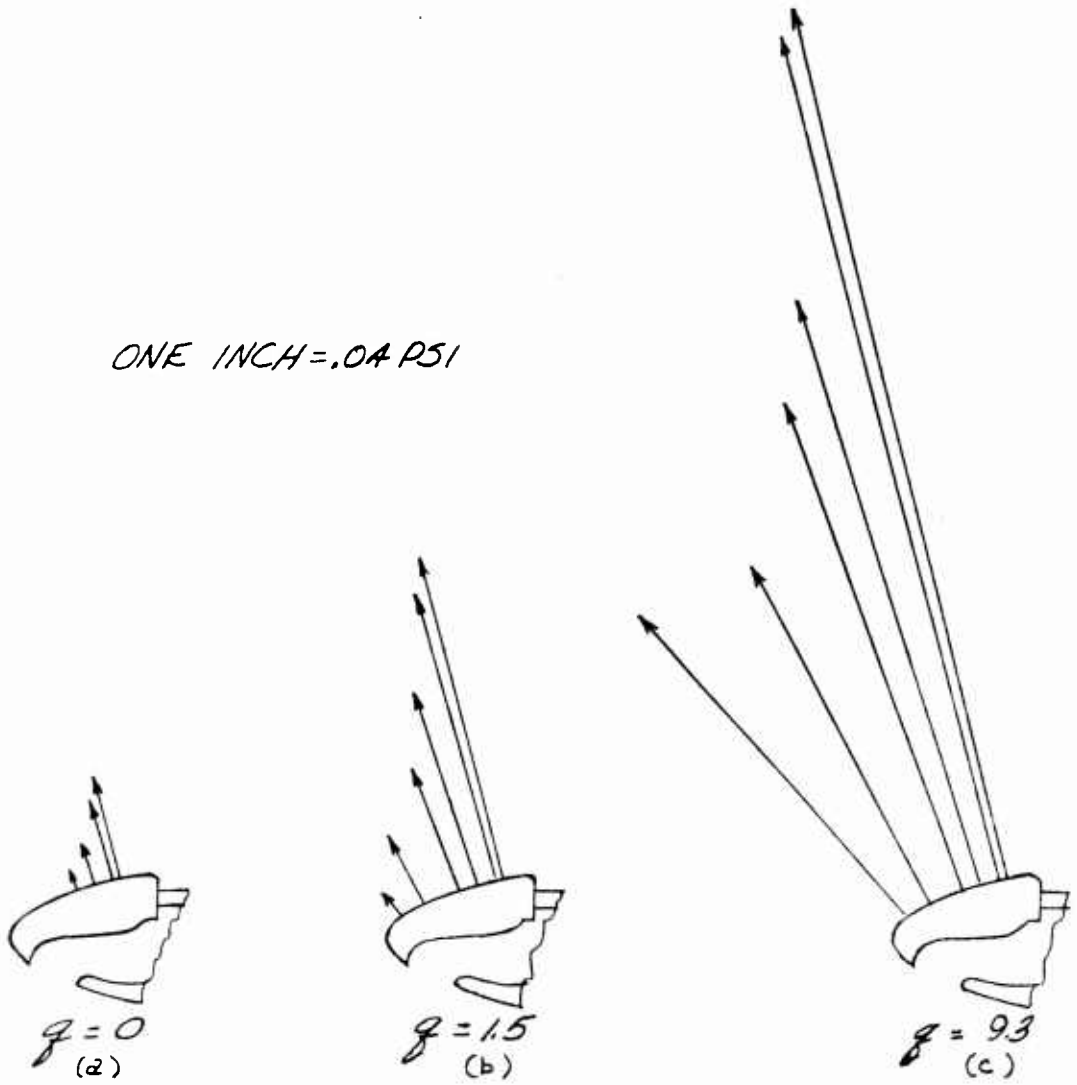

Figure 41. Effect of Forward Velocity on Leading Edge Pressures at Constant Fan RPM in Ground Effect — Configuration "B" Ducts (α = 0°, h/c = 0.115, δ_V = 30°/30°/30°)

negative pressures ahead of the fan inlet are not only the major contributors to the increase with speed of the undesirable nose-up moment but, at the same time, prevent a droop in lift which would otherwise occur due to the drop in base pressures.

It appears reasonable to expect that the aerodynamic forces and moments in the high-speed, or supercritical, regime will tend to be the same as those on the

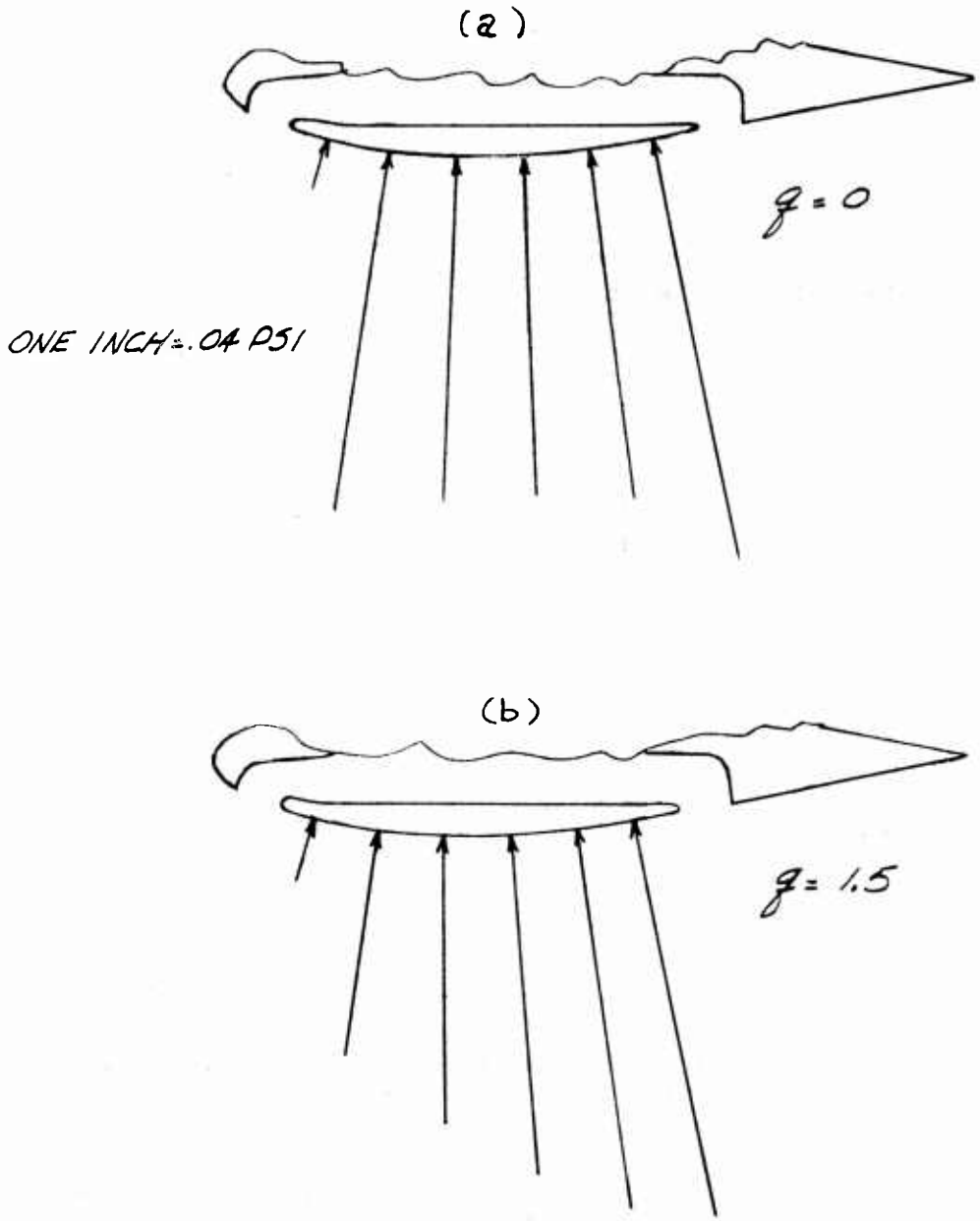

Figure 42. Effect of Forward Velocity on Base Pressure in Ground Effect — Configuration "B" Ducts (α = 0°, h/c = 0.115, δ_V = 15°/-15°/0°)

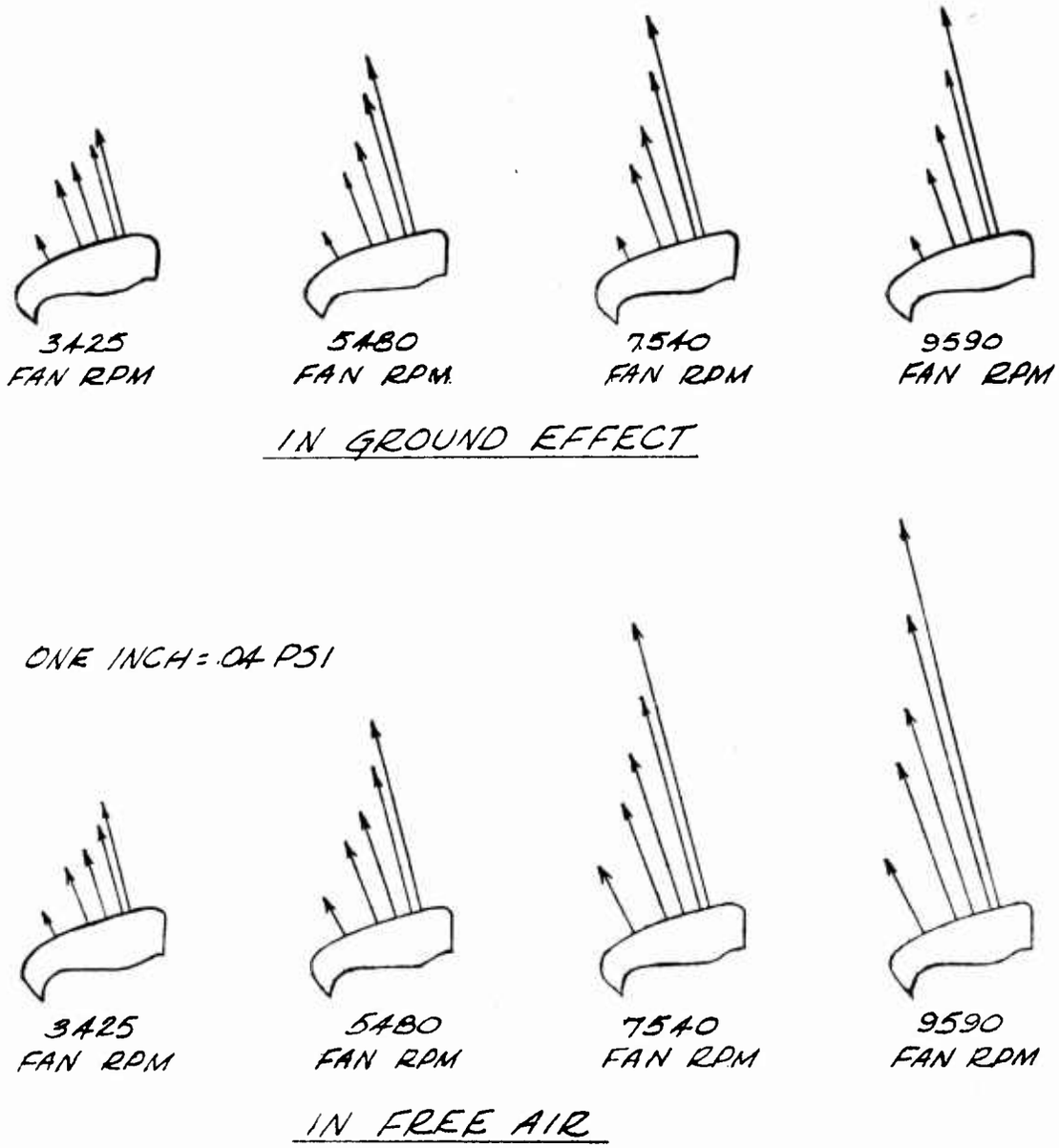

Figure 43. Effect of Forward Velocity on Upper Surface Leading Edge Pressures in and Out of Ground Effect – Configuration "B" Ducts
($q = 1.5$, $\delta_V = 30°/-15°/30°$, $\alpha = 0°$)

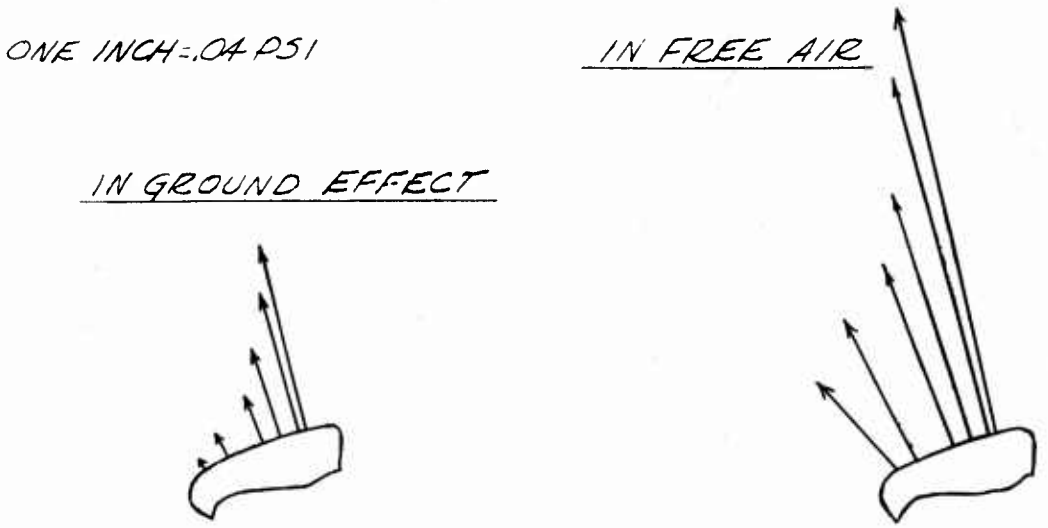

Figure 44. Effect of Ground on Upper Surface Leading Edge Pressures — Configuration "B" Ducts (q = 1.5, α = 0°, δ_V = 0°/0°/0°, Fan RPM = 9,590)

vehicle when in free air. Figure 43 presents some pressure data on the leading edge of the upper surface which appears to confirm this expectation. Data is shown for four fan rpm, both in ground effect and in free air, at a tunnel q of 1.5 and zero angle of attack. Decreasing fan rpm is indicative of increasing forward speed in powered model testing (see previous section). At 9,590 fan rpm, the pressures in free air are considerably higher than those in ground effect. This indicates that the flow over this surface is slower in ground effect, which would be the case if the jet efflux were being forced back over the model and did not have time to accelerate to free-stream velocity as described in the subcritical flow regime. As forward speed increased (decreasing fan rpm), it can be seen that at 3.425 fan rpm, the pressures in and out of ground effect are essentially the same, indicating that the flow over the model is the same for the two conditions just as described for the supercritical regime. It also can be seen from the figure that the transition takes place smoothly with no sudden discontinuities.

These flow patterns apparently have a strong effect on the ram drag experienced by the GETOL vehicle. Ram drag is here defined as that momentum lost as a result of stopping a stream tube of air of the same diameter as the fan. It has been observed, however, that for operation in ground effect under certain speed and flow deflection conditions, a ram-drag recovery may be experienced; i.e., the full theoretical ram drag does not materialize. Once again referring to

Figures 43 and 44 — and to the 9,590 fan rpm comparison in particular — the flow over the upper surface and into the fan at less than supercritical speed must be at a lower velocity in ground effect than in free air to produce the pressure pattern shown. Since the velocity is lower in ground effect, the momentum of the air being turned into the fan is less, and the ram drag is thus necessarily lower in ground effect than in free air. This hypothesis on the behavior of ram drag is strengthened by the observation (Reference 5) that ground-effect machines with raised "flower pot" inlets which are largely free of jet efflux burble — such as the SRN-1 — experience full theoretical ram drag; configurations such as the Princeton machine with flush inlets similar to the subject GETOL model experience much-reduced ram drag.

In summary, the subject model experienced changes with speed in the surrounding flow field similar if not identical to those described by Walker. It also appears that the quantitative behavior of pitching moment, lift, and ram drag can be directly related and attributable to these flow patterns.

Methods of Improving Lift-To-Thrust Ratio

A target value of the lift-to-static thrust ratio in ground effect for the GETOL research program was set at 1.40. This value was not attained with the "A" ducts (Figure 32) but was achieved with the "B" ducts by deflecting the front slot aft 15° and the rear slot forward 15°. The improvement obtained by this deflection of thrust into the base in ground effect can be seen in Figure 45. It is believed that further improvement can be realized by deflecting the tip slot inboard approximately 15°; however, design of the model tip slots precluded testing such a configuration. The lift-to-thrust ratio also would be improved by extending the peripheral slot across the fuselage to produce an unbroken curtain and by designing a fan more compatible to operation with a duct than was used during these tests. Additional studies based on GEM experience and theory would provide even further improvements in lift-to-thrust ratio. As a result of the above findings, the basic exit nozzle deflection configuration was set as 15°/-15°/0° (front slot/rear slot/tip slot). Also shown in Figure 45 are the drag-to-lift ratio and center-of-pressure movement due to this inward thrust deflection. Figure 46 presents the effects of this configuration out of ground effect. There is a slight improvement in free air lift also, but negative base pressures produce a lift-to-thrust ratio less than 1.0 in both cases.

Effect of Thrust Deflection

The method of obtaining forward thrust to accelerate to transition speed initially was intended to be equal deflection of the vanes at all slots. Figures 47 and 48

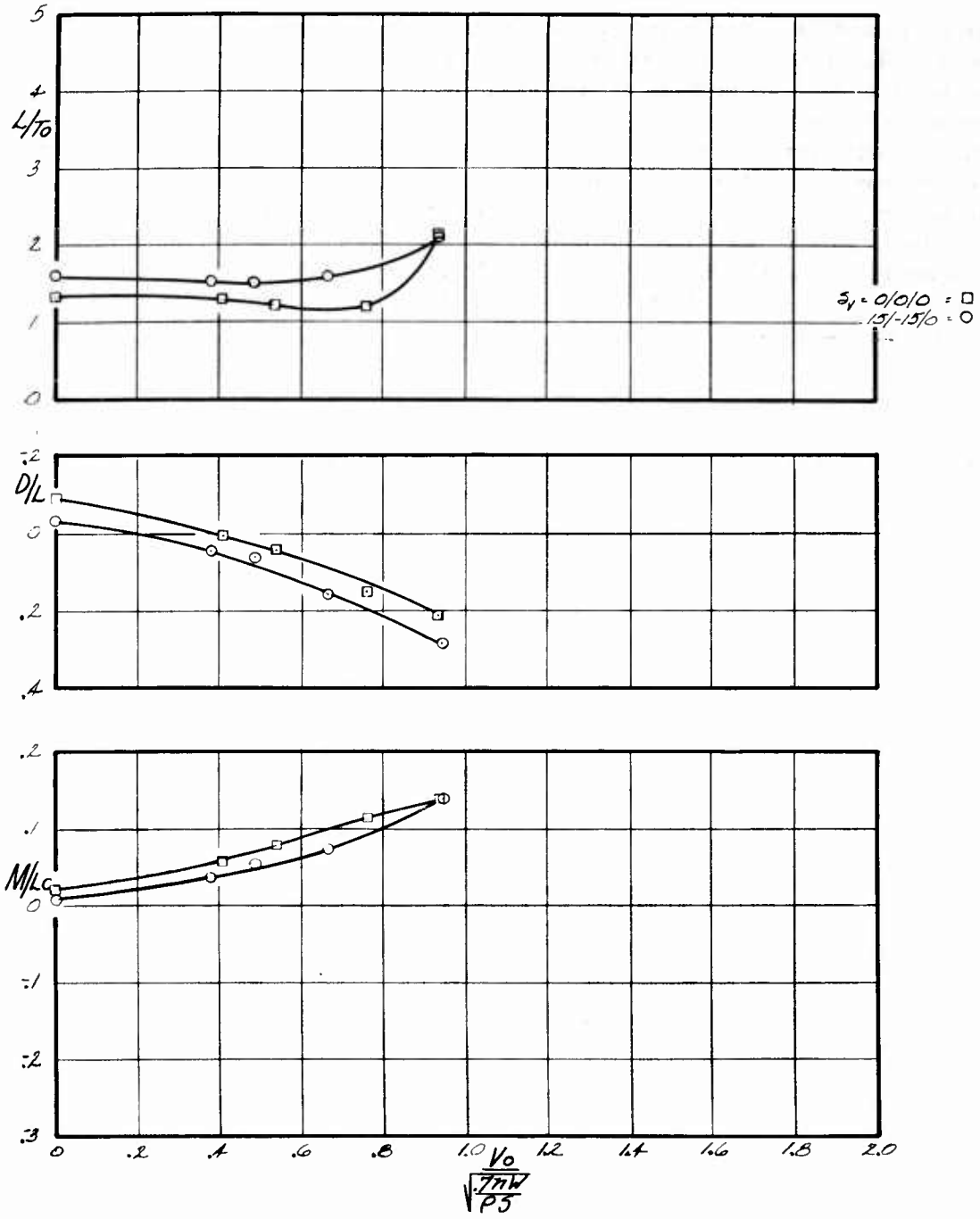

Figure 45. Effect of Canting Front and Rear Slots Inward in Ground Effect With Trimmer Forward — Configuration "B" Ducts
($h/c = 0.115$, $\alpha = 0°$, $\delta_F = 45°$)

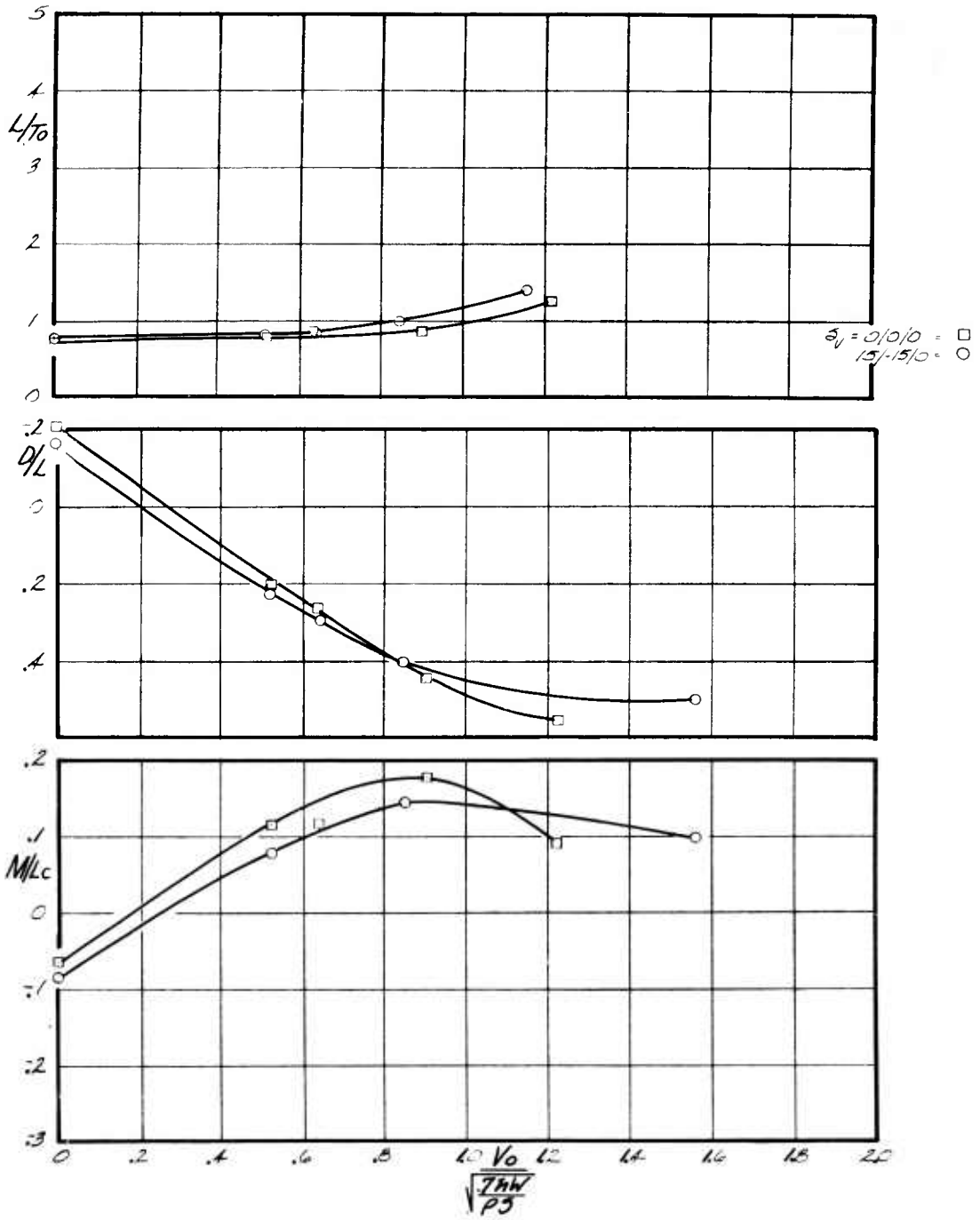

Figure 46. Effect of Canting Front and Rear Slots Inward in Free Air With Trimmer Forward — Configuration "B" Ducts
(h/c = 1.95, α = 0°, δ_F = 45°)

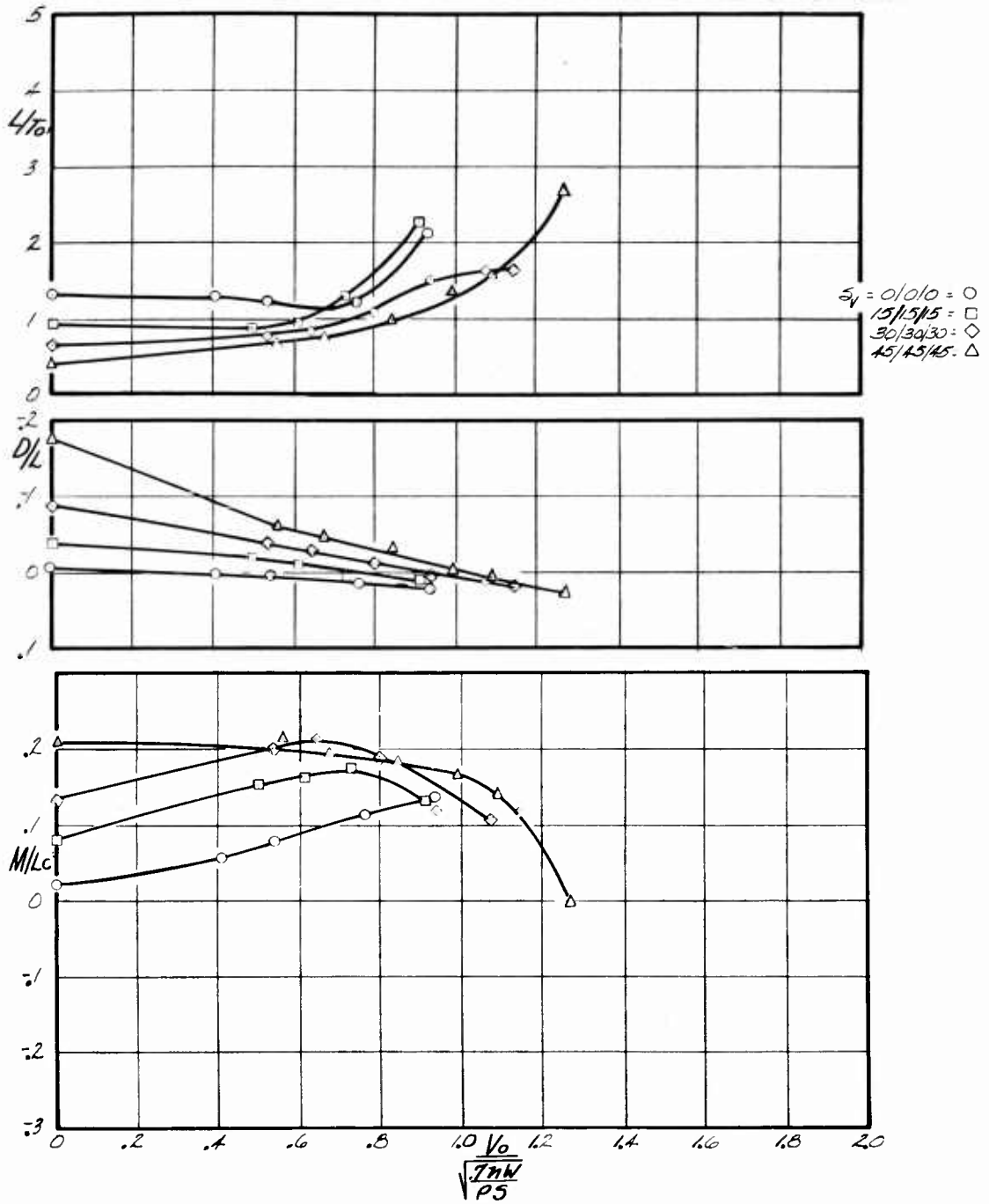

Figure 47. Effect of Equal Vane Deflection in Ground Effect With Trimmer Forward — Configuration "B" Ducts (h/c = 0.115, α = 0°, δ_F = 45°)

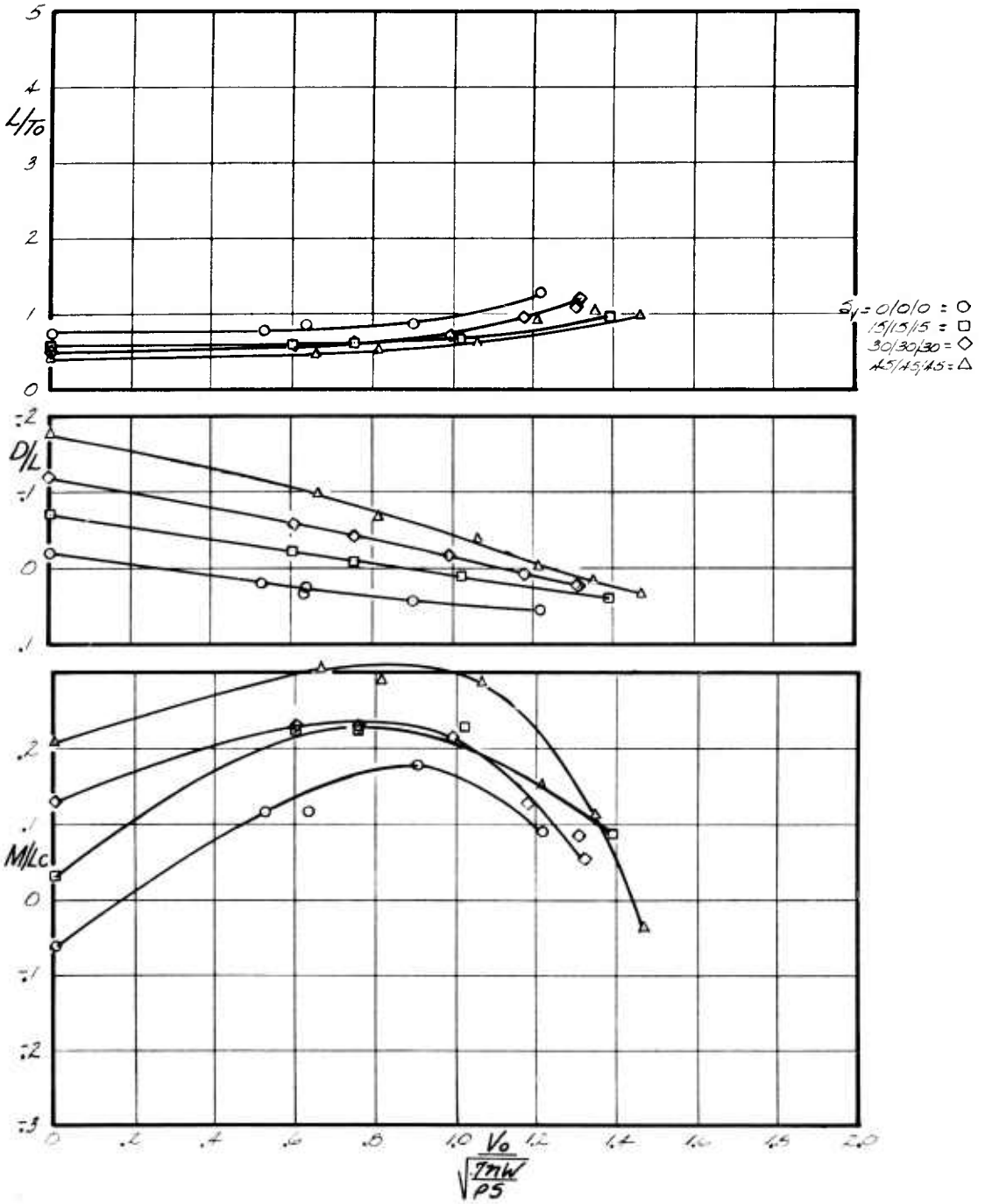

Figure 48. Effect of Equal Vane Deflection in Free Air With Trimmer Forward — Configuration "B" Ducts (h/c = 1.95, α = 0°, δ_F = 45°)

present results of equal vane deflection in and out of ground effect. Large lift losses occur both in ground effect and in free air, with the losses in ground effect being much larger than can be directly attributed to decrease in the vertical component of thrust. The resulting lift-to-thrust and drag-to-lift ratios are too low for any practical use. The drag-to-lift ratio increases negatively with increasing thrust deflection, as would be expected, to a maximum static acceleration of 1.75g.

Falloff in accelerating force at a constant-thrust deflection is proportional to forward speed as the ram drag builds up. The forward movement of center of pressure with increasing thrust deflection results from two causes. As the thrust is deflected, the moment arm of the thrust from the rear slot shortens faster than the arm of the thrust from the forward slot. Figure 49 shows that the pressures on the upper surface ahead of the fan show a marked negative increase as thrust is deflected. This phenomenon apparently is because, with no thrust deflection or small rearward deflection of the front slot, some of the air from the front slot is flowing forward where it is turned back over the model by free-stream velocity. As it passes over the upper surface, it does not have time to accelerate to free-stream velocity and, therefore, causes smaller than expected negative pressures before turning into the fan. As the rearward thrust deflection angle increases, less air flows forward; thus, the velocity over the upper surface is more nearly equal to free stream, and higher negative pressures result. Study has shown that the upper surface pressures ahead of the fan with 45° thrust deflection are essentially the same as the free air pressures, thus upholding the above hypothesis. That these upper surface pressures, with no thrust deflection, are lower in ground effect than in free air also may be a factor in explaining the conclusion that ram drag is lower in ground effect than in free air. This subject is discussed in greater detail later in the report.

The large losses in lift and large forward shifts of center of pressure produced by equal vane deflections lead to the conclusion that this was not an acceptable method of handling the thrust deflection programming. Therefore, data was obtained deflecting the thrust from each slot individually.

Figures 50 and 51 show the effect of deflecting first the thrust from the tip slot, and then from the front slot, in and out of ground effect. When the thrust from the tip slot is deflected 30° aft, there is a marked decrease in total lift produced. However, when the thrust from thr forward slot is also deflected 30°, there appears to be no additional loss in hovering lift. Neither does the deflection of the thrust from the front slot produce any additional accelerating force in ground effect. Maximum center-of-pressure shift caused by tip thrust deflection is approximately 4% forward. Once again, deflection of thrust from the front slot

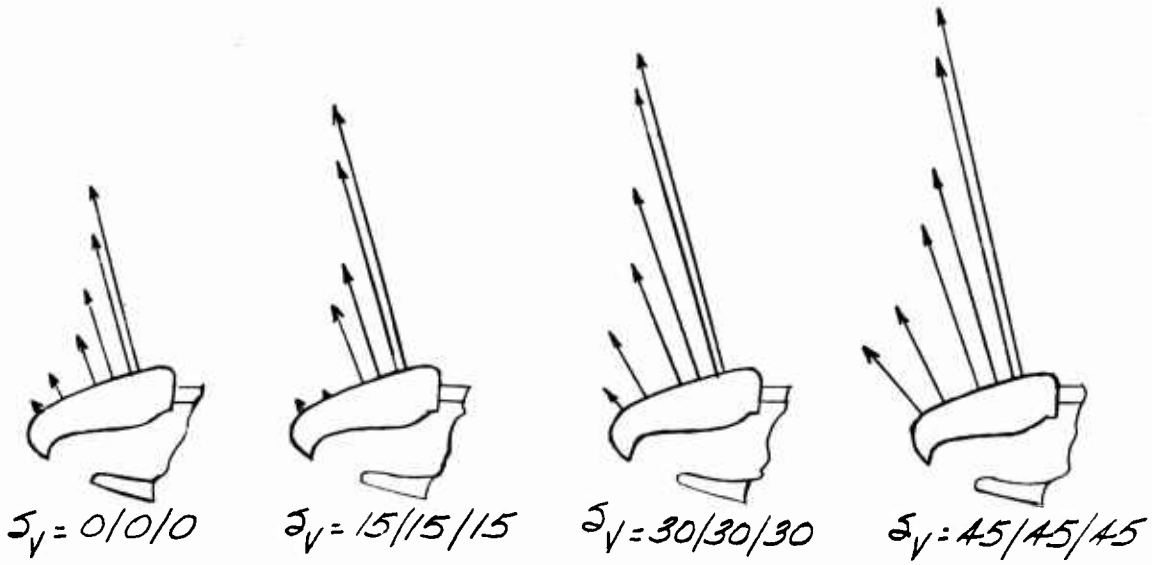

Figure 49. Effect of Equal Vane Deflection on Upper Surface Leading Edge Pressures in Ground Effect — Configuration "B" Ducts ($\alpha = 0°$, $q = 1.5$, $h/c = 0.115$)

to 30° produces no additional change. With both front and tip slot thrust deflected 30°, the lift-to-thrust ratio increases more rapidly with forward velocity than with only the tip thrust deflected. Therefore, it seems advisable to deflect the front and tip slots together, rather than the tip alone initially. An additional effect to be considered, however, is the change caused by trimming out the pitching moments. Although described in detail later, it is sufficient to say that when the moment is trimmed out, it is preferable first to deflect the tip slot and then, at some given velocity, to deflect the front slot.

Deflection of the thrust from the front and tip slots having been considered, the effect of deflecting the rear slot thrust remains to be considered. Figures 52 and 53 show the effect of deflecting the rear slot from zero to 45° while the tip and front slots are constant at 45°. Note that the trimmers is aft in these two figures, whereas all previous figures were with trimmer forward. The effect of the trimmer being aft is that the lift-to-thrust ratio is slightly higher and the center of pressure further aft. From the two figures it can be seen that deflecting the thrust from the rear slot causes a large loss in lift and a 15% forward shift of the center of pressure in ground and approximately 25% forward shift out of ground. It also can be seen that the accelerating force is improved only

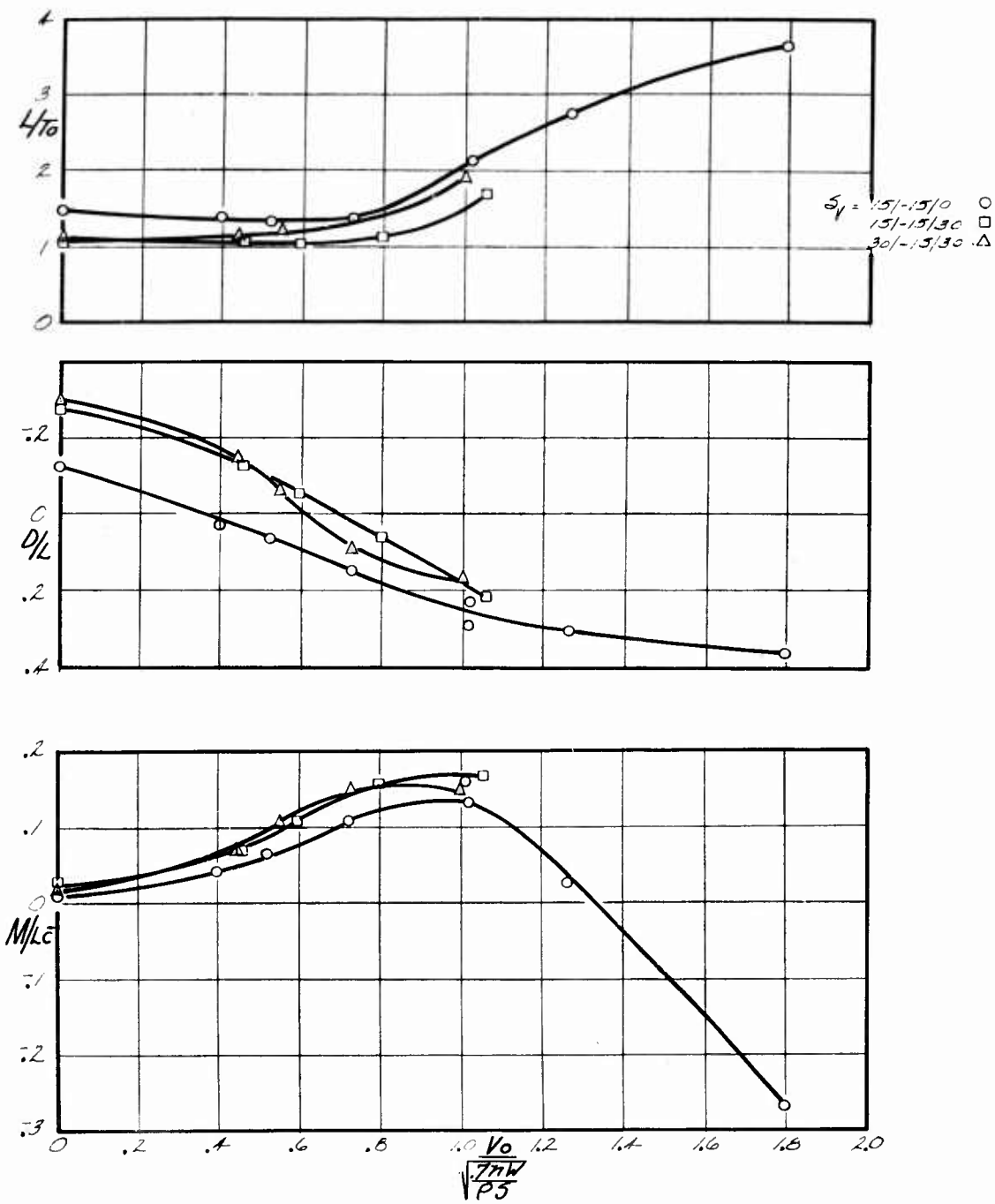

Figure 50. Effect of Tip and Front Vane Deflections in Ground Effect With Trimmer Forward — Configuration "B" Ducts
($h/c = 0.115$, $\alpha = 0°$, $\delta_F = 30°$)

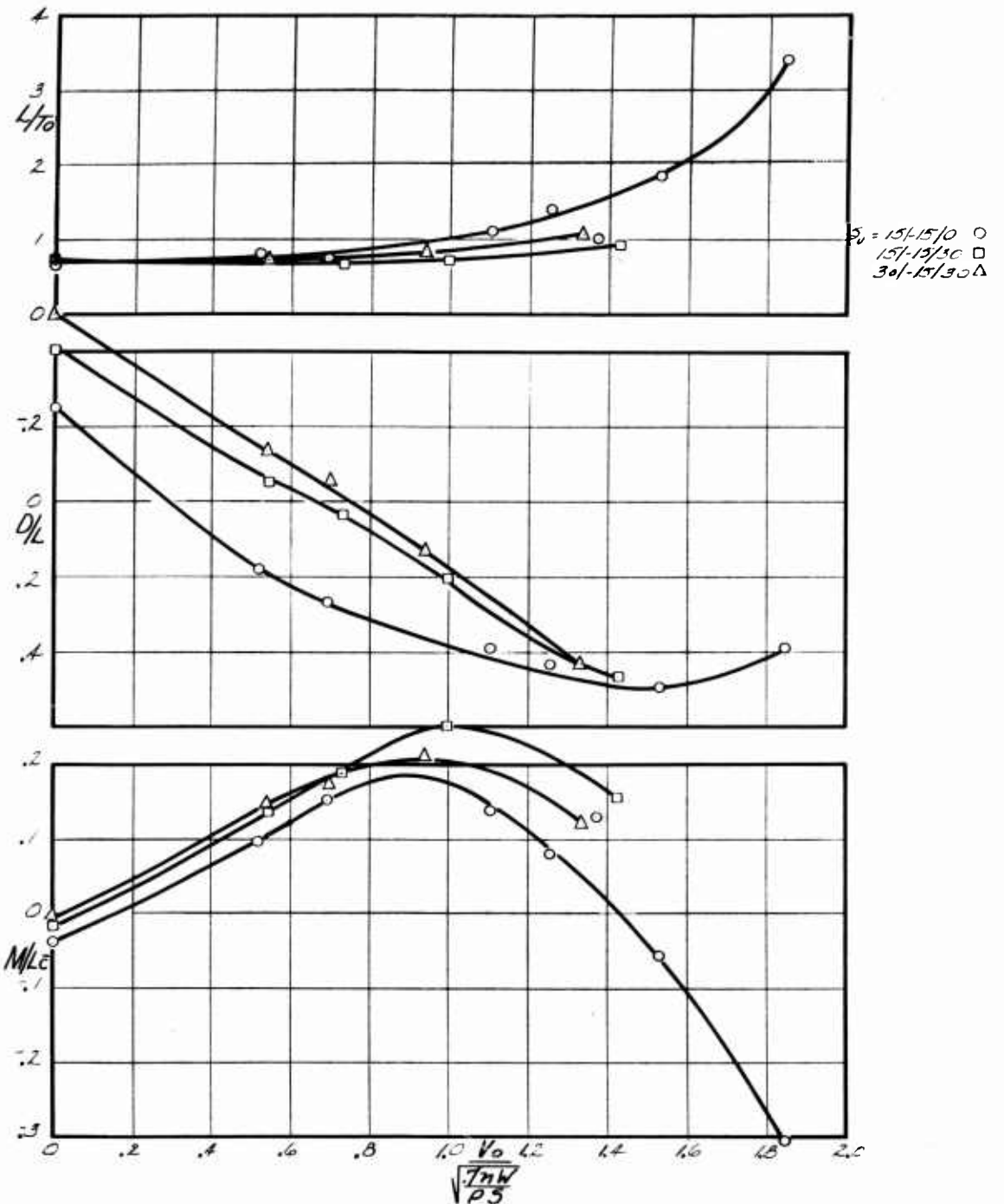

Figure 51. Effect of Tip and Front Vane Deflections in Free Air With Trimmer Forward — Configuration "B" Ducts (h/c = 1.95, α = 0°, δ_F = 30°)

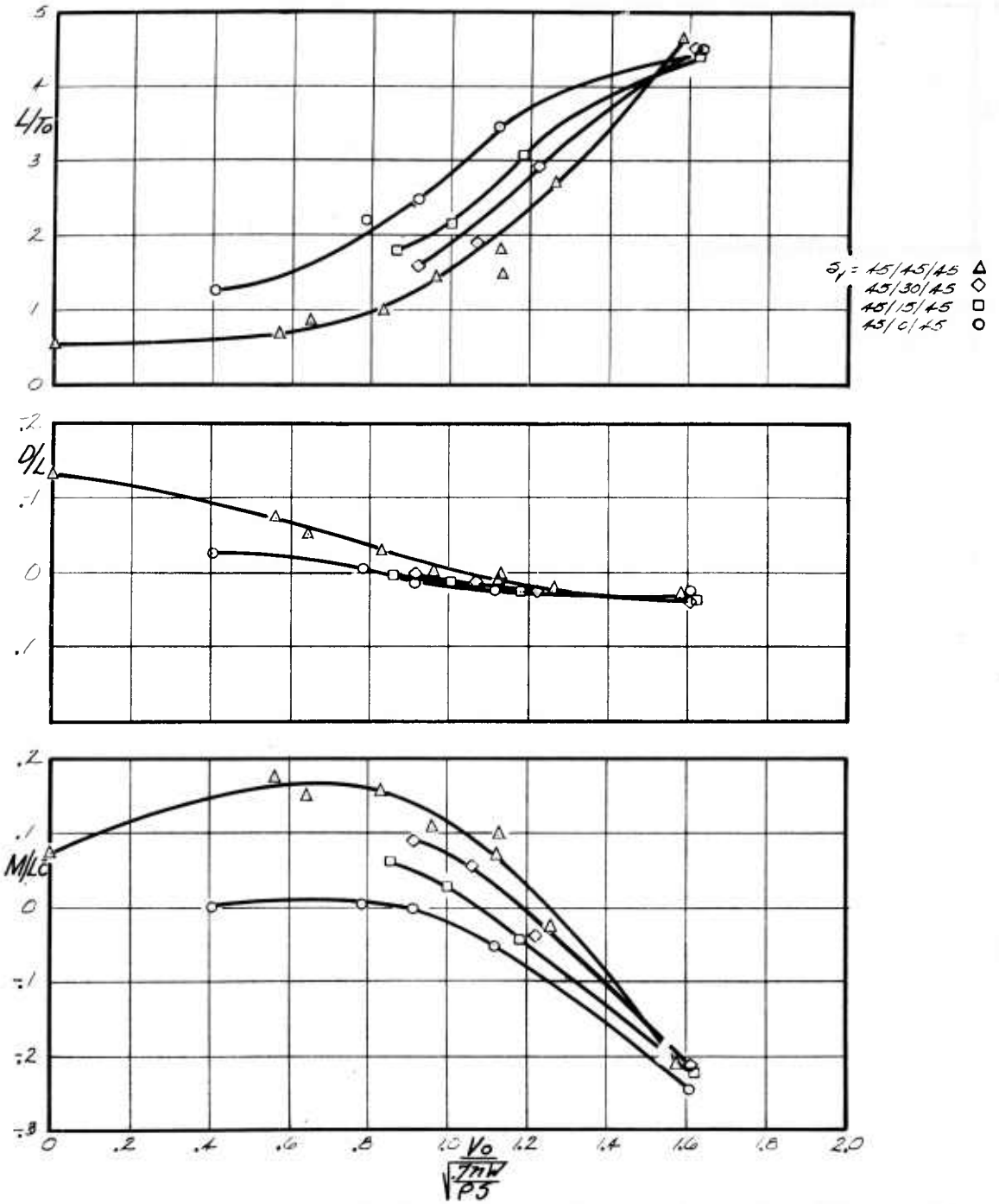

Figure 52. Effect of Rear Slot Deflection in Ground Effect With Trimmer Aft — Configuration "B" Ducts (h/c = 0.115, α = 0°, δ_F = 45°)

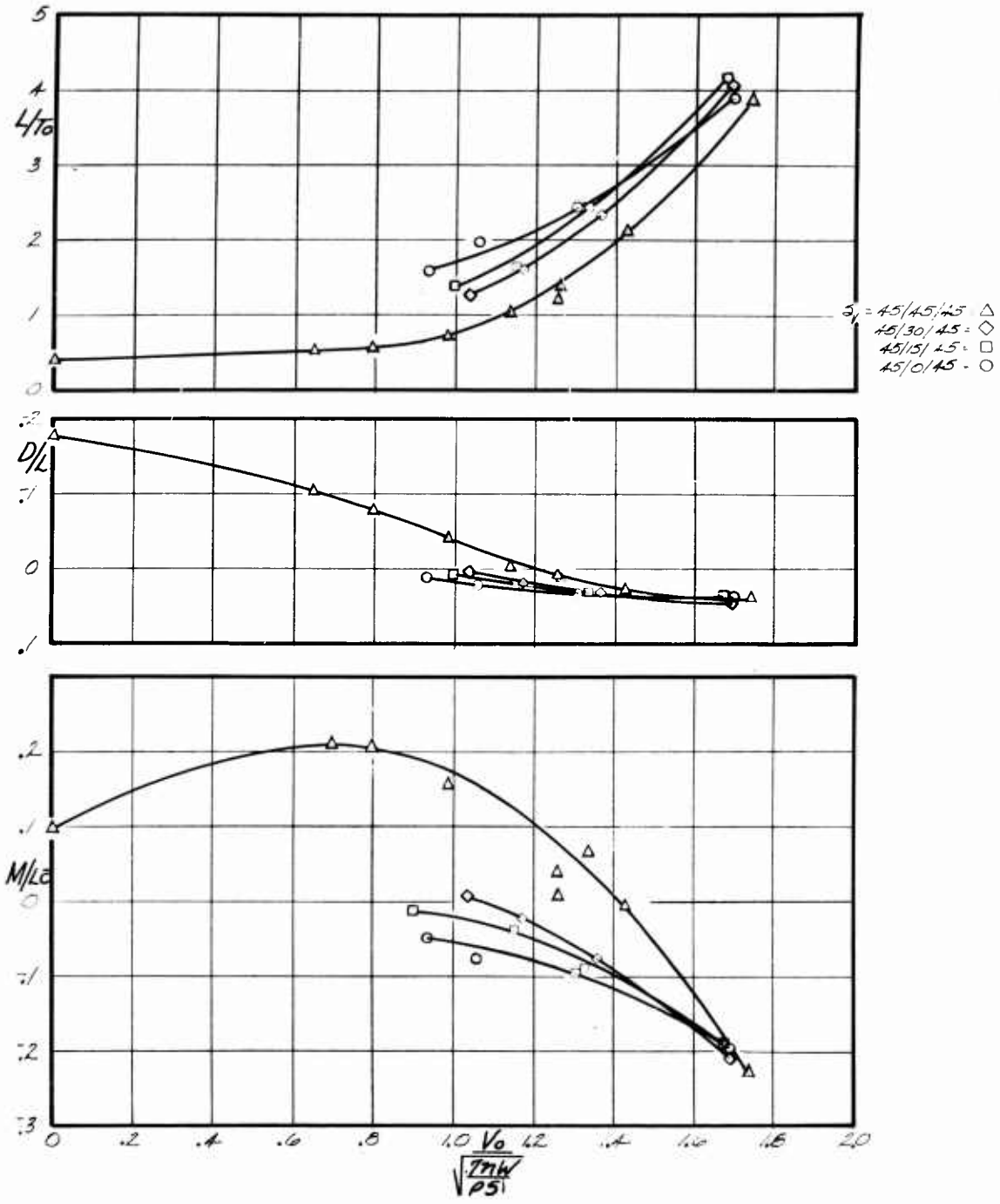

Figure 53. Effect of Rear Slot Deflection in Free Air With Trimmer Aft — Configuration "B" Ducts (h/c = 1.95, $\alpha = 0°$, $\delta_F = 45°$)

slightly by the use of rear slot deflection. The loss of lift occurs because base pressures are simply pumped from under the model when the rear curtain is deflected aft. The large center-of-pressure shift is due to the greatly foreshortened moment arm of the thrust from the rear slot when it is deflected aft. The above considerations make it inadvisable to use rear slot deflection for accelerating force except at velocities near transition speed.

Figures 54 and 55 present data with the front and rear slots deflected forward to produce a decelerating force. This data also is presented with the trimmer in the aft position. In ground effect, the only appreciable change is the increase in drag. Out of ground, the center of pressure moves aft approximately 5% in addition to the large drag increase. In view of this data, there appears to be no problem in achieving deceleration capability.

In summary, it may be said that all vane deflections, with the exception of inward deflection, gave disappointing results due to excessive lift losses over what would have been predicted by the cosine law. If used, the most satisfactory programming of thrust deflection for forward acceleration appears to be to first deflect the tip slot, then the front slot, and avoid deflection of the rear slot until near transition speed. For the fan pressure ratio tested, it does not appear possible to provide sufficient acceleration by means of deflected thrust to attain transition speed; therefore, the cruise engines, or some nozzle bypass scheme, would have to be used to provide additional accelerating force.

Origin of Pitch-Up

The subject of pitch-up is ever present in any discussion of a vehicle which makes transition from a powered, air-moving lift system at hover and very low speeds to aerodynamic lift at flying speeds. The following explains the origin of this pitch-up as it applies to the GETOL vehicle.

Figures 56 and 57 are representative plots of the center-of-pressure movement as read from the main and fan balances for three-exit vane configurations — 15°/-15°/0°, 15°/-15°/15° and 30°/30°/30° — all in ground effect. The fan balance data includes only the moments acting on the fan-duct assembly, whereas, the main balance data includes the moments on the fan-duct assembly, plus those on the wing-fuselage. Therefore, the increment between the two curves is that center-of-pressure movement due to forces acting on the exterior of the model. In general, the moments on the fan balance are caused by pressures on the lip of the fan and the forces at the duct exits. The nose-up moment on the fan balance in Figure 57 is due to the fact that with the thrust deflected aft 30°/30°/30°, the moment arm of the thrust vector from the rear slot is considerably shorter than

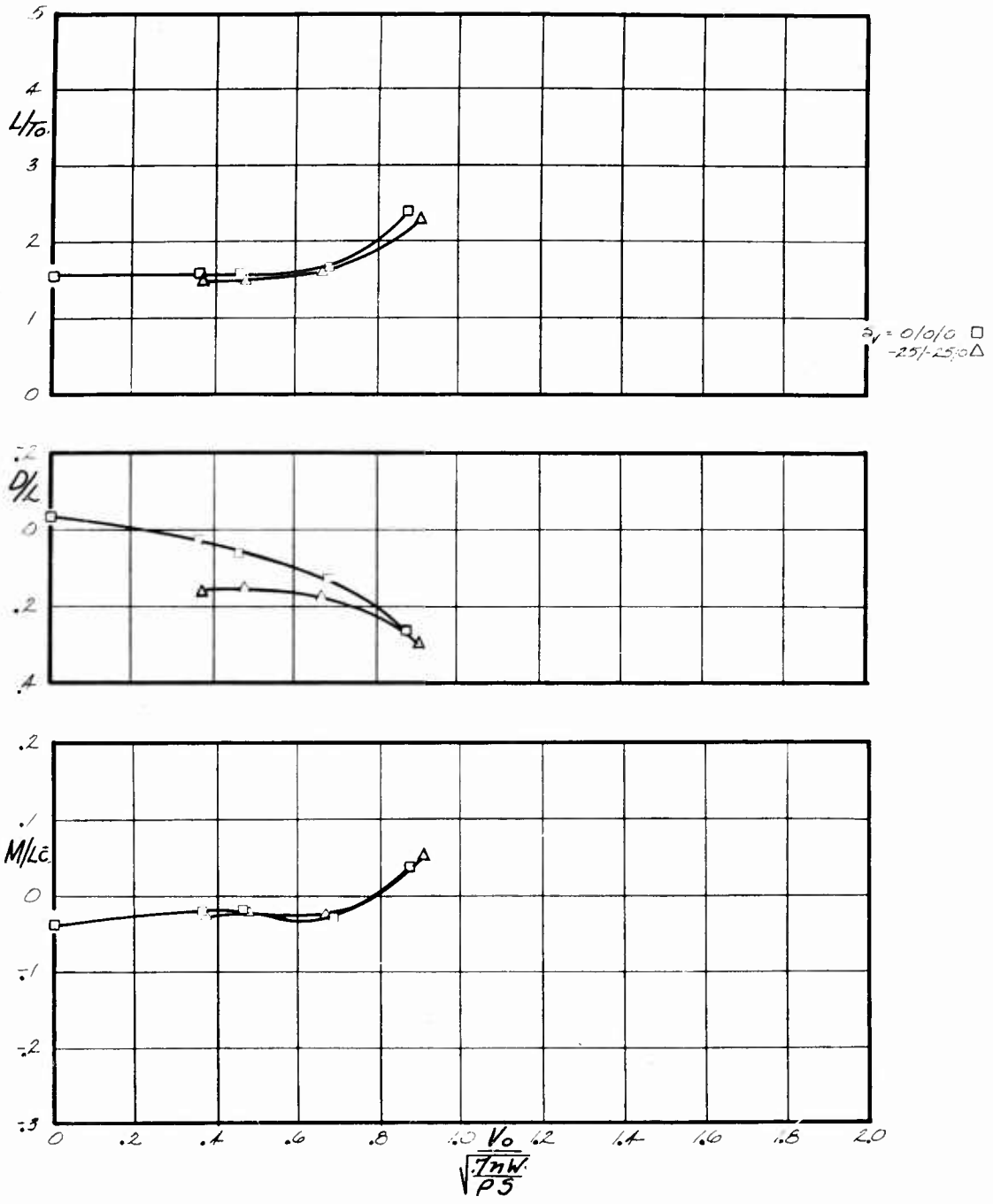

Figure 54. Effect of Deflecting Thrust Forward for Deceleration in Ground Effect With Trimmer Aft — Configuration "B" Ducts ($h/c = 0.115$, $\alpha = 0°$, $\delta_F = 45°$)

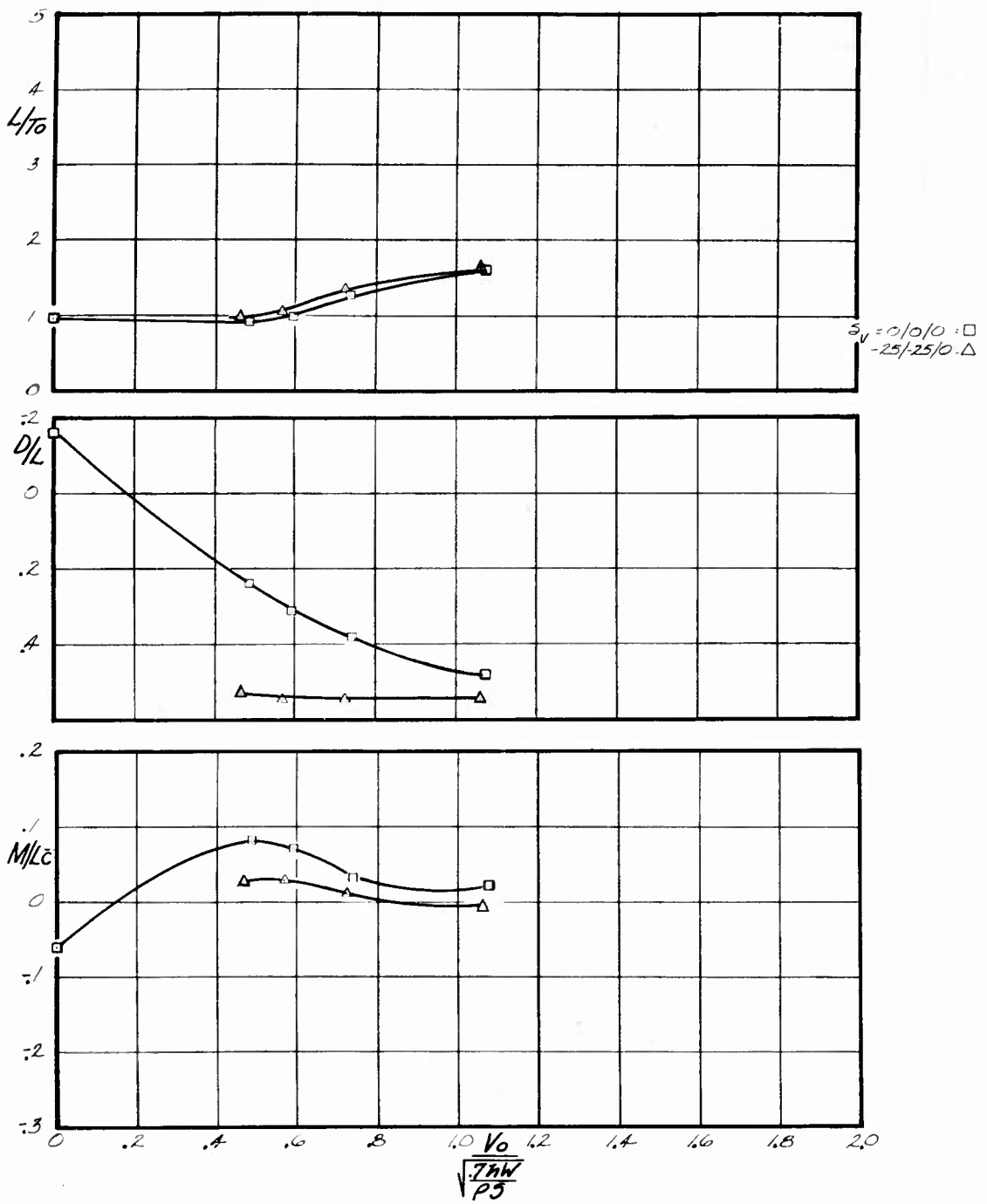

Figure 55. Effect of Deflecting Thrust Forward for Deceleration in Free Air With Trimmer Aft — Configuration "B" Ducts
(h/c = 1.95, α = 0°, δ_F = 45°)

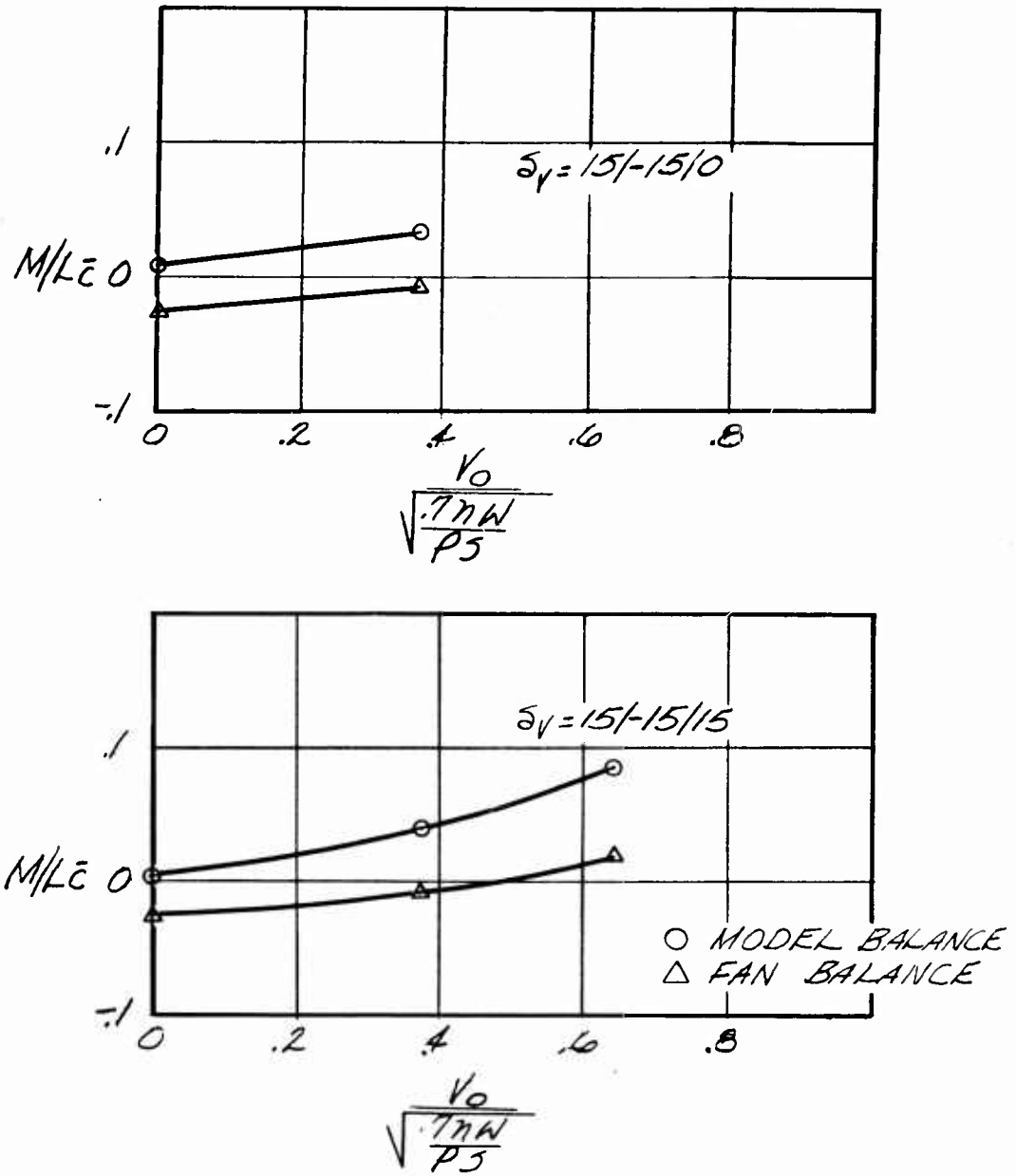

Figure 56. Center of Pressure Variation With Forward Velocity in Ground Effect With Trimmer Forward — Configuration "B" Ducts ($h/c = 0.115, \alpha = 0°$)

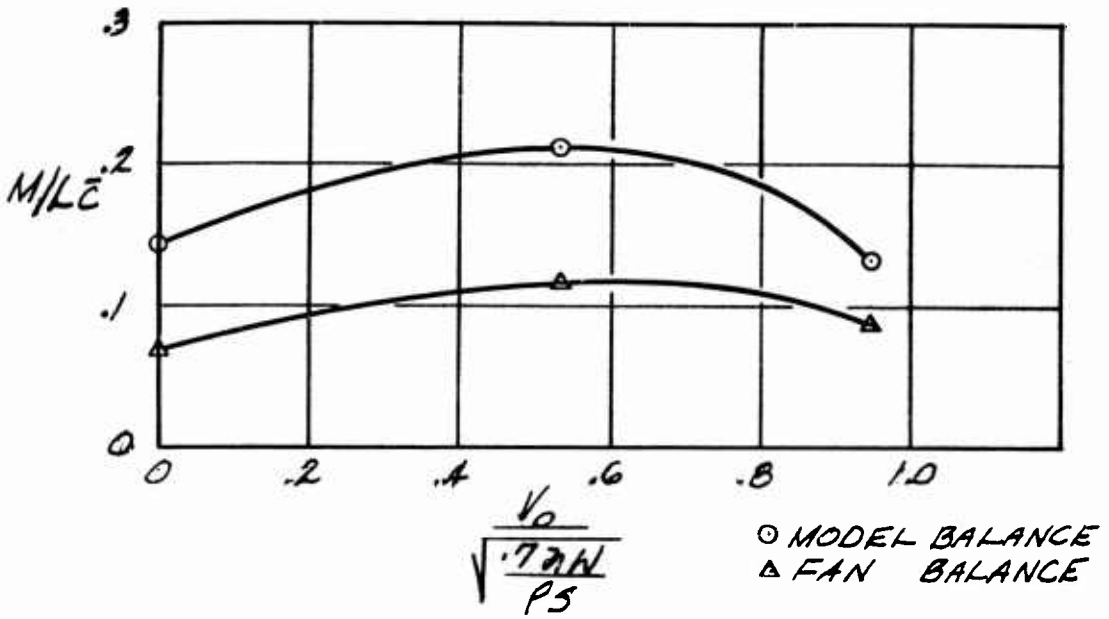

Figure 57. Center of Pressure Location With Forward Velocity in Ground Effect With Trimmer Forward — Configuration "B" Ducts ($h/c = 0.115$, $\delta_V = 30°/30°/30°$, $\alpha = 0°$)

that from the front slot. Figures 58 through 64 show the surface pressures acting on the wing at the fan centerline with tunnel q's of 0 and 1.5 for the 15°/-15°/0° and 15°/-15°/15° cases, and tunnel q's of 0, 1.5 and 9.3 for the 30°/30°/30° case. Fan rpm is 9,590 in every case. The vectors are plotted to a scale of 1 inch equals 0.04 psi pressure. In the static condition, the pressures fore and aft of the fan on the upper surface of the wing are approximately equal and in the same direction, so produce little pitching moment. The pressures on the base, between the front and rear slot, are fairly well balanced fore and aft so that they do not produce any appreciable pitching moment. Therefore, the increment on the figures, at hover, must be the result of the negative pressures acting on the undersurface of the wing aft of the rear slot. These pressures, and the incremental pitching moment at hover, are higher for the 30°/30°/30° thrust deflection case than for either of the other two because of the direction of flow from the rear slot. When air is blown over the model, the situation changes somewhat. The pressures on the base remain oriented approximately the same and, if anything, tend to produce a nose-down pitching moment, while the pressures at the rear undersurface of the wing increase negatively and produce a slightly larger nose-up moment than at hover. The most significant change with forward speed is in the pressures on the upper surface ahead of the fan. As can

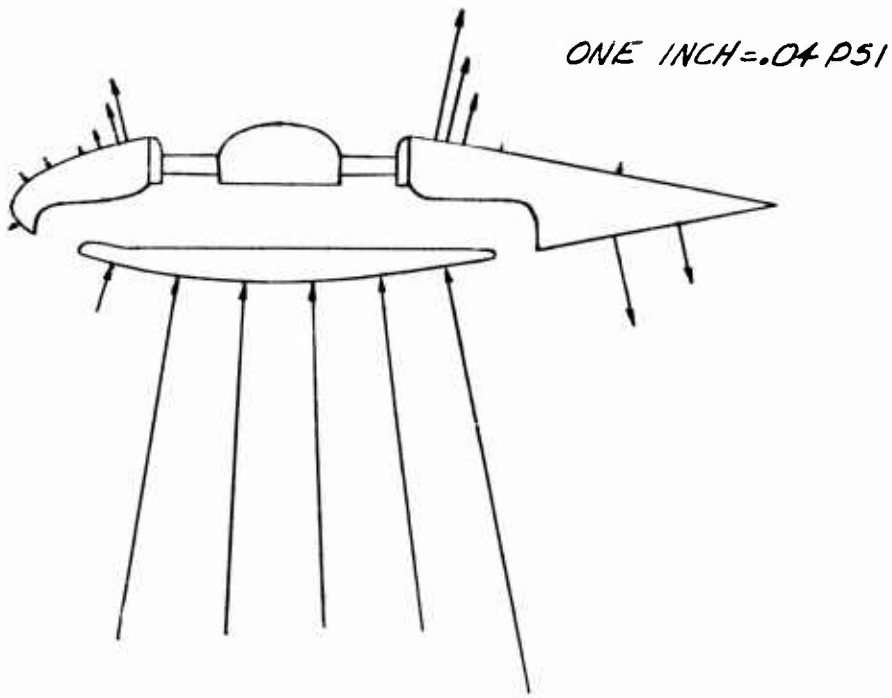

Figure 58. Pressure Distribution at Fan Centerline in Ground Effect With Trimmer Forward — Configuration "B" Ducts ($q = 0$, $h/c = 0.115$, $\delta_V = 15°/-15°/0°$, RPM = 14,000, $q_{jet} \cong 27$ PSF, $\alpha = 0°$)

be seen from the illustrations, these pressures increase quite markedly with forward velocity and in conjunction with the pressures aft of the fan (which have reversed from the static condition) produce a definite nose-up pitching moment as a function of forward speed. This is the origin of pitch-up on the GETOL vehicle. Note that although Figure 64 indicates a larger center-of-pressure shift at 9.3 q_T than at hover or 1.5 q_T, Figure 57 shows that it does not materialize. This is probably due to the increased effectiveness of the horizontal tails in producing nose-down pitching moment by virtue of the higher Reynolds' number at higher tunnel q.

Study of the pressure data in Figures 58, 60 and 62 reveals the effect of deflecting the thrust on the base pressures and total lift. Figure 58, the basic configuration with no rearward thrust deflection for acceleration, reveals an essentially even base pressure distribution with the exception of the area directly behind the front slot. This is probably a result of the front slot being deflected 15° aft. Figure 60 differs from the above figure only by the 15° deflection of the tip slot.

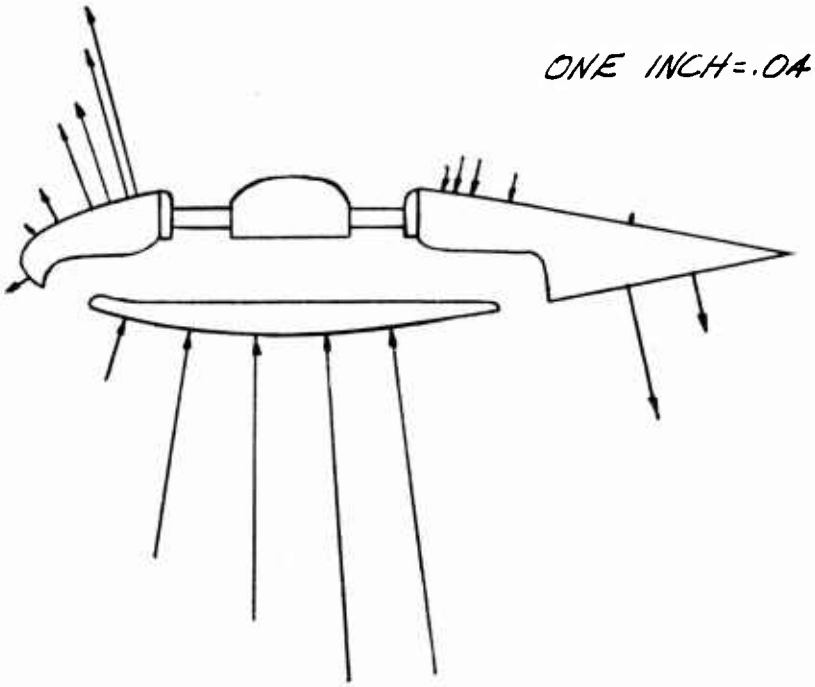

Figure 59. Pressure Distribution at Fan Centerline in Ground Effect With Trimmer Forward — Configuration "B" Ducts ($q = 1.5$, $h/c = 0.115$, $\delta_V = 15°/-15°/0°$, RPM = 14,000, $q_{jet} \cong 27$ PSF, $\alpha = 0°$)

As can be seen, the low-pressure area aft of the rear slot has been widened and the level of the rest of the base is somewhat reduced. Figure 62, which has all vanes deflected 30° aft, has blown the base pressure away to the extent that a portion of the base feels negative pressures. This supports and explains the force data presented in the preceding section as to the effect of thrust deflection on the longitudinal characteristics.

Effect of Angle of Attack

The effect of angle of attack on lift-to-thrust ratio, drag-to-lift ratio and center-of-pressure movement, both in and out of ground effect, is shown in Figures 65 and 66 with trimmer forward, and on Figures 67 and 68 with trimmer aft. Angle-of-attack effect on base pressures in and out of ground effect with trimmer forward, is shown in Figures 69 and 70 at a tunnel dynamic pressure of 1.5 psi and 9,590 rpm. Angle of attack, in the low-speed range, produced an almost negligible effect on lift and center-of-pressure movement, but did cause an increase in drag due to the tilting of the thrust vector. As the angle of attack increased, aerodynamic lift became a factor at progressively lower speeds and thus caused

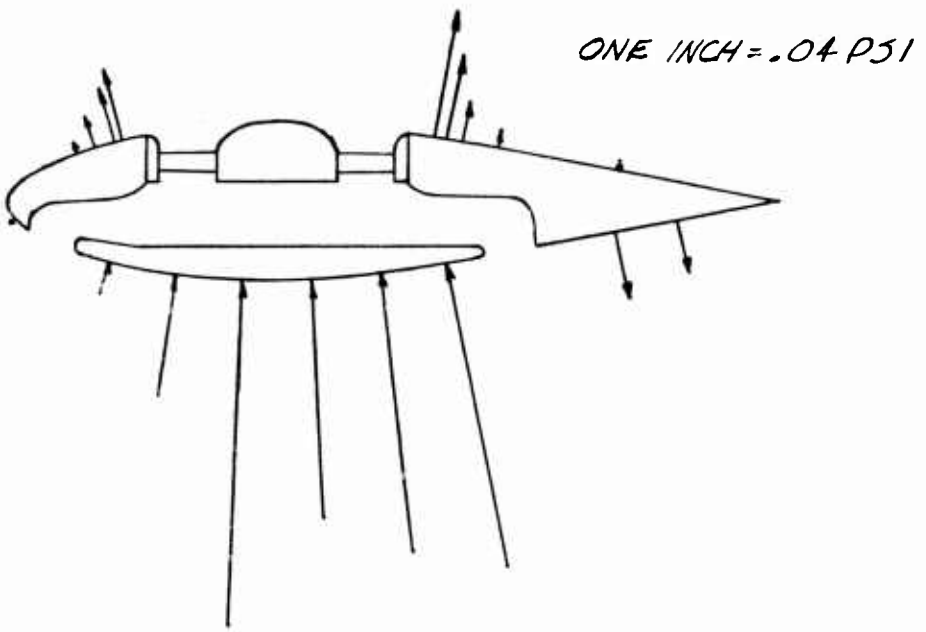

Figure 60. Pressure Distribution at Fan Centerline in Ground Effect With Trimmer Forward — Configuration "B" Ducts ($q = 0$, $h/c = 0.115$, $\delta_V = 15°/-15°/15°$, RPM = 14,000, $q_{jet} \cong 27$ PSF, $\alpha = 0°$)

the break in the lift-to-thrust ratio curve to occur at progressively lower speeds. The character of the force data is explained by the pressure profiles of Figures 69 and 70 which indicate only small differences in lift between the two angles of attack in the low-speed range.

Note that the effect of angle of attack is less marked with the trimmer aft than forward. This is attributed to flow leaking out the sides of the open area where the rear slot was moved aft and detrimentally affecting the flow around the horizontal tails. If the lift of the horizontal tail is affected, the change also would appear on the pitching moments, as shown in the illustrations. With the trimmer forward, the effectiveness of the horizontal tails causes the center-of-pressure curve to break at lower speeds after a shorter incremental forward movement as the angle of attack increases. With the trimmer aft, however, the reverse is true, indicating that the horizontal tails are not producing the same effect as with the trimmer forward. Further study of the center-of-pressure curves indicates that a slight attitude instability occurs at hover and in the low-speed range. With the trimmer forward, and in ground effect with the trimmer aft, the curves cross over as the horizontal tails become effective and attitude stability is achieved at higher forward speeds. The drag-to-lift ratio, initially more positive with

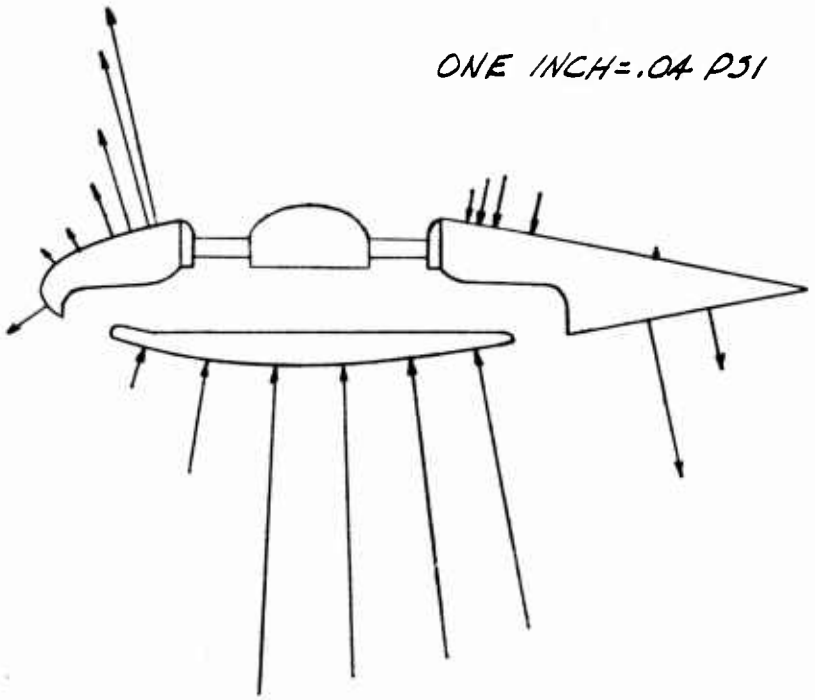

Figure 61. Pressure Distribution at Fan Centerline in Ground Effect With Trimmer Forward — Configuration "B" Ducts (q = 1.5, h/c h/c = 0.115, δ_V = 15°/-15°/15°, RPM = 14,000, $q_{jet} \cong 27$ PSF, α = 0°)

increased angle of attack due to the tilting of the thrust vector, reverses and becomes decreasingly positive with increasing angle of attack beyond the velocity at which the lift curve break occurs.

In summary, it may be said that angle of attack:

1. Causes the sharp increase in lift-to-thrust ratio to occur at lower forward speed.

2. Causes increased drag at hover, but decreased drag-to-lift ratio at the higher speeds.

3. Causes the center of pressure to move aft after a shorter forward movement.

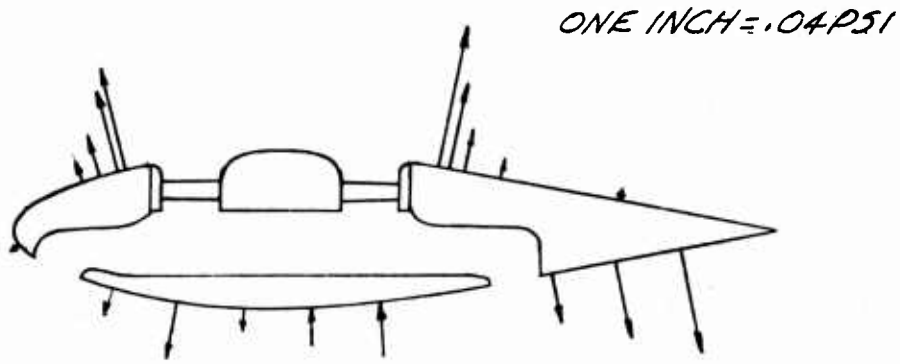

Figure 62. Pressure distribution at Fan Centerline in Ground Effect With Trimmer Forward — Configuration "B" Ducts (q = 0, h/c = 0.115, δ_V = 30°/30°/30°, RPM = 14,000, $q_{jet} \cong$ 27 PSF, α = 0°)

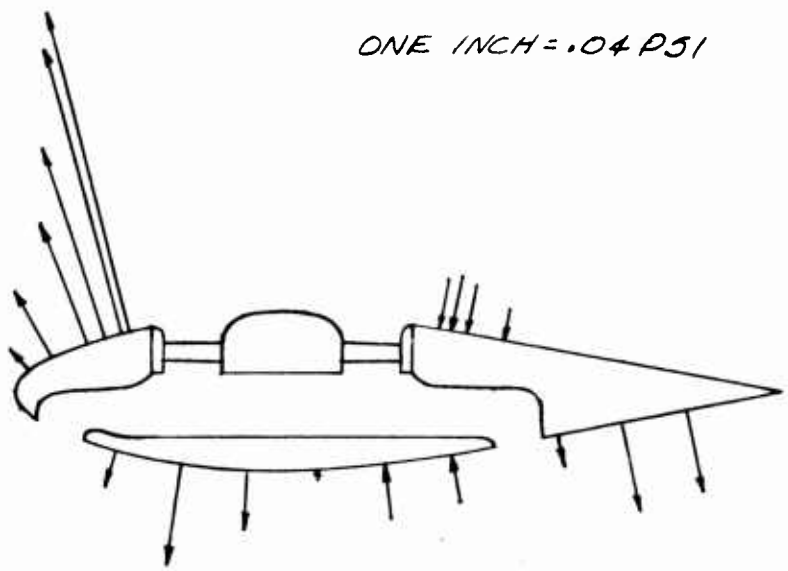

Figure 63. Pressure Distribution at Fan Centerline in Ground Effect With Trimmer Forward — Configuration "B" Ducts (q = 1.5, h/c = 0.115, δ_V = 30°/30°/30°, RPM = 14,000, $q_{jet} \cong$ 27 PSF, α = 0°)

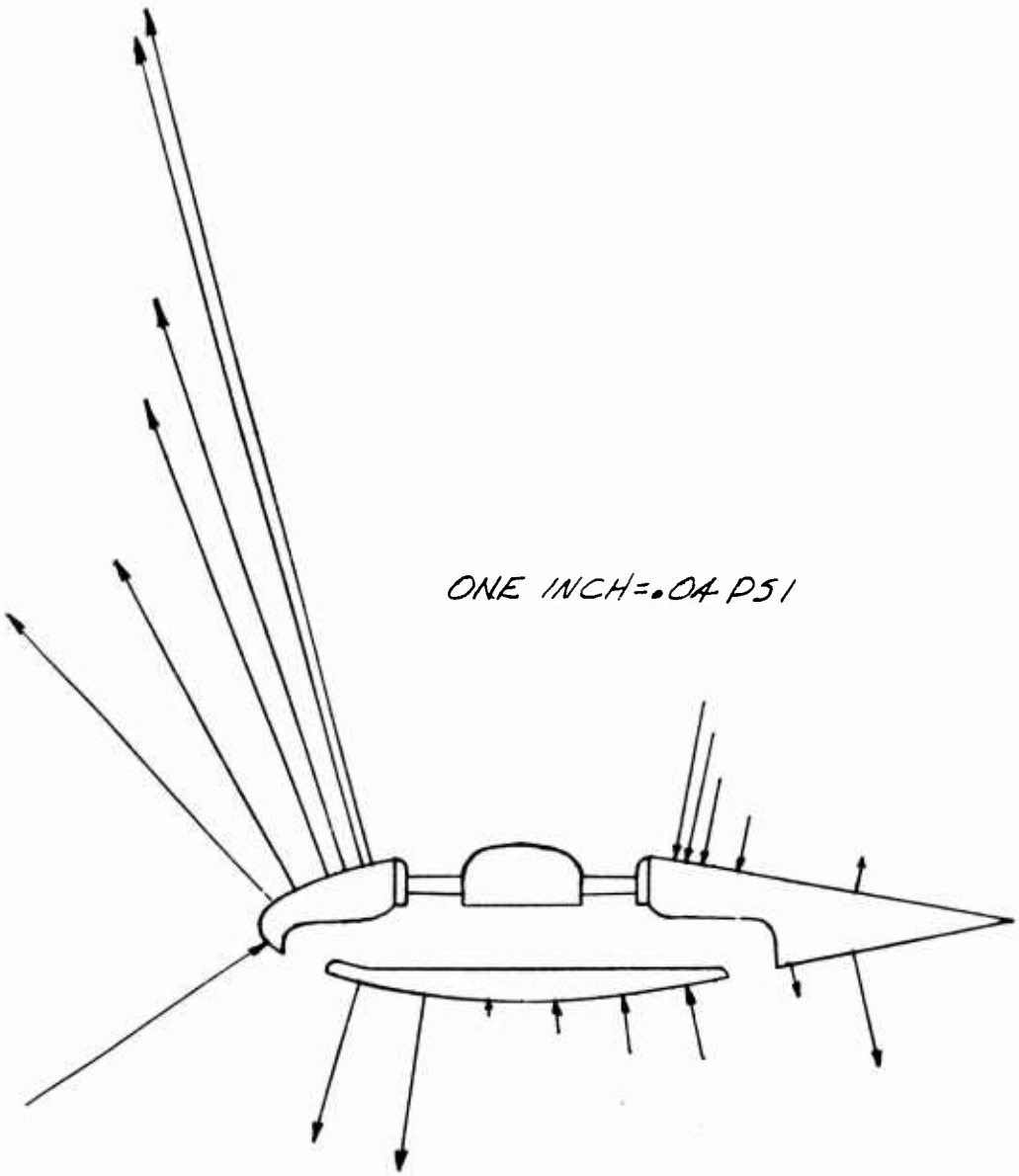

Figure 64. Pressure Distribution at Fan Centerline in Ground Effect With Trimmer Forward — Configuration "B" Ducts ($q = 9.3$, $h/c = 0.115$, $\delta_V = 30°/30°/30°$, RPM = 14,000, $q_{jet} \cong 27$ PSF, $\alpha = 0°$)

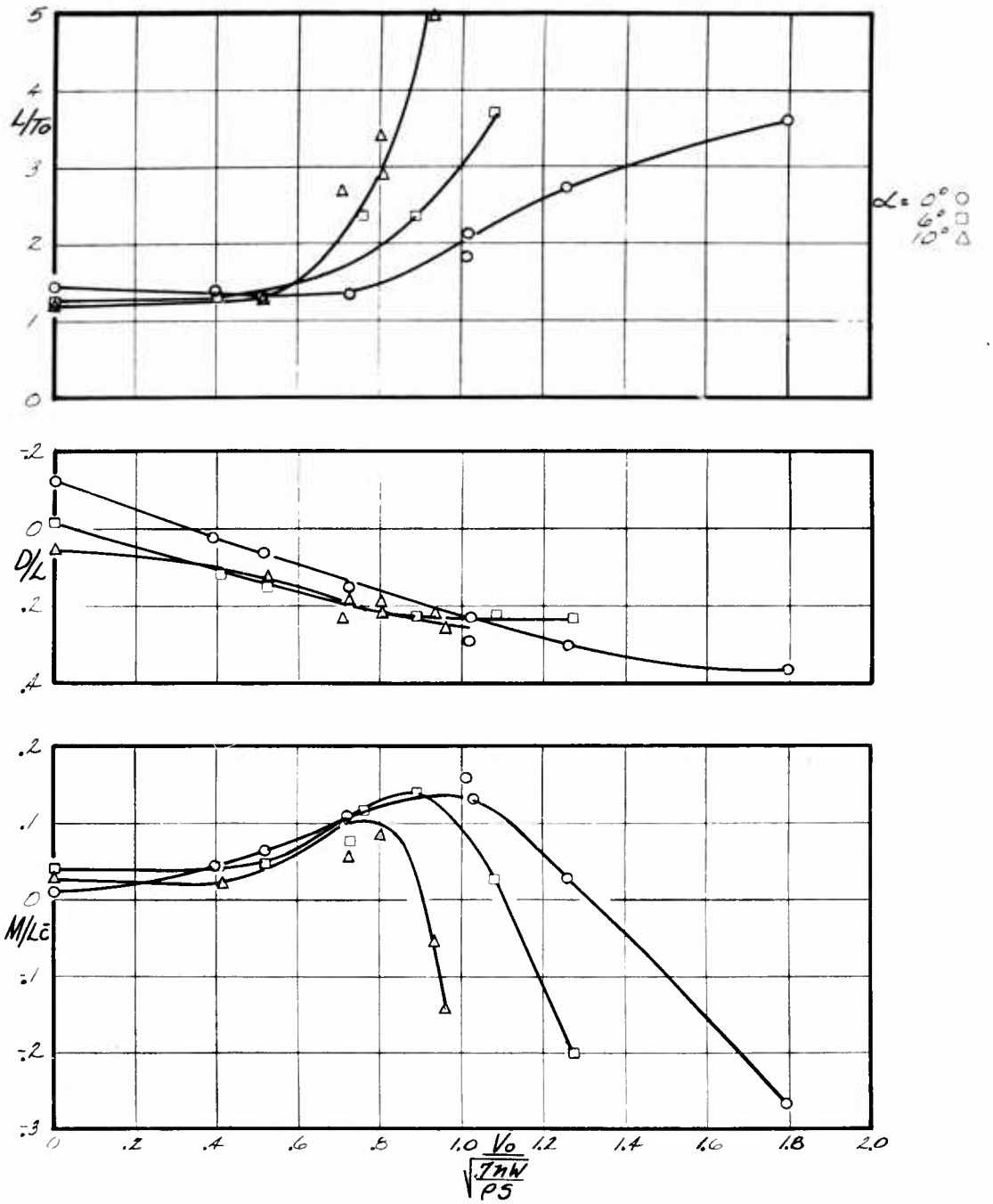

Figure 65. Effect of Angle of Attack in Ground Effect With Trimmer Forward — Configuration "B" Ducts (h/c = 0.115, δ_V = 15° /-15° /0° , δ_F = 30°)

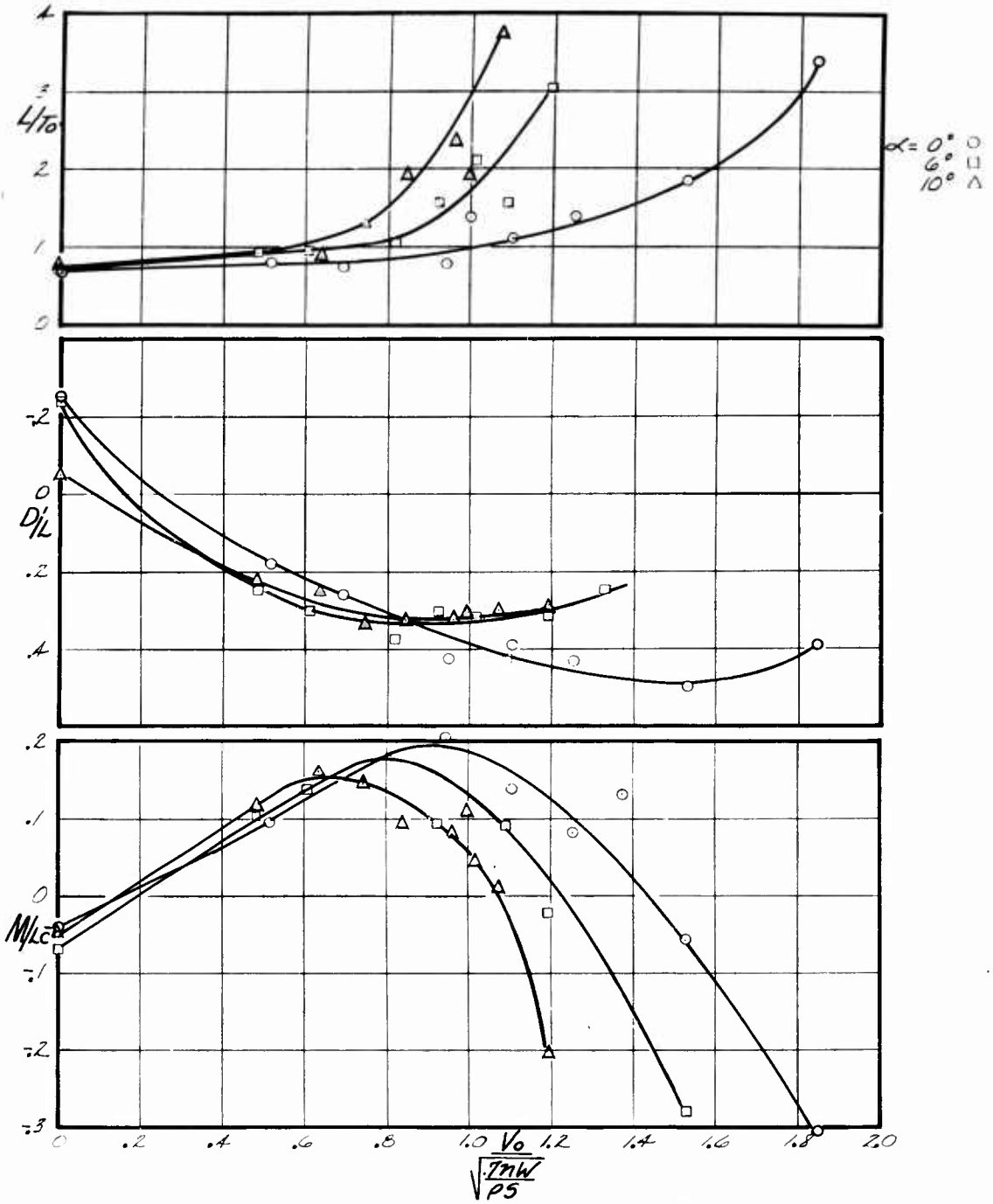

Figure 66. Effect of Angle of Attack in Free Air With Trimmer Forward — Configuration "B" Ducts (h/c = 1.95, δ_V = 15° /-15° /0° , δ_F = 30°)

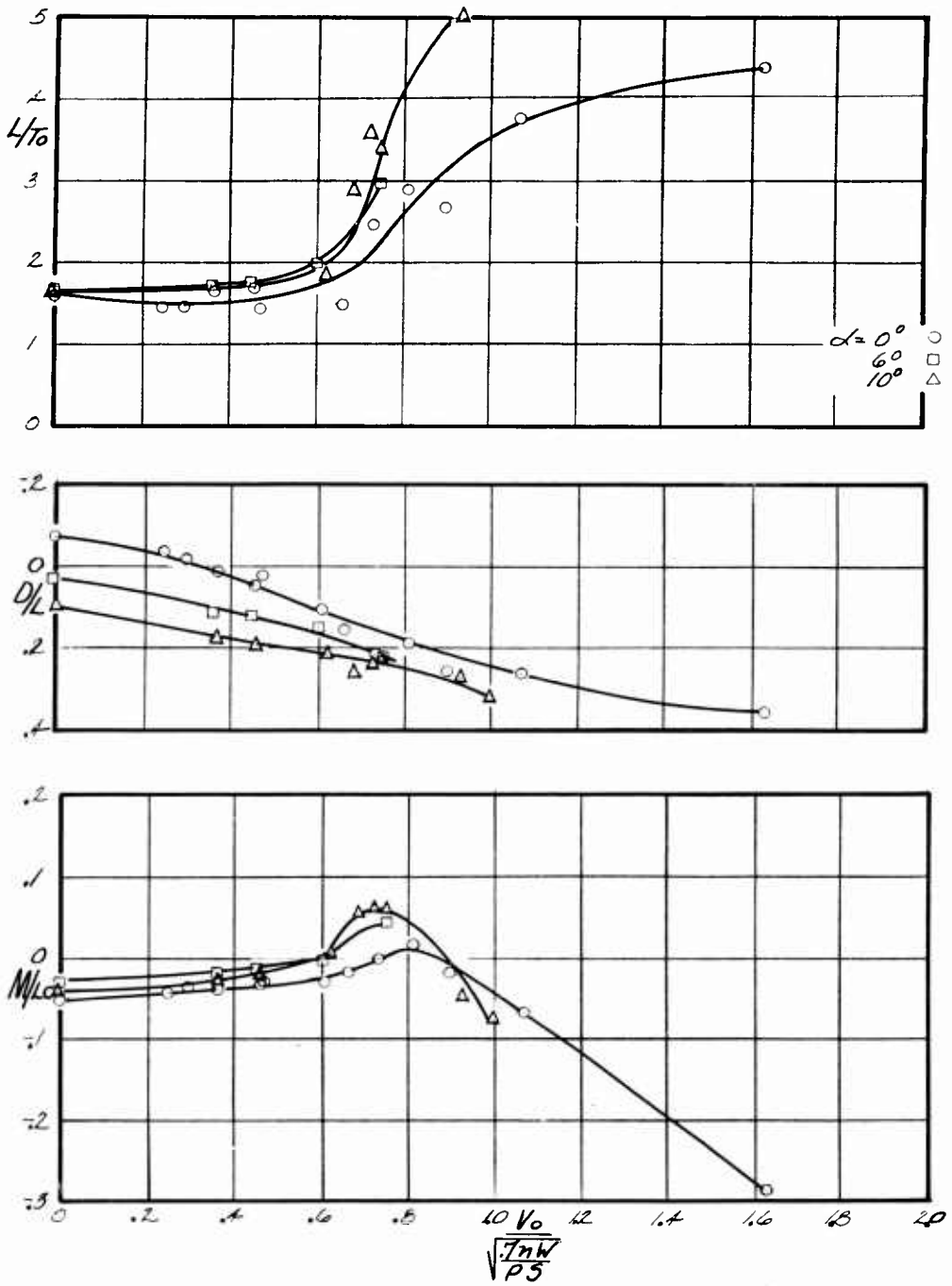

Figure 67. Effect of Angle of Attack in Ground Effect With Trimmer Aft — Configuration "B" Ducts (h/c = 0.115, δ_V = 15°/-15°/0°, δ_F = 30°)

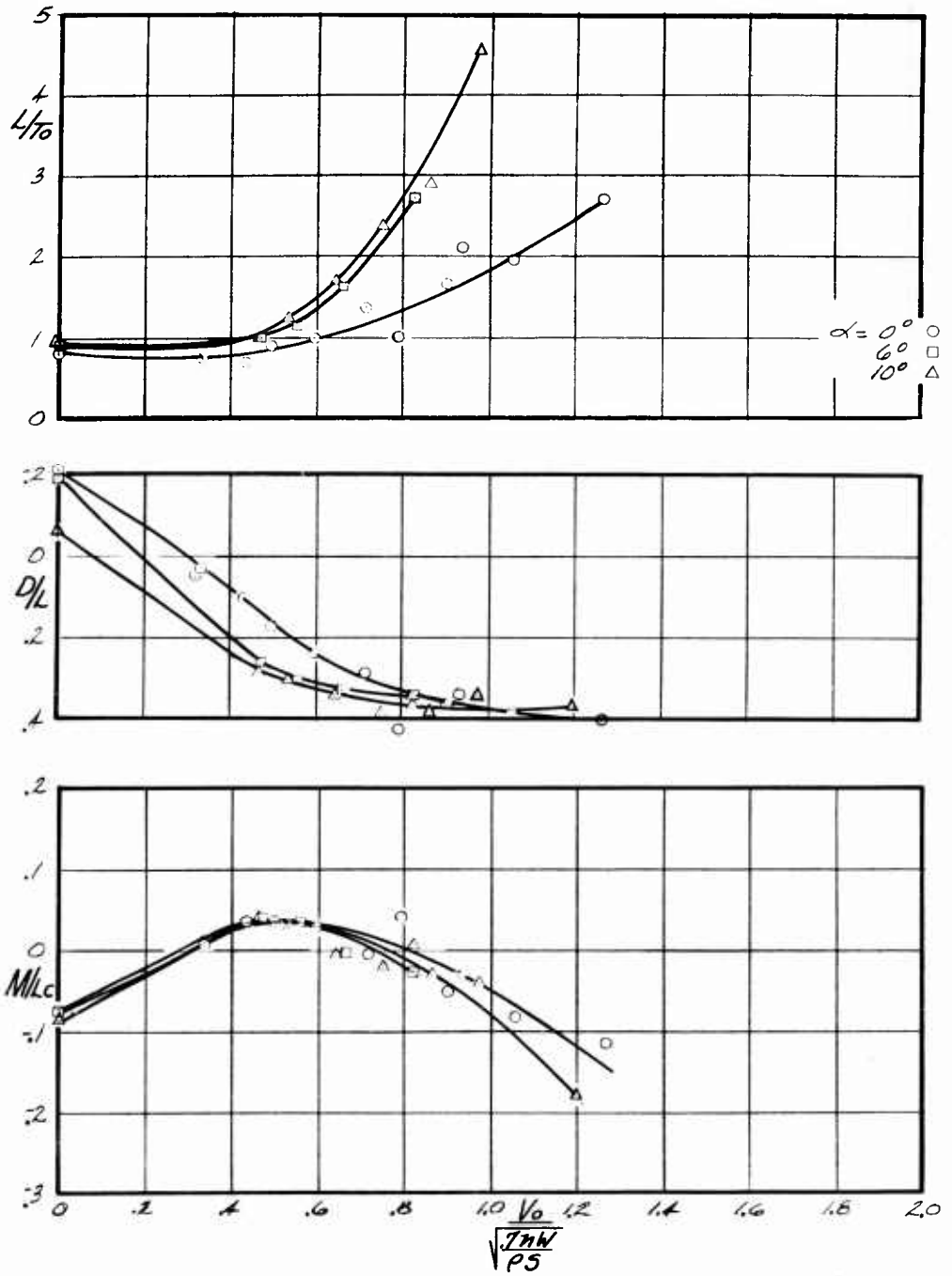

Figure 68. Effect of Angle of Attack in Free Air With Trimmer Aft — Configuration "B" Ducts (h/c = 1.95, δ_V = 15° /-15° /0° , δ_F = 30°)

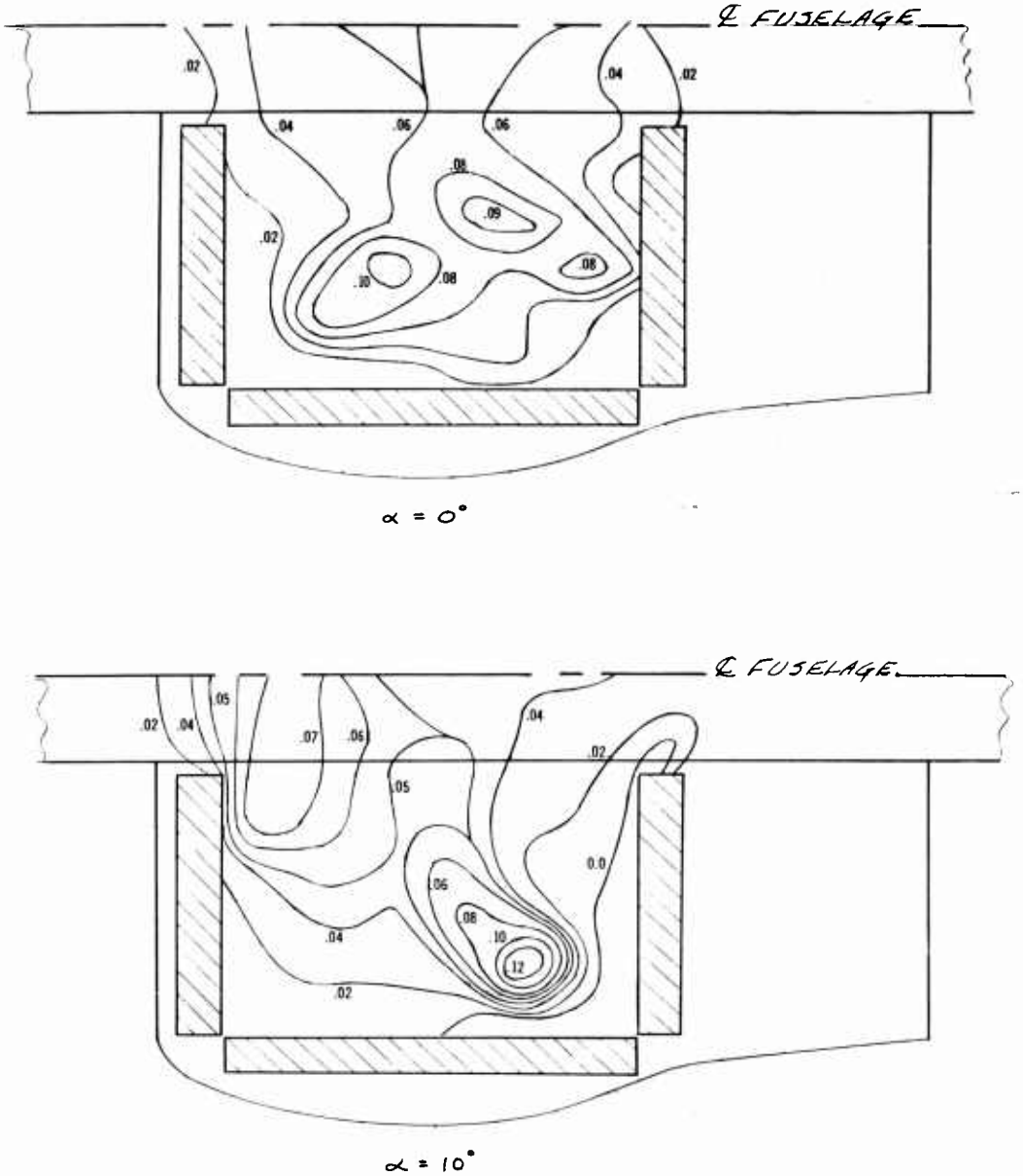

Figure 69. Effect of Angle of Attack on Base Pressure Distribution in Ground Effect With Trimmer Forward — Configuration "B" Ducts ($h/c = 0.115$, $\delta_V = 15°/-15°/0°$, $q = 1.5$ PSF, RPM = 14,000, $q_{jet} \cong 27$ PSF, Isobars ~ PSI)

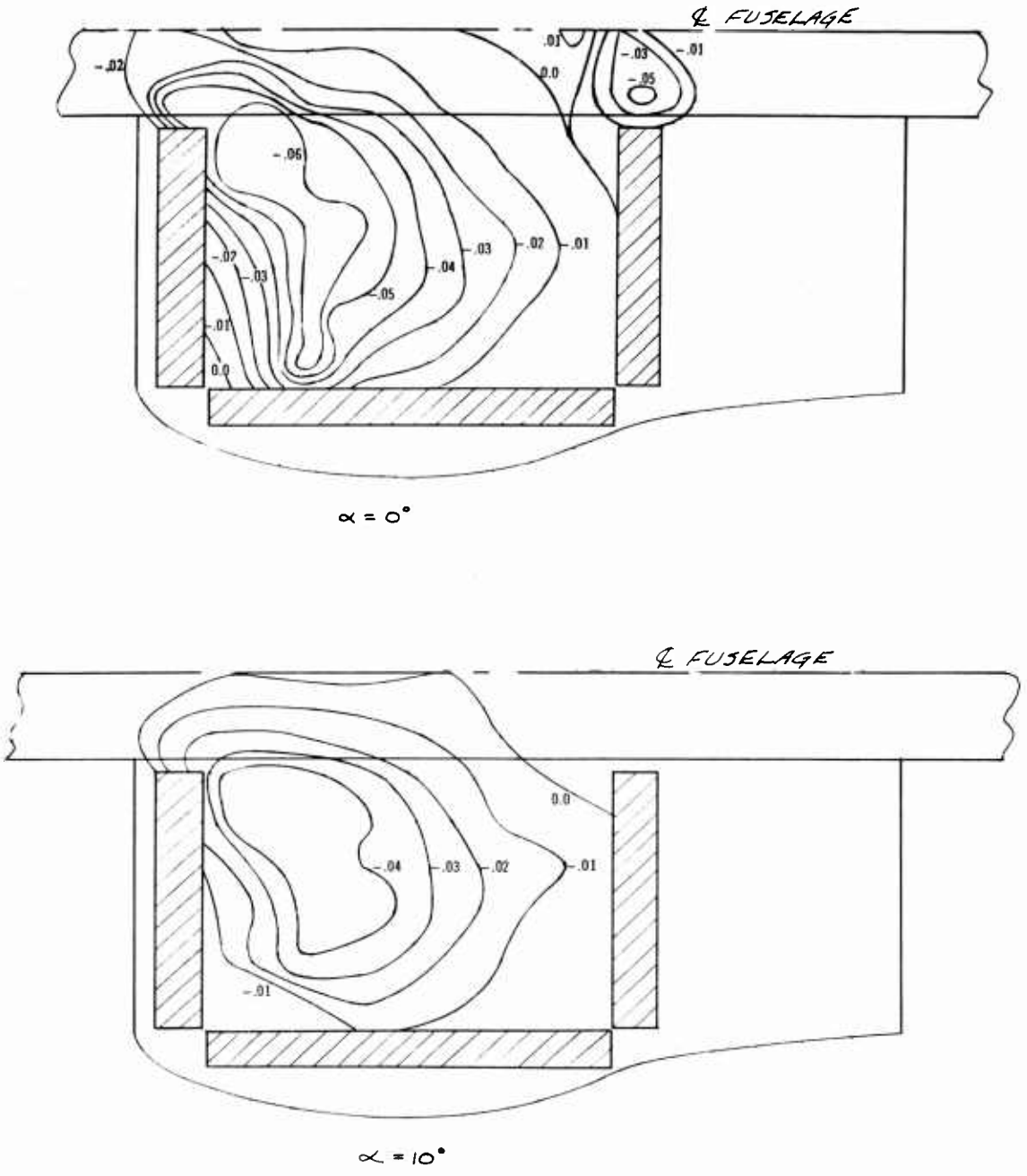

Figure 70. Effect of Angle of Attack on Base Pressure Distribution in Free Air With Trimmer Forward — Configuration "B" Ducts ($h/c = 1.95$, $\delta_V = 15°/-15°/0°$, $q = 1.5$ PSF, RPM = 14,000, $q_{jet} \cong 27$ PSF, Isobars ~ PSI)

4. Causes the center of pressure to move aft at lower speeds with the trimmer forward.

5. Causes increased pitch-up with the trimmer aft due to change in effectiveness of the horizontal tails.

Effect of Height

The variation of the longitudinal characteristics with height-to-chord ratio is presented in Figure 71 for the trimmer-forward configuration and in Figure 72 for the trimmer-aft configuration. Data is shown at tunnel q's of 0 and 1.5 in each case. The curves are of the same general shape in each configuration but do show a level change. The lift-to-thrust ratio increases smoothly with decreasing height with the characteristic sharp increase occurring below a height-to-chord ratio of 0.3. Figure 36 showed that a region of instability occurred in the lift-to-thrust ratio curve with the "A" ducts; however, the "B" configuration ducts, with approximately equal exit slots, did not experience this phenomenon. The static drag-to-lift ratio curve, as with the "A" ducts, increases negatively with increasing height due to the change in direction of the resultant thrust vector out of ground effect. At forward speed, the ram drag is predominant and so produces a more positive drag as height increases. The center of pressure, statically, moves forward approximately 6.5% as the height moves from out of ground effect to a height-to-chord ratio of 0.06. Once again, as in the case of the "A" ducts, this center-of-pressure shift is due to negative pressures acting on the undersurface of the wing, aft of the rear slot. With forward speed, the center-of-pressure shifts aft approximately 8% as the height moves from out of ground effect to in ground effect. Pressure data shows this shift to be due to an increase in the negative pressures on the upper surface of the wing ahead of the fan.

In summary, it may be said that lift increases with decreasing height, drag increases statically and decreases at forward speed with decreasing height, and the center of pressure moves forward statically and aft at forward speed with decreasing height.

Effect of Trimmer Position

A trimmer, as described in the Phase I section of this report, was installed on the model in an attempt to alleviate the pitch-up tendency encountered during acceleration from hover to transition speed. Three distinct positions of the trimmer were tested in the wind tunnel:

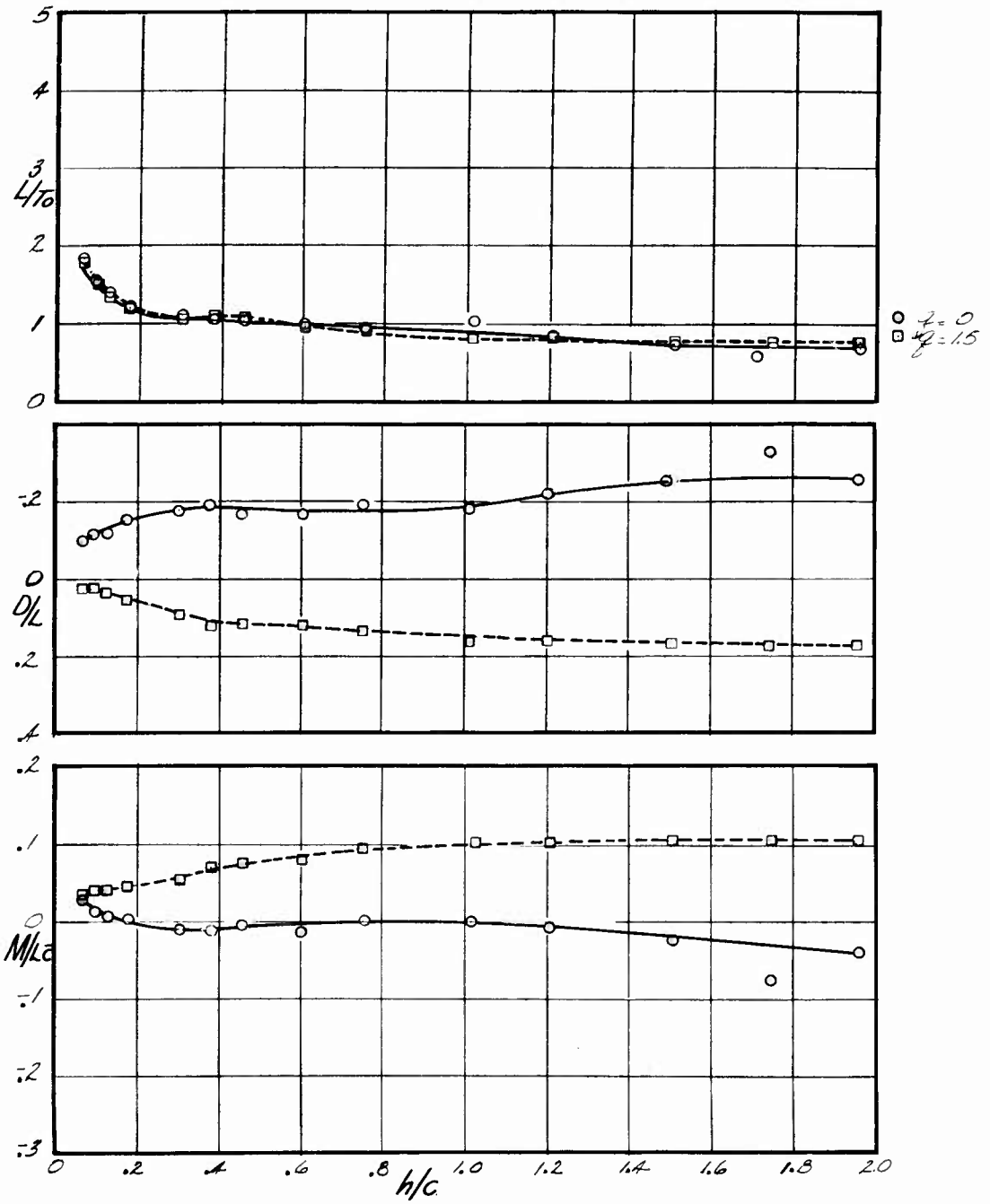

Figure 71. Effect of Height With Trimmer Forward — Configuration "B" Ducts ($\alpha = 0°$, $\delta_V = 15°/-15°/0°$, $\delta_F = 30°$)

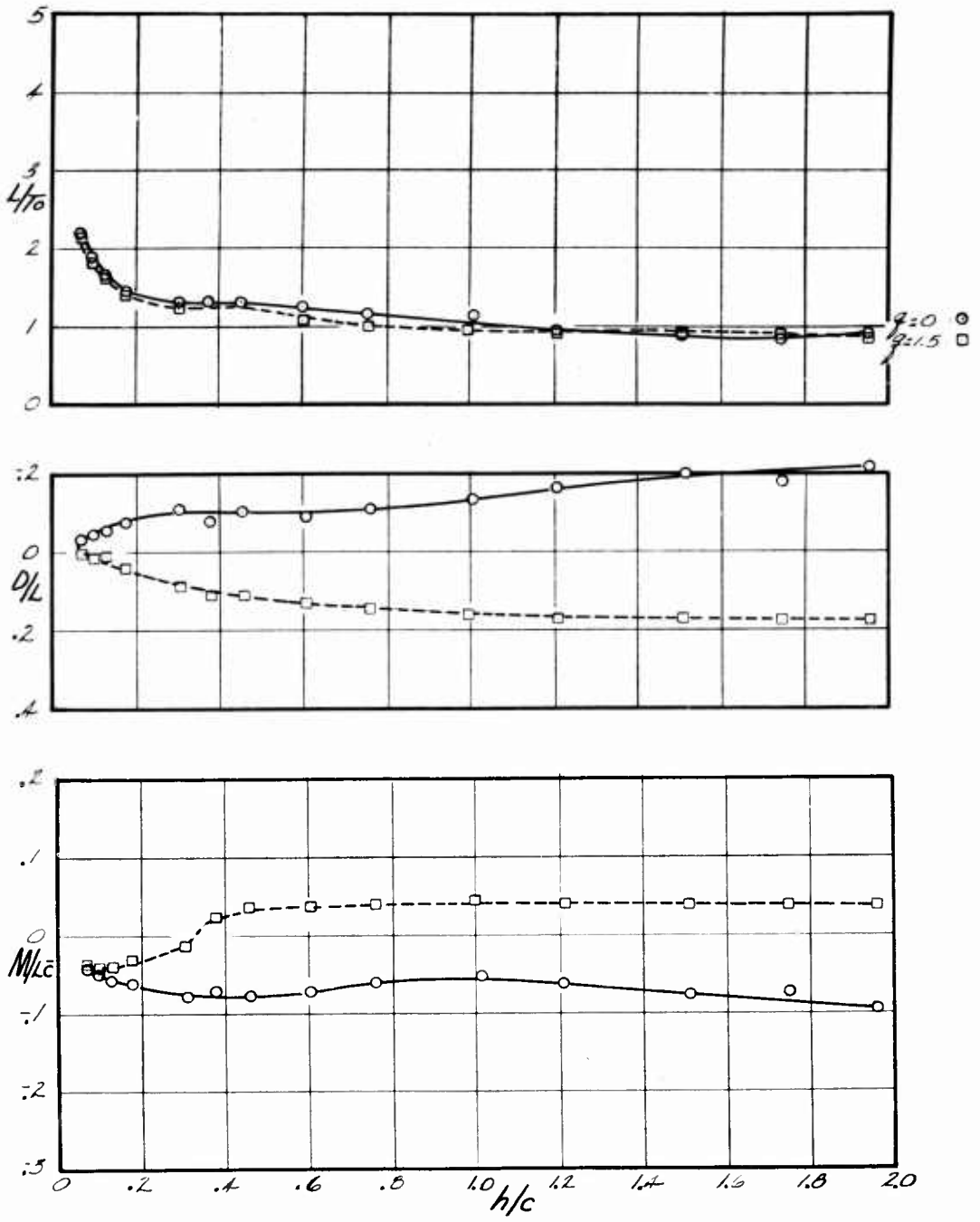

Figure 72. Effect of Height With Trimmer Aft — Configuration "B" Ducts (α = 0°, δ_V = 15°/-15°/0°, δ_F = 30°)

1. Trimmer forward — the rear duct wall in its basic position forming a symmetrical duct fore and aft around the fan centerline.

2. Trimmer intermediate — the rear wall of the aft slot moved 7.9% of wing chord to the rear from its basic position.

3. Trimmer aft — the rear wall of the aft slot moved 15.8% of wing chord to the rear from its basic position.

When the back wall of the aft slot was displaced to the rear, the base of the model was left in its basic position, thus leaving, in effect, a rear slot of a width that was the basic width plus the amount the rear wall was displaced. It was believed that flow from the duct to the rear slot would adhere to the upper surface of the duct and so be displaced to the rear a distance equal to the amount the rear wall had been moved aft. Tuft studies on a static test setup proved this assumption to be valid, and thus a method was provided for obtaining nose-down pitching moments.

Figures 73 and 74 show the effect of the rearward movement of the trimmer in both free air and ground effect. Base pressure profiles for the trimmer forward and aft configurations in and out of ground effect are shown in Figures 75 and 76. As can be seen from the moment curves in Figures 73 and 74, the trimmer functioned quite satisfactorily. The moment produced by the trimmer also increased with forward velocity so that the peak forward movement of center of pressure was realized at a lower forward speed. The data shows that slightly more rearward movement of the trimmer would be required to trim out all the nose-up pitching moment encountered in the configuration tested; however, there is no question as to the ability of achieving trim at any forward velocity. Lift, at hover and in the low-speed range, was not greatly affected by the movement of the trimmer, but there was some increase with the trimmer moved aft as a result of the increase in base area.

The pressure profiles in Figures 75 and 76 show that the increased lift evident in the force data was definitely due to the pressures in the area where the rear slot had been moved aft. It will be noticed that the family of lift-to-thrust ratio curves with trimmer position appears quite similar to the family produced by varying angle of attack. Although sufficient data is not available to explain fully the occurrence of the break at lower speeds with aft movement of the trimmer, two hypotheses may be advanced. One supposition is that by moving the rear slot aft, the normally negative pressures on the undersurface of the wing aft of the rear slot are removed. If these negative pressures increase with velocity with the trimmer forward, then their removal would produce an increase in total lift

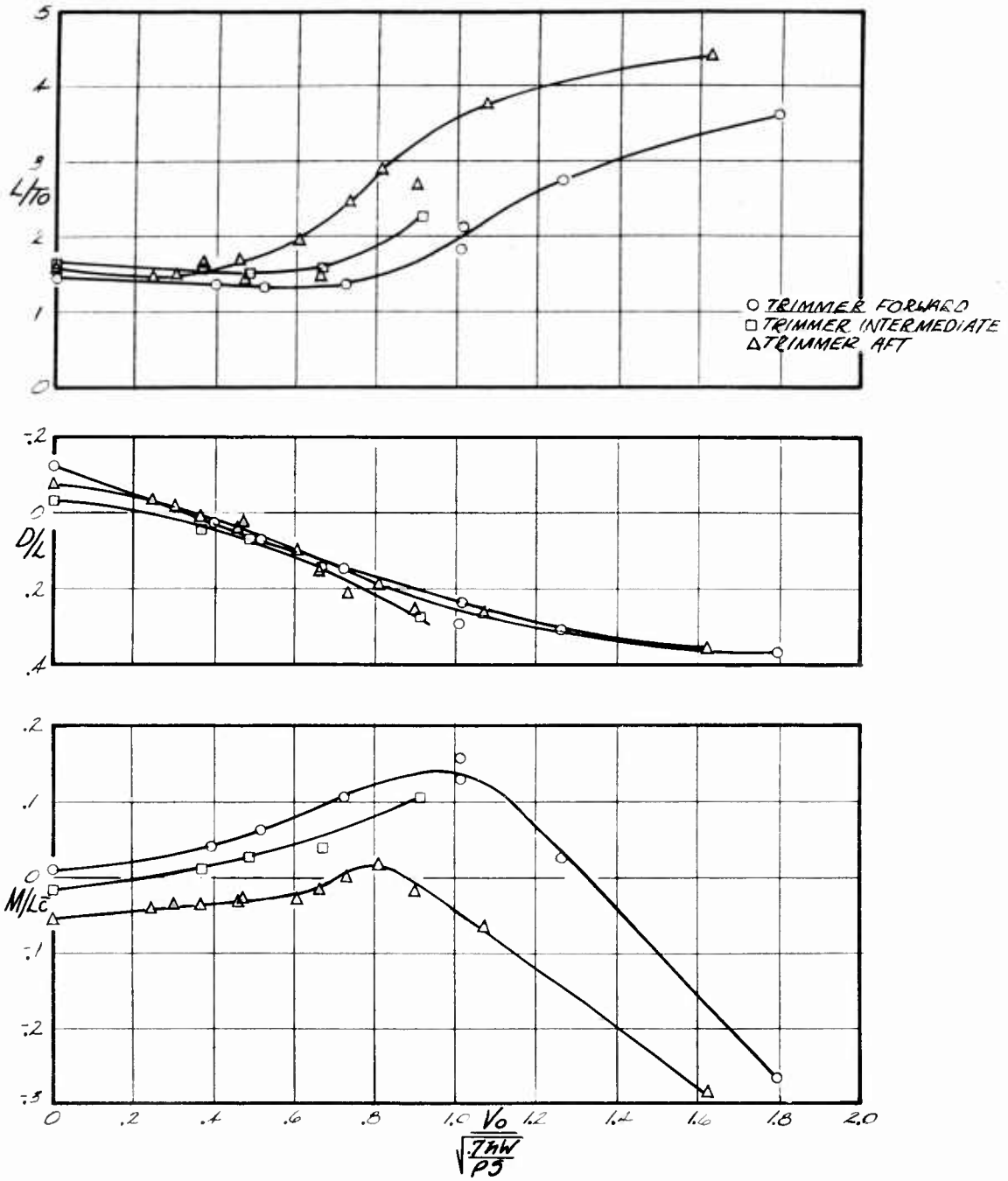

Figure 73. Effect of Trimmer Position in Ground Effect — Configuration "B" Ducts (h/c = 0.115, δ_V = 15°/-15°/0°, α = 0°, δ_F = 30°)

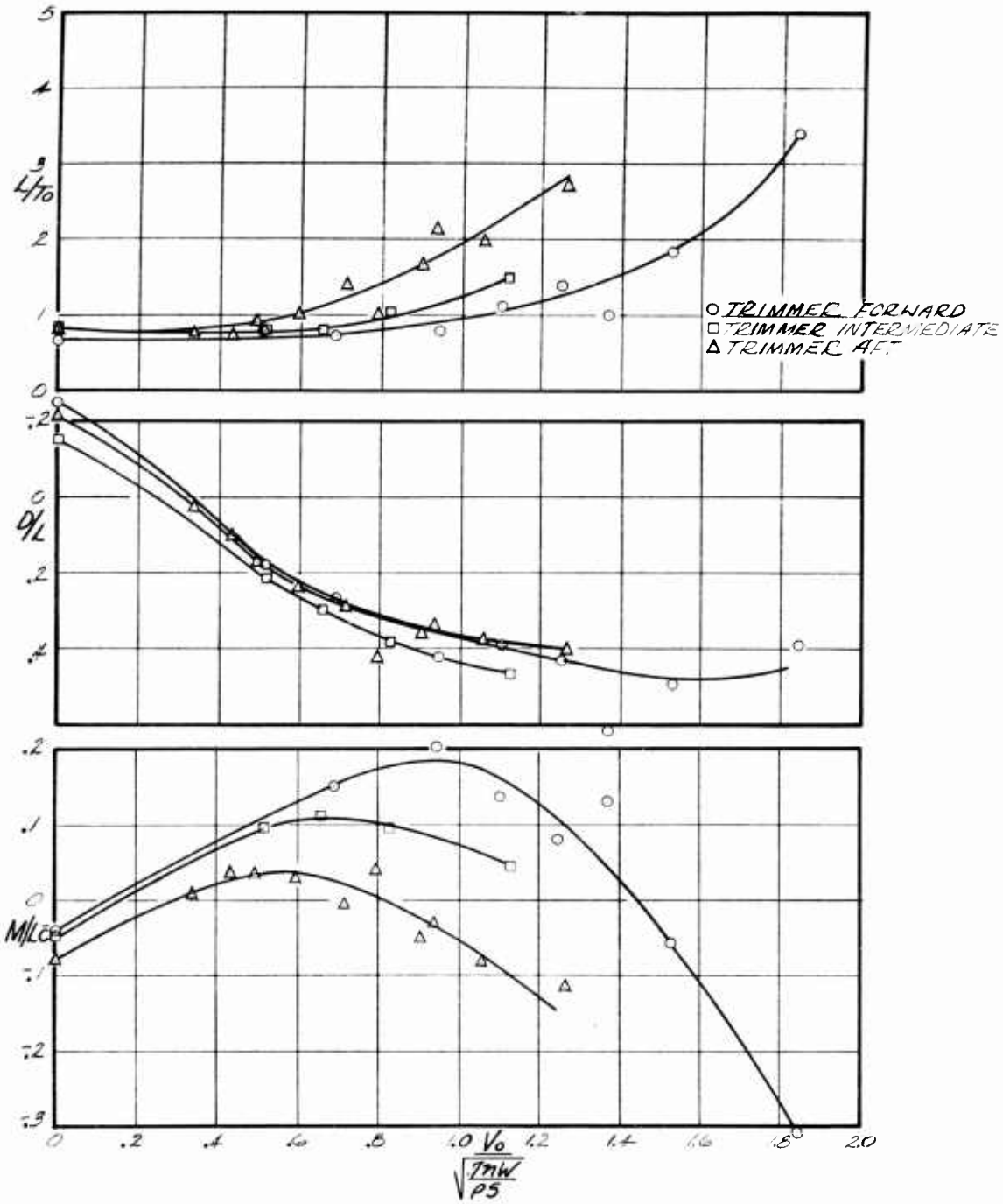

Figure 74. Effect of Trimmer Position in Free Air — Configuration "B" Ducts ($h/c = 1.95$, $\delta_V = 15°/-15°/0°$, $\alpha = 0°$, $\delta_F = 30°$)

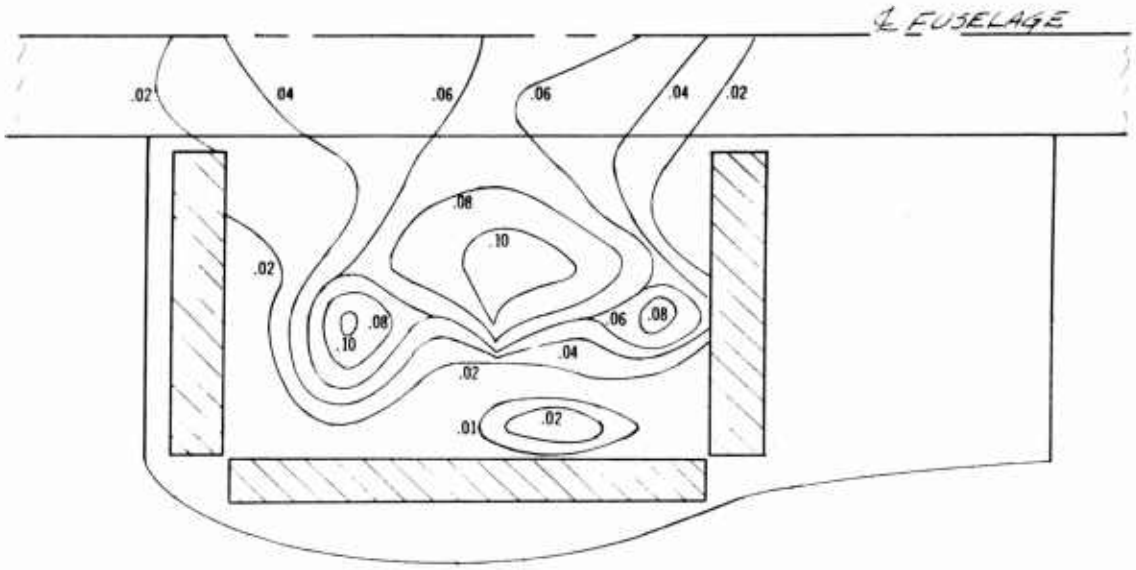

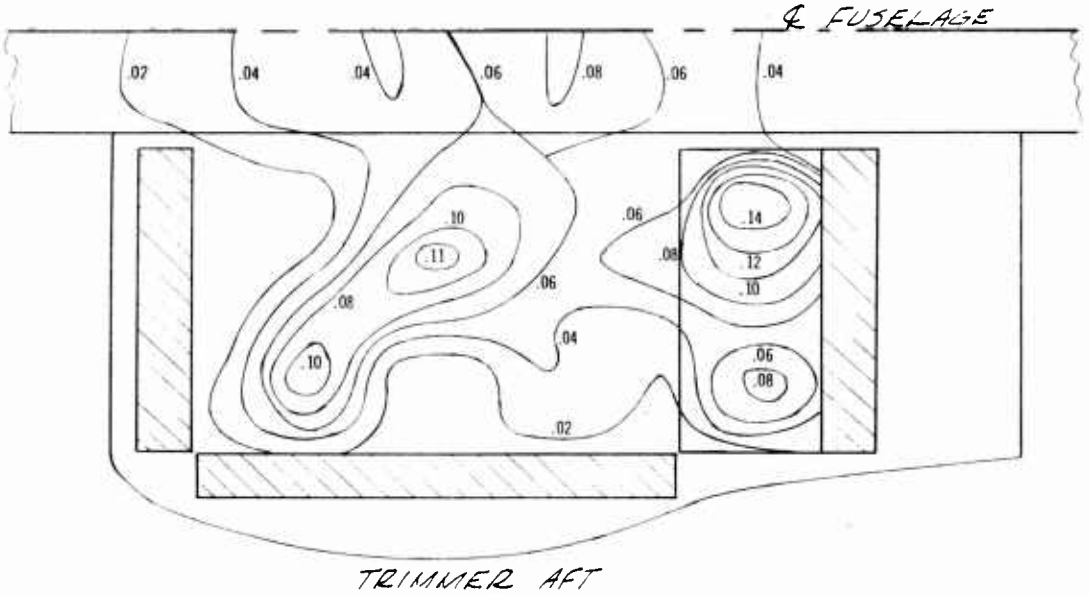

Figure 75. Effect of Trimmer Position on Base Pressure Distribution in Ground Effect — Configuration "B" Ducts (h/c = 0.115, δ_V = 15° /-15° /0° , α = 0° , q = 0 PSF, RPM = 14,000, $q_{jet} \cong$ 27 PSF, Isobars ~ PSI)

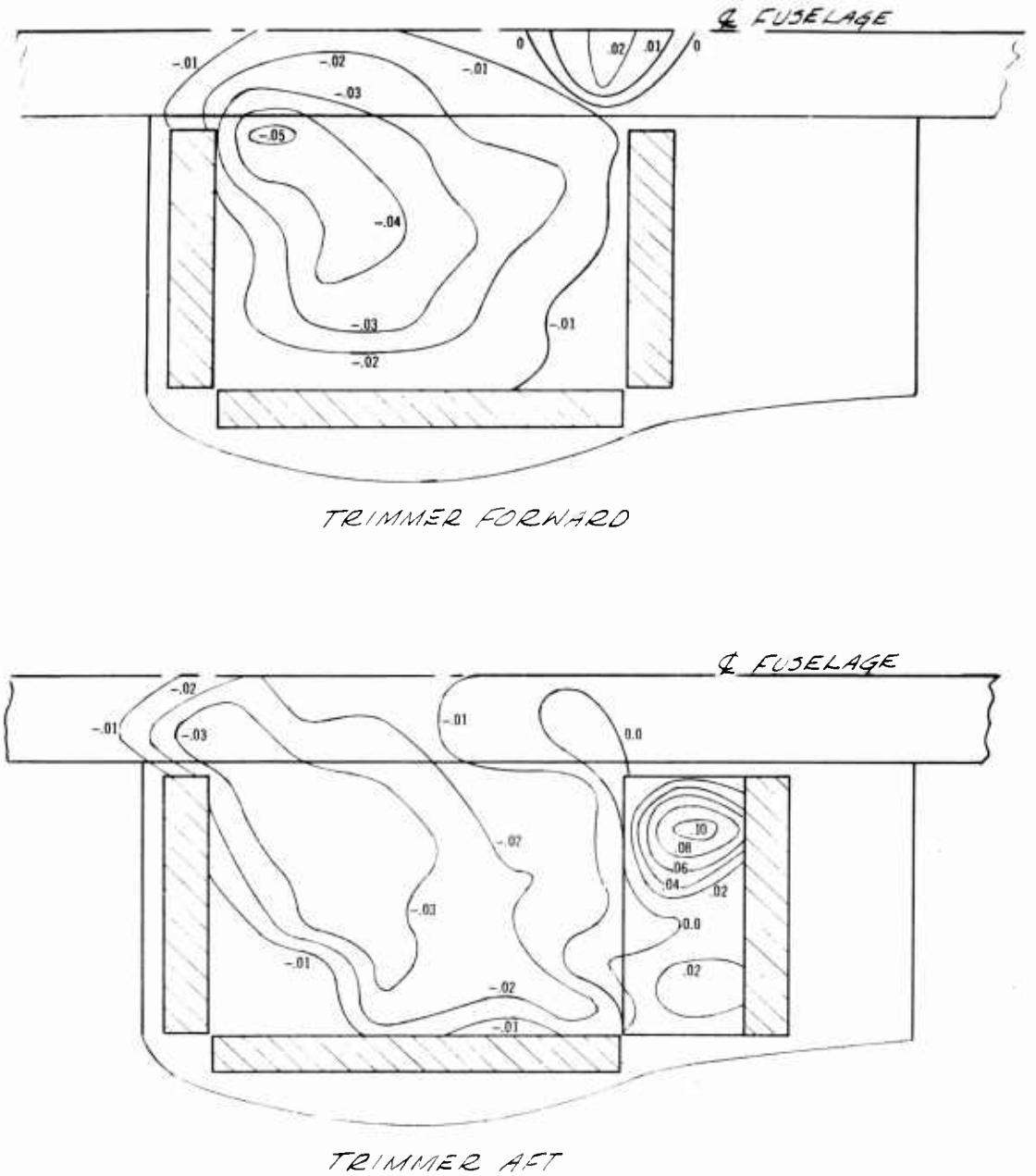

Figure 76. Effect of Trimmer Position on Base Pressure Distribution in Free Air — Configuration "B" Ducts (h/c = 1.95, δ_V = 15° /-15° /0° , α = 0° , q = 0 PSF, RPM = 14,000, $q_{jet} \cong$ 27 PSF, Isobars ~ PSI)

with velocity. Another point is that by moving the rear slot nearer the trailing edge of the wing, a boundary layer control condition could be induced on the rear portion of the top surface of the wing which would produce negative pressures in that area and increase the total lift. The drag-to-lift ratio is not appreciably affected by the movement of the trimmer. The significant item here is the difference in level between the in-ground and out-of-ground-effect data. The ratio is higher negatively out of ground effect due to the change in direction of the resultant thrust vector between in and out of ground, and the slope with speed is greater out of ground due to the increased percentage of ram drag realized as compared to in ground effect.

In summary, it may be said that moving the trimmer aft (1) increased the total lift statically; (2) caused the upward break in the lift-to-thrust ratio curve to occur at a lower speed; (3) resulted in small, if any, effect on the drag-to-lift ratio; and (4) produced a nose-down pitching moment.

Effect of Flap Deflection

A full span, 10% chord plain flap was tested at deflections of 0°, 30°, 45° and 60° to determine its effect on the longitudinal characteristics with the fan operating. Typical results are shown in Figures 77 and 78 for in ground effect and free-air conditions. In ground effect, the flap was almost completely ineffective. Close inspection of the data also leads to the conclusion that the flap was stalled above 30° deflection. The data presented is with the trimmer in the aft position and, in this configuration, the rear wall of the aft slot protrudes below the wing lower surface to the extent that it completely blocks off the flap; consequently, the ineffectiveness of the flap as shown by this data is not a complete surprise. An actual GETOL aircraft would not have this protuberance, and it would be expected that a flap should be more effective. The flap is slightly more effective in free air than in ground effect, but it is also evident from this data that the flap stalls above 30°. Drag increases somewhat with flap deflection, but once again the stalled condition is evidenced. The peak forward movement of center of pressure out of ground effect is flattened out by deflections up to 30°, but with no significant change above this value.

In summary, the plain flap tested on the model was ineffective in ground effect, only slightly effective in free air, and in both conditions stalled at deflections above 30°. While the configuration of the model undoubtedly influenced the resulting data, a more efficient flap should be devised if a flap is to be used at all.

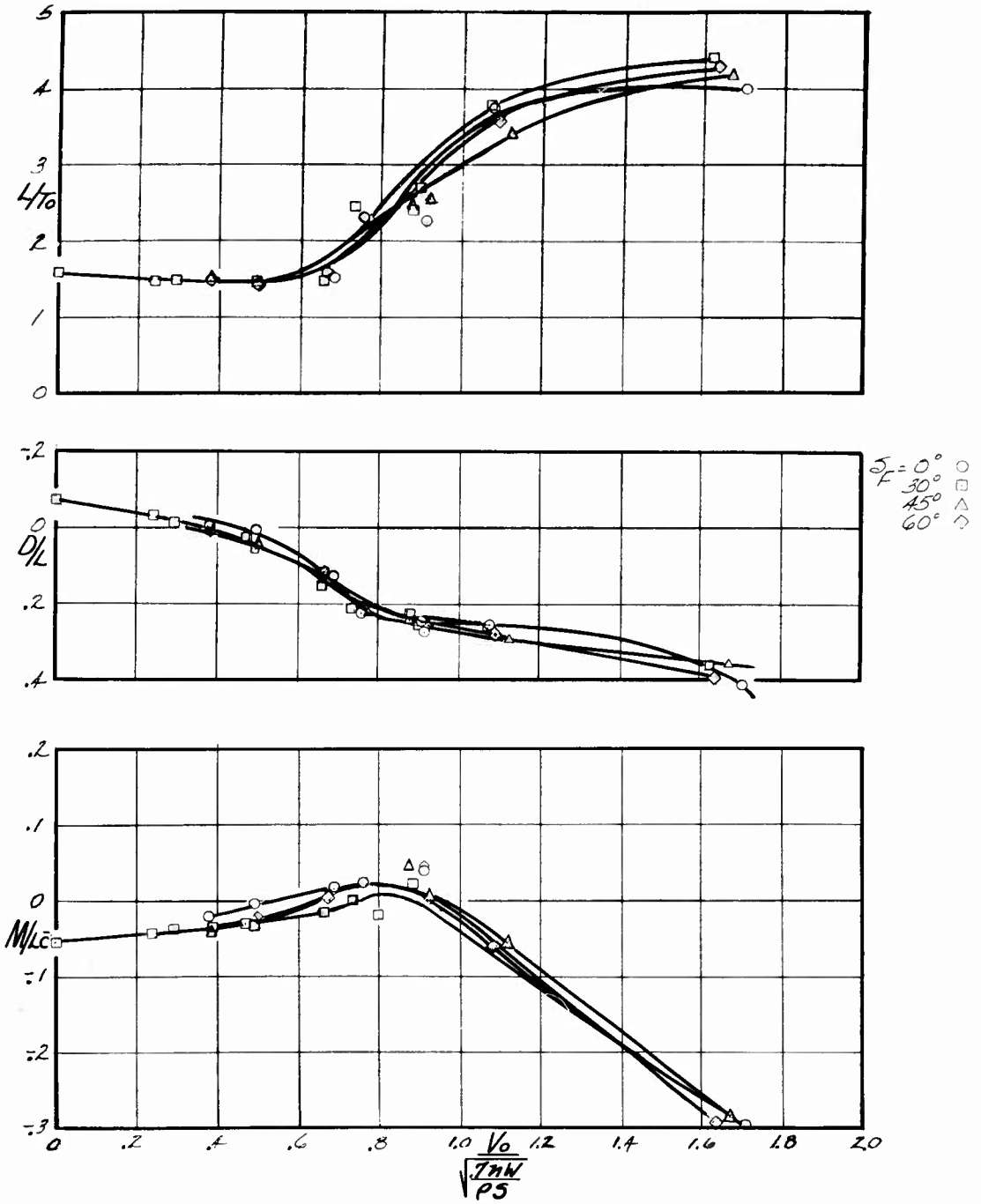

Figure 77. Effect of Flap Deflection in Ground Effect With Trimmer Aft — Configuration "B" Ducts (h/c = 0.115, δ_V = 15°/-15°/0°, α = 0°)

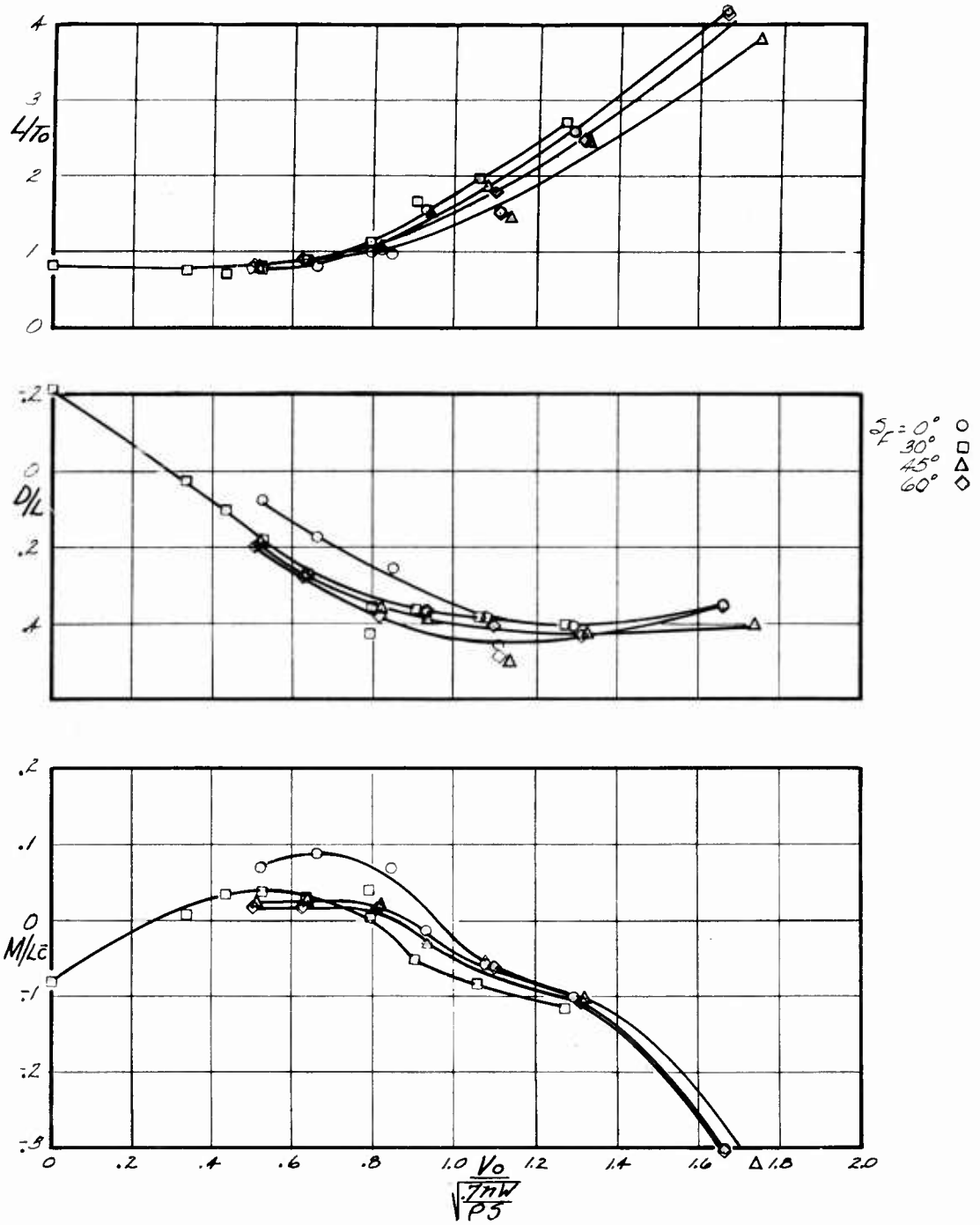

Figure 78. Effect of Flap Deflection in Free Air With Trimmer Aft — Configuration "B" Ducts (h/c = 1.95, δ_V = 15°/-15°/0°, α = 0°)

Effect of Horizontal Tail Incidence

The horizontal tails on the model were tested at deflections of 15°, 10° and ±5° with positive deflection considered to be stabilizer leading edge up. The results, as shown in Figures 79 and 80 for in and out of ground effect, were consistent and encouraging. Lift-to-drag ratio and center-of-pressure movement progressed smoothly in the expected direction as stabilizer deflection varied from -5 to 15°. Drag-to-lift ratio was not materially affected by altering the tail incidence either in or out of ground effect. An encouraging item to note is that with the proper combination of trimmer position and stabilizer incidence, pitch trim can be maintained throughout acceleration to transition in ground effect. No tail-off data was obtained during these tests; therefore, no attempt has been made to present an analysis of the flow field around the horizontal tails.

Effect of Control Devices

The trimmer, as the name implies, was conceived to provide longitudinal trim throughout the speed range from hover to transition. Additional longitudinal control capability must be provided in this speed range to allow for maneuvering the aircraft. Aerodynamic controls do not become effective until a velocity of 65 to 75 knots has been attained; therefore, some type of reaction control is necessary. Two items tested during the final test were inlet stators and control plugs in the nozzle exits.

Effect of Inlet Stators

Variable stators were placed in the fan inlet to alter the direction of flow into the fan. For this particular test, an attempt was made to direct the flow into the fan in such a way as to decrease the angle of attack of the fan blades in the front half of the fan and to increase the angle of attack of the fan blades in the rear half of the fan. The intent was to produce nose-down pitching moment. Data for the stator deflections of 0°, 10° and 20° in and out of ground effect is presented in Figures 81 and 82. Reference to the center-of-pressure curves shows that the stators did produce pitching moment in the desired direction; however, the magnitude of the moment was not as large as desired. Also, the incremental moment decreased with forward velocity until it became nonexistent at about stall speed. A large loss in lift also was associated with the use of the stators. Based on these considerations, the inlet stator concept does not appear promising.

Effect of Control Plugs

The second method to be tested of obtaining pitch control was the use of plugs in the exit nozzles which closed off 30% of the area. The intent was to decrease the

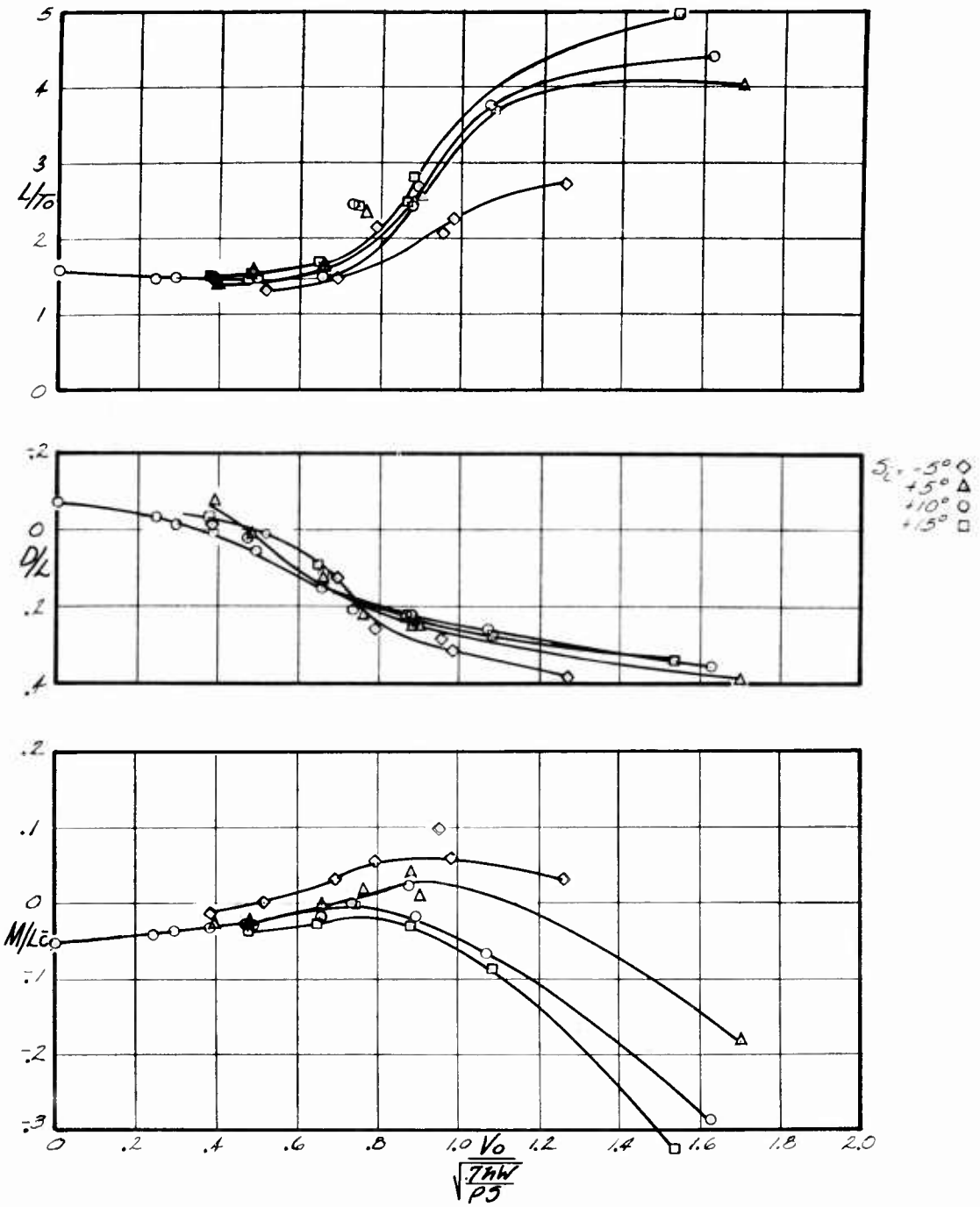

Figure 79. Effect of Tail Incidence in Ground Effect With Trimmer Aft — Configuration "B" Ducts (h/c = 0.115, δ_V = 15°/-15°/0°, α = 0°, δ_F = 30°)

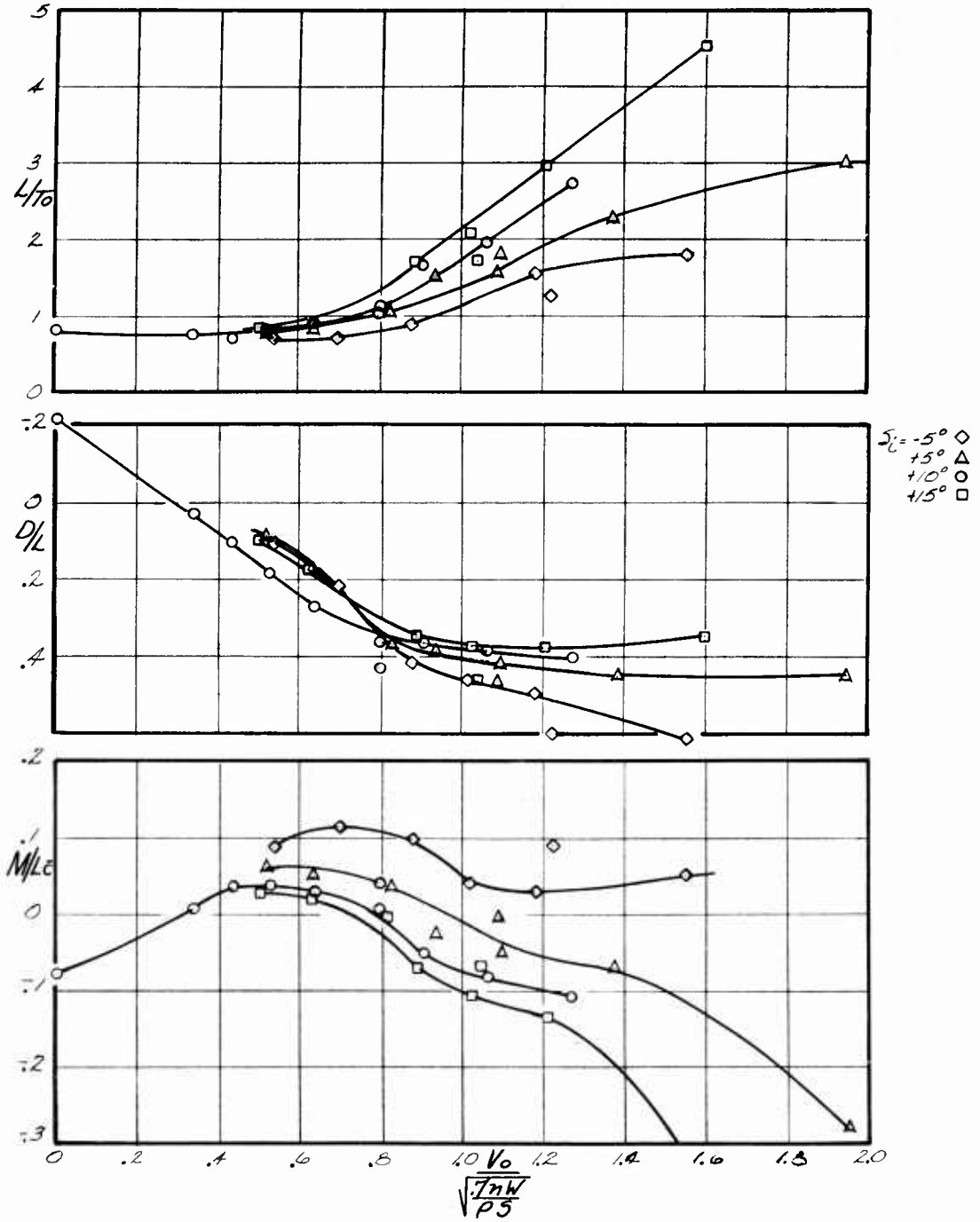

Figure 80. Effect of Tail Incidence in Free Air With Trimmer Aft — Configuration "B" Ducts (h/c = 1.95, δ_V = 15°/-15°/0°, α = 0°, δ_F = 30°)

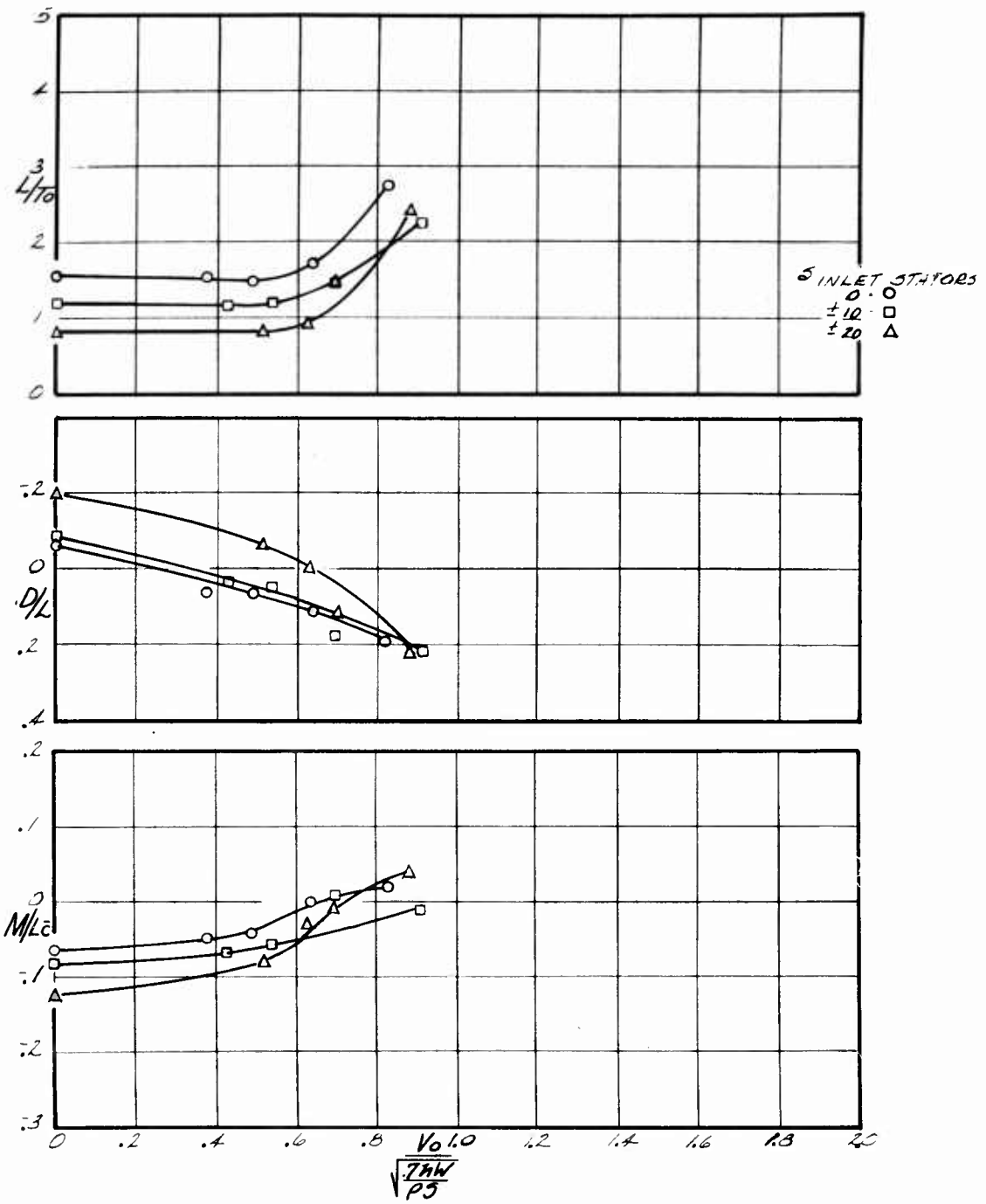

Figure 81. Effect of Inlet Stators in Ground Effect With Trimmer Aft — Configuration "B" Ducts (h/c = 0.115, δ_V = 15°/-15°/0°, α = 0°, δ_F = 30°)

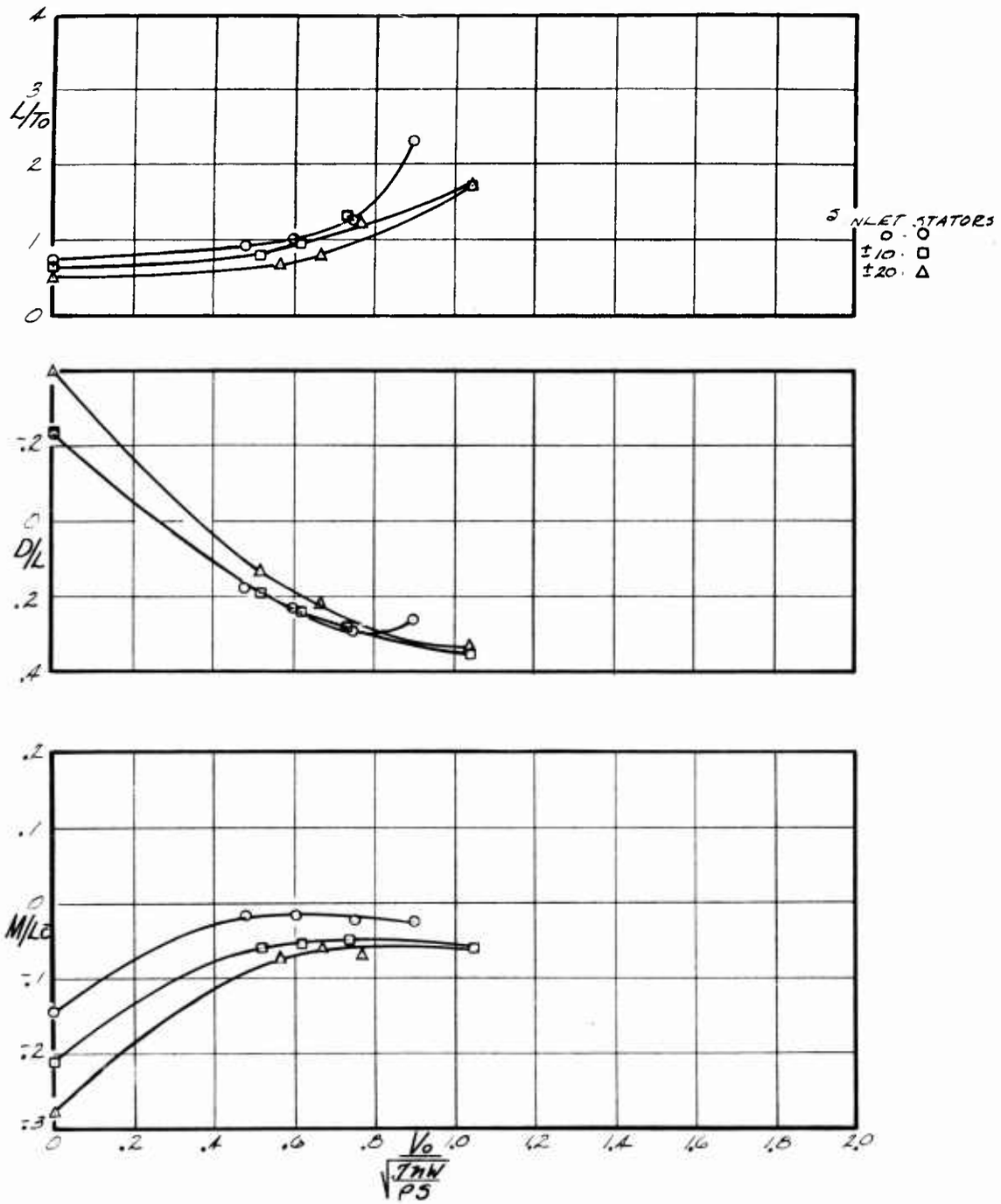

Figure 82. Effect of Inlet Stators in Free Air With Trimmer Aft — Configuration "B" Ducts (h/c = 1.95, δ_V = 15°/-15°/0°, α = 0°, δ_F = 30°)

flow either through the fore or aft nozzle by partially plugging it and thus produce a pitching moment. Data with plugs in both the front and rear slot is presented in Figures 83 and 84 for in and out-of-ground-effect conditions. As can be seen from the figures, the plugs were completely unsuccessful. With a plug in the front slot, a small nose-down moment was generated as expected. However, when a plug was put in the rear slot, nose-down moment still developed; in any case, the magnitude of the moment was so small that it would be worthless for pitch control.

Further work obviously remains to be accomplished on a longitudinal control system at hover and low speeds. The Phase III section of this report contains further information on this subject.

Effect of Roll Angle

Figures 85 through 88 show the effect of roll angle on longitudinal and lateral-directional characteristics, both in and out of ground effect. In this case, the in-ground-effect data is presented at a height-to-chord ratio of 0.175 rather than the 0.115 at which all previous ground effect data has been presented. This was to allow sufficient wing tip clearance when the model was rolled. Roll angle, either in or out of ground effect, had no appreciable effect on the longitudinal characteristics.

The lateral-directional characteristics presented are lateral movement of the center of pressure in per cent span (R/Lb), fore and aft movement of the center of pressure as applied to side force, in per cent chord ($\frac{N}{Y\bar{c}}$) and lateral acceleration (Y/L). Considerable scatter is shown throughout the lateral-directional data both in this section and later in the yaw data section. The model was rolled left wing down during the testing; therefore, a center-of-pressure movement to the left would be expected since the pressures on the left wing base should have been higher when it was closer to the ground plane. However, the data indicates that if any movement is taking place, it is a small movement to the right. This apparently is caused by the base pressure being blown out from under the left wing when it is rolled down. Out of ground effect, the center-of-pressure movement with roll angle is negligible. It is expected that there would be no fore-and-aft movement with roll angle, and the data bears this out reasonably well, although there is considerable scatter in the data. Lateral acceleration with roll angle is shown by the data to be to the left as would be expected since the resultant thrust vector would be in that direction with left wing down roll. Further testing is required in this area.

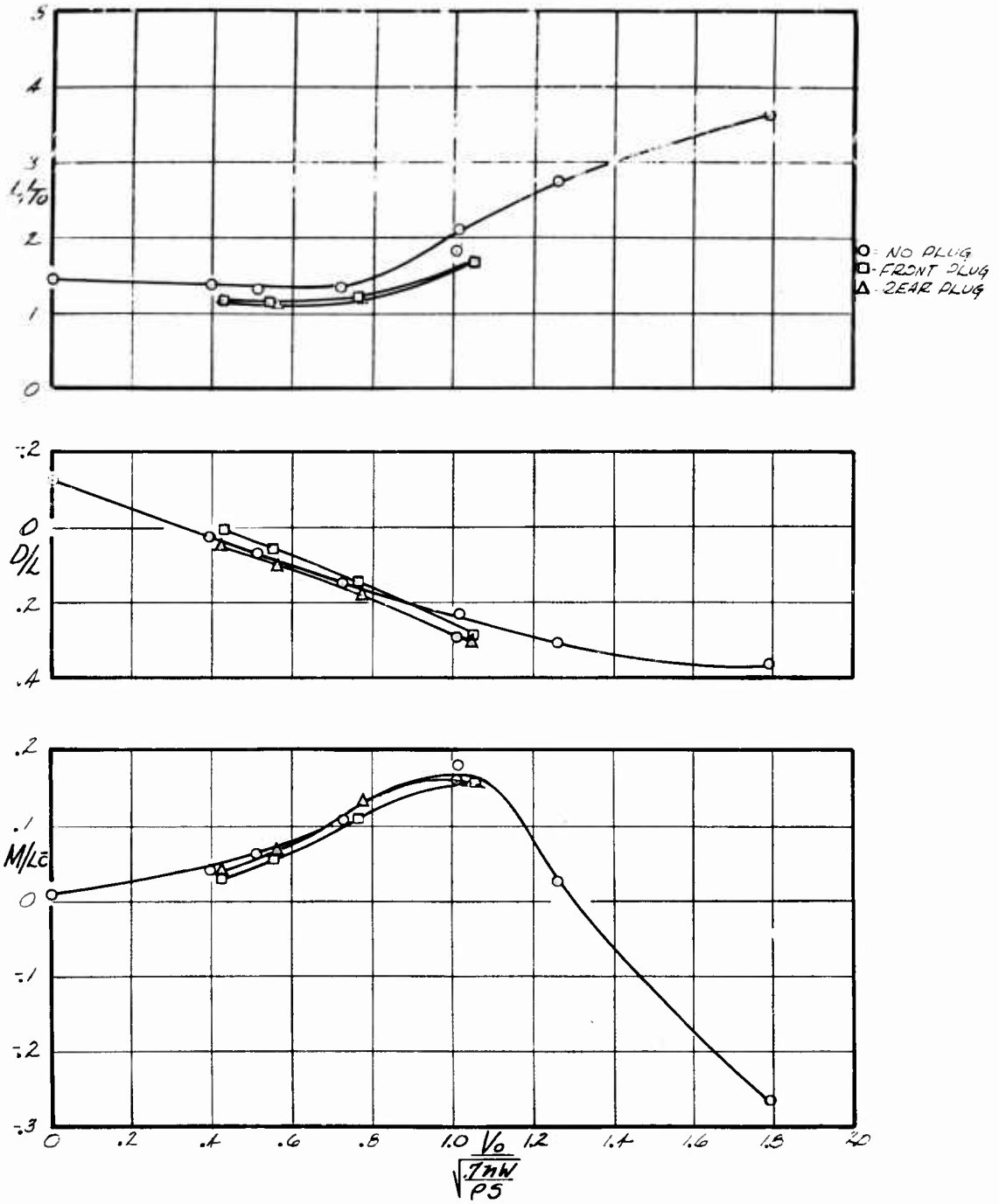

Figure 83. Effect of Control Plugs in Ground Effect With Trimmer Forward — Configuration "B" Ducts (h/c = 0.115, δ_V = 15°/-15°/0°, α = 0°, δ_F = 30°)

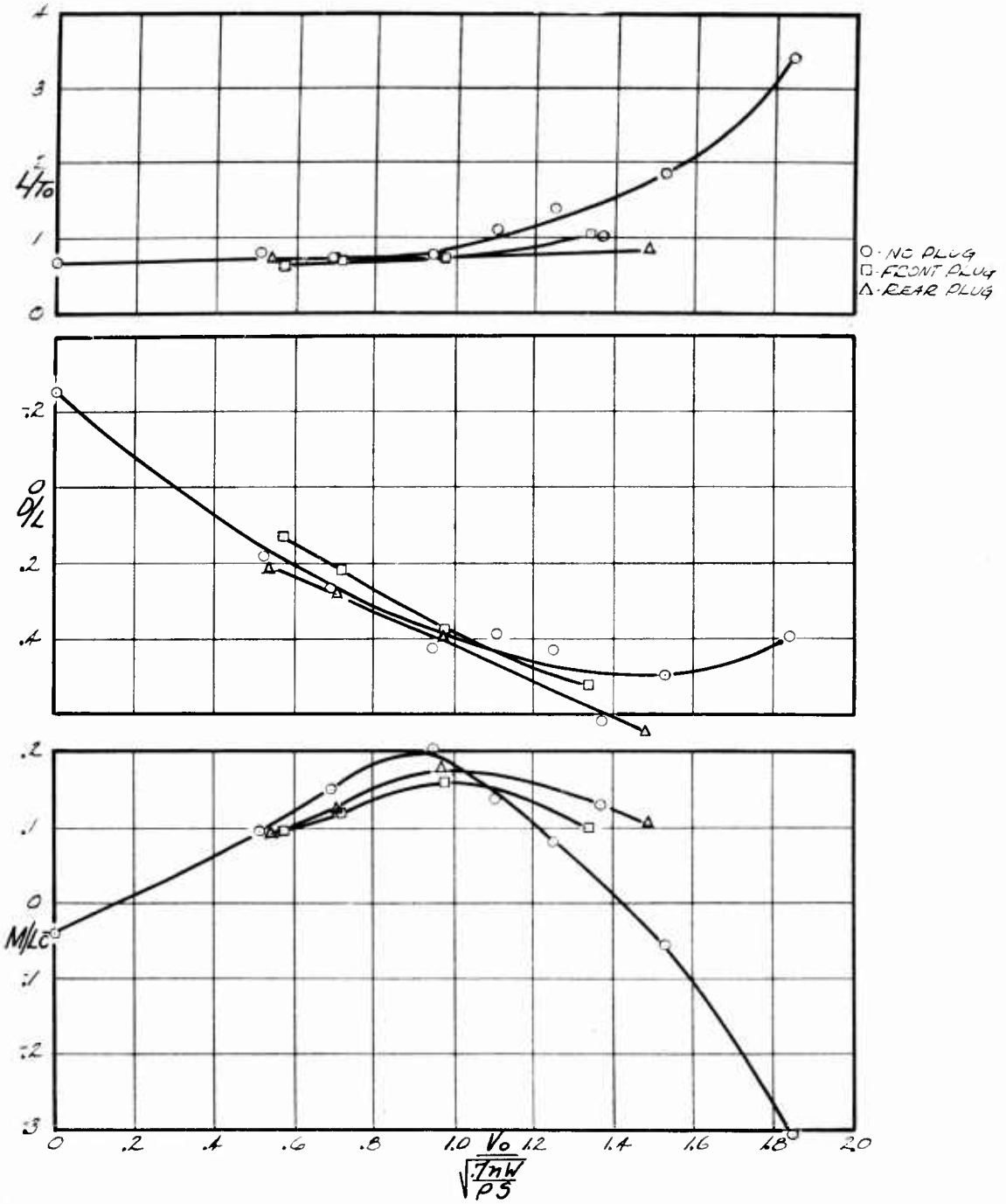

Figure 84. Effect of Control Plugs in Free Air With Trimmer Forward — Configuration "B" Ducts (h/c = 1.95, δ_V = 15° /-15° /0° , α = 0° , δ_F = 30°)

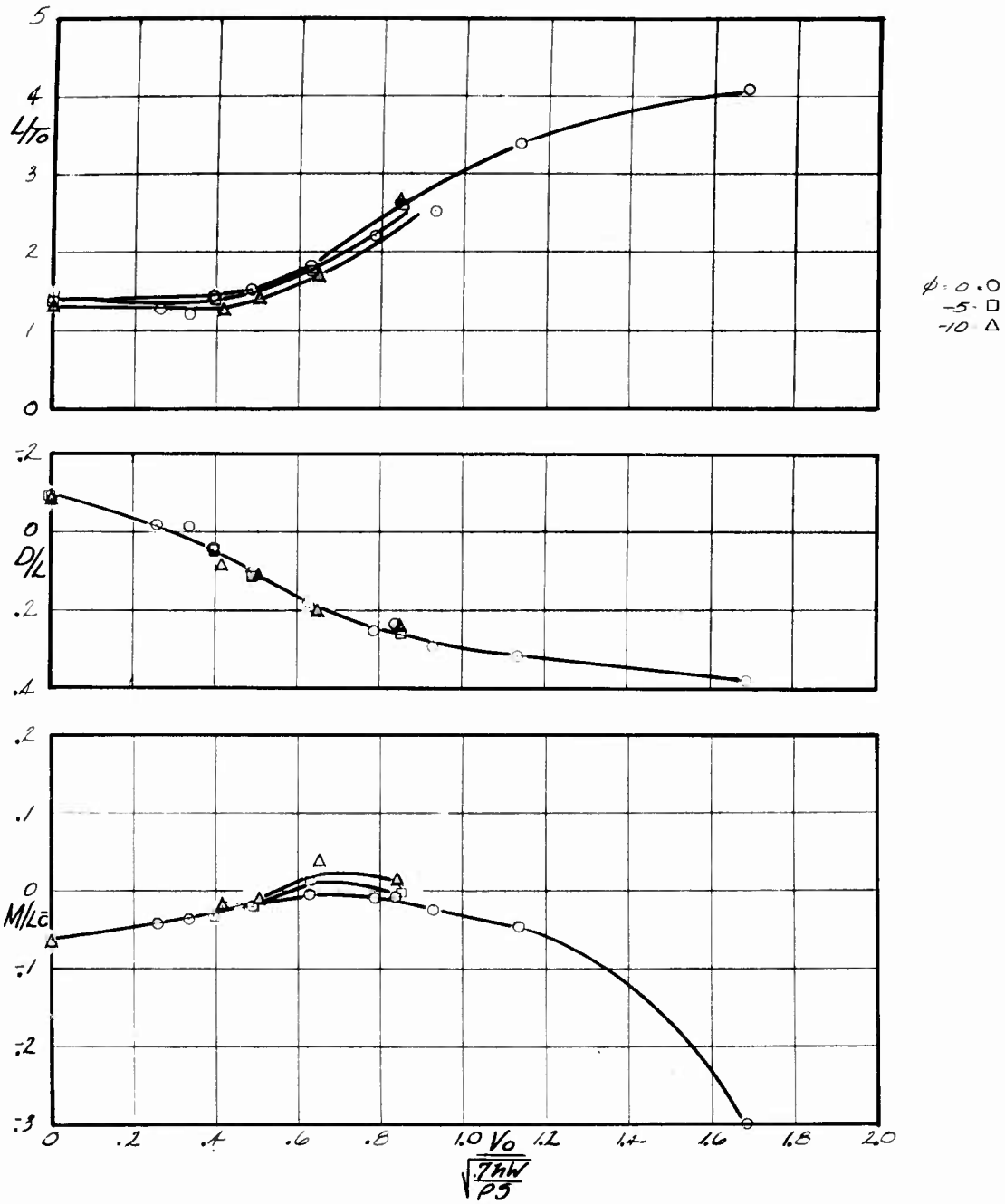

Figure 85. Effect of Roll Angle on Longitudinal Characteristics in Ground Effect With Trimmer Aft — Configuration "B" Ducts (h/c = 1.75, δ_V = 15°/-15°/0°, α = 0°, δ_F = 30°)

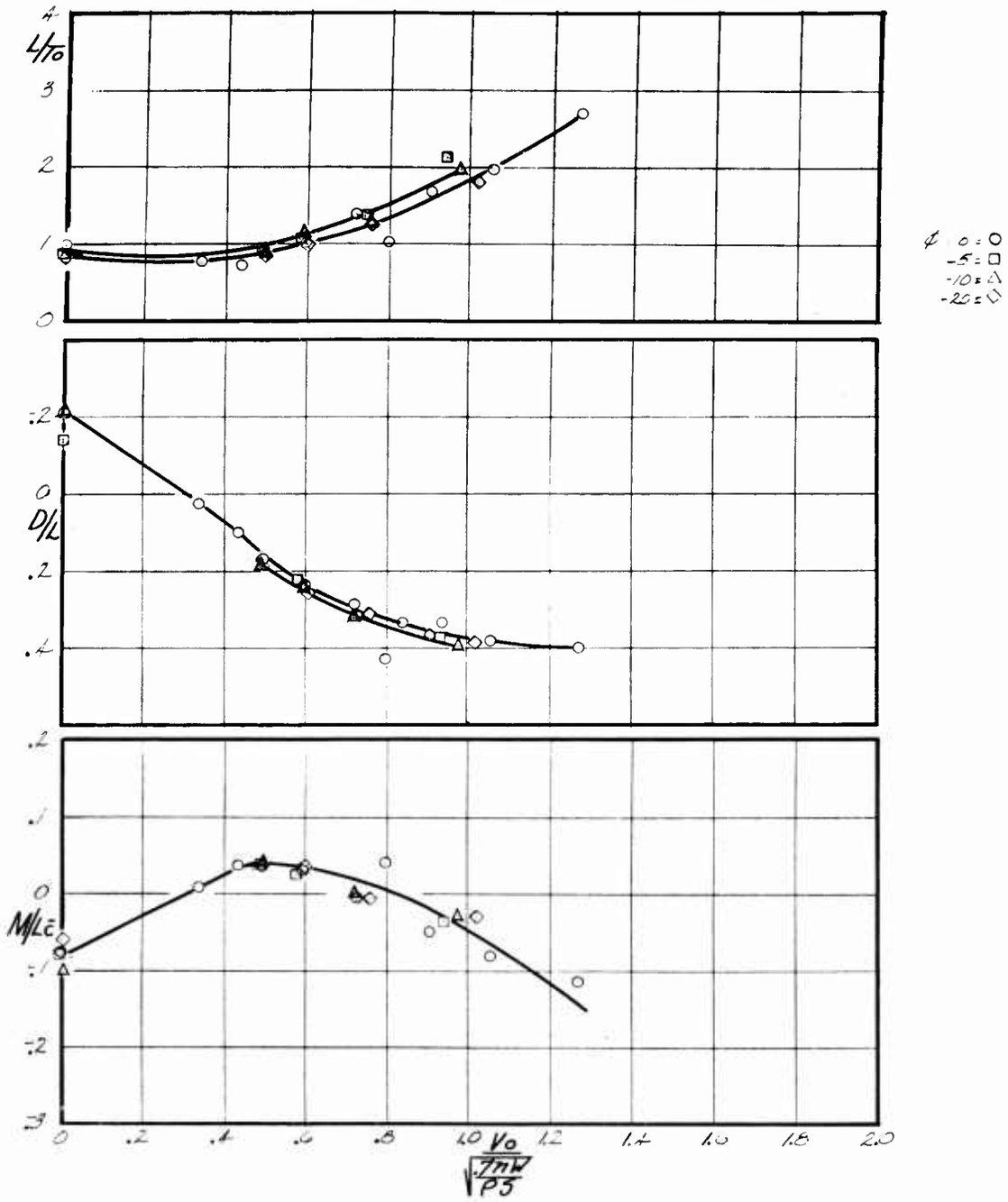

Figure 86. Effect of Roll Angle on Longitudinal Characteristics in Free Air With Trimmer Aft — Configuration "B" Ducts (h/c = 1.95, δ_V = 15° /-15° /0° , α = 0° , δ_F = 30°)

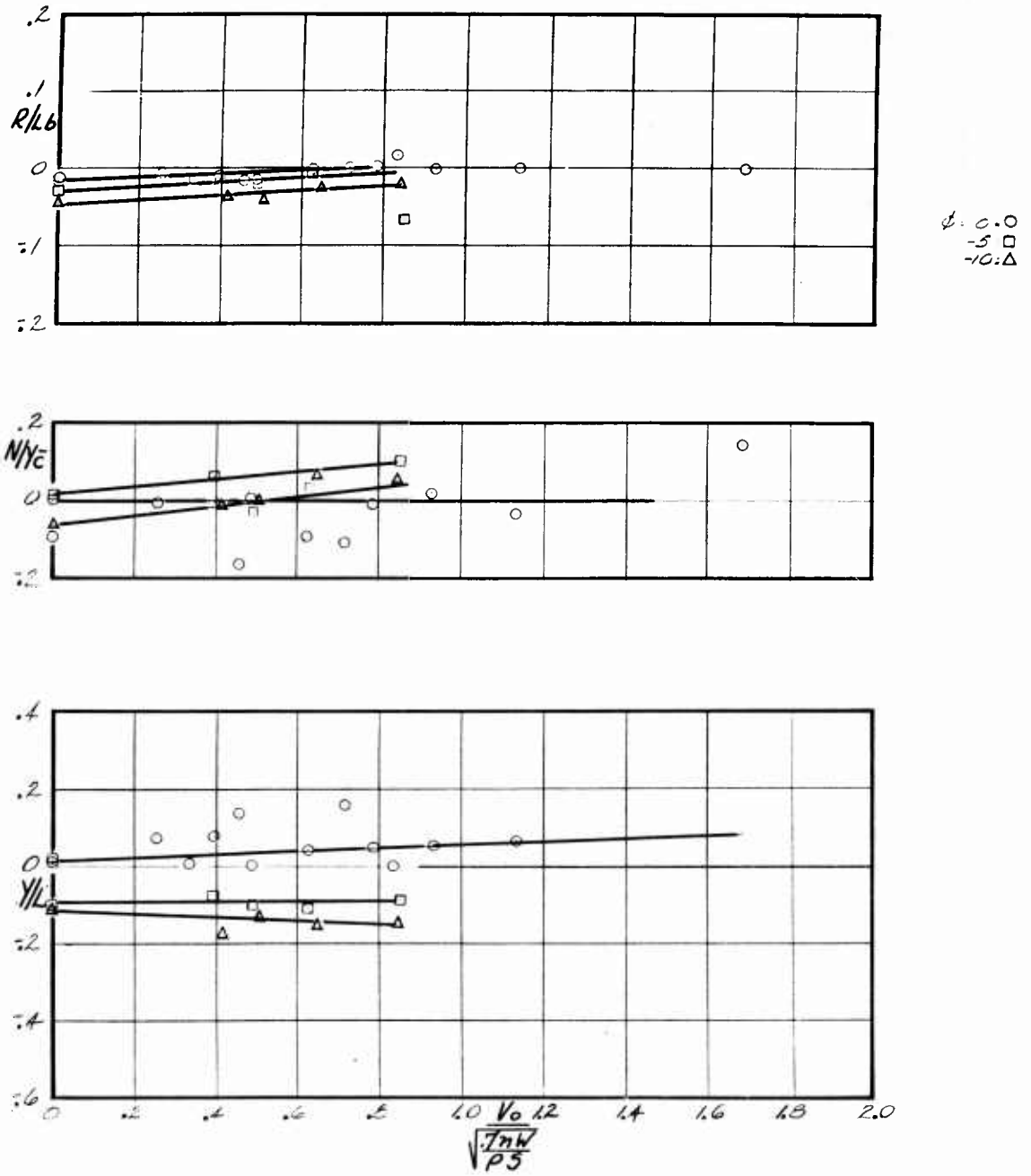

Figure 87. Effect of Roll Angle on Lateral Directional Characteristics in Ground Effect With Trimmer Aft — Configuration "B" Ducts (h/c = 0.175, δ_V = 15°/-15°/0°, α = 0°, δ_F = 30°)

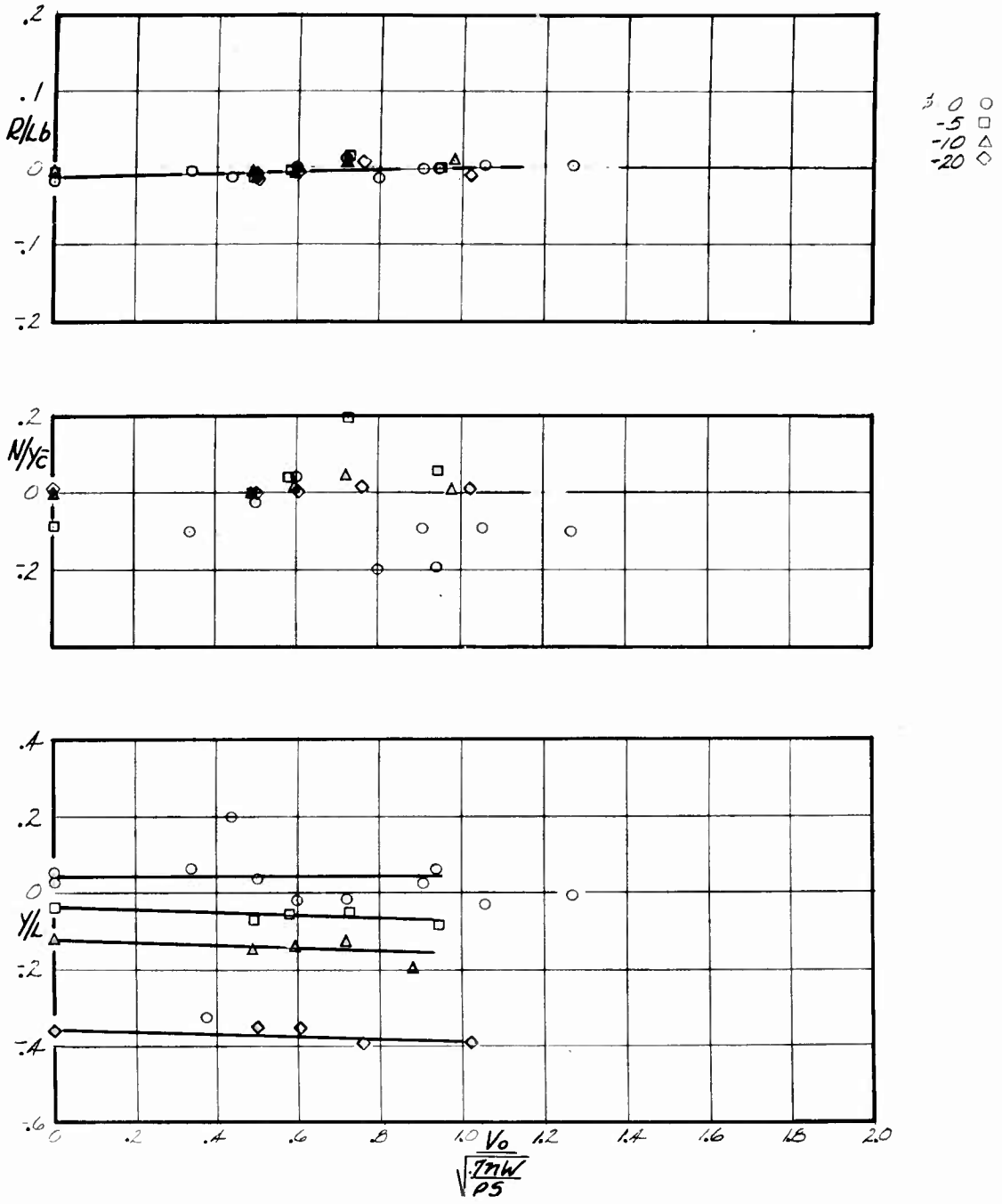

Figure 88. Effect of Roll Angle on Lateral Directional Characteristics in Free Air With Trimmer Aft — Configuration "B" Ducts (h/c = 1.95, δ_V = 15°/-15°/0°, α = 0°, δ_F = 30°)

Effect of Yaw Angle

The model was yawed nose left 10° and 20° during the final test to determine the effect of yaw with the fans operating. The longitudinal characteristics in and out of ground effect are shown in Figures 89 and 90 and the lateral-directional characteristics in Figures 91 and 92. Yawing the model produced essentially negligible effects on the longitudinal characteristics except for a small increase in drag. Of course, this would be expected with the fuselage turned partially into the free stream. There was so much scatter in the lateral-directional data due to yaw that it is quite difficult to interpret what is happening. When the model is yawed nose left, there is apparently some spanwise movement of the center of pressure to the right, the effect being more prominent in free air than in ground effect. If the model were stable directionally, nose-left yaw would produce a nose-right yawing moment, indicating a rearward shift of the center of pressure. The in-ground-effect data bears out this relationship. The free-air data exhibits so much scatter that drawing any conclusion from it is impossible; however, there seems to be no reason to assume that the relationship examined above should change. With a side force to the left as indicated above, the lateral acceleration would obviously be to the left, and this is borne out by the data. The relationship appears best represented by the free-air data of Figure 92, which shows the direction of the acceleration to be very definitely to the left. Further yaw testing is certainly necessary before definite conclusions as to the yaw characteristics can be drawn.

Power-Off Characteristics

Several runs were made during the final test with the fans and exit nozzles covered to determine roughly some of the cruise characteristics of the test configuration. Figure 93 shows representative results of these runs at four height-to-chord ratios. In this particular case, the flap deflection and tail incidence were both zero degrees, and the thrust deflection vanes were all retracted to provide as smooth a model as possible. The lift-curve slope decreased from 0.094 to 0.061 per degree and the angle of zero lift decreased from 2.7° to 0.3° as the model progressed from in ground effect to free air. This is the normal classic effect of the ground plane on lift-curve slope. The drag polars show minimum drag to be approximately 200 counts less in free air than in ground effect, but crossing over at a lift coefficient of about 0.7. The pitching moment curves show a large positive pitching moment shift as the model moves into ground effect. The horizontal tails on the model were mounted on the wing tips and thus operate in an upwash field produced by the wing tip vortices. As the model comes into the presence of the ground plane, the strength of these tip vortices apparently decreases so that the effective angle of attack of the horizontal

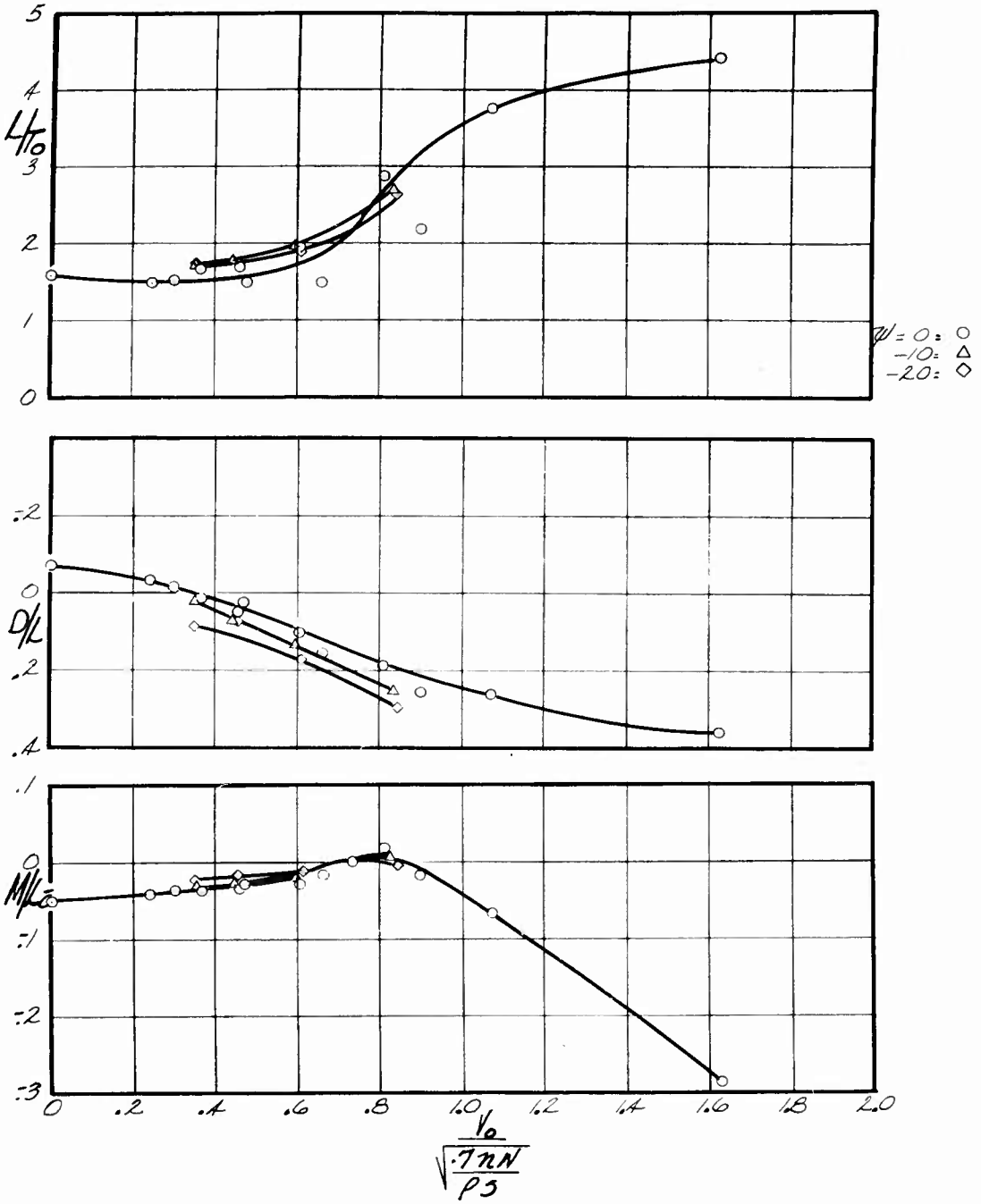

Figure 89. Effect of Yaw on Longitudinal Characteristics in Ground Effect With Trimmer Aft — Configuration "B" Ducts (h/c = 0.115, δ_V = 15° /-15° /0° , α = 0° , δ_F = 30°)

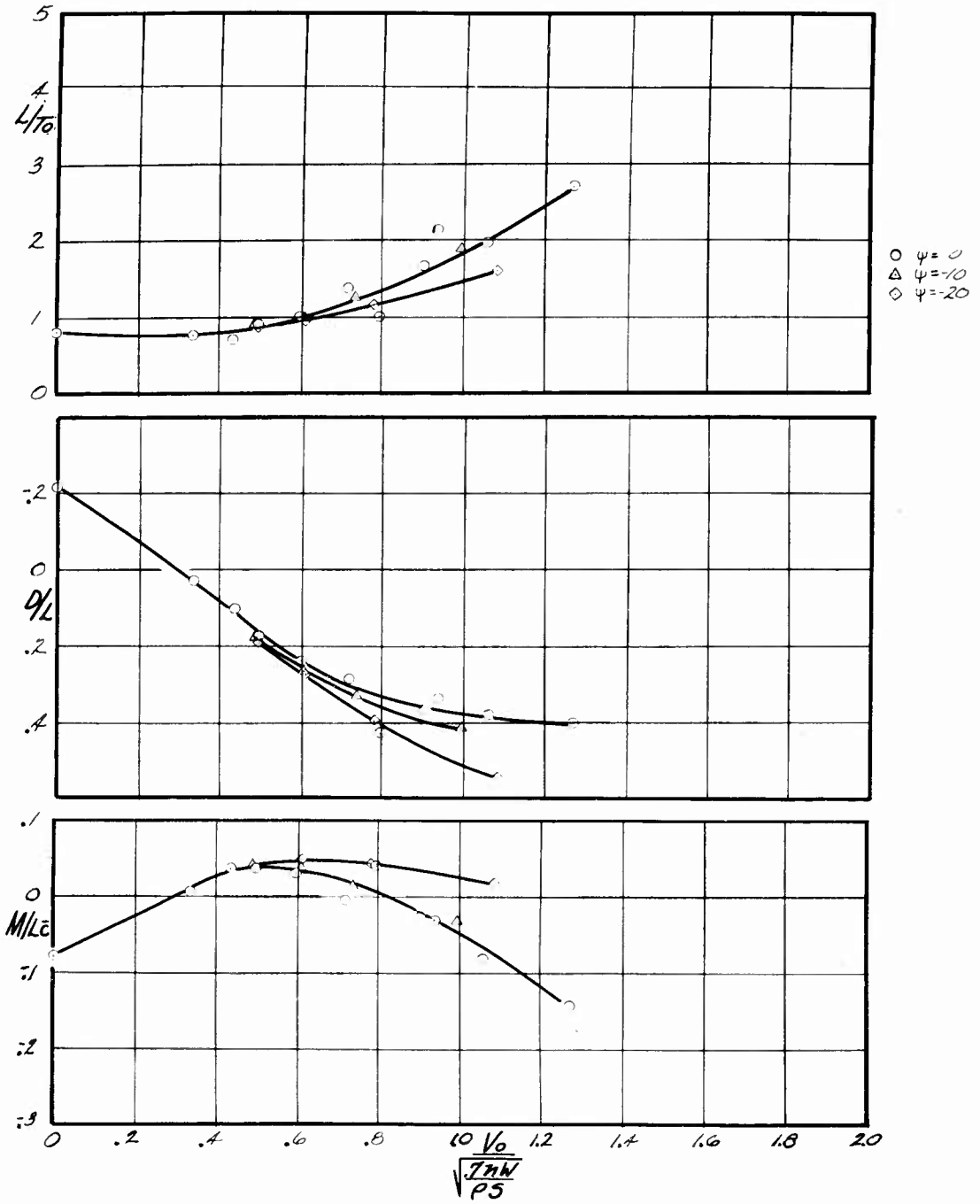

Figure 90. Effect of Yaw on Longitudinal Characteristics in Free Air With Trimmer Aft — Configuration "B" Ducts (h/c = 1.95, δ_V = 15°/-15°/0°, α = 0°, δ_F = 30°)

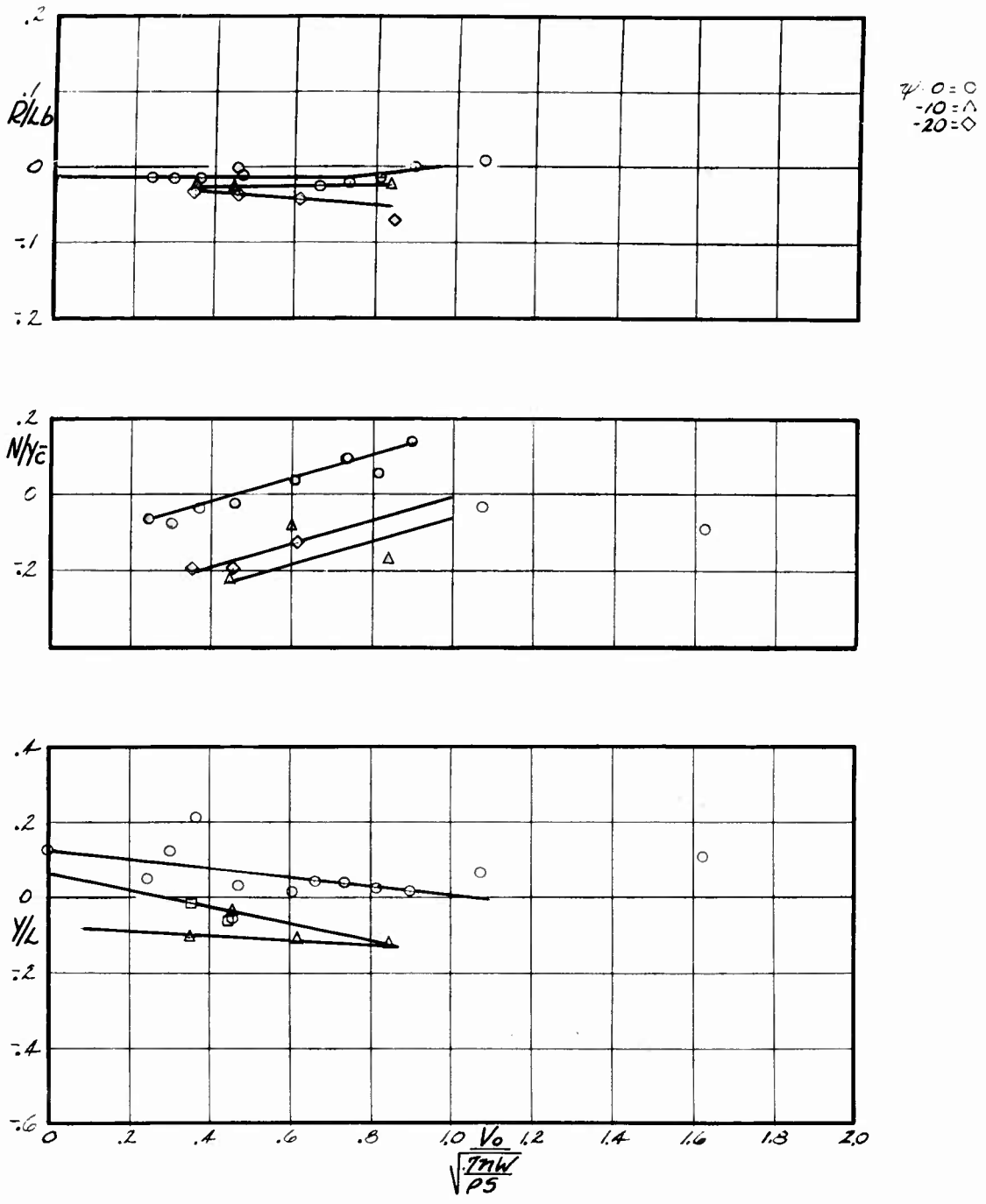

Figure 91. Effect of Yaw on Lateral Directional Characteristics in Ground Effect With Trimmer Aft — Configuration "B" Ducts (h/c = 0.115, δ_V = 15° /-15° /0° , α = 0° , δ_F = 30°)

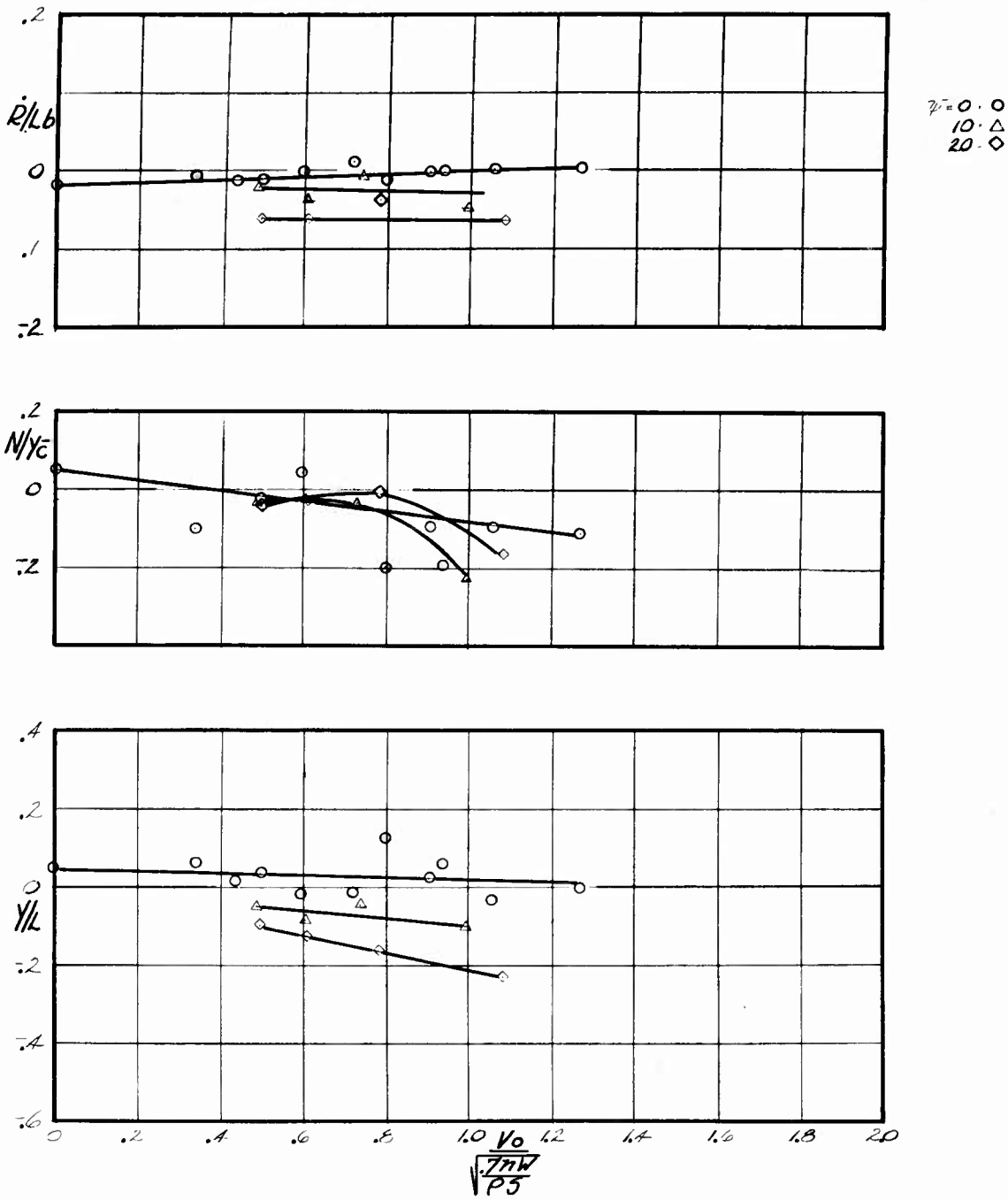

Figure 92. Effect of Yaw on Lateral Directional Characteristics in Free Air With Trimmer Aft — Configuration "B" Ducts (h/c = 1.95, δ_V = 15° /-15° /0° , α = 0° , δ_F = 30°)

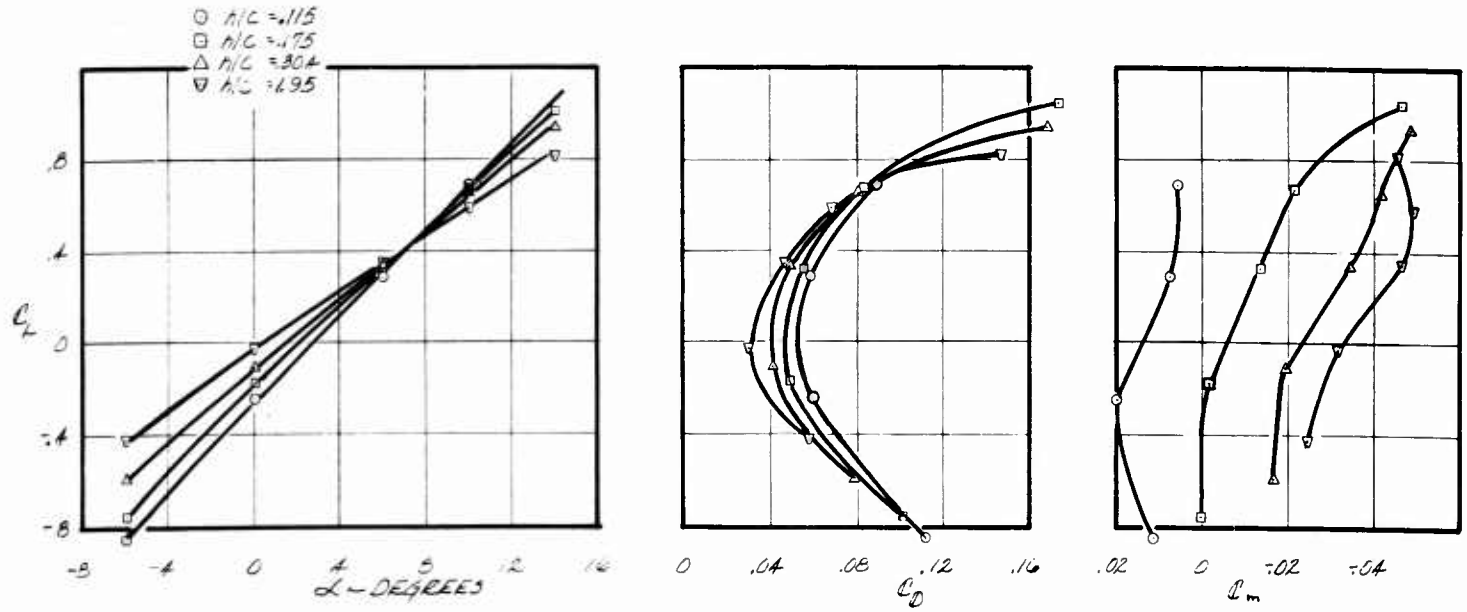

Figure 93. Cruise Configuration Characteristics — All Thrust Deflection Vanes Retracted ($q = 9.3$, $\delta_i = 0°$, $\delta_F = 0°$)

tail is reduced and an incremental nose-up pitching moment results. Note also that the model displays static longitudinal stability through only a short range in free air and then indicates a region of pitch-up beginning at a lift coefficient of approximately 0.4. This situation is unacceptable from a flying-qualities standpoint and requires that increased horizontal tail effectiveness be obtained. The solution arrived at for the transport airplane, which is presented in Phase III of this report, was to add a conventional horizontal tail to the vehicle leaving the prior tail as a fixed outboard wing panel and aileron.

Ram Drag Characteristics

Ram drag, as defined in a previous section of the report, is that momentum lost by stopping a stream tube of air of the same diameter as the fan. Also, a ram-drag recovery may be experienced in certain conditions. The drag data from the GETOL tests has been examined to evaluate the ram drag experienced by the GETOL vehicle in and out of ground effect.

As an adjunct to the ram-drag study, some time also was spent analyzing the weight flow data determined from the wind-tunnel tests. It will be recalled that six radial rakes were mounted aft of the fan to evaluate weight flow. Comparison was made between the weight flow as measured by these rakes and the theoretical value as determined from the measured thrust. When a rather large discrepancy appeared in this comparison, further comparisons were made between two sets of pressure data taken on the static test setup; one from the rakes aft of the fan and the second from rakes at the duct exit nozzles. A large discrepancy was noted in this comparison also, and since it was felt that the rakes at the exit nozzles were more accurate than those aft of the fan, it was decided to ignore the weight flow data gathered during the testing and use theoretical values calculated from the measured thrust. Figure 94 shows these values of weight flow for the free-air and in-ground-effect conditions. The data shows total weight flow for both fans.

Using the weight-flow values as determined above, a theoretical value of ram drag was determined. The wind-tunnel drag data then was reduced to evaluate the experimental values of ram drag in and out of ground effect. The results of this analysis are shown in Figure 95 where a comparison is made of experimental and theoretical ram drag in and out of ground effect. The comparison shows that in free air 100% of theoretical ram drag is experienced experimentally, while in ground effect only approximately 65% of the theoretical value appears. These results support the hypothesis presented in the section on the nature of the flow fields and their effects.

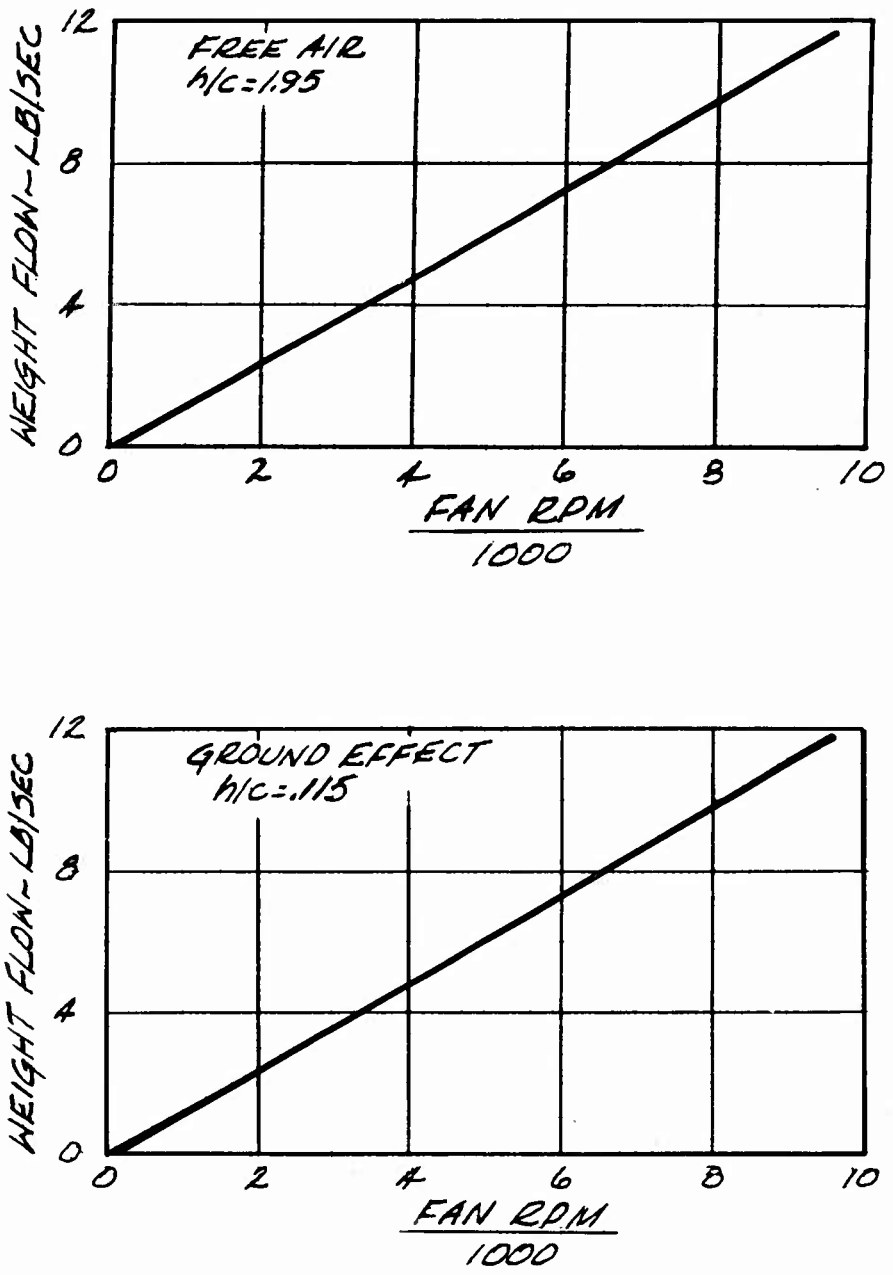

Figure 94. Weight Flow Characteristics With Fan RPM In and Out of Ground Effect — Trimmer Forward ($q = 1.5$, $\alpha = 0°$, $\delta_V = 15°/-15°/0°$)

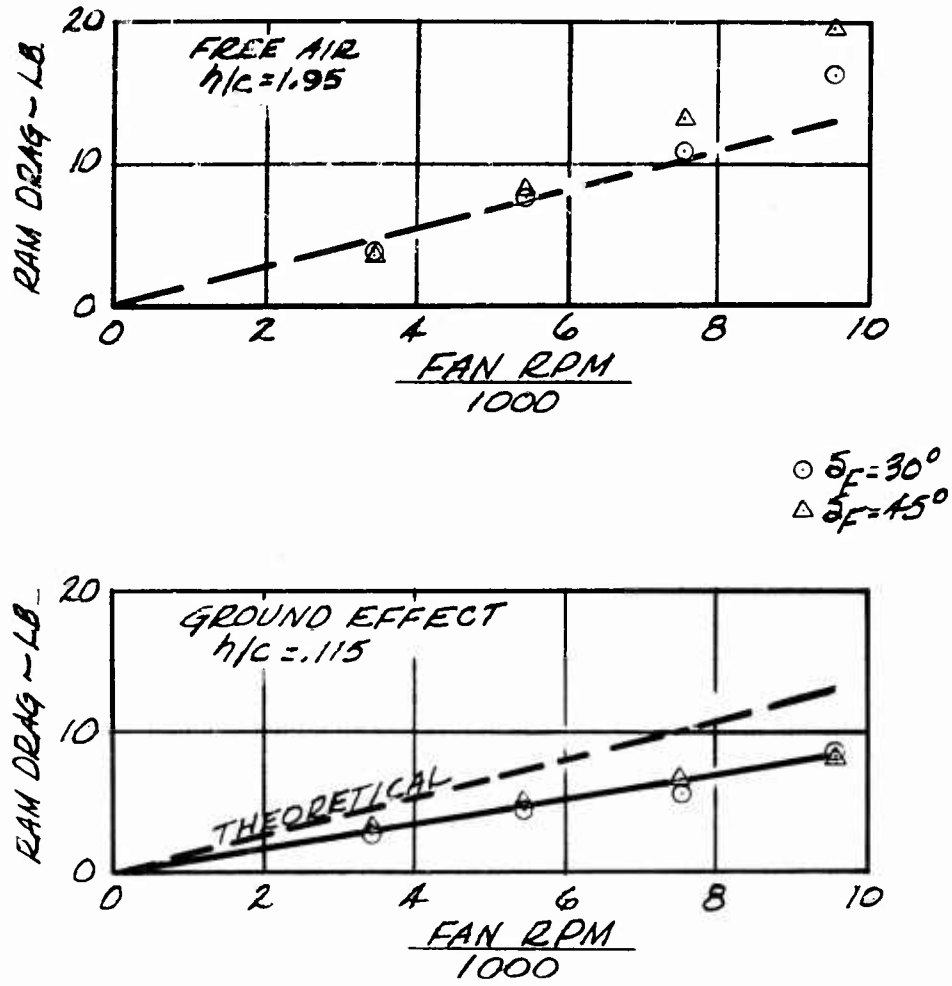

Figure 95. Ram Drag Characteristics In and Out of Ground Effect — Trimmer Forward ($q = 1.5$, $\alpha = 0°$, $\delta_V = 15°/-15°/0°$)

Another item stated by Walker (Reference 4) is that, in the presence of the ground plane, the flow from the rear slot must turn aft before it leaves the area of the vehicle — it cannot blow straight down as in free air. Evidently some pressure or force is exerted by this air which is flowing aft and is transmitted by some means through the curtain into the model. Further study and testing certainly is necessary before a complete understanding of ram drag is attained.

GENERAL HANDLING CHARACTERISTICS

This section presents a general discussion of the handling characteristics of a GETOL vehicle with a configuration similar to that tested in the wind tunnel. Specific numbers, quantitatively defining the flying qualities of a particular vehicle, are not dealt with here, but are reserved for the predesign study presented in Phase III of this report. However, the background information derived from studies of specific configurations and the results of all previous wind-tunnel tests, in conjunction with the test reported in this phase, provide a basis for this discussion.

The take-off, transition, and landing operations of a GETOL vehicle are unique, but possess qualitites of both VTOL and conventional airplanes. Both take-off and landing operations are similar to conventional aircraft in that combinations of a ground run (at hover height) and a flare are employed. The similarity to VTOL aircraft lies in the ground-hovering operation and in the transition to the conventional flight mode. Since there are no requirements specified for a GETOL-type vehicle, V/STOL and conventional airplane specifications must be used as guides for evaluation and early design efforts. Guided by these specifications, handling characteristics associated with the GETOL concept are discussed as follows.

Hovering Characteristics

The unique characteristics of the GETOL concept in hovering with respect to GEMs and VTOL aircraft is the hovering height. VTOL aircraft hovering operations are predominately free of the ground effects; therefore, the design is dominated by the requirements for height control and the characteristically neutral pitch and roll attitude stability. On the other hand, GEM operates very close to the ground over its entire speed range, thus requiring strong positive attitude stability. These extremes bracket the GETOL concept. Wind tunnel test results show that the GETOL configuration with a plain peripheral nozzle is slightly unstable in both pitch and roll at the design hovering heights. Therefore, control-system requirements similar to the V/STOL requirements are indicated when

using this data. At this time, positive attitude stability is believed to be highly desirable, if not mandatory. Consequently, the control system is likely to be driven by an automatic stabilizing system. Experimental ground-effect-machine data, however, indicates that the configuration may be made inherently stable by use of dual slots on base compartmenting. In this case, requirements as stringent as the V/STOL requirements should not be necessary.

Ground maneuvering will be accomplished either by tilting the lift vector or by introducing lateral and axial forces. An integrated combination of the two methods may prove desirable. However, since attitude control will be required for the unstable configuration tested in the wind tunnel, the lift vector tilting method appears to be the most compatible system. Further, this method is consistent with previous V/STOL concepts and the currently proposed V/STOL requirements. Therefore, a 3-axis angular acceleration control system is considered. Helicopter specifications (see Reference 6) require angular control accelerations which vary inversely with approximately the cube root of weight. These requirements are repeated in the V/STOL specifications proposed by NASA in Reference 7. However, the author of these proposed specifications currently believes that the hovering control requirements should be independent of weight and on the order of magnitude of 1, 1, and 2 radians/sec.^{2} for pitch, yaw, and roll control. Recent unpublished results of fixed base flight simulator studies under IFR conditions, conducted at Canadair, Limited, indicate that the variation of maximum available control with weight is correct but that the initial slope of acceleration versus control deflection should be independent of weight. Canadair personnel believe that the correct requirement consists of a gain through neutral control which is consistent with the 1, 1, and 2 radians/sec.^{2} maximum control suggested by Ames Research Center personnel, with a secondary gain through large control inputs which yields the current helicopter specification requirements for maximum control.

Since only the maximum control requirements are of interest at present, those of Reference 7 with one exception are used as a guide in Phase III of this report. The exception is that only half of the yaw control and damping requirements is used based on results of the X14A flight testing published in Reference 8.

Longitudinal Characteristics

The predominant characteristic in the longitudinal mode, in addition to the attitude instability metnioned above, is the large pitch trim change experienced during acceleration from hover through transition velocity. As speed is increased, nose-down control will be required to compensate for pitch-up. Rotation and climb-out will be normal. Acceleration to transition velocity will be

accompanied by an increasing nose-up control requirement as the lift system power is reduced. Details of the transition characteristics are unknown but sufficient latitude in programming the cleanup sequence exists to assure acceptable characteristics.

In the cruise configuration, the GETOL configuration as tested exhibits insufficient static stability to allow a reasonable operating cg range if full advantage of the GETOL system is to be realized. The addition of a conventional horizontal tail appears necessary to allow a cg range which is compatible with the ground-effect lift-system geometry while maintaining acceptable cruise dynamic stability characteristics.

The variable position aft slot system as tested to provide pitch trim in the ground-effect mode is not directly applicable as a control system due to the large mass displacement which would be required. Development of an equivalent system is required such as described in Phase III.

Lateral-Directional Characteristics

The significant lateral-directional characteristic associated with this configuration is the noticeably poor Dutch Roll damping. This characteristic is discussed in Reference 9 and in Phase III. The poor damping is caused by the large inertia to damping ratio and the large dihedral effect associated with the wing tips. This Dutch Roll oscillation most likely will fall into the emergency operation region defined in Reference 7. Therefore, either a significant configuration change or a full-time automatic damping system appears required.

The control systems for cruise operation will be conventional and, therefore, will require very little development effort. Systems for the ground-effect mode, however, will require a wind tunnel development program since no satisfactory system has been tested to date. Concepts for these systems are presented in Phase III.

PHASE III — TRANSPORT APPLICATION

The objective of Phase III was to use information derived from the wind tunnel tests of Phase II to obtain a representative GETOL aircraft configuration. The configuration was evaluated with respect to:

1. Cruise performance.
2. Take-off and landing performance.
3. Cruise handling qualities.
4. Take-off and landing handling qualities.

An assault transport vehicle was chosen to be a representative U. S. Army GETOL configuration. This vehicle would have payload capability in excess of 10 tons and ferry range capability in excess of 3,000 miles.

The aircraft is more completely described as follows:

Take-off weight		82,570 pounds
Useful load		28,722 pounds
Lift-system gas generators	2 at	21,000 pounds thrust each
Lift fan diameter		100 inches
Cruise engines (regenerative)	2 at	4,891 SHP/each
Propellers	2 at	14-foot diameter
Basic wing area		1,856 square feet

The airplane has a fuselage whcih provides water-meaneuvering capability on lakes and rivers. Figure 96 is a three-view drawing of the aircraft. Figure 97 is an inboard drawing.

WEIGHT DERIVATION

Due to the unique wing configuration, the usual weight estimating techniques could not be used. In lieu of the normal techniques, a weight was determined by using a preliminary stress analysis and preliminary design layouts. It was found that most gages would be set, not by structural requirements, but by

1

GENERAL DATA

		WING		TAIL	
		BASIC	HORIZ.	VERT.	HORIZ.
AREA	SQ.FT.	1856	464	185.6	382
ASPECT RATIO		1.6	1.0	1.0	3.5
TAPER RATIO		1.0	.6	.575	.65
INCIDENCE	DEG.	3	3	–	–
DIHEDRAL	DEG.	–	3	–	1.5
SWEEPBACK	DEG.	0	0 @ T.E.	45 @ L.E.	0 @ 50C
THICKNESS	t/c	.22	.16	.16	.12
VOL. COEFF.	$\bar{V}$		.125	.739	.239

FANS (2)

DIAMETER	INS.	100
DRIVE	GAS COUPLE	TIP TURBINE
CAPTURE AREA	SQ.FT.	54.541
HUB AREA	SQ.FT.	13.448
NET (F) AREA	SQ.FT.	41.094

WING EXITS

L.E. @ T.E. / SIDE	SQ.FT.	49.50
TIP / SIDE	SQ.FT.	29.00
BASE AREA / SIDE	SQ.FT.	572.25

ENGINES

CRUISE (2) REGENERATIVE TURBO PROP ENGINES OF 4091 SHP EACH (ALLISION T-56 TYPE)

FANS: (8) GAS GENERATOR ENGINES OF 21,000 # THRUST EA (G.E. - LT200 DIRECT LIFT ENGINE TYPE)

PROPELLERS: (2) 14'-0" DIAMETER 4 BLADE VARIABLE PITCH

GROUND HANDLING GEAR - M.L.G. - 56 x 11-24 PR. N.L.G. - 18 x 4.4 - 10 PR.

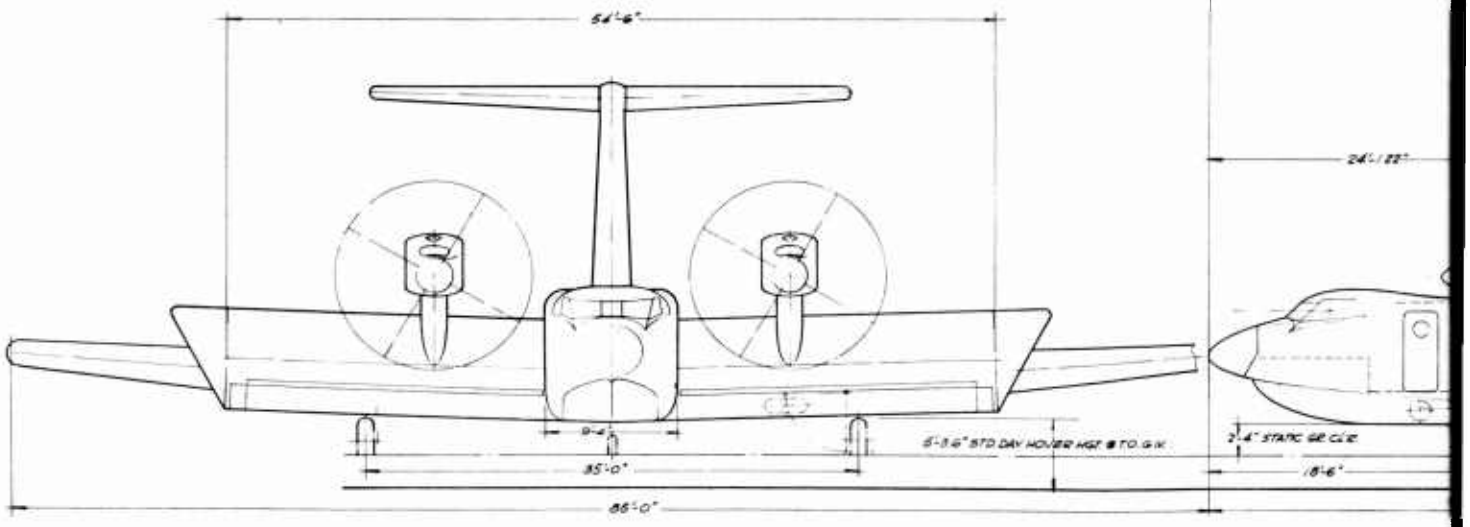

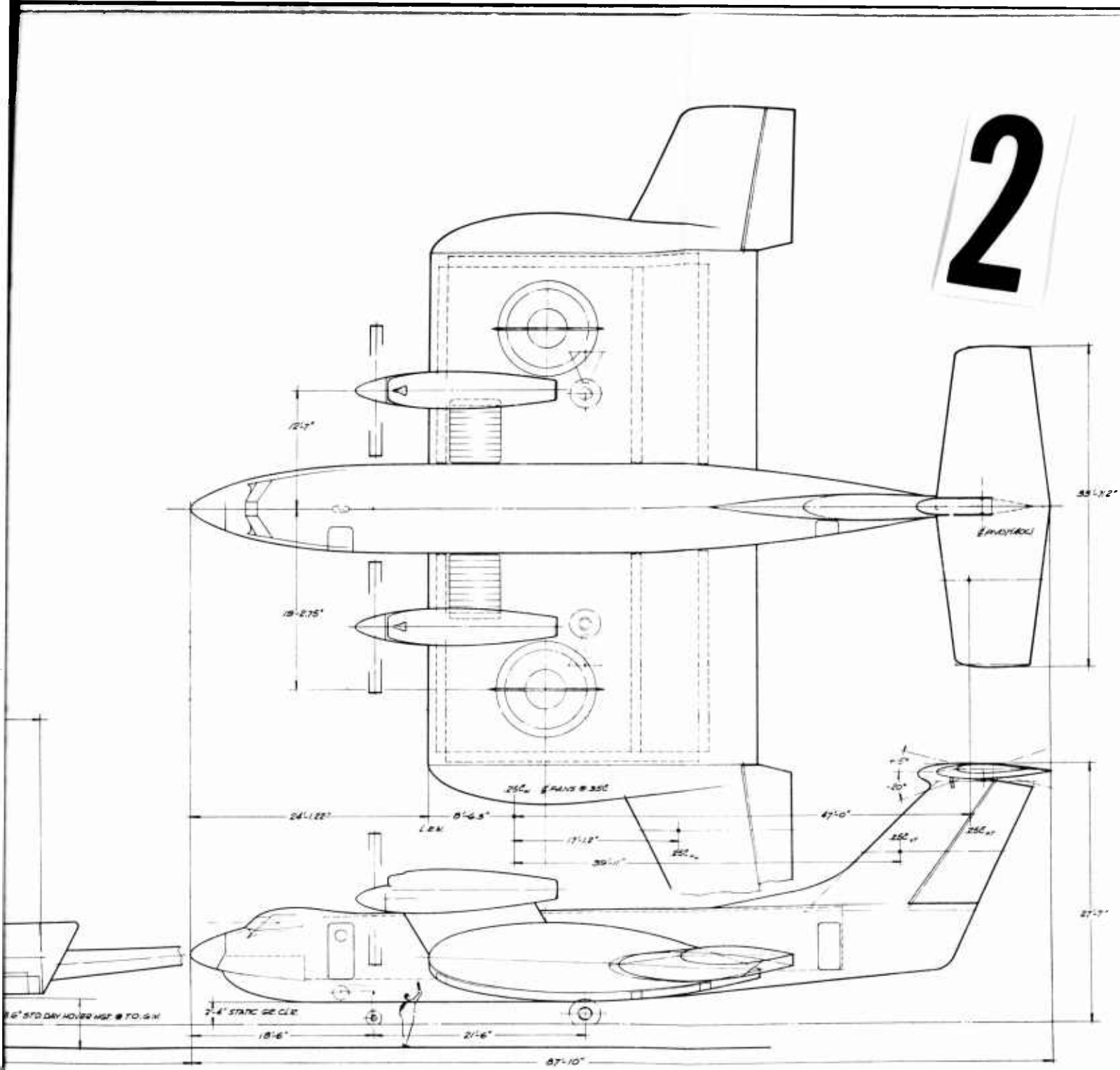

Figure 96. General Arrangement — Ground Effect Take-Off and Landing

1

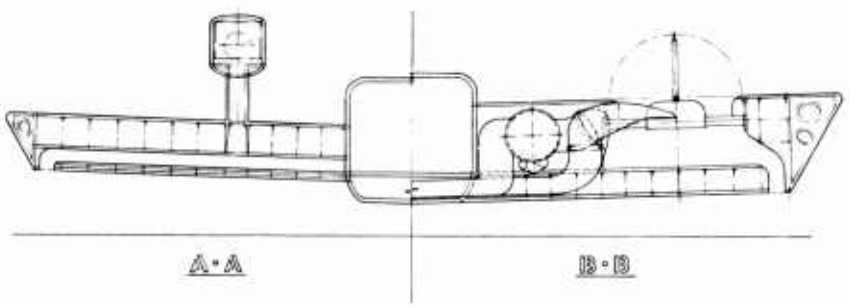

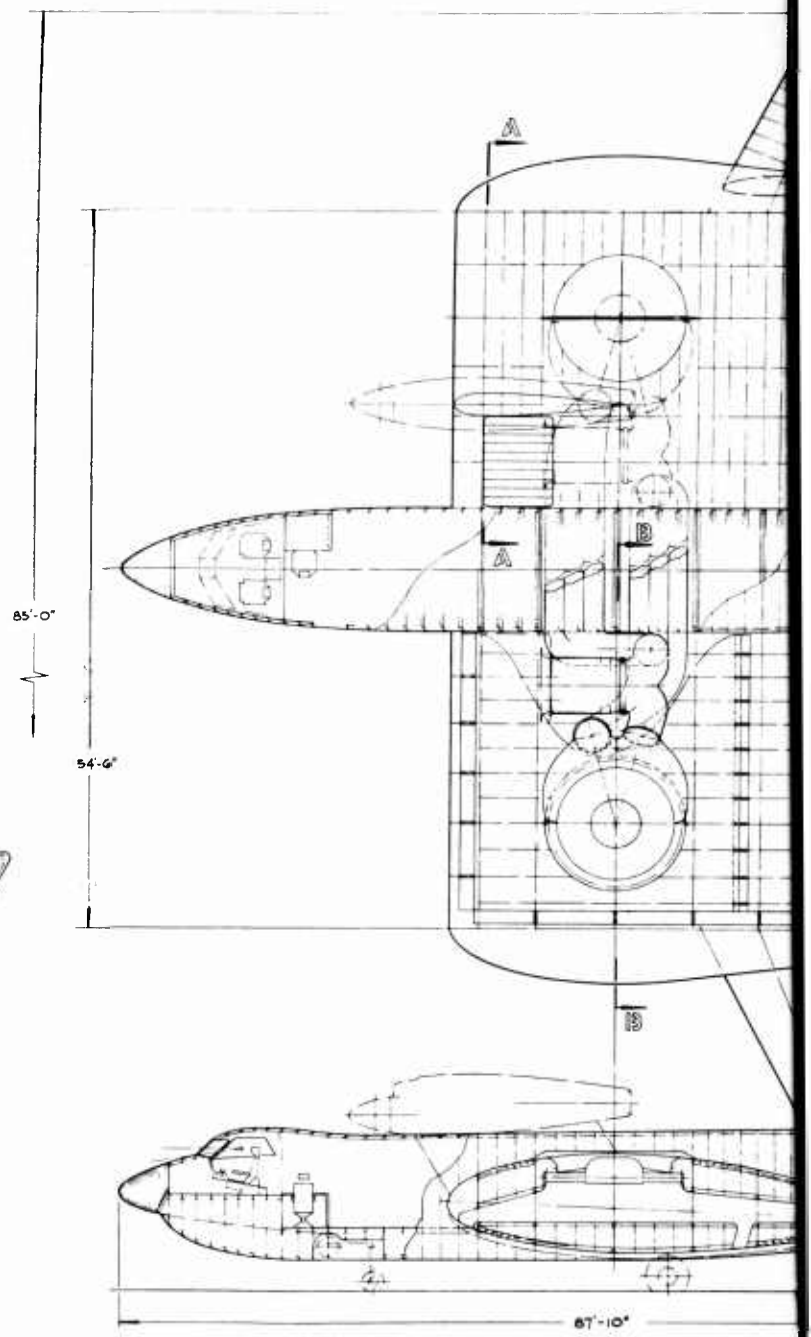

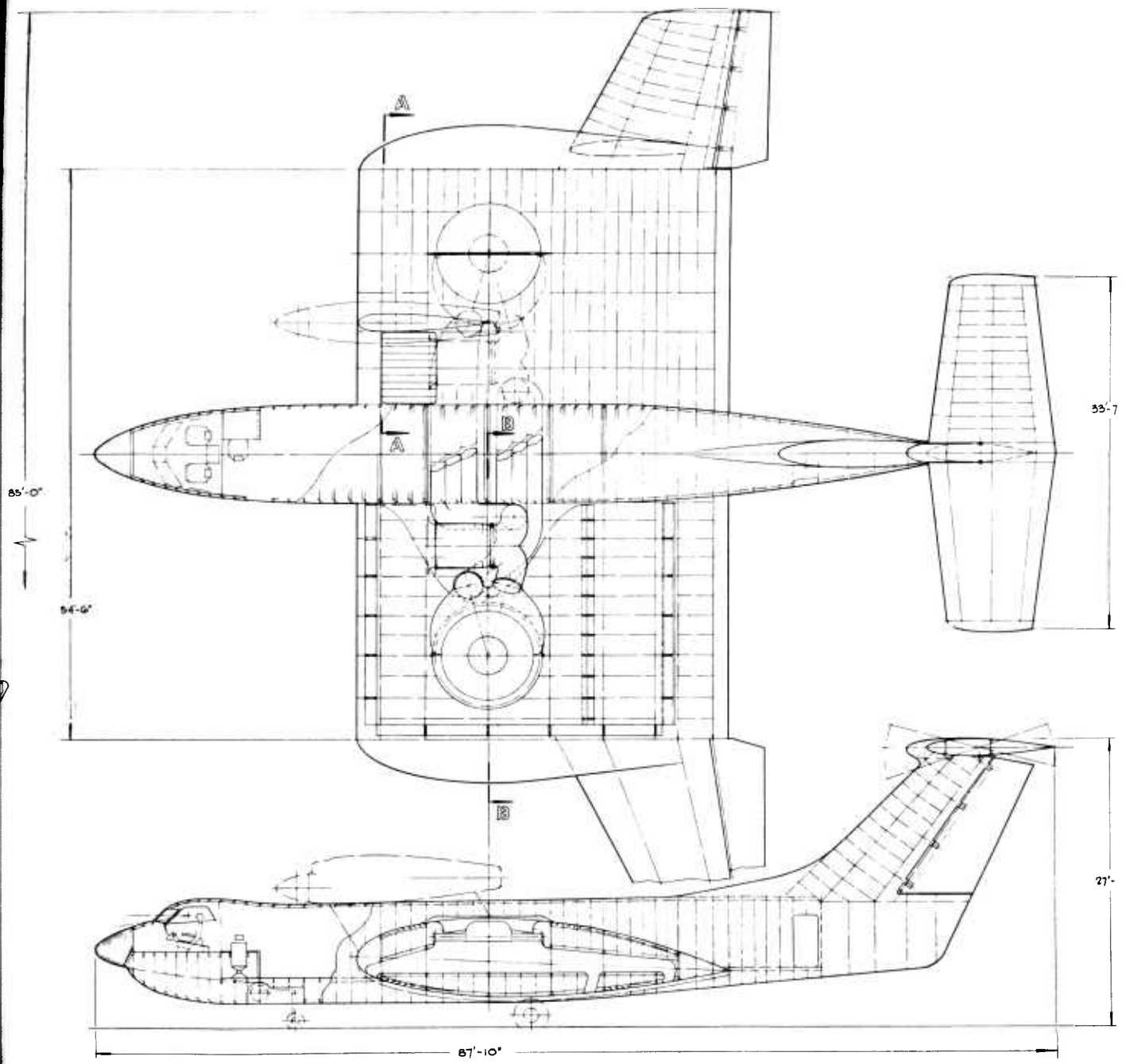

Figure 97. Structural Inboard

fabrication, handling, serviceability, and fuel-tight requirements. The weights of other structural components were derived by using conventional preliminary weight estimating techniques. Powerplant weights were obtained from the engine manufacturers. Weights for other systems and equipment were obtained by comparison with other airplanes that have similar mission requirements. A detailed weight statement is shown in Table 1.

CRUISE PERFORMANCE

Drag Basis

The cruise-drag basis consisted of a component drag buildup to establish the zero lift drag plus a modification of experimental trimmed drag due to lift data derived from a test on a similar configuration with an aspect ratio one wing in the Convair Low-Speed Wind Tunnel. The modification consisted of altering the wind tunnel data of Reference 10 for variations in wing-aspect ratio, tail-area-to-wing-area ratio, and tail-aspect ratio. The drag at a cruise altitude of 10,000 feet is shown in Figure 98.

Cruise Engine Performance

Since it is expected that regenerative turboprop engines will be available during the expected GETOL development time, they have been used as cruise engines for this configuration. The engines selected are Allison Model 501 MHR-type regenerative turboprop engines rated for take-off at 4,891 SHP each. The specific fuel-consumption values have been increased 3% to account for installation losses and another 5% to comply with the provisions of Mil Spec 5011A. The engine performance at a cruise altitude of 10,000 feet is shown for one engine in Figure 99.

Propellers

The propellers are four-bladed with a diameter of 14 feet. The activity factor is 180 and the integrated design lift coefficient is 0.3. This propeller has an efficiency of approximately 0.85 as computed for 10,000-foot cruise by the method of Reference 11. The static thrust-to-horsepower ratio is approximately 2.68 when computations from the same reference are used.

High-Speed Performance

The aircraft has a high speed at sea level of 306 knots for a gross weight of 71,000 pounds which corresponds to a condition of 40% fuel used and zero

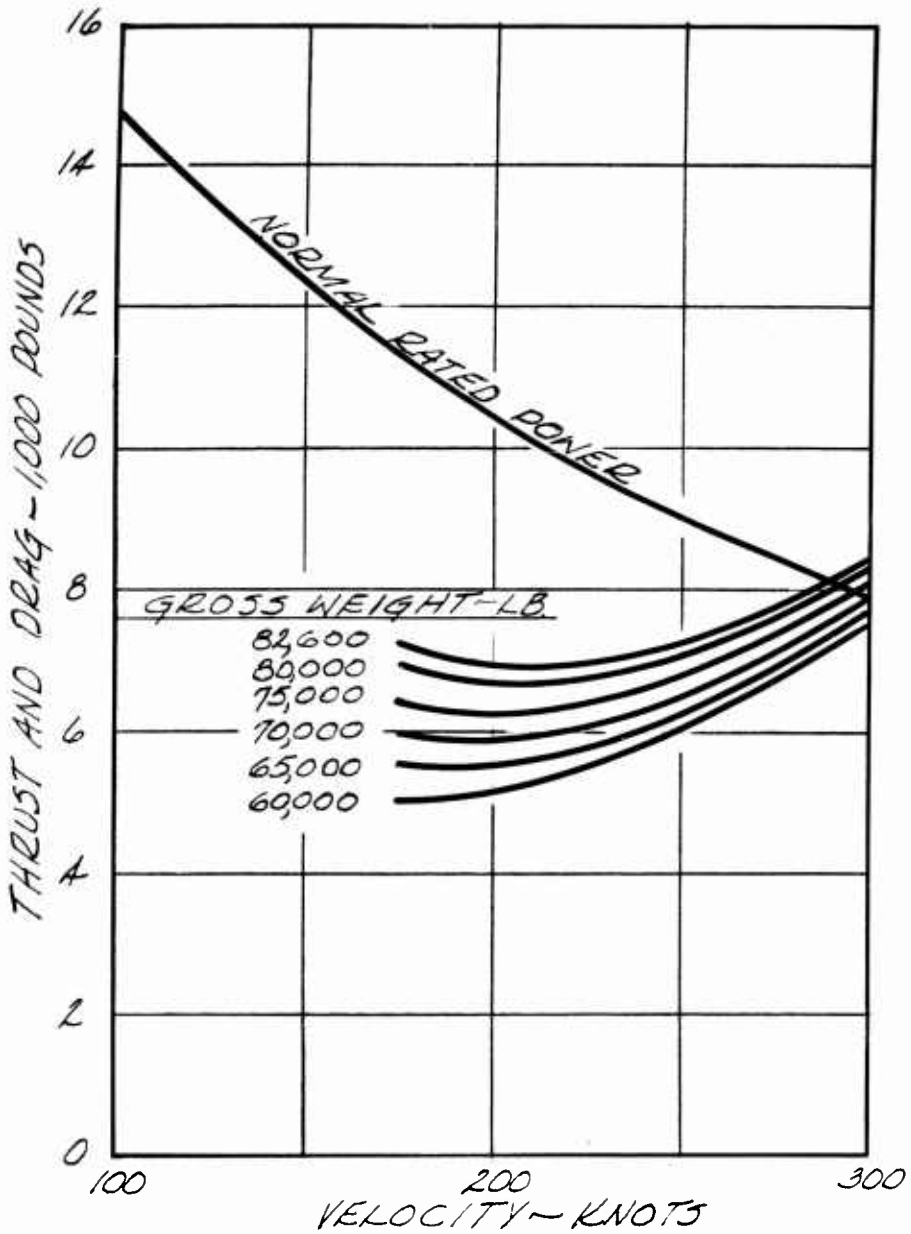

Figure 98. Cruise Drag, Altitude = 10,000 Feet

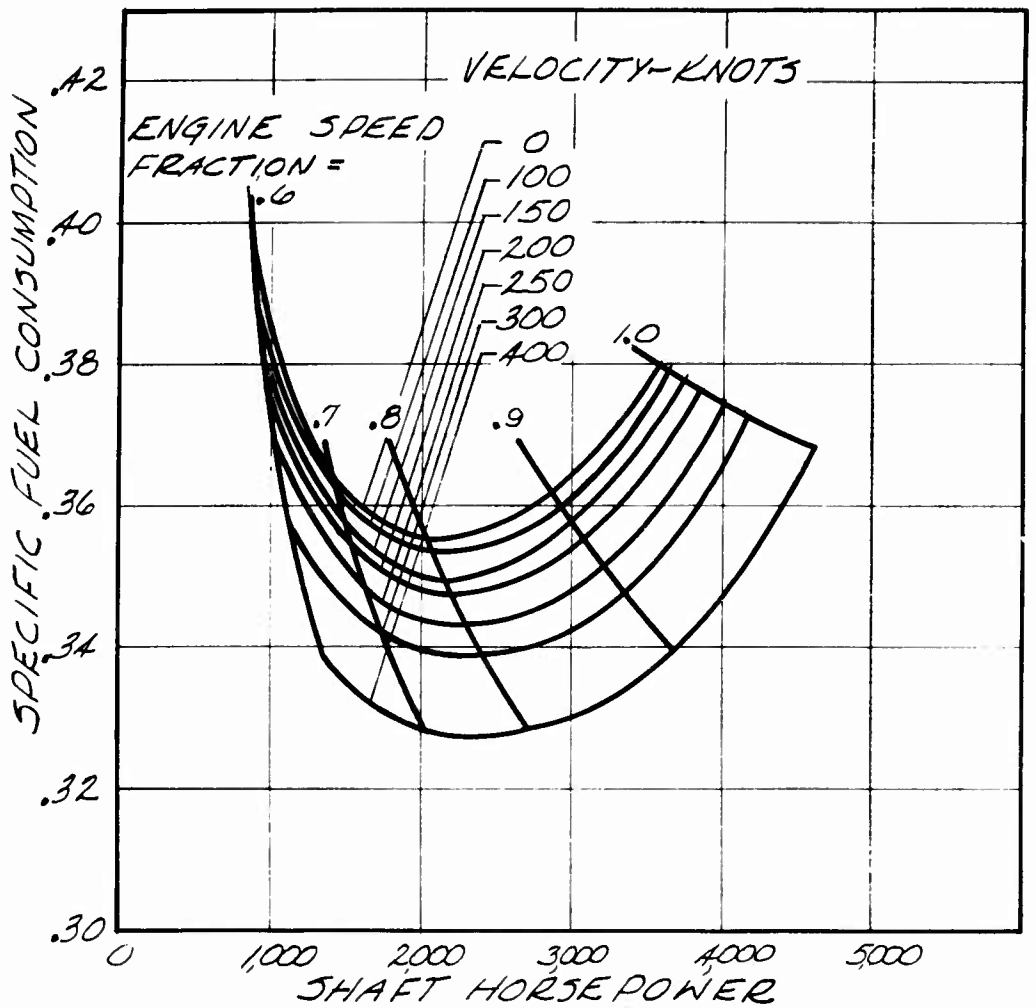

Figure 99. Cruise Engine Performance (Allison 501 MHR-Type)
Standard Day, One Engine Only, Altitude = 10,000 Feet

TABLE 1
GETOL ARMY SUPPORT

Dwg. No. SD-62-27012

			Weight (Pounds)
Structure			(23,486)
Wing (Includes outer panel)			11,425
Tail			2,150
Hull			5,350
Landing Gear			2,060
Nacelle			1,661
Surface Controls			840
Propulsion	Cruise	Lift	(21,767)
	(9,592)	(12,175)	
Engine	5,600	2,950	
Air Induction	42	770	
Exhaust	285	150	
Lubrication	205	50	
Fuel System	1,050	-	
Engine Controls	100	40	
Starting	150	100	
Propellers/Fans	2,160	5,315	
Ducts and Controls	-	2,800	
Systems			
Instruments			(7,260)
Hydraulic and Electrical			650
Avionics			1,275
Furnishings			2,060
Heat and Vent			750
APU			385
Weight Empty			(52,513)
Crew (2)			400
System Fuel and Oil			935
Basic Operating Weight			(53,848)
Military Payload			28,722
Gross Weight			82,570

payload. Maximum performance is indicated in the curve of Figure 100 for this same weight.

Mission Performance

Mission performance for this aircraft is illustrated by its range payload capabilities. The airplane is capable of transporting an 8-ton payload for a range of over 1,200 nautical miles. The complete range payload performance is shown in Figure 101. Note that at zero range, the payload differs from the total useful load by the take-off fuel allowance plus the reserves and also that there is no weight or space limit on the payload weight. The mission is defined using Mil Spec 5011A as a basis as follows:

1. Fuel allowance for starting engines, take-off, and acceleration to climb speed is the sum of the following items:

   a. Normal rated power on the cruise engines, 5 minutes.

   b. Normal rated power on the lift system (helicopter requirement), 2 minutes.

2. Climb on course to an altitude of 10,000 feet for cruise.

3. Cruise out at 215 knots at 10,000 feet.

4. Land (no fuel consumed, no distance credit).

5. Reserves: 10% of initial fuel (helicopter requirement) or 2 minutes normal rated power on the lifting system, whichever is larger.

TAKE-OFF AND LANDING PERFORMANCE

Take-offs and landings were calculated for the transport configuration by a digital computer and were based on wind tunnel test data. The take-offs were calculated for full airplane gross weight, while landings were calculated at a reduced airplane weight, representing 40% fuel load plus full military payload.

Wind Tunnel Data

Vane configurations which were tested with two or three trimmer positions (aft nozzle position) were chosen for use in the take-off and landing computations.

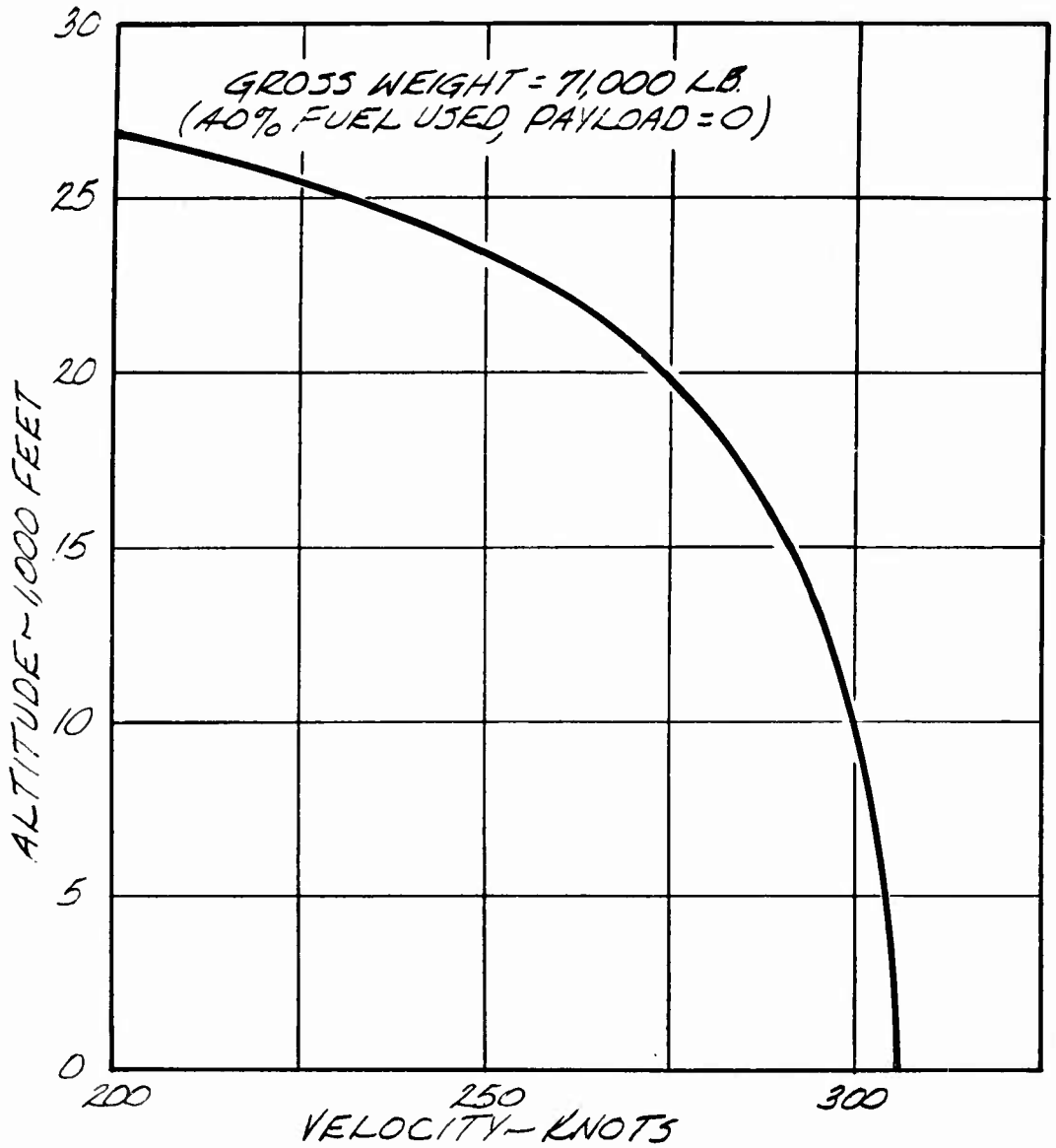

Figure 100. Maximum Performance

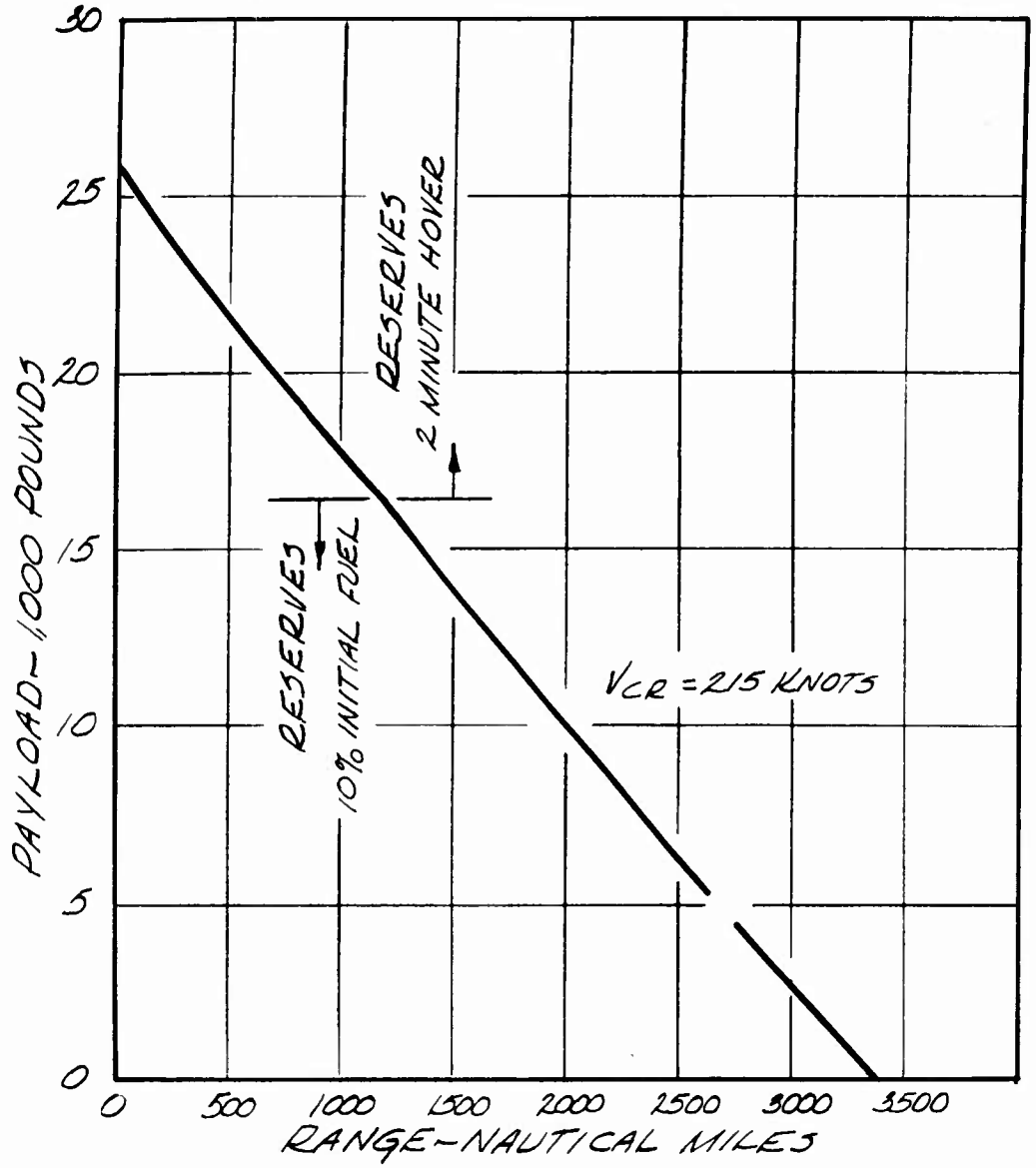

Figure 101. Mission Performance, Altitude = 10,000 Feet, Take-Off Gross Weight = 82,570 Pounds

The data was replotted for trim conditions, i.e., zero moment. Thus, values of lift-to-thrust ratio and drag-to-lift ratio used in the calculations represent interpolated values for a trimmer position giving zero moment.

The wind tunnel model drag was additionally modified by allowing for a cleaner nozzle vane installation and a higher pressure ratio fan in the full-scale airplane. Model drag data on a cruise configuration with the nozzle vanes installed and with the vanes removed provided a basis for the former modification. The latter drag modification, and the change in ram drag because of the change in fan pressure ratio, was based on calculated values of fan airflow for both the model fans and the airplane fans.

Propeller and Nozzle Thrust

The propeller configuration was chosen on the basis of high thrust performance for both the static and cruise conditions. The propellers are four-bladed, 14 feet in diameter, have an activity factor of 180, and a design-C_L of 0.3. The full-power propeller thrust at low speeds is shown in Figure 102.

The nozzle thrust was calculated for two 100-inch diameter fans powered by two 21,000-pound thrust gas generators with due allowance for duct losses. The maximum nozzle thrust obtainable is 61,553 pounds.

Calculative Procedure

An iterative process was used to compute take-offs and landings, with equal time increments. The airplane normal and tangential accelerations are calculated for a given condition, resulting in increments of velocity and distances, thus determining new conditions for the succeeding iteration. An IBM 1620 digital computer was used for these calculations, the procedure being programmed in Fortran computer language.

Take-Off and Landing Procedures

The take-offs presented consist of accelerating from zero velocity and climbing above a height of 50 feet to a speed of 1.2 times the stall speed (137.5 knots for the transport airplane). The airplane is allowed to accelerate at full power and, as the lift begins to increase with increase in speed, the airplane is allowed to climb. When a 50-foot height is reached, the fan thrust is lowered and adjusted to maintain a 0.8 load factor pushover to level flight. Acceleration then continues at a constant altitude. Angle of attack nominally is maintained constant, except for changes in vane configuration and/or angle of attack at discrete points during the take-off.

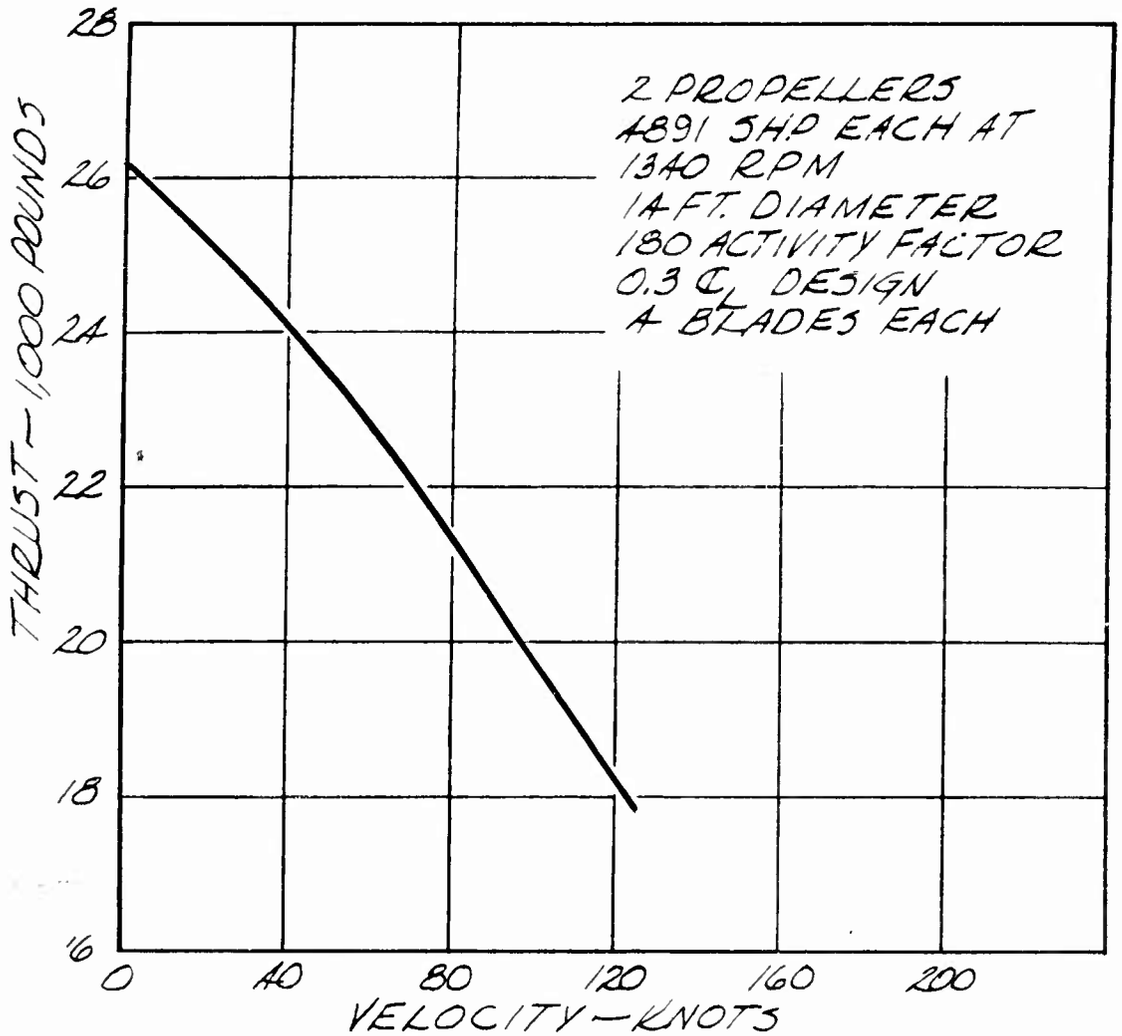

Figure 102. Take-Off Propeller Thrust, Maximum Power

Landings were calculated in a similar manner to take-offs. Thus, the airplane decelerates from 1.2 times the stalling speed at a constant height, then pushes over by lowering fan thrust and maintaining a load factor of 0.8. The fans are then brought to full power for the remainder of the landing. The airplane pulls up as a result of the lift increasing in the presence of the ground. Final deceleration in ground effect is aided by reverse propeller thrust.

Take-Off Performance

The results of the take-off calculations are plotted to show the flight path in terms of height versus horizontal distance traversed. Figure 103 illustrates the take-off performance of the transport airplane obtainable with a constant vane configuration of 15° /-15° /0° . Three take-off paths are shown, representing flights at three distinct angles of attack, 0° , 6° , and 10° . Note that the angle of attack was limited to zero degrees until a speed of 60 knots had been reached; this allowed a greater hovering height, since the lift-to-thrust ratio is greater at zero velocity for this angle than for the higher angles. Note also that selected values of speed and elapsed time have been marked on the flight paths, so as to give an indication of comparative accelerations along portions of the take-off.

It is encouraging that a take-off can be accomplished without varying the vane configuration while maintaining zero angle of attack. The 15° /-15° /0° vanes provide little propulsive thrust, especially at the higher speed. Moreover, lift-to-thrust ratio increases little with forward speed at this angle of attack. Thus, it is expected that the take-off performance would be relatively poor.

By rotating the airplane to a positive angle of attack, a much improved take-off results, as shown in Figure 103. This is mainly due to the increase in available lift. A height of 50 feet is obtained in 1,000 to 1,200 feet, while transition speed (1.2 times the stalling speed) is reached in 35 seconds or less. Remember that this take-off performance is obtained without manipulating the nozzle vanes.

Figure 104 shows the relatively small effect vectoring the tip slot has on the take-off performance. Vectoring the tip slot actually increases the distance to reach 50 feet, since the lift-to-thrust ratio is decreased. Total time to transition speed is lessened by only 2 seconds.

In an effort to increase the take-off acceleration when out of ground effect, both front slot and tip slot vectoring were increased when the airplane levelled off. The results are shown in Figure 105. Vanes of 15° /-15° /30° were maintained until the airplane reached level flight, and then changed to 30° /-15° /30° . Both 6° and 10° angle of attack are shown. The flight path at 10° angle of attack was

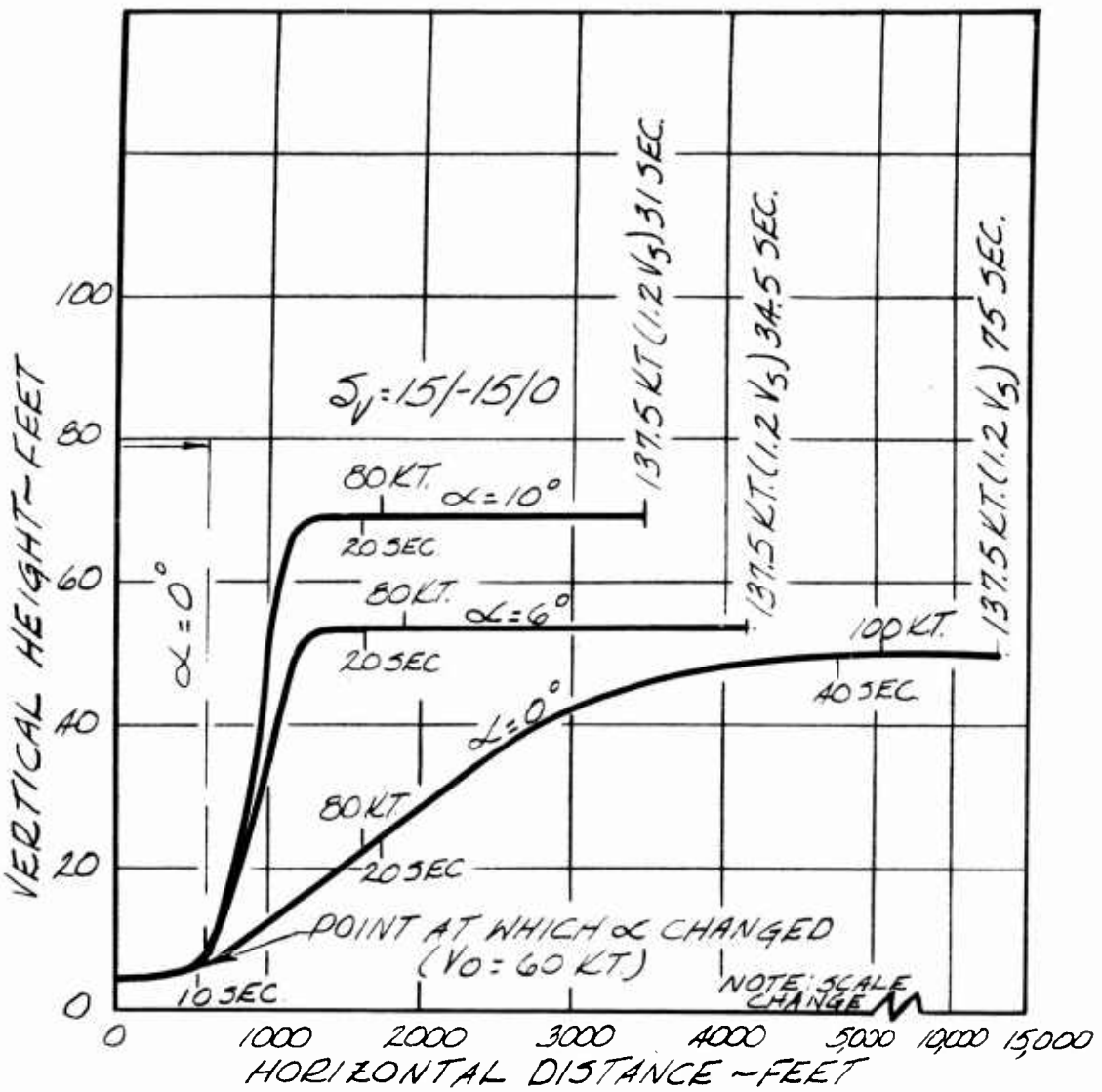

Figure 103. Effect of Angle of Attack (With Constant Vane Configuration) On Take-Off Performance, Gross Weight = 82,500 Pounds, Time Shown is Elapsed Time From Start of Take-Off

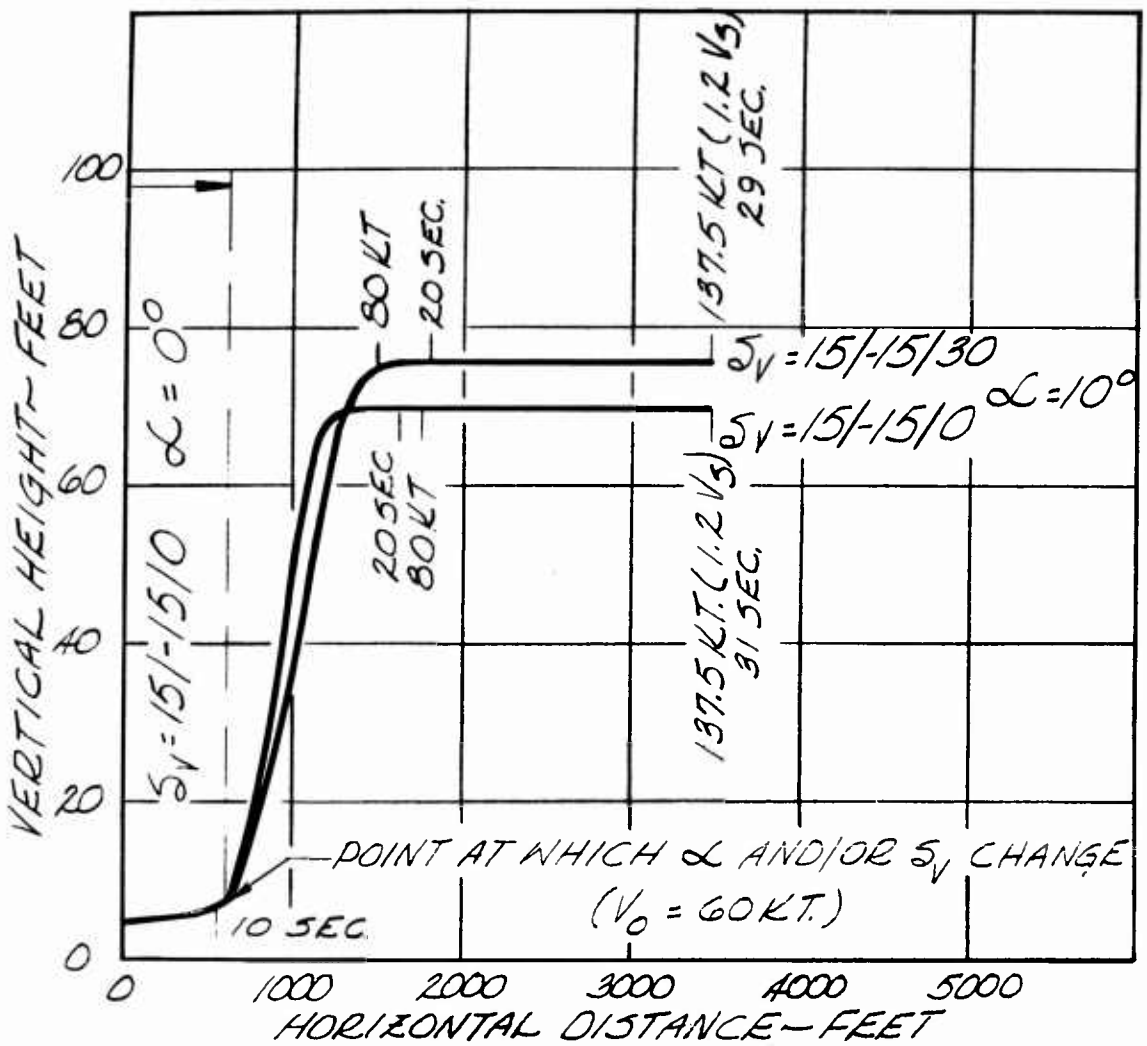

Figure 104. Effect of Vane Configuration On Take-Off Performance, Gross Weight = 82,500 Pounds, Time Shown is Elapsed Time From Start of Take-Off

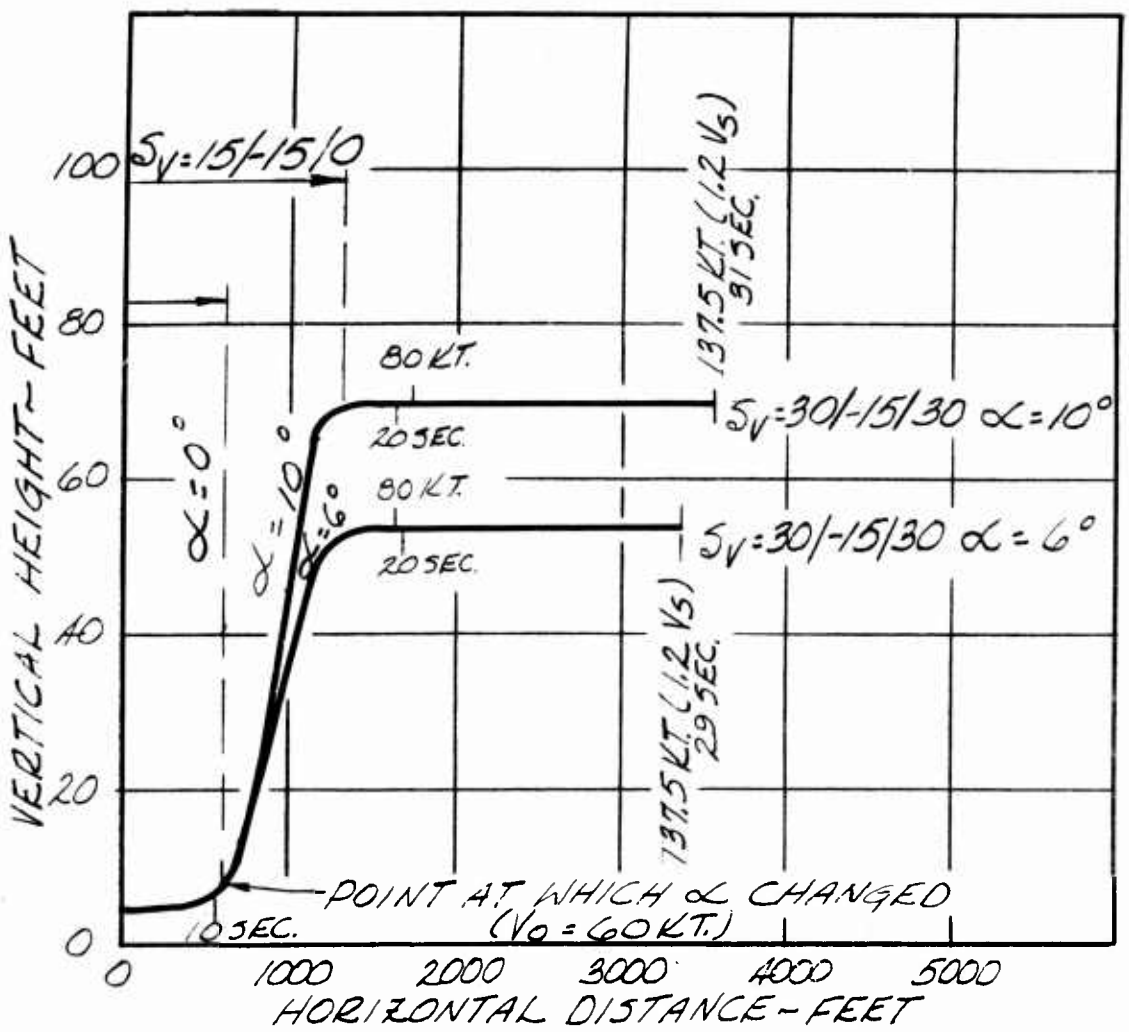

Figure 105. Effect of Angle of Attack (With Changing Vane Configuration) On Take-Off Performance, Gross Weight = 82,500 Pounds, Time Shown is Elapsed Time From Start of Take-Off

unchanged, but improved for 6° ; total time and distance to transition speed for the latter being 29 seconds and 3,400 feet.

Effects of vectoring the front and tip slots are shown in Figure 106. Here, two configurations are shown, both at 10° angle of attack. In both cases, the take-off field lengths and times are of the same order of magnitude as are obtainable without vectoring.

For the configuration studied, it appears that the increase in propulsive thrust due to thrust vectoring is not commensurate with the loss in lift suffered. In ground effect, this results in a shallower climb to 50 feet, although a slightly higher speed may be reached (Figure 104). Out of ground effect, in the range of velocities attained by the airplane, the net propulsive force from the nozzle is in the drag direction for all configurations studied. When the nozzle thrust is vectored, the drag is reduced for the same gross thrust, but since the thrust must be increased to maintain constant lift, the drag is of the same order as for the unvectored configuration. Thus, little or no change in overall take-off performance accrues (compare Figures 104 and 106), and the choice of vane configuration narrows to ones which improve hovering height. Allowing the nozzle vanes to remain unchanged during the take-off results in operational simplicity, a desirable characteristic.

Landing Performance

The landing flight path obtainable with a vane configuration of 15° /-15° /0° is shown in Figure 107. It is similar to the take-offs previously discussed, except that the landing path commences at transition speed (1.2 times the stalling speed) and at a height above 50 feet. The airplane decelerates by idling the propeller engines to about 60 knots; from there to zero velocity, reverse thrust is applied. The angle of attack is maintained at 10° . The total landing distance is 3,550 feet, but less than 1,000 feet is consumed below 50 feet in height. The total time is 30 seconds. Thus, landing performance is much the same as the take-off performance, the only change in procedure being to adjust the propeller thrust.

A vane configuration which produces negative propulsive thrust, namely -25° /-25° /0° , also was used to compute a landing. This is shown in Figure 108. The angle of attack was zero degrees, and no propeller thrust was used throughout the landing. Note that deceleration out of ground effect is faster than with 15° /-15° /0° vanes and could undoubtedly be improved in ground effect by use of reverse propeller thrust.

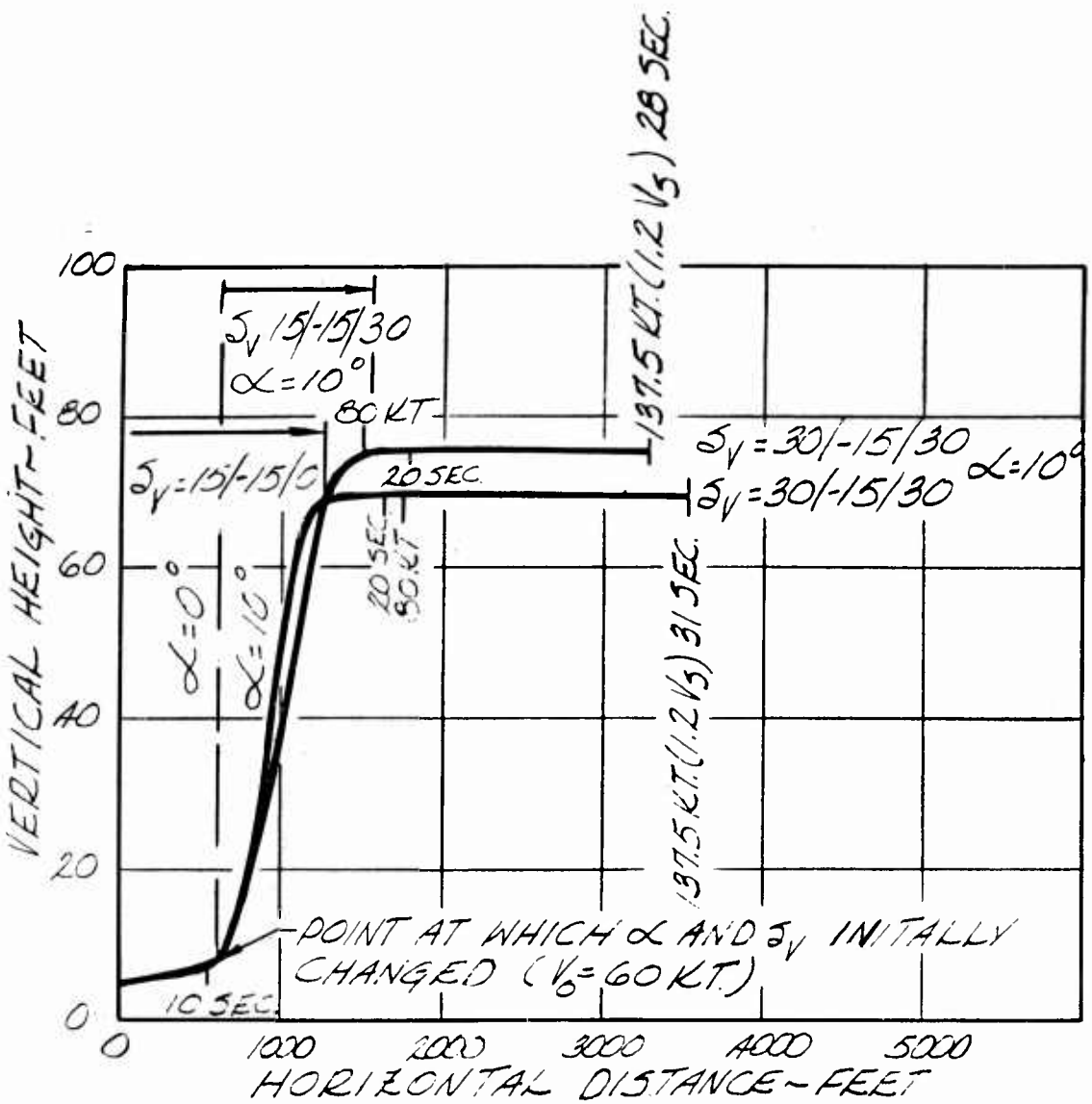

Figure 106. Take-Off Performance With Alternate Nozzle Thrust Vectoring, Gross Weight = 82,500 Pounds, Time Shown is Elapsed Time From Start of Take-Off

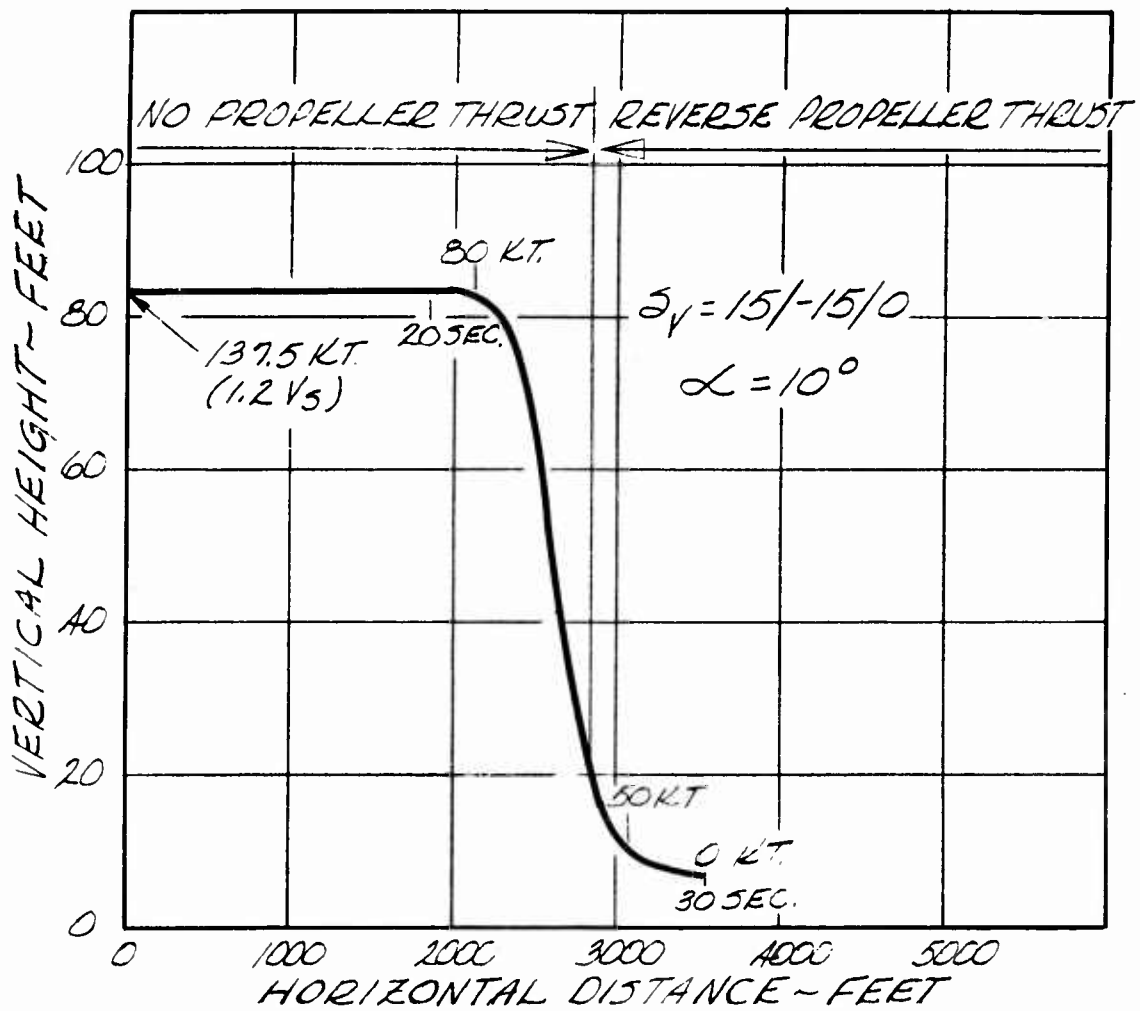

Figure 107. Landing Performance With Nonthrusting Vane Configuration, Gross Weight = 71,000 Pounds

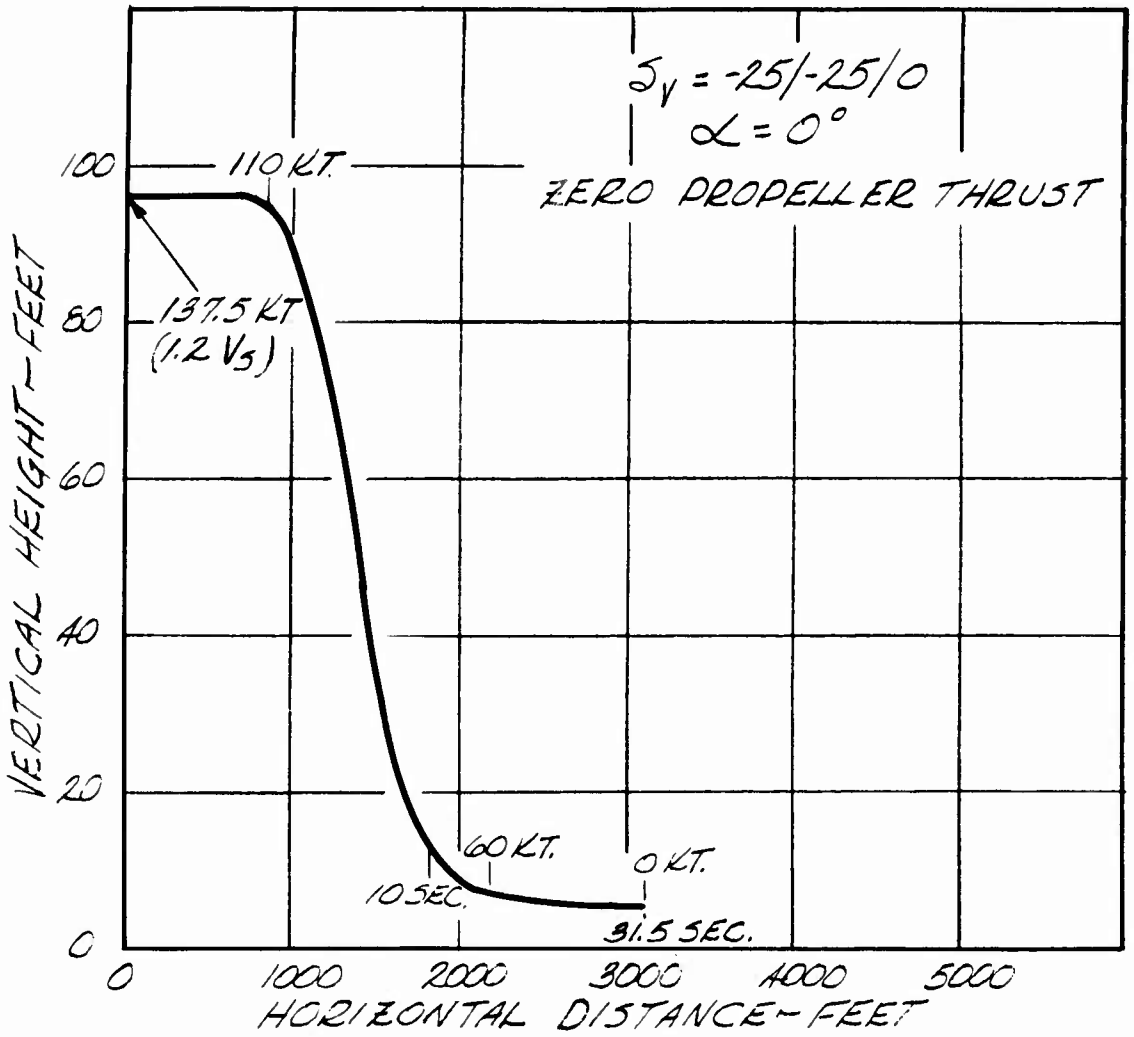

Figure 108. Landing Performance With Reverse Thrusting Vane Configuration, Gross Weight = 71,000 Pounds

Nonstandard Day Performance

A change in ambient temperature will not require a change in the magnitude of the useful load for this configuration. The operating height normally will be adjusted as required to provide a lift-to-thrust ratio compatible with the vehicle weight and the system thrust as affected by the ambient temperature. No calculations have been made in this regard for this particular vehicle. However, previous studies on similar GETOL configurations have substantiated this argument.

STABILITY AND CONTROL

A discussion of the general handling characteristics associated with the GETOL concept is presented in Phase II. The information in this section serves as a partial basis for the discussion. Specific characteristics for this particular configuration are presented to illustrate the discussion in Phase II and to indicate the capability of achieving acceptable handling characteristics with the GETOL concept.

The wind tunnel test program reported in Phase II was intended primarily to investigate the ground-effect phenomena associated with the basic concept. Therefore, tests of the various configurational parameters required for a comprehensive predesign study effort were not included. With the exception of the longitudinal mode, very little information is available upon which to base the ground effect control system estimates. The effects of the conventional empennage and the pylon-mounted propellers incorporated on the specific configuration defined herein have not been established nor have wake surveys been conducted. Consequently, much of the data basis for defining handling characteristics has been established from elementary estimates. In the conventional operating mode, the deficiency of wind tunnel data is not considered significant to the analysis since classical estimating techniques should be adequate. However, in the ground operation mode, the complexity of the flow field precludes making accurate estimates to account for the geometric deviations from the test configuration. The ramifications of this fact are discussed where applicable to qualify the information.

Low-Speed Operation

Assumed hovering control requirements are shown in Table 2. The development of these requirements is based on the requirements proposed by NASA in Reference 7, with modifications as follows (see discussion of General Handling Characteristics in Phase II):

TABLE 2
ASSUMED HOVERING CONTROL REQUIREMENTS

Axis	Specification		Weight (lb.)	Inertia (slug-ft.^{2})	Minimum Damping (sec.$^{-1}$)	Maximum Control Accel. (rad./sec.^{2})
	Minimum Attitude Response (deg. in 1 sec.)	Minimum Damping (ft. - lb. rad./sec.)				
Pitch	$\frac{180}{\sqrt[3]{W+1,000}}$	$8(I_y)^{0.7}$	82,570	630,435 to 718,987	0.165 to 0.140	0.182 to 0.181
Roll	$\frac{324}{\sqrt[3]{W+1,000}}$	$18(I_x)^{0.7}$	82,570	540,286 to 465,817	0.345 to 0.361	0.348 to 0.350
Yaw	$\frac{165}{\sqrt[3]{W+1,000}}$	$13.5(I_z)^{0.7}$	82,570	1,083,851 to 1,096,963	0.211 to 0.210	0.170 to 0.170

1. Yaw requirement is reduced by a factor of 2 based on recent X14A test results presented in Reference 8.
2. Roll requirements is converted to an equivalent value for a time period of 1 second rather than 0.5 second, based on the recommendation of Ames Research Center personnel.
3. Control system time constants of 0.1 second are assumed.

Several control system concepts have been qualitatively investigated to establish the most promising concept. These systems are defined and discussed in Reference 12. Inadequate data is available to establish confidently the best system at this time; however, an early judgment has been made. The control systems are illustrated in Figure 109. The longitudinal system is derived directly from the wind tunnel tests of the variable aft slot position. The test data verified the effectiveness of the system in the extreme forward and aft control configurations. The characteristics through the intermediate control range (with partial flow through each slot) are assumed to be acceptable, based on elementary ground

effect theory. The lateral, directional, and thrust-vectoring systems are integrated through an intermix system operating on flow deflector vanes in the tip slots. Lateral control is achieved by differential "pinching" of the tip slot areas. Directional control and axial force control (for take-off acceleration augmentation) are achieved by either differential or symmetrical tip slot thrust vectoring.

A summary of the estimated maximum effectiveness of these control systems with respect to the requirements is shown in Table 3. Also shown is the estimate of the lift system design thrust margins required to accommodate these systems. The basis for defining the required thrust margins is a ficticious configuration with no control systems, trimmed about the mid cg point (0.37$\bar{c}$), and operating at a hover height equal to that obtainable with full control input. These thrust margins are presented for future comparisons with other possible GETOL systems or with the many V/STOL systems. As indicated in Table 3, the systems are potentially adequate to satisfy the requirements and are mechanically acceptable. A cursory examination of the tip vane intermix system indicates that reasonable control combinations are obtainable.

Typical take-off and landing static longitudinal control requirements are shown in Figures 110 and 111. The control requirements are all within the capability of the system with the exception of the 0 to 20-knot speed range during take-off. This excessive nose-up control requirement is caused by the large nose-down moment assumed from the propellers. This may require a gradual application of power for the take-off procedure. However, power effects on stability and control derivatives in the ground operation mode are unknown. Further wind tunnel testing is required to establish these effects.

CONVENTIONAL FLIGHT OPERATION

Data Basis

The data basis for the conventional flight mode of operation is presented in Table 4. Where possible, GETOL wind tunnel data was employed to establish this basis. Tail-off static longitudinal derivatives were derived primarily from the data of Reference 10 and static lateral-directional derivatives were extracted from the data of Reference 13. The remainder of the derivatives were established by elementary estimating techniques in which the unique GETOL wing configuration was treated as a simple, low aspect-ratio wing. The techniques of Reference 14 were relied upon to determine many of the lateral-directional rotary derivatives.

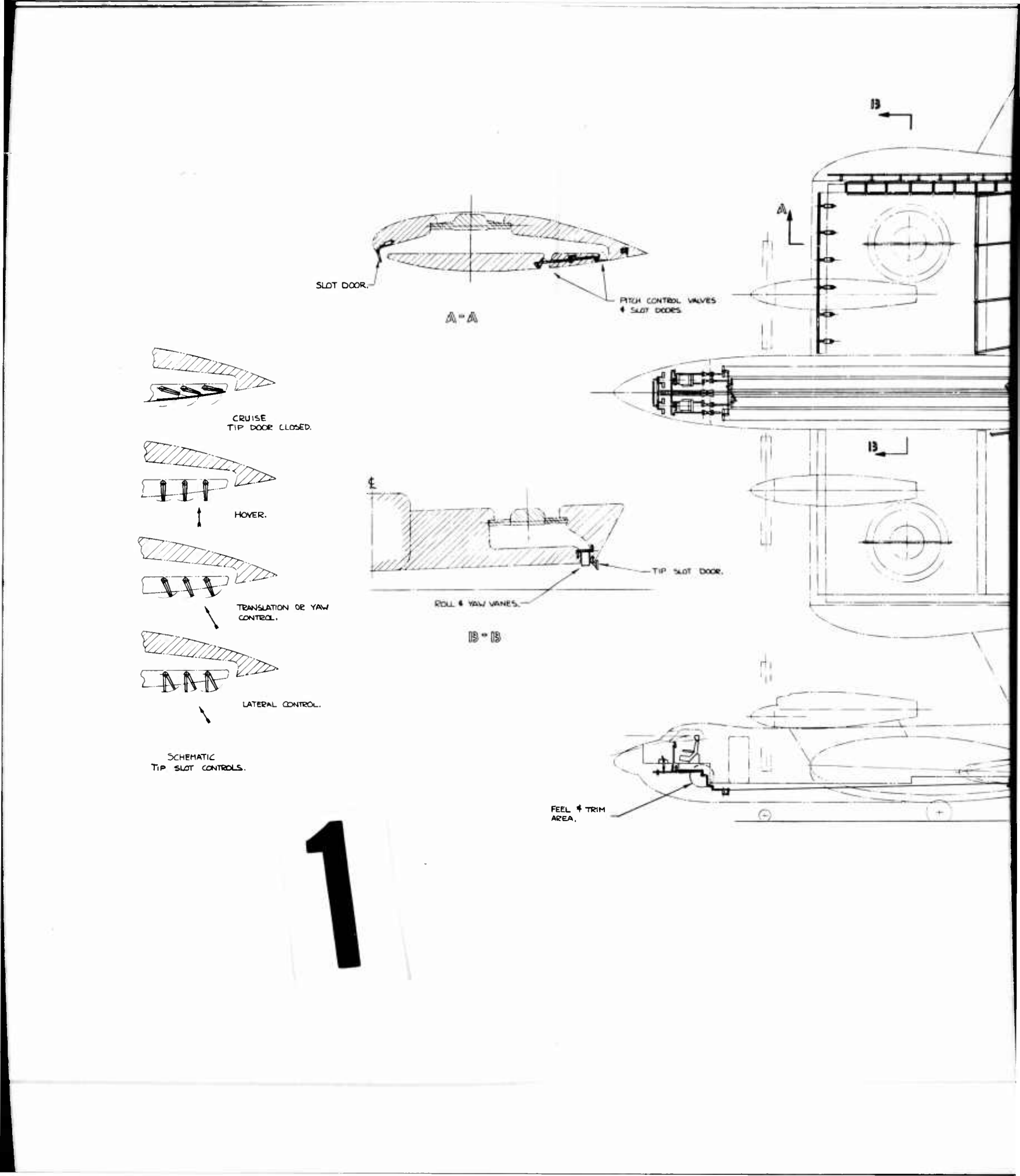
B
A
SLOT DOOR.
PITCH CONTROL VALVES & SLOT DOORS.
A - A
B
℄
TIP SLOT DOOR.
ROLL & YAW VANES.
B - B
CRUISE
TIP DOOR CLOSED.
HOVER.
TRANSLATION OR YAW CONTROL.
LATERAL CONTROL.
SCHEMATIC
TIP SLOT CONTROLS.
FEEL & TRIM AREA.

1

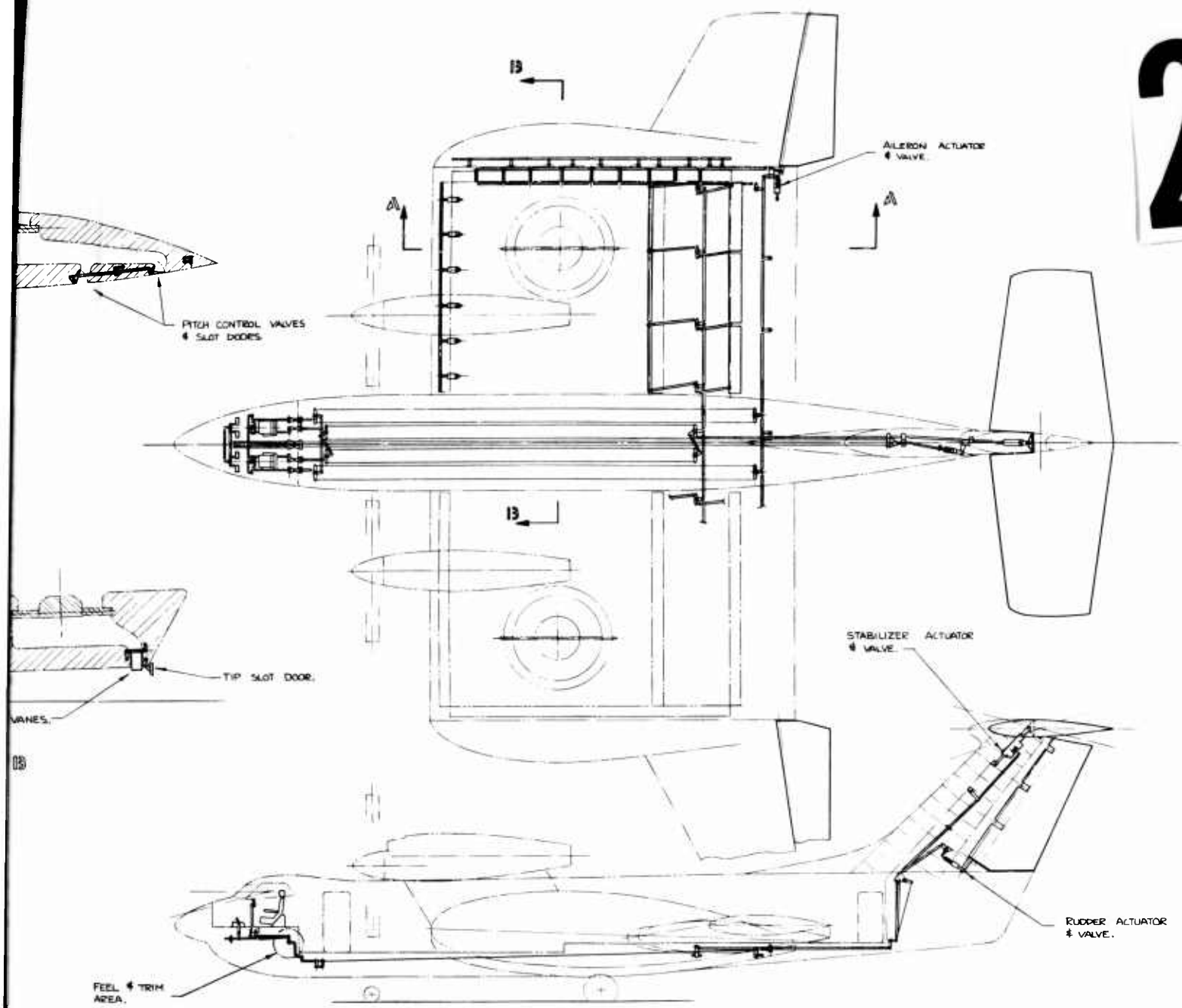

Figure 109. Controls Inboard

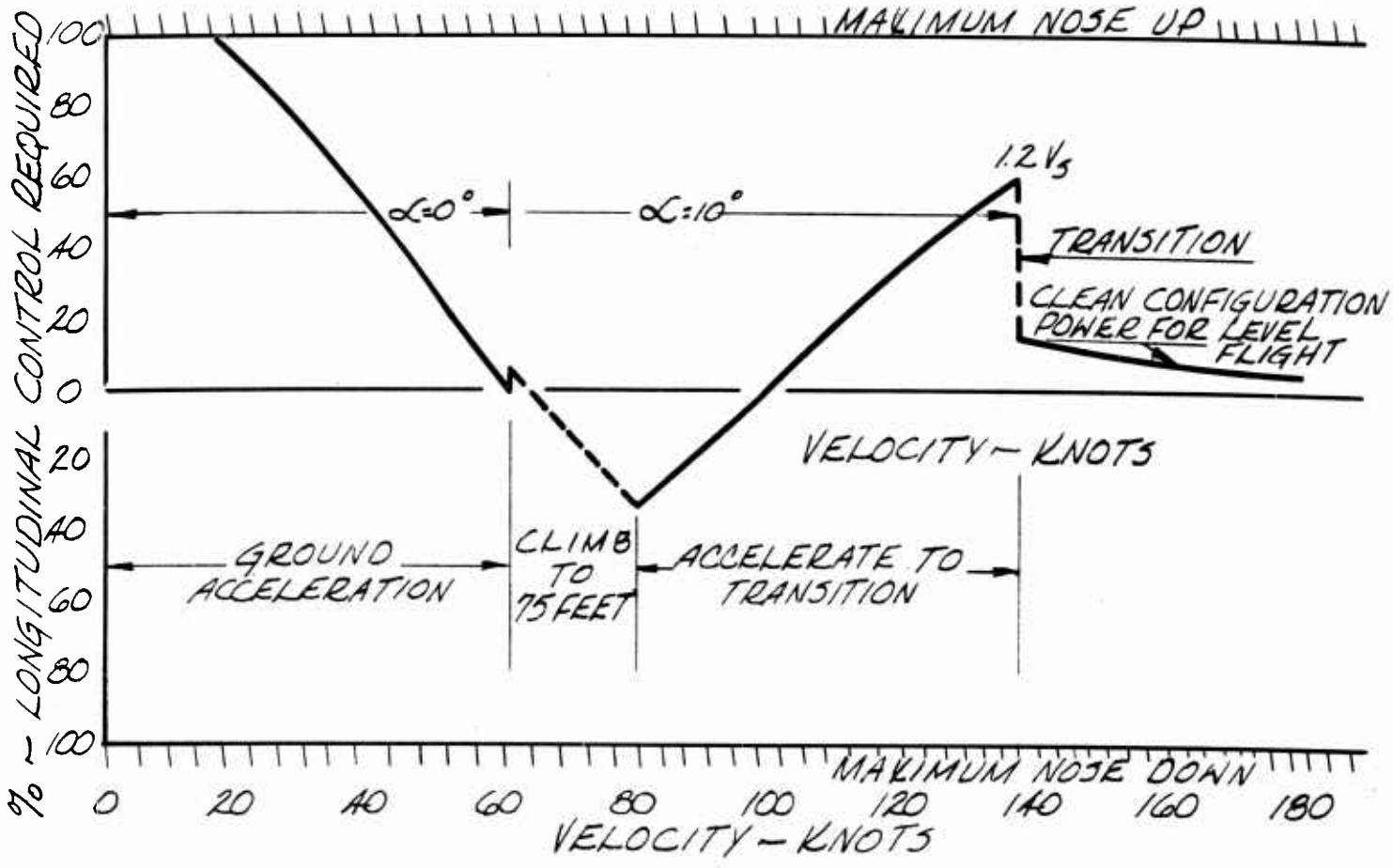

Figure 110. Control Required During Take-Off to Transition Maximum Take-Off Thrust CG = 0.37$\bar{c}$ Gross Weight = 82,500 Pounds

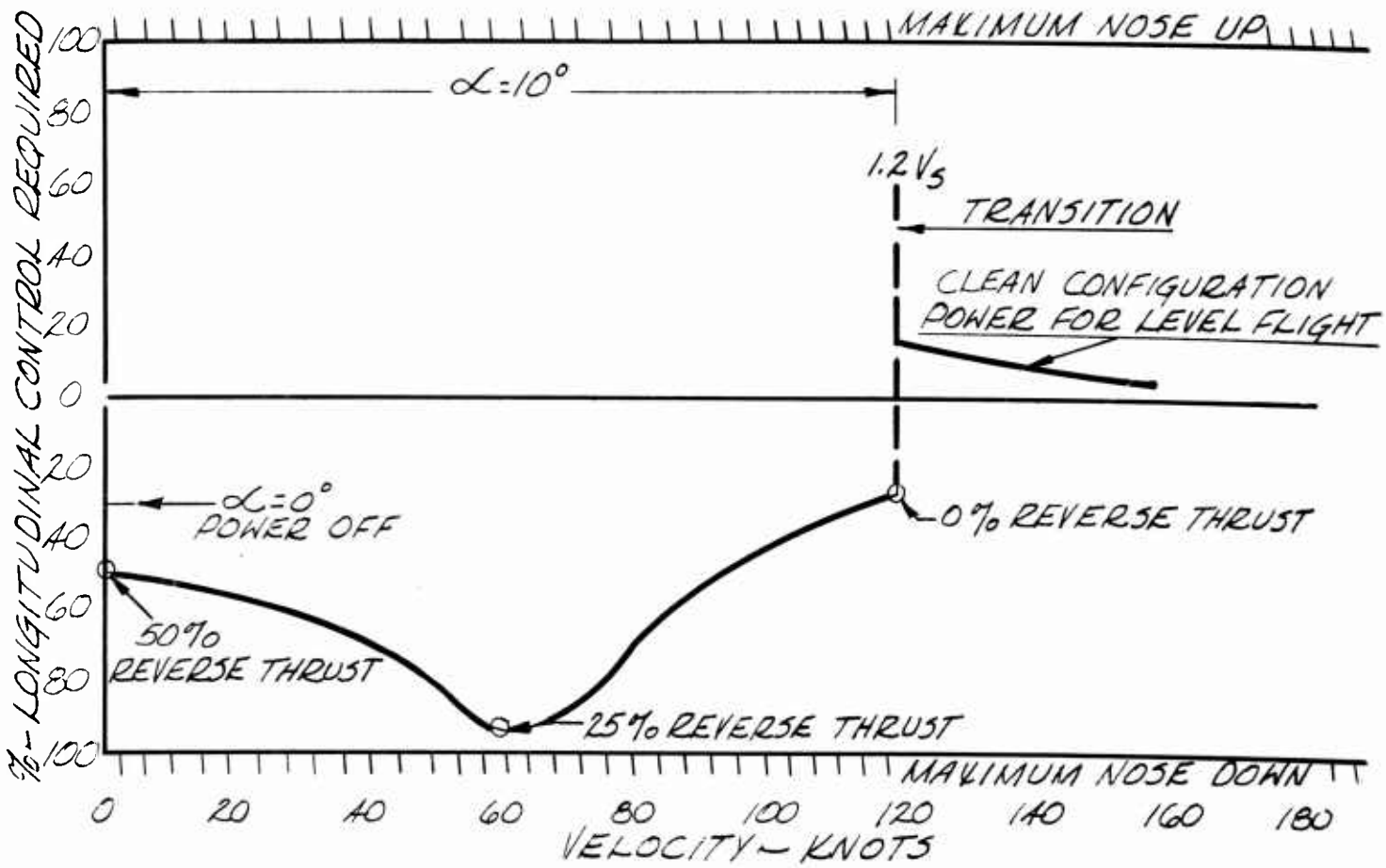

Figure 111. Control Required for Normal Landing Gross Weight = 62,200 Pounds CG = 0.37$\bar{c}$

TABLE 3
HOVERING CONTROL SYSTEM DESIGN SUMMARY

Axis	Hovering Requirement	System Effectiveness	Required Lift System Design Thrust Margin
Pitch	±4.62% chord center of pressure shift from cg	+7.6% chord and -4.0% chord from 37% chord point (Marginal nose-up control)	Approximately 7%
Roll	±0.35 rad./sec.^{2} roll acceleration	±0.40 rad./sec.^{2} available with ±35% tip thrust modulation	0% for first order effect. Actual margin unknown
Yaw	±0.17 rad./sec.^{2} yaw acceleration	±0.19 rad./sec.^{2} available with ±20° tip thrust vectoring	Approximately 10%

Longitudinal Characteristics

Static longitudinal stability in the conventional flight mode of operation is illustrated in Figure 112 as speed stability. The neutral point location of 45% chord results in adequate stability over the assumed cg range. Maneuver stability shown in Figure 113 indicates a maneuver point at approximately 48% chord. Note that the small stabilizer deflection requirements for trim and maneuvering indicate that a fixed stabilizer with a conventional elevator control system would be adequate in this flight regime. The all-moving stabilizer designed was assumed to allow for unknowns in the low-speed operating range. Adequate control in this low-speed regime probably can be obtained with the hovering control system, thereby relieving any requirement for an all-movable stabilizer.

Longitudinal short-period dynamic stability parameters are shown in Figure 114. The requirements of both References 7 and 15 are superimposed to show compliance. The parameters for this configuration generally fall within the acceptable boundary of Reference 7. This boundary is considered applicable rather than the boundary of Reference 15 since it is derived from more recent information.

TABLE 4
DATA BASIS FOR CONVENTIONAL FLIGHT CHARACTERISTICS CALCULATIONS

Longitudinal

$W = 82,570$ lb.

$I_{yy} = 630,435$ slug-ft.^{2}

Aerodynamic Derivatives/Rad.

Derivative $\backslash$ CG	$0.345\bar{c}$	$0.370\bar{c}$	$0.395\bar{c}$
C_{L_α}	-	4.2	-
C_{M_α}	-0.441	-0.336	-0.231
$C_{L_{\dot{\alpha}}}$	-	0	-
$C_{m_{\dot{\alpha}}}$	-	-0.0119	-
$C_{L_{\dot{\theta}}}$	-	0.097	-
$C_{m_{\dot{\theta}}}$	-	-0.0721	-
$C_{L_{\delta_S}}$	-	0.601	-
$C_{m_{\delta_S}}$	-0.743	-0.756	-0.772

Lateral-Directional

$W = 71,120$ lb.

$I_{xx} = 465,817$ slug. ft.^{2}

$I_{zz} = 1,096,963$ slug-ft.^{2}

Incidence of principal axis with flight path assumed = 0.

Aerodynamic Derivatives/Rad.

Derivative $\backslash$ V_o Knots	128	175	250
C_L	0.690	0.371	0.181
C_{n_β}	0.263	0.235	0.219
C_{ℓ_β}	-0.404	-0.273	-0.196

TABLE 4 (Continued)

Aerodynamic Derivatives/Rad.

Derivative	V_o Knots 128	175	250
C_{y_β}	-0.290	-0.367	-0.412
C_{n_r}	-0.143	-0.171	-0.191
C_{ℓ_r}	0.382	0.271	0.200
C_{y_r}	0	0	0
C_{n_p}	-0.110	-0.058	-0.029
C_{ℓ_p}	-0.246	-0.242	-0.242
C_{y_p}	0	0	0

Lateral-Directional Characteristics

The lateral-directional characteristics considered herein are maximum roll control, one-engine-out control, and dynamic stability. The 40% chord ailerons deflected 20° will provide a roll helix angle of 0.1 to 0.15 which is well in excess of 0.07 requirement of Reference 4. The rudder is more than adequate for control of an engine-out condition, requiring only 18° of rudder deflection at $1.2V_S$ to hold zero degrees sideslip. Lateral-directional oscillation parameters are compared with the requirement of Reference 7 in Figure 115. As evidenced, poor damping characteristics are exhibited. This is caused by the large ratio of inertia to damping and the large dihedral effect from the wing tips. A single point for low-speed flight is shown for a 60% increase in C_{n_r} and a 90% decrease in C_{ℓ_β} representing a major wing tip shape modification. These changes are sufficient to yield parameters acceptable for emergency operation but not for normal operation. Means of reducing $C_{\ell\beta}$ and the inertia levels must be investigated to achieve acceptable characteristics. A stability augmentation system appears required.

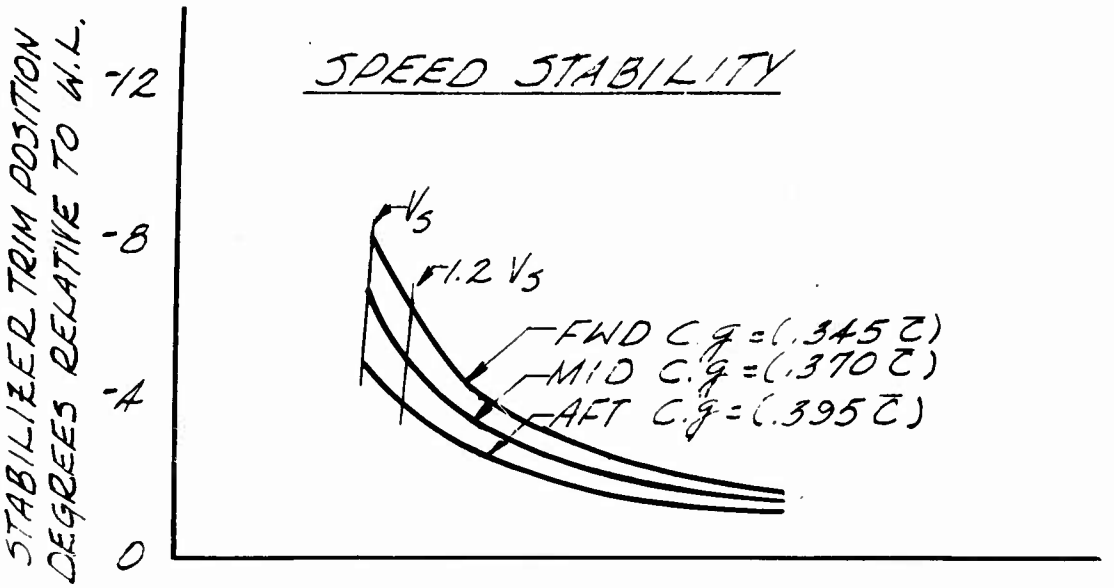

Figure 112. Clean Configuration Power for Level Flight

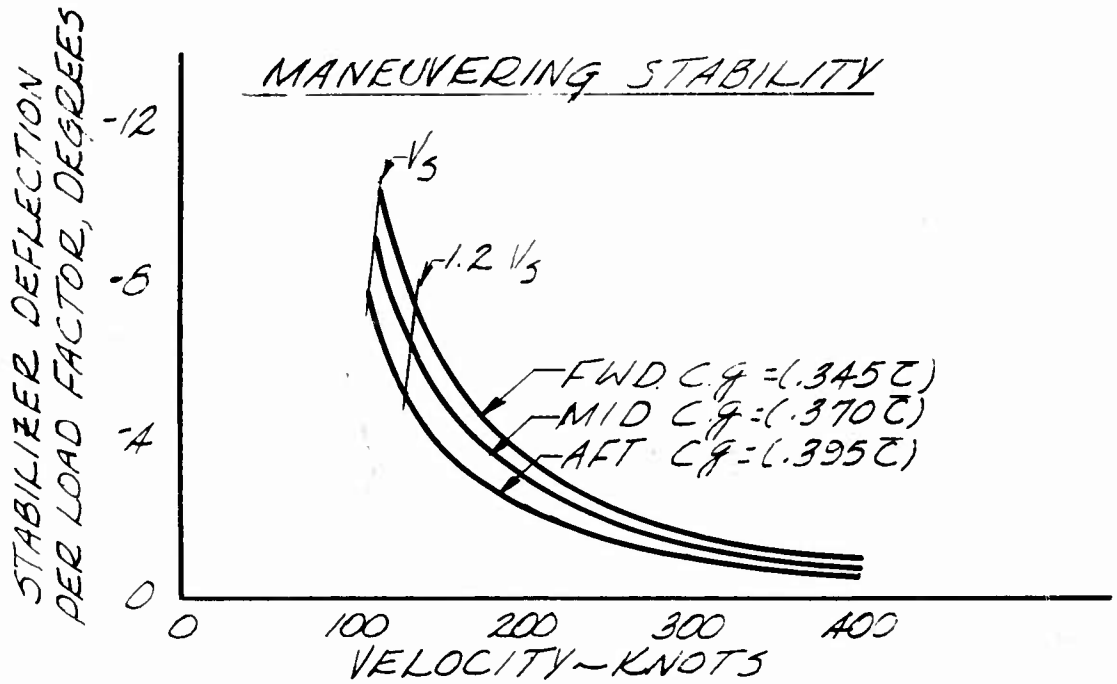

Figure 113. Clean Configuration Power for Level Flight

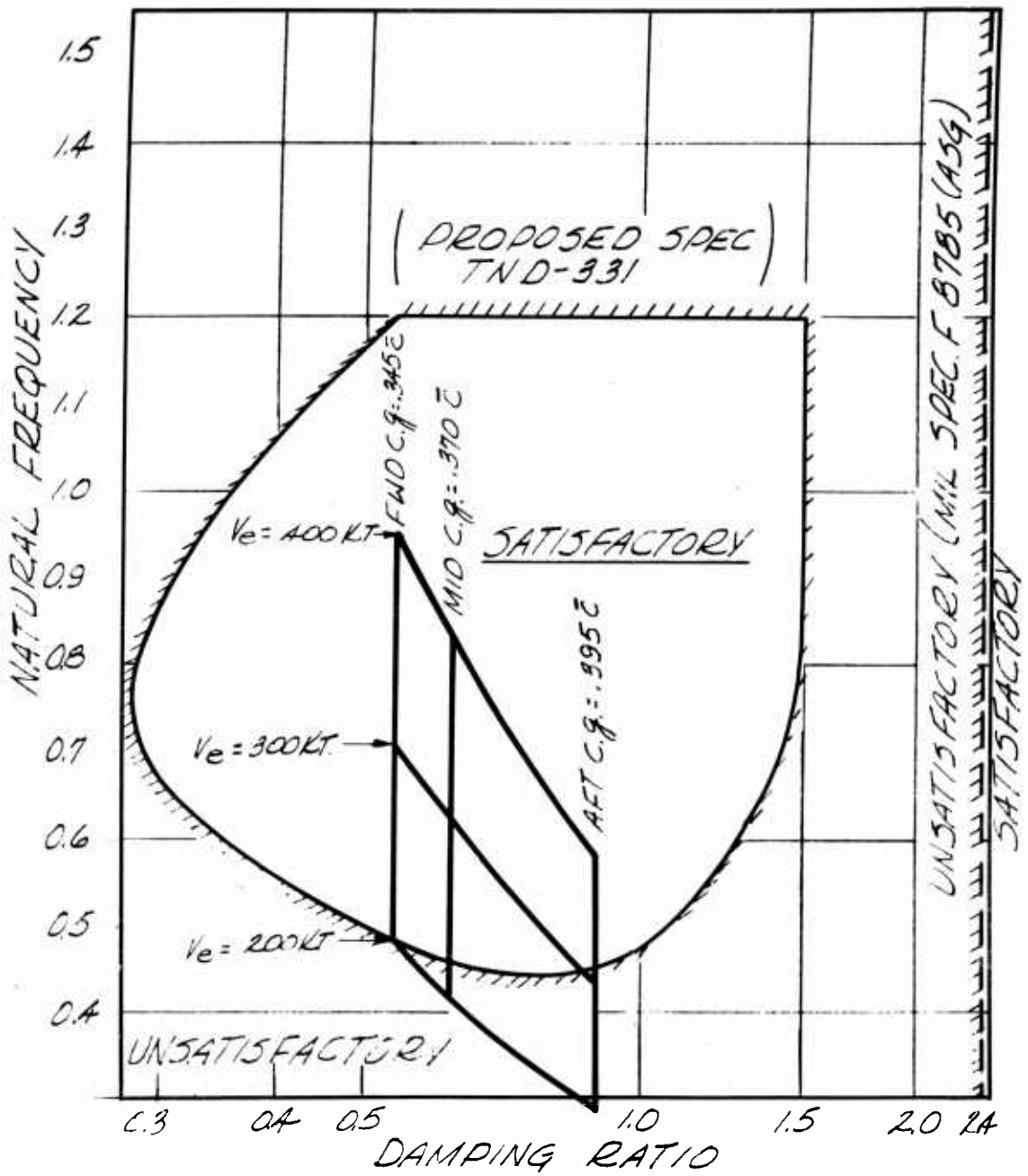

Figure 114. Longitudinal Dynamic Stability Parameters

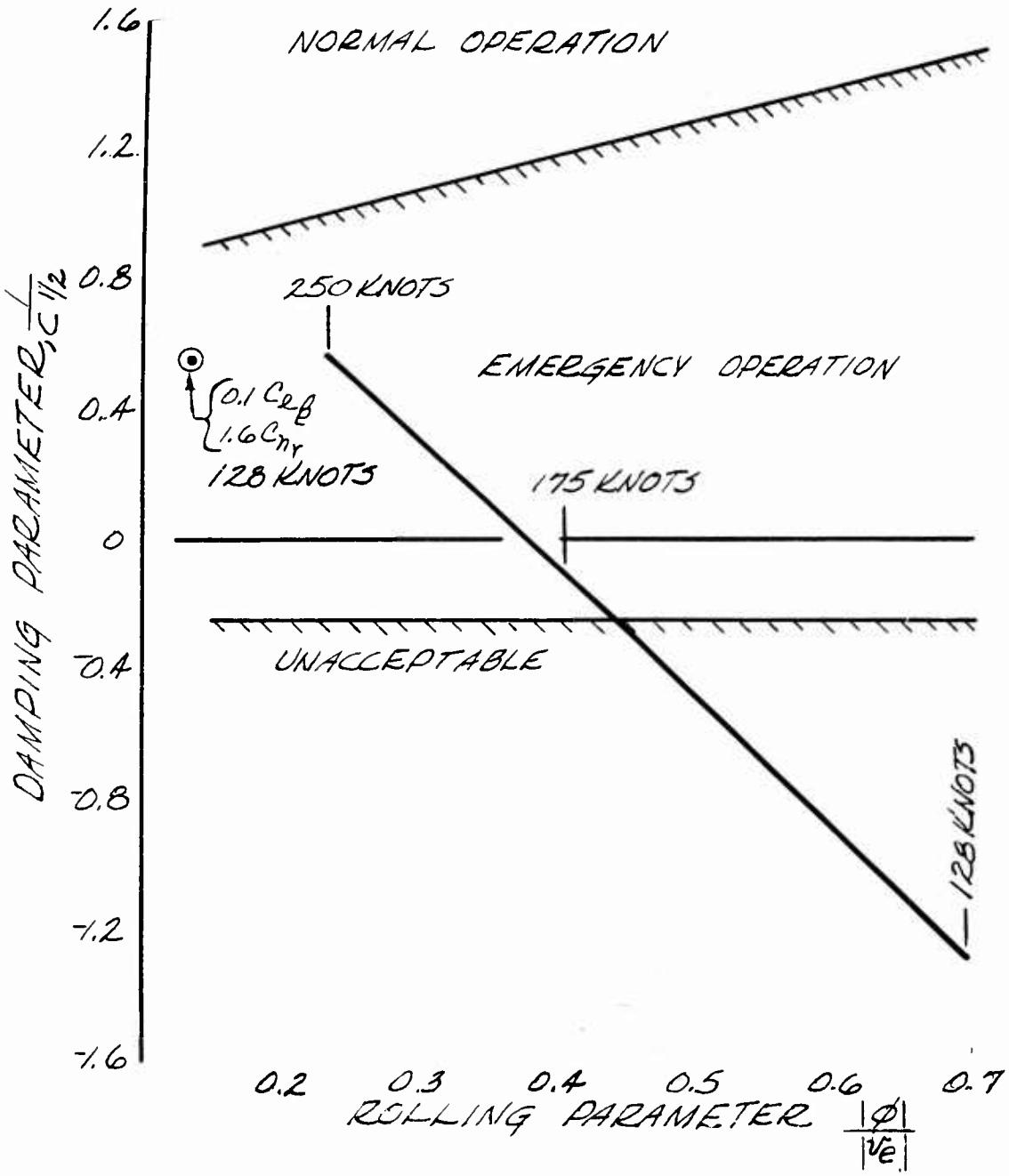

Figure 115. Lateral-Directional Dynamic Stability

REFERENCES

1. Prunty, J., A Verification of the Structural Advantages of a Low Aspect Ratio VTOL/STOL Configuration, Convair Report ACPD-60-027, San Diego, California, 13 July 1960.

2. Wolkovitch, J., Interim Report on Wind Tunnel Tests on Unpowered Model of PD-104 VTOL Configurations, Convair Aero Memo A-PD-010, San Diego, California, 17 March 1959.

3. Davis, Walter B., Procedures for Correlation of the Aerodynamic Characteristics of V/STOL Aircraft, paper presented at IAS National Meeting on the Future of Manned Military Aircraft, San Diego, California, 1-3 August 1960.

4. Robinson, H. L., Preliminary Study of Scaling Laws for Powered Lift Fan Models and Specifications for the First General Electric X353-5 Convair VTOL Model, Convair Aero Doc VTOL-021, San Diego, California, August 1961.

5. Walker, Norman K., Some Notes on the Lift and Drag of Ground Effect Machines, Norman K. Walker Associates, Inc., Bethesda, Maryland, September 1962.

6. Helicopter Flying and Ground Handling Qualities; General Requirements For, Military Specification MIL-H-8501A, 7 September 1961.

7. Anderson, Seth B., An Examination of Handling Criteria for V/STOL Aircraft, NASA TN D-331, Ames Research Center, Moffett Field, California, July 1960.

8. Rolls, L. Stewart, and Drinkwater III, Fred J., A Flight Determination of the attitude Control Power and Damping Requirements for a Visual Hovering Task in the Variable Stability and Control X-14A Research Vehicle, NASA TN D-1328, Ames Research Center, Moffett Field, California, May 1962.

9. Wolkovitch, J., Stability and Control of the PD-104 Configuration SD-60-00007 With 2 x 120" Diameter Horizontal Lift Fans, Convair Aero Doc VTOL-005, San Diego, California, March 1960.

10. Durigan, O. S., Additional Low-Speed Wind Tunnel Tests of a 0.0615 Scale Model of the PD-104 VTOL Airplane to Determine the Effectiveness of Various Horizontal Tail Configurations, Convair Report CVAL 293, San Diego, California, 23 May 1960.

11. Hamilton Standard Division, United Aircraft Corporation, Generalized Method of Propeller Performance Estimation, Hamilton Standard Report Number PDB 6101.

12. Piszkin, S., Some Considerations of GETOL Stability and Control Systems, Convair Aero Doc VTOL-034, San Diego, California, 21 September 1962.

13. Reynolds, H. A., Additional Low-Speed Wind Tunnel Tests of a 0.057-Scale Model of the Configuration -104 VTOL Airplane to Determine the Aerodynamic Effects of Various Wing Tip Modifications and Various Fuselage and Engine Nacelle Configurations, Convair Report CVAL 276A, B, San Diego, California, 31 August 1959.

14. Campbell, John P. and McKinney, Marion O., Summary of Methods for Calculating Dynamic Lateral Stability and Response and for Estimating Lateral Stability Derivatives, NACA TN 2409, Langley Aeronautical Laboratory, Langley Field, Virginia, July 1951.

15. Flying Qualities of Piloted Airplanes, Military Specification MIL-F-8785 (ASG).

DISTRIBUTION

U. S. Army Aviation Test Board	1
Army Research Office, Durham	2
Office of Chief of R&D, D/A	1
Army Research Office, OCRD	1
U. S. Army Combat Developments Command Transportation Agency	1
U. S. Army Aviation and Surface Materiel Command	1
U. S. Army Transportation Research Command	20
U. S. Army Research & Development Group (Europe)	1
Air University Library, Maxwell AFB	1
Bureau of Naval Weapons	5
Bureau of Ships	1
U. S. Naval Ordnance Test Station	1
David Taylor Model Basin	1
U. S. Army Standardization Group, Canada	1
Canadian Army Liaison Officer, U. S. Army Transportation School	3
British Army Staff, British Embassy	4
U. S. Army Standardization Group, U.K.	1
NASA-LRC, Langley Station	2
Ames Research Center, NASA	2
Lewis Research Center, NASA	1
NASA Representative, Scientific and Technical Information Facility	1
U. S. Government Printing Office	1
Defense Documentation Center	10
U. S. Patent Office	1
U. S. Army Mobility Command	3
U. S. Army Materiel Command	1
Institute of Naval Studies	1
Naval Air Development Center	1

General Dynamics/Convair, San Diego, Cal., GETOL RESEARCH PROGRAM, (Final Report), TRECOM Technical Rept 63-1, August 1963, 165 pp. (Contract DA 44-177-TC-722) USATRECOM Task 1D121401A14701, (formerly Task 9R38-11-011-01).

Unclassified Report

This report presents the results of an experimental research program to determine the aerodynamic characteristics of a ground-effect take-off and landing (GETOL) aircraft and to

(over)

General Dynamics/Convair, San Diego, Cal., GETOL RESEARCH PROGRAM, (Final Report), TRECOM Technical Rept 63-1, August 1963, 165 pp. (Contract DA 44-177-TC-722) USATRECOM Task 1D121401A14701, (formerly Task 9R38-11-011-01).

Unclassified Report

This report presents the results of an experimental research program to determine the aerodynamic characteristics of a ground-effect take-off and landing (GETOL) aircraft and to

(over)

General Dynamics/Convair, San Diego, Cal., GETOL RESEARCH PROGRAM, (Final Report), TRECOM Technical Rept 63-1, August 1963, 165 pp. (Contract DA 44-177-TC-722) USATRECOM Task 1D121401A14701, (formerly Task 9R38-11-011-01).

Unclassified Report

This report presents the results of an experimental research program to determine the aerodynamic characteristics of a ground-effect take-off and landing (GETOL) aircraft and to

(over)

General Dynamics/Convair, San Diego, Cal., GETOL RESEARCH PROGRAM, (Final Report), TRECOM Technical Rept 63-1, August 1963, 165 pp. (Contract DA 44-177-TC-722) USATRECOM Task 1D121401A14701, (formerly Task 9R38-11-011-01).

Unclassified Report

This report presents the results of an experimental research program to determine the aerodynamic characteristics of a ground-effect take-off and landing (GETOL) aircraft and to

(over)

ascertain the feasibility and potential of a GETOL aircraft system. The objective of the GETOL concept is to produce an aircraft that would eliminate conventional landing gear and provide a capability for take-off and landing over unprepared terrain.

The program included static-room and wind-tunnel testing. The data and results from the tests provided the basis for the design analysis and layouts of the GETOL aircraft study contained in this report.

The acquisition of basic GETOL aerodynamic data and analysis should be considered as the significant technical achievement of this program.

ascertain the feasibility and potential of a GETOL aircraft system. The objective of the GETOL concept is to produce an aircraft that would eliminate conventional landing gear and provide a capability for take-off and landing over unprepared terrain.

The program included static-room and wind-tunnel testing. The data and results from the tests provided the basis for the design analysis and layouts of the GETOL aircraft study contained in this report.

The acquisition of basic GETOL aerodynamic data and analysis should be considered as the significant technical achievement of this program.

ascertain the feasibility and potential of a GETOL aircraft system. The objective of the GETOL concept is to produce an aircraft that would eliminate conventional landing gear and provide a capability for take-off and landing over unprepared terrain.

The program included static-room and wind-tunnel testing. The data and results from the tests provided the basis for the design analysis and layouts of the GETOL aircraft study contained in this report.

The acquisition of basic GETOL aerodynamic data and analysis should be considered as the significant technical achievement of this program.

General Dynamics/Convair, San Diego, Cal., GETOL RESEARCH PROGRAM, (Final Report), TRECOM Technical Rept 63-1, August 1963, 165 pp. (Contract DA 44-177-TC-722) USATRECOM Task 1D121401A14701, (formerly Task 9R38-11-011-01).

Unclassified Report

This report presents the results of an experimental research program to determine the aerodynamic characteristics of a ground-effect take-off and landing (GETOL) aircraft and to

(over)

General Dynamics/Convair, San Diego, Cal., GETOL RESEARCH PROGRAM, (Final Report), TRECOM Technical Rept 63-1, August 1963, 165 pp. (Contract DA 44-177-TC-722) USATRECOM Task 1D121401A14701, (formerly Task 9R38-11-011-01).

Unclassified Report

This report presents the results of an experimental research program to determine the aerodynamic characteristics of a ground-effect take-off and landing (GETOL) aircraft and to

(over)

General Dynamics/Convair, San Diego, Cal., GETOL RESEARCH PROGRAM, (Final Report), TRECOM Technical Rept 63-1, August 1963, 165 pp. (Contract DA 44-177-TC-722) USATRECOM Task 1D121401A14701, (formerly Task 9R38-11-011-01).

Unclassified Report

This report presents the results of an experimental research program to determine the aerodynamic characteristics of a ground-effect take-off and landing (GETOL) aircraft and to

(over)

General Dynamics/Convair, San Diego, Cal., GETOL RESEARCH PROGRAM, (Final Report), TRECOM Technical Rept 63-1, August 1963, 165 pp. (Contract DA 44-177-TC-722) USATRECOM Task 1D121401A14701, (formerly Task 9R38-11-011-01).

Unclassified Report

This report presents the results of an experimental research program to determine the aerodynamic characteristics of a ground-effect take-off and landing (GETOL) aircraft and to

(over)

ascertain the feasibility and potential of a GETOL aircraft system. The objective of the GETOL concept is to produce an aircraft that would eliminate conventional landing gear and provide a capability for take-off and landing over unprepared terrain.

The program included static-room and wind-tunnel testing. The data and results from the tests provided the basis for the design analysis and layouts of the GETOL aircraft study contained in this report.

The acquisition of basic GETOL aerodynamic data and analysis should be considered as the significant technical achievement of this program.

ascertain the feasibility and potential of a GETOL aircraft system. The objective of the GETOL concept is to produce an aircraft that would eliminate conventional landing gear and provide a capability for take-off and landing over unprepared terrain.

The program included static-room and wind-tunnel testing. The data and results from the tests provided the basis for the design analysis and layouts of the GETOL aircraft study contained in this report.

The acquisition of basic GETOL aerodynamic data and analysis should be considered as the significant technical achievement of this program.

ascertain the feasibility and potential of a GETOL aircraft system. The objective of the GETOL concept is to produce an aircraft that would eliminate conventional landing gear and provide a capability for take-off and landing over unprepared terrain.

The program included static-room and wind-tunnel testing. The data and results from the tests provided the basis for the design analysis and layouts of the GETOL aircraft study contained in this report.

The acquisition of basic GETOL aerodynamic data and analysis should be considered as the significant technical achievement of this program.

ascertain the feasibility and potential of a GETOL aircraft system. The objective of the GETOL concept is to produce an aircraft that would eliminate conventional landing gear and provide a capability for take-off and landing over unprepared terrain.

The program included static-room and wind-tunnel testing. The data and results from the tests provided the basis for the design analysis and layouts of the GETOL aircraft study contained in this report.

The acquisition of basic GETOL aerodynamic data and analysis should be considered as the significant technical achievement of this program.

UNCLASSIFIED